Hierarchically Organized (Hybrid) Silica Monoliths for the Application as Stationary Phases in HPLC

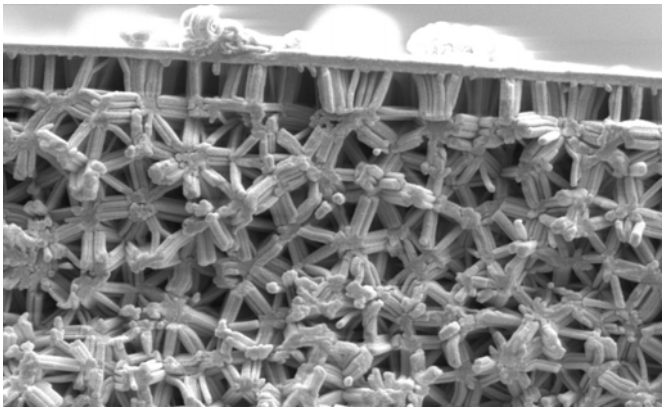

Dissertation zur Erlangung des akademischen Grades
Doktor der Naturwissenschaften
(Dr. rer. nat.)

eingereicht an der
Fakultät für Naturwissenschaften
der Universität Ulm

vorgelegt von
Sarah Hartmann
aus Starnberg

2009

Amtierender Dekan: Prof. Dr. Axel Groß

Erstgutachterin: Prof. Dr. Nicola Hüsing
Zweitgutachter: Prof. Dr. Boris Mizaikoff

Tag der Promotion: 17. 03. 2010

Abstract

This work deals with the sol-gel processing by employing diol-modified silanes as precursors towards hierarchically organized (hybrid) silica monoliths. With regard to their application as stationary phases in high performance liquid chromatography (HPLC), an important aspect is the hierarchical structuring with defined pore size domains in the mesoscopic and the macroscopic range.
In order to avoid limitations of the diffusion pathways and the mass transfer within the monolithic column, a homogeneous co-continuous macroporous framework is desired, while an integrated mesoporous network allows for the separation of the chemical compounds. The sol-gel synthesis in combination with the employment of a structure-directing agent is a promising approach towards the synthesis of materials with integrated advanced functionalities as it allows for the design of the hierarchical pore size domains and can be performed in aqueous media at moderate temperatures and pressures. Adjusting the synthesis parameters, such as the choice and ratio of the structure-directing agent, e.g. Pluronic P123 or polydimethylsiloxane-based co-polymers (Tego Glide 440 and LA-S 687), the concentration of the acid catalyst, the gelation and aging temperature, etc., allows for a deliberate control of the final pore architecture of the silica monoliths with respect to the desired morphology on the different length scales.

As in this work, diol-modified silanes are employed as precursors for the formation of the silica network, the influence of the chemical nature of the released diol on the phase separations in the mesoscopic and macroscopic range and hence on the resulting structural properties are studied.

Besides well-defined pore size domains, the application of silica materials as stationary phases in HPLC, *e.g.* in the Reversed Phase (RP) mode, requires tailored surface properties, such as hydrophobic pore walls, which can be achieved by the incorporation of functional organic groups. Hybrid inorganic-organic silica monoliths have been synthesized via two different approaches. First by the direct synthesis approach at which the organic-modified silica network is generated by co-condensation of the ethylene glycol-modified methyl- or phenylsilane (MeGMS, PhGMS) with the ethylene glycol-modified silane (EGMS). The second approach is the post-synthetic functionalization of the silica surface via silylation

reactions with chlorotrimethylsilane (TMCS), or chlorododecyldimethylsilane and via end-capping (by combining both silylation agents) resulting in a hydrophobic surface by simultaneous preservation of the hierarchical pore architecture.

The last chapter of this work deals with the application of selected monoliths as stationary phases in HPLC experiments. In collaboration, the hierarchically organized hybrid silica monoliths have been tested in standardized Normal Phase (NP) and in Reversed Phase (RP) experiments at Merck KGaA, Darmstadt.

Kurzfassung der Dissertation

Das Ziel dieser Arbeit ist die Synthese hierarchisch strukturierter (Hybrid-) Silika Monolithen mit Hilfe des Sol-Gel Verfahrens unter Verwendung diol-modifizierter Silane. Ein wichtiges Kriterium im Hinblick auf die Anwendung der Monolithe als stationäre Phasen in der Hochleistungsflüssigkeitschromatographie (HPLC) ist hierbei die hierarchische Strukturierung mit definierten Porengrößendomänen im meso- und im makroporösen Bereich. Ein homogenes, bikontinuierliches Makroporennetzwerk ermöglicht die ungehinderte Diffusion der mobilen Phase und gewährleistet zugleich einen hohen Massentransport innerhalb der Trennsäule, während das integrierte, geordnete Mesoporensystem für die Auftrennung der chemischen Komponenten verantwortlich ist. Der Sol-Gel Prozess unter Verwendung von struktur-dirigierenden Agenzien bietet die Möglichkeit Materialien mit integrierten Funktionalitäten durch das individuelle Design der hierarchisch organisierten Porengrößendomänen in Anlehnung an die Natur in wässrigen Lösungen bei geringen Drücken und Temperaturen zu synthetisieren. Durch Einstellen der Syntheseparameter wie die Wahl des struktur-dirigierendes Agens z.B. die Verwendung von unterschiedlich hoch konzentrierten Templatphasen des amphiphilen Block Copolymeres Pluronic P123 oder amphiphiler Polydimethylsiloxan-basierter Tenside wie Tego Glide 440 und LA-S 687, die Konzentration der Säure (Katalysator), die Gelierungs- und Alterungstemperatur, etc. können die individuell erwünschten Morphologien in den verschiedenen Größenbereichen gestaltet werden.

Da in dieser Arbeit diol-modifizierte Silane als Precursoren für die Bildung des Silika-Netzwerks eingesetzt werden, wird zusätzlich der Einfluss der Polarität des freigesetzten Diols auf die Phasenseparation im makroskopischen und im mesoskopischen Bereich und damit auf die resultierenden strukturellen Eigenschaften untersucht.

Für die Anwendung von Silika Materialien als HPLC Säulen ist nicht nur eine definierte Porenarchitektur von Bedeutung, sondern auch maßgeschneiderte Oberflächeneigenschaften, die durch das Einbringen funktioneller, organischer Gruppen eingestellt werden können. So ist zum Beispiel für die Anwendung in der „Reversed Phase“ (RP) HPLC eine hydrophobe Oberfläche der Poren notwendig um eine gute Trennleistung zu erzielen. Die Synthese anorganisch-organischer Hybridmonolithe wird in dieser Arbeit durch zwei verschiedene Ansätze verwirklicht. Im ersten Synthesepfad werden Phenyl- und Methyl-Gruppen durch

Cokondensation des Ethylenglykol-modifizierten Methyl- oder Phenylsilans (MeGMS, PhGMS) mit dem Ethylenglykol-modifizierten Silan (EGMS) direkt in das Silika Netzwerk eingebracht, während das zweite Verfahren eine post-synthetische Funktionalisierung darstellt. Hierbei erfolgt die Einbringung der organischen, funktionellen Gruppen durch Silylierung der Silika Oberfläche mit Chlorotrimethylsilan (TMCS), Chlorododecyldimethylsilane oder durch „end-capping" mit beiden Silylierungsagenzien, wodurch eine hydrophobe Oberfläche unter Erhalt der hierarchischen Porenarchitektur generiert wird.

Das letzte Kapitel dieser Arbeit befasst sich mit der Anwendung ausgewählter Monolithe als stationäre Phasen in der HPLC. Hierfür wurden hierarchisch strukturierte, (Hybrid-) Silika Monolithe sowohl in standardisierten Normal Phasen (NP-) als auch in RP-HPLC Experimenten in den Laboren von Merck KGaA, Darmstadt, untersucht.

List of Abbreviations and Symbols

(1/2)3D	(one / two-) three-dimensional
2D	two-dimensional
3D	three-dimensional
α	selectivity
δ	chemical shift (NMR)
ΔD	shrinkage in diameter / %
Δm	mass loss
ΔL	shrinkage in length / %
γ	surface tension
λ	wave length
μ	dipole moment
ν^1	molar volume
$\tilde{\nu}$	wave number
ρ	density
σ	cross-section area
θ	scattering angle (XRD, SAXS), contact angle
% v/v	volume percent
A	Eddy-diffusion, turbulent diffusion
a	lattice constant
a.u.	arbitrary units
B	longitudinal diffusion
bp	boiling point
BET	Bunauer, Emmett, Teller
BJH	Barrett, Joyner, Halenda
c	concentration / mol l^{-1} or M
C	mass transfer
CP	cross polarization
CPG	Controlled Pore Glass
d_{hkl}	repeating unit
D_{BJH}	diameter calculated according to Barrett, Joyner and Halenda
EDL	electrical double layer
EO	ethylene oxide

FCC	face centred cubic
FSM-16	Folded sheet materials no. 16´
H	height equivalent of a theoretical plate
HCPS	hexagonally close-packed spheres
hkl	Miller indices
HMS	Hexagonal molecular sieves
HPLC	High Performance Liquid Chromatography
IR	infrared
IUPAC	International Union for Pure and Applied Chemistry
k’	retention factor
KIT-16	Korea Advanced Instititute of Science and Technology, no. 6
L	length
(L)LC	(lyotropic) liquid crystalline
M	molar, mol l^{-1}
MAS	magic angle spinning (solid-state NMR)
M41S	mesoporous molecular sieves
MCM-41	Mobile Composition of Matter No.41
MCM-48	Mobile Composition of Matter No.48
MCM-50	Mobile Composition of Matter No.50
MOF	metal organic framework
mol %	mol percent
N	number of theoretical plates
NMR	nuclear magnetic resonance
NP	Normal phase
P	packing parameter
$p_{(c)}$	(critical) pressure
p/p_0	relative pressure
PO	propylene oxide
ppm	pars per million
PZC	point of zero charge
q	scattering vector
R,R^1	alkyl groups
R	resolution
$R^{(m)}$	(micelle) radius
R^{Hg}	pore radius (mercury porosimetry)
RP	Reversed Phase

RPLC	Reversed Phase Liquid Chromatography
RT	room temperature
SAXS	small angle X-ray scattering
SBA-11	Santa Barbara no. 11
SBA-15	Santa Barbara no.15
S^{BET}	specific surface area calculated according to Brunauer, Emmett and Teller
SEC	Size Exclusion Chromatography
SEM	Scanning Electron Microscopy
$t_{age\ /\ g\ /\ PS\ /\ R}$	aging / gelation / phase separation / retention time
$T_{(c\ /\ g\ /\ age)}$	(critical / gelation / aging) temperature
TEM	Transmission Electron Microscopy
TGA	thermogravimetric analysis
TLCT	True Liquid Crystal Templating
T_{USP}	Tailing (according to USP)
t_{wall}	pore wall thickness
u	linear flow velocity
USP	United States Pharmacopeia
V_0	initial adsorbed volume
V^{Hg}	cumulative pore volume (mercury porosimetry)
$W_{0.5}$	full width at half-maximum
wt %	weight percent

Precursor Abbreviations

BDMS	tetrakis(3-hydroxybutyl) orthosilicate, 2,3-butane diol-modified silane
EGMS	tetrakis(2-hydroxyethyl) orthosilicate, ethylene glycol-modified silane
HDMS	tetrakis(2-hydroxyhexyl) orthosilicate 1,2-hexane diol-modified silane
MeGMS	tris(2-hydroxyethoxy)methylsilane ethylene glycol-modified methylsilane
MTMS	trismethoxymethlysilane

PGMS	tetrakis(2-hydroxypropyl) orthosilicate, 1,2-propane diol-modified silane
PhGMS	tris(2-hydroxyethoxy)phenylsilane ethylene glycol-modified phenylsilane
PTMS	trimethoxyphenylsilane
TEOS	tetraethylorthosilicate
TMOS	tetramethylorthosilicate

Chemicals and Structure-Directing Agents

CTAB	cetyltrimethylammonium bromide
DDMCS	chlorododecyldimethylsilane
EtOH	ethanol
F127	Pluronic™ F127 (EO_{97}-PO_{69}-EO_{97})
LAS	LA-S 687
P123	Pluronic™ P123 (EO_{20}-PO_{70}-EO_{20})
PD	1,2-propane diol
PDMS	polydimethylsiloxane
PEG	poly(ethylene glycol)
PEO	poly(ethylene oxide)
T44	Tego Glide 440
TTAB	tetradecyltrimethylammonium bromide
TiP	tetra-iso*p*ropylorthotitanate
TMCS	chlorotrimethylsilane

Polymers

PC	polycarbonate
PE	polyethylene
PEEK	polyaryletheretherketone
PMMA	poly(methyl methacrylate)
PP	polypropylene
PVDF	poly(vinylidene fluoride)

Table of Contents

LIST OF ABBREVIATIONS AND SYMBOLS III

TABLE OF CONTENTS VII

LIST OF TABLES X

LIST OF FIGURES XIII

CHAPTER 1
INTRODUCTION 1

1.1. MOTIVATION 1
1.2. POROUS MATERIALS 3
1.3. SOL-GEL CHEMISTRY 9
1.3.1. Precursors 13
1.3.2. Introduction of the Mesoporous System 15
1.3.2.1. Exotemplating 15
1.3.2.2. Endotemplating 15
1.3.3. Design of the Macroporous System 21
1.3.4. Surface Modification 23
1.3.4.1. Post-Synthetic Grafting 24
1.3.4.2. Direct Functionalization (Co-condensation) 25
1.3.5. Requirements for HPLC 26

CHAPTER 2
HIERARCHICALLY ORGANIZED SILICA (HYBRID-)MONOLITHS BY EMPLOYING ETHYLENE GLYCOL-MODIFIED PRECURSORS 29

2.1. PURELY INORGANIC SILICA MONOLITHS 29
2.1.1. Motivation 29
2.1.2. Synthesis of the Gels 31
2.1.3. Influence of the HCl Concentration 34
2.1.3.1. Influence on the different pore size regimes 37
2.1.4. Composition of the Template Phase and the Si-Content 43
2.1.5. The Acid Anion 54
2.1.6. Gelation / Aging Temperature and Time 58
2.2. INORGANIC-ORGANIC HYBRID SILICA MONOLITHS 64

2.2.1. In-situ Modification by Co-condensation *64*
2.2.1.1. Synthesis of the Inorganic-Organic Hybrid Silica Gels 64
2.2.1.2. Inorganic-Organic Hybrid Silica Monoliths 66
2.2.2. Surface modification by post-synthetic grafting *78*
2.3. CONTAINER MATERIAL 83
2.4. CONCLUSION 87

CHAPTER 3
NEW DIOL-MODIFIED SILANES AS PRECURSORS FOR THE SOL-GEL PROCESS 90

3.1. MOTIVATION 90
3.2. SYNTHESIS AND CHARACTERIZATION OF THE PRECURSORS 91
3.3. INFLUENCE OF THE RELEASED DIOL ON THE HIERARCHY 94
3.4. CONCLUSION 105

CHAPTER 4
COMPARISON OF TEOS, SILICIC ACID AND SODIUM SILICATE TO EGMS 106

4.1. MOTIVATION 106
4.2. SYNTHESIS OF THE GELS 107
4.3. INFLUENCE OF THE TYPE OF PRECURSOR 108
4.3.1. TEOS as Sole Precursor in Comparison to EGMS *108*
4.3.2. Silicic Acid and Sodium Silicate as Precursors *113*
4.4. CONCLUSION 119

CHAPTER 5
PDMS-BASED BLOCK CO-POLYMERS AS STRUCTURE-DIRECTING AGENTS IN THE SYNTHESIS OF HIERARCHICALLY ORGANIZED SILICA MONOLITHS 120

5.1. INTRODUCTION 120
5.2. SYNTHESIS OF THE GELS 122
5.3. RESULTS AND DISCUSSION 123
5.3.1. Critical Micelle Concentration *123*
5.3.2. Hierarchical Silica Gels *125*
5.3.3. Silica Gels with a Tailored Surface *133*
5.4. CONCLUSION 137

CHAPTER 6
APPLICATION OF HIERARCHICALLY ORGANIZED SILICA MONOLITHS AS HPLC COLUMNS 138

6.1. MOTIVATION 138
6.2. APPLICATION AS HPLC COLUMNS 139
6.2.1. EGMS-derived Silica Monoliths 142
6.2.2. MeGMS / EGMS-derived Hybrid Silica Monoliths 152
6.3. CONCLUSION 158

CHAPTER 7
EXPERIMENTAL 160

7.1. ANALYTICAL METHODS 160
7.1.1. Nitrogen Sorption 160
7.1.2. Mercury Porosimetry 166
7.1.3. Small Angle X-ray Scattering (SAXS) 167
7.1.4. Electron Microscopy 170
7.1.4.1. Scanning Electron Microscopy (SEM) 170
7.1.4.2. Transmission Electron Microscopy (TEM) 170
7.1.5. Nuclear Magnetic Resonance Spectroscopy (NMR) 171
7.1.6. Thermogravimetric Analysis (TGA) 171
7.2. SAMPLE PREPARATION 172
7.2.1. Materials 172
7.2.2. Synthesis of the Precursors 173
7.2.3. Preparation of the Monoliths 175
7.2.3.1. Preparation of Pure Silica Monoliths with Pluronic P123 175
7.2.3.2. Synthesis of Inorganic-Organic Hybrid Monoliths by Employing Pluronic P123 183
7.2.3.3. Synthesis of Silica Monoliths by Employing New Diol-Modified Silanes 191
7.2.3.4. Comparison of TEOS, Silicic Acid and Sodium Silicate to EGMS 193
7.2.3.5. PDMS-based Co-Polymers as Structure Directing Agents 198

CHAPTER 8
CONCLUSION 202

REFERENCES 207

List of Tables

Table 1 The different denotations of the pore classes with respective pore diameter and examples. 3

Table 2 Denotations of relevant mesoporous systems 6

Table 3 Listing of the investigations and their varied parameters 33

Table 4 Physicochemical data of the silica gels prepared from different HCl concentrations 37

Table 5 Physicochemical characteristics of the silica gels prepared with varied composition 44

Table 6 Physicochemical characteristics of the silica gels prepared with varied Si content 52

Table 7 pKa-values of the acids and the observed times for the gelation and the phase separation 54

Table 8 Physicochemical data of the silica gels prepared with different acid 55

Table 9 Physicochemical properties of the samples gelled and aged for 3 and 7 d at different temperatures 60

Table 10 Physicochemical data of the inorganic-methyl hybrid silica gels prepared with a varied content of MeGMS 67

Table 11 Physicochemical properties of phenyl-modified hybrid silica gels prepared with varying contents of PhGMS 72

Table 12 Physicochemical properties of the different silylated silica monoliths 79

Table 13 Physicochemical properties of the different silylated hybrid silica gels 80

Table 14 Determined shrinkage in length (L) and in diameter (D) of the silylated monoliths 82

Table 15 Physicochemical data of the silica monoliths gelled and aged in different container materials. 84

Table 16 Physicochemical data of the hybrid monoliths gelled and aged in different container materials 85

Table 17 Classification of the Bragg reflections of the various phase types 96

Table 18 Gelation times of the silica monoliths prepared from the diol-modified silanes 99

Table 19 Physicochemical data of the silica monoliths prepared with PGMS 101

Table 20 Physicochemical data obtained for the silica gels prepared with BDMS 101

Table 21 Physicochemical data for the TEOS-derived silica monoliths 109

Table 22 Physicochemical data of the silica gels synthesized from silicic acid by employing P123 / 1 – 0 M HCl = 30 / 70 wt %. 114

Table 23 Physicochemical data of the silica gels synthesized from silicic acid by employing P123 / 1 – 0 M HCl = 40 / 60 wt %. 115

Table 24 Physicochemical data of the silica gels synthesized from basic sodium silicate solution 115

Table 25 Data of the different silica monoliths prepared with LA-S 687 in different HCl concentrations. 127

Table 26 Data of silica monoliths prepared with Tego Glide 440 at different HCl concentrations 129

Table 27 Testing parameters of the applied HPLC tests 140

Table 28 Chromatographic data obtained from Normal Phase (NP) Si standard tests at RT. 143

Table 29 Chromatographic data obtained from Reversed Phase (RP) tests at RT. 143

Table 30 Listing of the RP separation experiments performed on the P1-1e column 150

Table 31 Chromatographic data obtained from Normal Phase (NP) Si standard tests for the hybrid methyl-modified silica monoliths 152

Table 32 Chromatographic data obtained from Reversed Phase (RP) standard tests for the hybrid methyl-modified silica monoliths 153

Table 33 Chromatographic data obtained from the re-testing 157

Table 34 Selected samples of possible structures including the corresponding equations 169

Table 35 Listing of the different synthesized diol-modified silanes. 173

Table 36 Listing of the data from ^{1}H- and spin-lock ^{29}Si-NMR of the diol-modified silanes 174

Table 37 Applied weight portions of the template phase P123 / 1 – 10^{-6} M HCl = 30 / 70 177

Table 38 Time intervals for the sol-gel transition (t_g) and the phase separation (t_{PS}) 177

Table 39 Shrinkage in diameter and the length of the silica monoliths. 178

Table 40 Composition, c(HCl), aging temperature, and the obtained average shrinkage 179

Table 41 Physicochemical data of the silica gels of the template variation in the HCl concentration range from 10^{-2} to 10^{-4} M. 180

Table 42 Composition, aging temperature T, gelation times, and the times for the phase separation ... 180

Table 43 Composition, time intervals for the gelation and phase separation of the silica gels gelled and aged at different temperatures T. 181

Table 44 Physicochemical properties of the silica gels gelled and aged in the range of 40 – 90°C 182

Table 45 Molar composition and weight portions of MeGMS and EGMS for the synthesis of the methyl-modified hybrid monoliths prepared at c(HCl) = 0.03 M 184

Table 46 Molar composition and weight portions of PhGMS and EGMS for the synthesis of the phenyl-modified hybrid monoliths prepared at c(HCl) = 0.03 M 185

Table 47 Physicochemical properties of the methyl-modified hybrid silica monoliths 185

Table 48 Physicochemical properties of the phenyl-modified hybrid silica monoliths 186

Table 49 Molar composition and weight portions of MeGMS and EGMS 187

Table 50 Molar composition and weight portions of PhGMS and EGMS 187

Table 51 Physicochemical properties of the supercritically dried methyl-modified hybrid silica gels ... 188

Table 52 Physicochemical properties of the supercritically dried phenyl-modified hybrid silica gels.... 188

Table 53 Acid concentration and content of MeGMS for the gel synthesis and the modification..... 189

Table 54 Material and dimensions of the container applied for the investigations 190

Table 55 HCl concentration, type, and Si-content of precursor applied for the synthesis of the silica samples 192

Table 56 Physicochemical properties of the silica monoliths prepared with EGMS (8.4 wt %) and HDMS (4.5 wt %) 193

Table 57 Composition, gelation and aging times of the TEOS-derived silica gels synthesized with c(HCl) = 1 M at 40°C. 194

Table 58 Composition, gelation and aging times of the TEOS-derived silica gels synthesized with c(HCl) = 10^{-1} M at 40°C. 194

Table 59 Composition, gelation and aging times of the TEOS-derived silica gels synthesized with c(HCl) = 10^{-2} and 10^{-3} M at 40°C. 195

Table 60 Physicochemical properties of the silica monoliths prepared with TEOS (8.4 wt %) 195

Table 61 Weight portions of template phase and silicic acid 196

Table 62 Composition, HCl concentration, times for gelation, phase separation and aging of the silicic acid –derived sol-gel systems 196

Table 63 Weight portions of template phase and sodium silicate 197

Table 64 Composition, HCl concentration, time periods for gelation, phase separation, and aging sodium silicate-derived sol-gel systems 197

Table 65 Weight portions of EGMS determined for the particular Si-content for the composition Si / surfactant / x M HCl = 8.4 / 30 / 70 199

Table 66 Weight portions of EGMS determined for the particular Si-content for the composition Si / surfactant / x M HCl = 8.4 / 10 / 90 200

Table 67 Weight portions of EGMS determined for the particular Si-content for the composition Si / surfactant / x M HCl = 8.4 / 20 / 80 200

Table 68 Physicochemical properties of the silica gels synthesized with Tego Glide 440 and LA-S 687200

List of Figures

Figure 1 Schematic topologies of the most prominent mesoporous systems 5

Figure 2 Schematic drawing of the EDL 10

Figure 3 Schematic drawing of interparticulate condensation reactions 11

Figure 4 Schematic drawing of some employable diol / polyol-modified silanes 14

Figure 5 Interactions between the inorganic precursor species with the head group 17

Figure 6 Phase diagram of Pluronic® P123 in aqueous solution 19

Figure 7 Schematic depiction of the TLCT mechanism 19

Figure 8 Schematic depiction of the co-operative mechanism 20

Figure 9 Phase separation and domain formation 23

Figure 10 Schematic drawing of the post-synthetic modification 24

Figure 11 Schematic drawing of the *in-situ* modification 25

Figure 12 Reaction scheme of the EGMS synthesis 31

Figure 13 Schematic depiction of the silica gel synthesis 32

Figure 14 Time intervals of the sol-gel transition (t_g) and the phase separation (t_{PS}) 34

Figure 15 Diagram representing the percentage of shrinkage 36

Figure 16 SAXS pattern of the dried silica monoliths prepared at different HCl concentrations 38

Figure 17 SEM images of the silica gels prepared with different HCl concentration 39

Figure 18 Evolution of the macroporous morphology of the silica gels 40

Figure 19 Macropore radii distribution of the silica gels prepared at varying HCl concentrations 42

Figure 20 Diagrams illustrating the shrinkage in length and diameter at varying template compositions 45

Figure 21 SAXS pattern of the resulting mesostructure of the silica monoliths prepared with different template compositions at 1 M HCl 46

Figure 22 SEM images presenting the macroporous morphology of the silica monoliths prepared with varied template composition at 1 M HCl 47

Figure 23 Macropore radii distribution of the silica gels derived from varied template composition at 1 M HCl 48

Figure 24 SAXS pattern illustrating the evolution of the mesoscopic ordering for a varied template composition at 10^{-1} M HCl 49

Figure 25 SEM images presenting the evolution of the macroporous morphology with varying template composition at 10^{-1} M HCl. 50

Figure 26 Macropore radii distribution of the silica gels prepared with varying composition of the template phase 50

Figure 27 Photo of the resultant silica monoliths prepared with different Si contents 51

Figure 28 SAXS pattern of the development of the periodical with decreasing Si-content 52

Figure 29 SEM pictures presenting the decreasing distinctive macroporous morphology 53

Figure 30 SAXS pattern for the mesoscopic ordering of the silica gels prepared with the different acids 56

Figure 31 Macropore radii distribution of the silica gels synthesized from different acids 57

Figure 32 SEM images of the hierarchically organized silica monoliths prepared with the different acids 58

Figure 33 Diagram presenting the gelation times and the onset of phase separation as function of the temperature 60

Figure 34 SAXS curves of the evolution of the mesoscopic ordering with increasing gelation and aging temperature 61

Figure 35 SEM pictures presenting the change of the macroporous morphology after aging for 3 d at different temperatures 62

Figure 36 SEM images presenting the macroporous morphology of the silica monoliths aged for 1 – 7 d at 40°C 63

Figure 37 Reaction scheme of the synthesis of the tris(2-hydroxyethyl)organosilane 65

Figure 38 SAXS pattern of the evolution of the mesoscopic ordering with increasing content of MeGMS 68

Figure 39 TEM images of the two selected hybrid silica gels 69

Figure 40 SEM images of the hybrid methyl-silica gels prepared with varied contents of MeGMS 70

Figure 41 Relationship between the composition of the sol and the resulting macroporous morphologies 71

Figure 42 SAXS pattern of the evolution of the mesoscopic ordering with varying PhGMS content 73

Figure 43 TEM images of the hybrid silica gels synthesized with 10 and 15 mol % PhGMS 73

Figure 44 SEM images of the macroporous framework of hybrid silica gels with PhGMS 74

Figure 45 Macropore radii distribution of the phenyl-modified hybrid silica gels 75

Figure 46 TG diagram of the mass loss of the different methyl-modified silica monoliths 76

Figure 47 Coupled IR-spectra of the released alkyl fragments 77

Figure 48 Schematic depiction of the surface modification reactions via the end-capping approach 78

Figure 49 SAXS pattern of the silylated silica gels prepared with 100% EGMS 81

Figure 50 SAXS pattern of the silylated hybrid silica gels 81

Figure 51 Photographs of the different modified monoliths and their wetting behaviour 83

Figure 52 SEM images of the resulting macroporous morphologies in the boundary region of the SiO_2 monoliths 86

Figure 53 SEM images of the resulting macroporous morphologies in the boundary region of the hybrid silica monoliths 87

Figure 54 Hierarchically organized silica monolith 88

Figure 55 Schematic depiction of the synthesis and the equilibrium reactions of the different diol-modified silanes. 92

Figure 56 Thermogravimetric diagram of the thermo-oxidative decomposition 93

Figure 57 SAXS diagrams showing the influence of each diol on the lyotropic liquid crystalline phase . 95

Figure 58 Correlation between the lattice constant a in dependency of the type and the content of the varied diols 98

Figure 59 Diagram of the gelation times for the different diol modified silanes at room temperature 99

Figure 60 Direct comparison of the SAXS pattern of silica gels 102

Figure 61 SEM and TEM images of the silica gels prepared with the different diol-modified silanes 104

Figure 62 Comparison of the gel times at 40°C for the EGMS- and the TEOS-derived silica gels 110

Figure 63 Photographs of the obtained silica monoliths prepared from TEOS 112

Figure 64 Photographs of the silica monoliths synthesized from EGMS 112

Figure 65 SAXS pattern of the TEOS-derived silica gels 113

Figure 66 SEM image of the co-continuous macroporous framework of the silica gel prepared from silicic acid 116

Figure 67 SAXS patterns indicating the mesoscopic ordering of the silica gels prepared with silicic acid 117

Figure 68 SAXS pattern of the silica gels derived from sodium silicate 118

Figure 69 TEM image presenting the mesoporous system of the silica gel derived from sodium silicate 118

Figure 70 Scheme of the linear PEO-PDMS-PEO polymer of the Tegopren 5 Series. 122

Figure 71 Pattern of the reduction of the surface tension for Tego Glide 440 (T44) and LA-S 687 (LAS). 125

Figure 72 Silica monolith made with LA-S 687 in purely aqueous media exhibiting pores of different size domains 126

Figure 73 Investigations of the mesopore systems. 127

Figure 74 SEM images of silica gels prepared with LA-S 687 in dilute HCl 129

Figure 75 Silica monolith prepared with Tego Glide 440 in H_2O 130

Figure 76 Structural investigations of the mesopore systems of the silica monoliths prepared with Tego Glide 440 131

Figure 77 SEM images of silica gels prepared with Tego Glide 440 at different HCl concentrations.... 132

Figure 78 Silica monoliths supercritically dried with CO_2 and subsequently heated to 400 or 600°C... 135

Figure 79 TGA curves presenting the thermal decomposition of the surfactant Tego Glide 440 within the pore systems of the silica gels 136

Figure 80 Chromatograms of the separation of toluene, nitrobenzene, and 2-nitroanisole with *n*-heptane / dioxane (95 / 5% v/v) by the different silica columns derived from EGMS 145

Figure 81 Chromatogram obtained by applying Chromolith™ Performance Si 146

Figure 82 Pore size distributions of the macropores (left) and the mesopores (right) of P1-1e..... 146

Figure 83 Van Deemter curves for the silica column prepared at 1 M HCl of nitrobenzene and 2-nitroanisole at RT. 147

Figure 84 Chromatograms of the separation of thiourea, biphenyl-2-ol, progesterone, 1-phenyl-1-hexanone, and anthracene for the different silica columns derived from EGMS 148

Figure 85 Van Deemter curves of the RP-system for the EGMS-derived silica column 149

Figure 86 Chromatograms of the investigations of the selectivity of P1-1e 151

Figure 87 Chromatograms of the separation of toluene, nitrobenzene, and 2-nitroanisole of the different hybrid methyl-modified silica columns 154

Figure 88 Van Deemter curves for the hybrid silica column prepared with 5 mol % MeGMS 155

Figure 89 Chromatograms of the separation experiments of thiourea, biphenyl-2-ol, progesterone, 1-phenyl-1-hexanone, and anthracene for the different methyl-modified hybrid silica columns156

Figure 90 Chromatograms of the re-testing 158

Figure 91 Classification of the different isotherms according to IUPAC 161

Figure 92 Classification of the different hysteresis loops 162

Figure 93 Schematic drawing of Bragg's Law 168

Figure 94 Schematic depiction of the surface hydrophobization via silylation 176

Chapter 1

Introduction

1.1. Motivation

Mesoporous materials have attracted a lot of interest as they meet the requirements for a wide field of applications such as sorption materials, support materials *e.g.* for heterogeneous catalysis, chemical sensors or for optical applications and chromatography. However, in some cases, such as chromatography, the separation of macromolecules and the release of pharmaceutical components, a sole mesoporous system is not effective enough. Therefore, an additional porosity on a greater length scale has to be introduced, like an interconnected macroporous framework, to allow for a high diffusion rate of solvent and to guarantee a high mass transport. Hierarchically organized materials combine the advantages of the different pore regimes with high surface areas resulting from meso- and / or microporosity and a high solvent flow through a bicontinuous macroporous network.

Today high-performance liquid chromatography (HPLC) is one of the mostly applied analysis methods for mixtures of compounds, the detection of impurities in drugs and pollutants or additives in food. Most of the employed HPLC columns are packed with 3 – 5 μm porous silica microparticles, which determine the separation performance by the quality of packing,

the size of the particles and their size distribution.[1-4] In consequence to the particulate character of these columns with no uniform diffusion pathways, the limiting factor of the separation time and performance is the high back pressure of the eluent. To reduce the back pressure and thus to improve the separation performance, the idea was developed of creating hierarchically organized silica or with respect to Reversed Phase liquid chromatography (RPLC) inorganic-organic hybrid silica monoliths, in which the formation of the interconnected macroporous and the mesoporous regimes ought to be controlled independently.

The ability to design hierarchically organized materials across varying length scales ranging from Ångstrøms up to micrometers is a key issue in the synthesis of materials with integrated advanced functionalities. Promising approaches towards these materials are soft-chemistry based techniques, which try to mimic biological processes in order to tailor the nanostructure of the resulting materials.[5, 6] Like in nature, the syntheses are performed in aqueous solutions at low temperatures and pressure favouring kinetically controlled products. As these systems are exceptionally sensitive towards slight changes of the reaction parameters *e.g.* pH-value, temperature, concentrations, polarity of the solvent, etc., inducing fundamental variances in the supramolecular assemblies, the resulting morphologies can be adjusted by fine tuning these parameters.

Besides the reaction parameters, the material of the vessel is a prominent factor for the evolution of a homogeneous macroporous morphology in the boundary region of the monolith surface. The intensity of interactions such as adhesion forces between gel surface and container deeply influences the surface region of the gel leading to a densification of the macroporous framework near the surface, which hinders the flow of the mobile phase. Thus, the chemical and physical properties of the container material play an important role in the synthesis of HPLC columns.

The long-term ambition for the synthesis of monolithic HPLC columns is the direct synthesis within the HPLC mould itself to reduce unnecessary synthesis steps. However, one critical issue is the shrinkage of the gel body during aging and drying due to evaporation of solvent and the formation of a concave interface inside the mesopores, that can cause the collapse of the monolithic shape.

1.2. Porous Materials

Today a great variety of different porous materials ranging from purely inorganic materials such as zeolites to inorganic-organic hybrid systems like organically modified silica phases, to purely organic materials like polymer foams or metal-organic frameworks (MOFs) is known. For the differentiation of porous materials, the International Union of Pure and Applied Chemistry (IUPAC) (table 1) established a classification with respect to the different pore size regimes.

Table 1 The different denotations of the pore classes with respective pore diameter and examples.

denotation	*pore diameter*	*examples*
microporous	< 2 nm	zeolites, MOF
mesoporous	2 ≤ d ≤ 50 nm	M41S phases, aerogels
macroporous	> 50 nm	porous glasses, foams

Microporous Materials. Besides metal-organic frameworks (MOF) the most prominent representatives for microporous materials are zeolites. Even though zeolites on the basis of aluminiumsilicates were discovered in the middle of the 18th century, their industrial applications as catalytic materials for the cracking of petrochemical products only started in the early 1960s.[7, 8] Until the 1970s only few amounts of zeolites were synthesized with the main focus on Zeolite Y for the petrochemical application. Only when the eutrophication of lakes and rivers became a severe problem in the 1980s caused by phosphoric compounds like pentasodium phospate used as ion exchangers in detergents, zeolites *e.g.* hydrated Zeolite A became an attractive candidate as anti-pollution water softener in detergents. Per definition zeolites are microporous crystalline oxides, typically composed of silicon, aluminium and oxygen, with cavities that are accessible by smaller windows and which cages are interconnected by either 1D-, 2D- or 3D-terminal channel systems (arrangement along one, two or three cartesian axes).[9, 10] This cage structure for example in Zeolite A allows for the capturing of calcium ions in the cage cavity in exchange of sodium ions as the affinity of the Ca^{2+} towards the anionic aluminiumsilicate framework is greater than for the Na^{+}. Today the assumption that zeolites consist exclusively of aluminiumsilicates is no longer valid. In 1978

the first aluminium-free zeolite, Silicalite, was synthesized, which does not exhibit an ion exchanging ability. And in 1982 a silicon-free zeolite was created consisting only of aluminiumphosphate, which exhibited also an electrostatically neutral framework. Even though all these zeolites possess a periodically arranged microporous network with a narrow pore size distribution and high specific surface areas, the limiting factor for the range of applications is the small pore size. As mentioned above the windows, which are the access to the cages are normally smaller than the cage itself, therefore the diffusion rate is dominated by the window diameter and is drastically limited for greater ions or molecules. For example in order to adsorb water molecules, the molecular sieve must have pores of a specific and ideally uniform size, as for the incorporation of a single H_2O molecule the windows and the cage have to exceed 0.25 nm.

Thus, to meet the requirements of separation and catalysis applications, new porous materials with narrow pore size distributions and pore sizes larger than 1 nm had to be discovered. When in 1988 the group of Davis et al. succeeded in the synthesis of a crystalline microporous aluminiumphosphate zeolite with uniform micropores larger than 2 nm, the kick-off was on for the development of new well-ordered materials with uniform mesopores.[11, 12]

Mesoporous Materials. For mesoporous materials, two different kinds of materials have to be distinguished. First the materials with a statistical arrangement of mesopores and second the materials with a periodical arrangement of the mesopores. The most prominent examples for the primary type are aerogels. Aerogels exhibit cylindrical, branched mesopores, which are well-accessible and generate a high specific surface area, however, the pores are randomly arranged.[13] In addition, most aerogels show a broad pore size distribution, as in general the synthesis of these kind of materials is conducted without the employment of structure-directing agents and the resulting pore sizes strongly depend on reaction conditions such as temperature, solvent, aging conditions, etc. Due to the fragility of the gel framework, the drying process is a crucial step to prevent the collapse of the porous architecture. Therefore different drying techniques were introduced such as the supercritical drying with CO_2, which eliminates the formation of a gas-liquid interface within the pore channels, or by modification of the inner pore surface *e.g.* by grafting with chlorotrimethylsilane, in order to reduce the contact angle between the meniscus and the pore walls and hence the capillary forces.[14]

The lack of uniformity of the pore sizes and the random arrangement of the pores in combination with the fragility of gel framework limits the applicability of aerogels for separation and catalysis applications.

In the early 1990s the groups of Yanagisawa et al. and Kresge et al. presented independently from each other the synthesis of periodically organized mesoporous materials via two different approaches.[15-17] The group of Mobile Oil Corporation succeeded in the synthesis of mesostructured M41S silica phases, the so-called Mobile Composition of Matter (MCM) materials, by a templating pathway analogous to the synthesis of zeolites, where supramolecular aggregates of surfactants were employed as structure-directing agents. Today several MCM materials are known, however, the most prominent materials are the 2D hexagonally arranged MCM-41 with a symmetry of P_{6m} and the MCM-48 with a cubic arranged mesoporous system of the symmetry I_{a3d}.

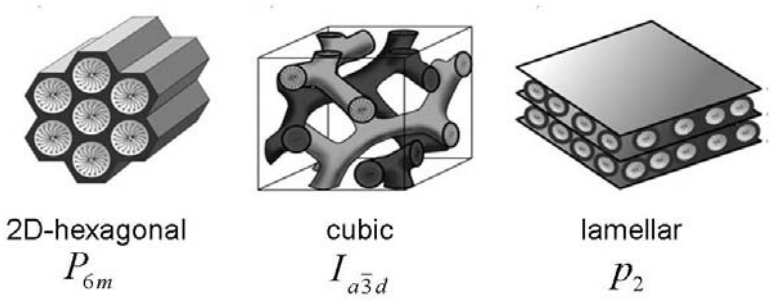

Figure 1 Schematic topologies of the most prominent mesoporous systems including the corresponding space group.[18] From left to right: The 2D-hexagonal array is found in MCM-41, the cubic arrangement corresponds to MCM-48 and the lamellar structure to MCM-50.

Yanagisawa and his co-workers chose another approach to create the mesostructured network. Starting with a single layered polysilicate kanemite, that was allowed to swell with the ionic surfactant alkyltrimethylammonium chloride, surfactant-kanemite complexes were formed in which the SiO_2 layers were condensed to form the silica network. Today many different mesostructured silica materials have been synthesized under various conditions as listed in table 2.

As these materials combine a periodically arranged mesopore system and uniform pore sizes in the theoretical range of 2 – 50 nm, a wider field of applications has been accessible than for zeolites as bigger molecules can be adsorbed within the mesoporous channels.

Table 2 Denotations of relevant mesoporous systems including their structures, abbreviations, and synthesis conditions.

denotation	*pore system /symmetry*	*synthesis conditions*
MCM-41 (Mobil composition of matter no. 41)	2D hexagonal / P_{6m}	basic conditions, cationic template
MCM-48 (Mobil composition of matter no. 48)	cubic / I_{a3d}	basic conditions, cationic template
MCM-50[19, 20] (Mobil composition of matter no. 50)	lamellar	basic conditions, cationic template
FSM-16 (folded sheet materials no. 16)	2D hexagonal	from kanemite, cationic surfactant
HMS (hexagonal molecular sieves)	Wormhole-like organization	acidic conditions, neutral amine templates
SBA-11 (Santa Barbara no. 11)	Cubic / $P_{m\bar{3}m}$	acidic conditions, neutral block co-polymer
SBA-15[21] (Santa Barbara no. 15)	2D hexagonal / P_{6m}	acidic conditions, neutral block co-polymer
KIT-6[22, 23] (Korea Advanced Instititute of Science and Technology, no. 6)	Cubic / I_{a3d}	acidic conditions, neutral block co-polymer, butanol

Macroporous Materials. Polymer foams with either isolated macropores or an interconnected macroporous network are among the most prominent representatives for macroporous materials. The introduction of the macropores into the polymer is usually conducted via physical or chemical blowing techniques by dissolving for example a gas or a volatile liquid in the polymer melt for the production of a thermoplastic foam (physical blowing) or by a chemical reaction releasing the gas during the foaming process (chemical blowing). The release of the blowing agent can be achieved via two different techniques. First by addition of an appropriate additive or second by a chemical reaction, *e.g.* as for the production of polyurethane foam by a side reaction of the polymerization reaction itself.[24] Among the class of inorganic macroporous materials, porous glasses such as CPG (controlled pore glass) have attracted some attention as chromatographic devices for bioseparation as the material consists

of a continuous phase of ordered macropores with a narrow pore size distribution. Further advantages of the glass bed are the inertness of glass towards bioactive systems and the fact that it can be sterilized without damage to the morphology. Haller et al. have developed CPGs with pore sizes ranging from 7 to 300 nm in diameter. [25-28]

Other macroporous silica materials have also been investigated as they are interesting for separation applications, biocatalysis and as membranes according to the high mass transfer they allow for.

The synthesis of macroporous, ordered materials has been extensively studied during the last decades. One of the most often applied approaches is the templation of close-packed colloidal crystals, which can be infiltrated by liquid or gas-phase precursors to enclose and freeze the structure of the template. After the formation of the silica network is completed, the templates can be removed by either chemical etching, thermal treatment or solvent exchange and an inverse silica matrix of the template is obtained. These structures are also known as inverse opals.[29]

However, one major problem of the purely macroporous network are the low specific surface areas and therefore a low loading of functional groups on the surface. To enhance the specific surface area, new approaches towards macroporous silica have been developed. For the enhancement of the specific surface area of macroporous particles, Galarneau and co-workers have suggested a pseudomorphic transformation, which is only conducted at the surface of the pores, while the macropores and the particle size is preserved. This approach generates silica materials with a high mechanical stability and a high loading of potential substitution sites for functional organic moieties on the surface.[30]

For the preparation of macroporous silica monoliths, Brook and Brennan have proposed a sol-gel process where allyl- and silyl-modified poly(ethylene glycol) (PEG) polymers are employed to promote the particle aggregation process in order to obtain the macroporous framework.[31]

Macroporous materials possess highly penetrable networks for larger molecules, such as biopolymers, however, low specific surface areas and the high throughput that limits the performance of a separation, make them no ideal candidates for HPLC columns.

Hierarchically Organized Materials. The combination of either microporous and macroporous, mesoporous and macroporous or microporous and mesoporous systems should provide the necessary amount of active sites combined with a high diffusion rate for separation

and catalysis applications. Examples from nature like sponges and diatoms show the advantages of hierarchically organized porous materials, as the interconnected framework consisting of large pores allows for a high solvent diffusion rate and thus ensures the mass transfer, while within the smaller pores the intrinsic functions, such as the adsorption of molecules are conducted. To mimic these natural materials in the laboratory, different approaches towards hierarchically organized materials have been developed. One method is to generate the macroporous network by the macrotemplating approach. Here the materials are obtained by either hard templates, such as polystyrene particles, which can be eliminated after the formation of macroporous network by leaching, or by micro-moulding techniques in which emulsion droplets or bacterial threads determine the final pattern of the macropores.[32-37] Another approach to introduce a bicontinuous macroporous network is by polymerization-induced phase separation. Here the resulting macroporous morphology is frozen by the sol-gel transition. One of the most prominent sol-gel procedures to introduce macroporous heterogeneity to form the macroporous architecture was presented by Nakanishi and co-workers in 1992.[38, 39] By employing a silicon alkoxide precursor in combination with a polar additive, such as poly(ethylene oxide) (PEO) or an amphiphilic surfactant under acidic conditions, the phase separation is induced by the polymerization of the siliceous species via spinodal decomposition, which occurs in the unstable region of the miscibility gap. The generated co-continuous structure is frozen in by the sol-gel transition and the resulting morphology is strongly dependent on the onset of the phase separation relative to the gelation point. Today the group of Nakanishi succeeds in creating silica materials with macropores ranging from 100 nm up to 30 μm.[40] However, in order to create hierarchically organized materials, the macrotemplating as well as the polymerization-induced phase separation approaches have to employ a second step to introduce the mesoporous system. Thus, the supramolecular templating approach was adopted from the synthesis of mesoporous materials. As structure-directing agents either ionic surfactants such as cetyltrimethylammonium bromide (CTAB)[41] and tetradecyltrimethylammonium bromide (TTAB)[42] or amphiphilic surfactants like Pluronic P123[40, 43-45],[46-50] and F127[51-54] are used to determine the arrangement and the size of the resulting mesopores.

1.3. Sol-Gel Chemistry

For the manufacturing of purely inorganic metal oxide, inorganic-organic hybrid materials, as well as organic polymer materials, the sol-gel process has become one of the mostly applied methods. Depending on the processing various materials, such as fibres, powders, films and monoliths can be obtained under mild synthesis conditions (moderate temperature, low pressures).

During the last decades, one major interest was on the adaption of coatings for different applications. For example, porous silica coatings are used today as antireflection coatings for solar collectors or for eyeglasses that have an additional anti-scratch coating beneath the antireflection coating made of a hybrid polymer. These applications are based on the work of Geffcken and Berger, who presented the preparation of thin oxidic films by employing alkoxides for the first time.[55-58]

The sol-gel process can be divided into two separate synthesis steps:

1. preparation of the sol
2. reaction to the gel

The sol is a colloidal solution with finely dispersed particles in the range of 1 to 100 nm.[59] Compared to the solvent phase, there is only a small amount of the dispersed phase present and therefore long-range forces, such as gravitation are negligible, while short-range forces such as surface charges and van-der-Waals interactions dominate the colloidal system. According to the Stern model, electrostatic forces are responsible for the stabilization of the sol. The adsorption of charged OH^- or H^+ (depending on the pH) on the surface leads to the formation of a electrical double layer (EDL) at the liquid-solid interphase. The consequence of the formation of the EDL is a repulsive interaction with other colloidal particles and therefore inhibits the aggregation to greater particles which would lead to the destabilization of the sol.[60] (Figure 2)

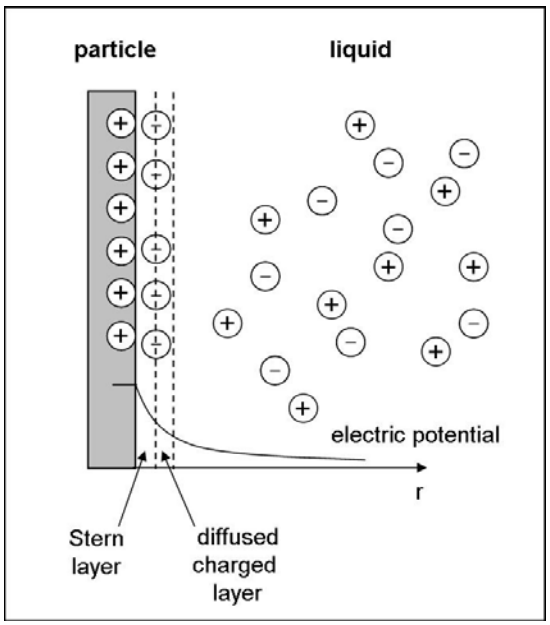

Figure 2 Schematic drawing of the EDL of a positively charged particle surface according to Stern. Attached to the particle surface is the Stern layer which electric potential decreases linearly. The electric potential of the diffused charged layer exponentially decreases towards 0.

The formation of the sol is based on hydrolysis and condensation reactions of the precursors, the starting compounds. There are various types of precursors for the sol-gel process, however, the most commonly applied molecules are metal alkoxides of the type $M^{n+}(OR)_n$ such as tetraethylorthosilicate (TEOS) and tetramethylorthosilicate (TMOS) for silica materials and tetra-isopropyl orthotitanate (TiP) for titania networks. (Scheme 1)

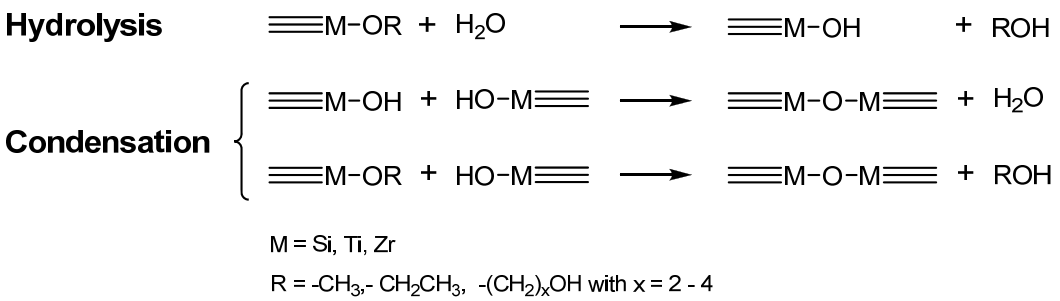

Scheme 1 Reaction scheme showing the hydrolysis and condensation reactions of metal alkoxides during sol-gel processing.

Due to destabilization of the sol by the hydrolysis and condensation reaction or/and by changes in temperature, pH, composition of the liquid phase, the particles in the solution start to grow and to aggregate leading to the formation of a solid network. The gel point is

characterized by an abrupt increase in viscosity, resulting in a "solid" which reacts elastically under minor mechanical stress.

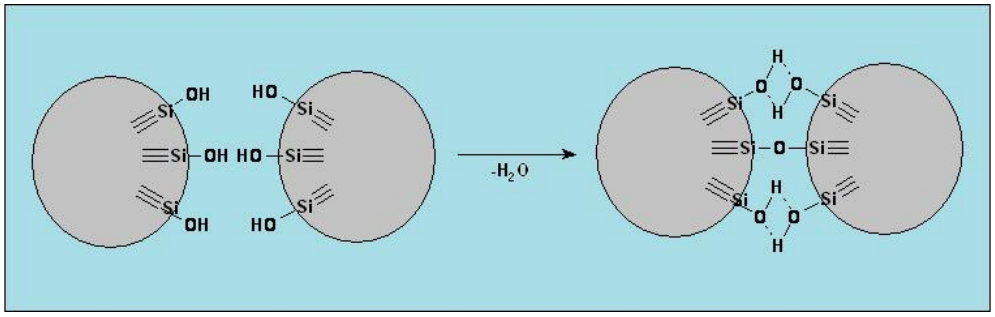

Figure 3 Schematic drawing of interparticulate condensation reactions.[60]

There are different theories to explain the mechanisms of the gelation process. The classical theory developed by Flory and Stockmayer mainly focuses on the question how large the polymer fraction has to become before an infinitely large molecule is formed.[59, 61, 62] For a silica system, the assumptions made for this theory include equal reactivity for all free silanol groups independent from the degree of polymerization. Additionally, polymers are not supposed to form intramolecular bonds, thus no ring formation occurs within the system. Therefore, every newly formed bond attributes to the expansion of the polymer until a critical degree of polymerization is reached, the gelation point. The theory suggests that the average molecular weight in the sol climax until the gel point, as a great "spanning supermolecule" is formed parallel to large oligomers, which are then integrated in the "supermolecule" after the sol-gel transition, leaving the sol depleted of large average molecular weights. For silica the calculation according to this model yields, that a pure silica gel is generated when 1/3rd of all possible siloxane bonds have formed.

The theory provides mathematical formulas for the calculation of the critical polymer fraction at the point of sol-gel transition and for the average weight distribution in the sol. However, in real systems the reactivity of the free silanol groups considerably depends on the degree of substitution of the Si atom. In combination with the assumption that no ring formation occurs during the polymerization, which is only likely for high polymer concentration, the classical theory is not an adequate explanation for the gelation process. A more refined model is the percolation theory presented by Stauffer.[63] In analogy to the classical theory, it is assumed that bond formation is to be random and the polymers are cross-linked including the possibility of ring formation by intramolecular reactions within the macromolecules. The base

for the simplest approach is a static lattice (constant dimensionality) model, in which monomers surround the lattice with a certain number of substitutions sites, which is equal to the amount of nearest neighbours. Macromolecules are formed (group of bonded lattice points), that are connected by direct or indirect bonds. When a critical value of bonds for a macromolcule is reached, a "spanning supermolecule" is formed, which is of finite size below the percolation threshold (sol) and of infinite size, if it is above the percolation threshold (gel). The gel can also be described as an infinite network built-up of connected monomers.[64] The threshold considerably depends on the nature of the lattice (dimensionality, random or periodical ordering) and in general cannot be exactly determined.[59, 63] Both theories exhibit serious deficiencies as they presume an equilibrium state and do not consider the kinetics of the gelation process. A kinetic approach towards the gelation process is the kinetic rate equation presented by Smoluchowski.[65] According to the kinetic approach, the particle growth results from collisions of two species in a dilute liquid system. These species can either be large macromolecules or/and small molecules, aggregating to a larger molecule or even to a particle. Depending on the domination of either small – large molecule collisions (Class III) or large – large molecule interactions (Class I), the resulting gels differ in growth kinetics and size distribution of the resulting particles. For example, while the domination of small – large molecule collisions results in aggregates with a "bell-shaped" size distribution and no gelation occurs as the formation of an infinite macromolecule requires an infinite time. In contrary, the predominance of large – large molecule collisions leads to a sol that is depleted from large molecules, but enriched with monomers. Therefore, the size distribution of the molecules within the solution constantly decreases with time and a gel network is formed, when the total mass of the "supermolecule" increases without limit (infinite).[59, 66] The real behaviour of gelling systems infers that the condensation reactions produce polymeric aggregates the growth of which is kinetically controlled. However, as the size of the aggregates increases, their density is reduced and thus the effective volume fraction of the polymeric aggregates is extended. Due to the growth, overlapping of the polymers can occur confining their mobility and the formation of further bonds can best be explained by a percolation process, where the sites form new bonds with other large polymer aggregates.[59]

After the sol-gel transition, the three-dimensional network is still fragile. There are still condensable oligomers and monomers present, that can form bonds with the condensed network or among each other leading to a firmer network. Additionally, Ostwald ripening also occurs after the gel point that leads to the growth of bigger particles at the expense of smaller

particles influencing the morphology of the resulting gel network. In monolithic materials synereses leads to spontaneous shrinkage of the gel body as free silanol groups on the surface react with each other resulting in a repulsion of the pore liquid and a densification of the network. The combination of all the processes emerging after the initial gelation that affect the resulting gel morphology are classified as aging. By tuning the aging conditions such as temperature, moisture, and aging time the resulting gel structure can be tailored to meet the requirements for different applications.

The resulting morphology of the gel considerably depends on the conditions during all three steps of sol-gel processing:

1. the sol: composition, pH, type of precursor, the degree of dilution, temperature
2. the gel: the conditions during the sol-gel transition, changes in solvent (evaporation), temperature, acid or base catalysis, etc.
3. the aging: synereses effects, Oswald ripening, further incorporation of monomers and small oligomers are all dependent on the temperature, the system (closed, open), the aging time, etc.

1.3.1. Precursors[49]

Even though the most famous precursors for the synthesis of structured silica materials are still TMOS and TEOS, there has been much effort to develop new biocompatible silicon source precursors. During the hydrolysis of TEOS and TMOS monovalent alcohols are released which are often detrimental to living cells, enzymes and proteins. Furthermore, the network formation of TEOS and TMOS requires either base or acid catalysis, which are not compatible with most biosystems. Diol- or polyol-modified precursors such as tetrakis(2-hydroxyethyl)orthosilicate, an ethylene glycol-modified silane (EGMS) and sugar-modified silanes seem to be the better choice for bioencapsulating sol-gel processes, as the released diol / polyol does not harm the biosystem. The synthesis of EGMS was first reported in the 1960s by the group of Mehrotra.[67] However, the autohydrolysis of the EGMS in contact with water was first considered as disadvantage. Only when Hoffmann and Sattler[68] recognized the compatibility of the released diol with the liquid crystalline (LC) phase of tetradecyl-

trimethylammonium bromide (TTAB) in water, which they employed as supramolecular template for the synthesis of mesostructured silica materials, diol and polyol-modified silanes attracted attention as possible candidates for bioencapsulation protocols into silica matrices. Since then various polyol-modified silanes have been synthesized and employed for different applications. For example, Brennan and Brook synthesized and employed diglycerylsilane, monosorbitylsilane as well as maltosyldisilane for the embedding of proteins within the silica matrix. Besides the successful entrapment of enzymes, these so synthesized silica monoliths additionally exhibited a reduced shrinkage compared to silica monoliths prepared from TEOS resulting from residual polyol inside the pores.[69] The employment of EGMS as water hydrolyzable silicon source precursor was described by Shchipunov et al.[70, 71] as well as by Hüsing and co-workers who also synthesized the glycerol analogue of EGMS and applied it for sol-gel processing of hierarchically organized silica materials.[48, 72]

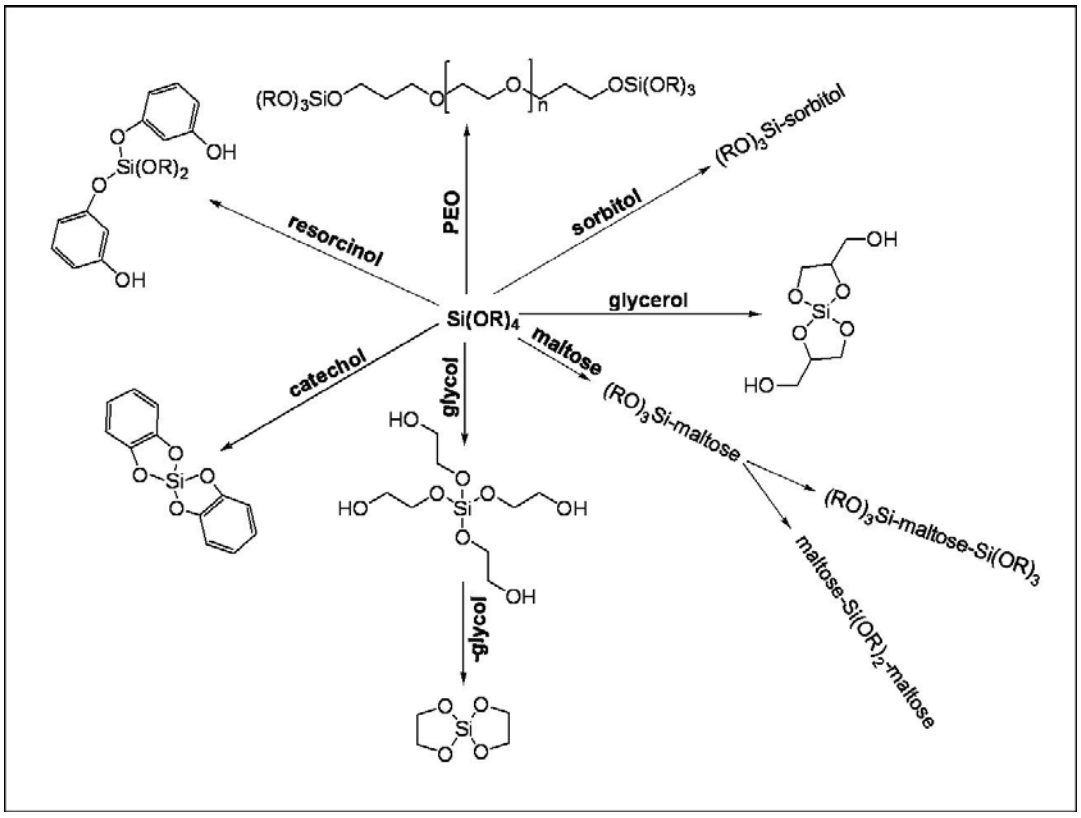

Figure 4 Schematic drawing of some employable diol / polyol-modified silanes for the sol-gel process. The drawing does not depict the real structures but can only give an impression of the molecules as most of them are in equilibrium with bridged and chelated species and in some cases even hypervalent silicon species are reported.[69, 71-73]

1.3.2. Introduction of the Mesoporous System

In the synthesis of porous materials, the focus is on the tailoring of the porous system to meet the requirements for their specific applications. The most prominent techniques to introduce the porosity into the material by simultaneously governing the size and the arrangement of the pores are templating methods. According to the suggestion of Schüth two different templating approaches are distinguished.[24]

1.3.2.1. Exotemplating

This technique is also known as confined space synthesis. For the creation of the pores, hard templates such as other porous materials or nanocasting are employed as negative imprints for the resulting gel network.[24, 74] Besides the generation of a porous bulk material also other nanomaterials, such as fibres, wires, and tubes, can be obtained.[75-77] Subsequent to the synthesis, the template has to be removed i.e. by leaching, for isolating the product and the porous system. This technique is most often applied for non-silicate materials. Ryoo et al. reported the synthesis of ordered mesoporous carbon materials by employing SBA-15 materials as templates, which resulted in carbon nanorods (inverse replica of the template pores) and carbon nanotubes (hollow replica of rod-like templates). By using the so-synthesized carbon materials as templates and by converting these with a silicon source precursor, the original structure, the SBA-15, could be re-generated.[78-80]

1.3.2.2. Endotemplating

The endotemplating approach is a “soft-matter” templating technique that is also known as supramolecular templating. Here supramolecular arrays of molecules such as lyotropic liquid crystalline (LC) phases of amphiphilic surfactants or block co-polymers function as structure-directing agents for the resulting mesoporous oxide network. Besides the employment of non-ionic co-polymers, also the employment of ionic surfactants is known for the preparation of ordered mesoporous materials. Depending on the predominant interactions between the head groups of the surfactant molecules and the surface charge of the inorganic precursor aggregates, different synthesis pathways can be distinguished according to Huo et al.[81, 82] Figure 5 shows the different pathways for the organization of organic surfactant molecules with the inorganic precursor molecules to form nanocomposites in dependence of the pH of

the liquid phase. The interactions of cationic surfactants (S^+) like cetyltrimethylammonium bromide (CTAB) with an inorganic precursor in basic media (I^-, deprotonated precursor molecules) can be described by the S^+I^- path. (Figure 5A) As the surfactant and the precursor molecules are oppositely charged, the positive Coulomb interactions forward the aggregation of the precursor in the hydrophilic domains of the surfactant arrays and therefore the formation of the composite. (Analogue S^-I^+ in acidic media, figure 5D) In general, positive interactions between the head groups of the surfactant and the inorganic precursor molecules are required for the assembly of the composite in the hydrophilic regions of the supramolecular arrays. Thus, if surfactant and precursor are equally charged for example a cationic surfactant S^+ with a protonated precursor molecule in acidic media I^+ (figure 5B) or an anionic surfactant S^- with a deprotonated precursor species I^- in basic media (figure 5C), the presence of a counterion is fundamental to establish the charge balance between the two species. These pathways are known as $S^+X^-I^+$ for two positively charged ions (figure 5B) and as $S^-M^+I^-$ for two negatively charged species (figure 5C). For non-ionic surfactants such as the amphiphilic block co-polymer Pluronic P123 a poly(ethylene oxide)-poly(propylene oxide)-poly(ethylene oxide) (EO_{20}-PO_{70}-EO_{20}) and non-ionic precursor molecules, the aggregation is based on van-der-Waals interactions between the hydrophilic head groups and the precursor molecule (S^0I^0). In the case of P123 or other amphiphilic polyether co-polymers, where the PEO blocks form the hydrophilic regime of the surfactant arrays, additional hydrogen bonds between the PEO segments and the precursor molecules intensify the composite formation. This pathway is also known as N^0I^0 with N representing the PEO blocks (figure 5E).

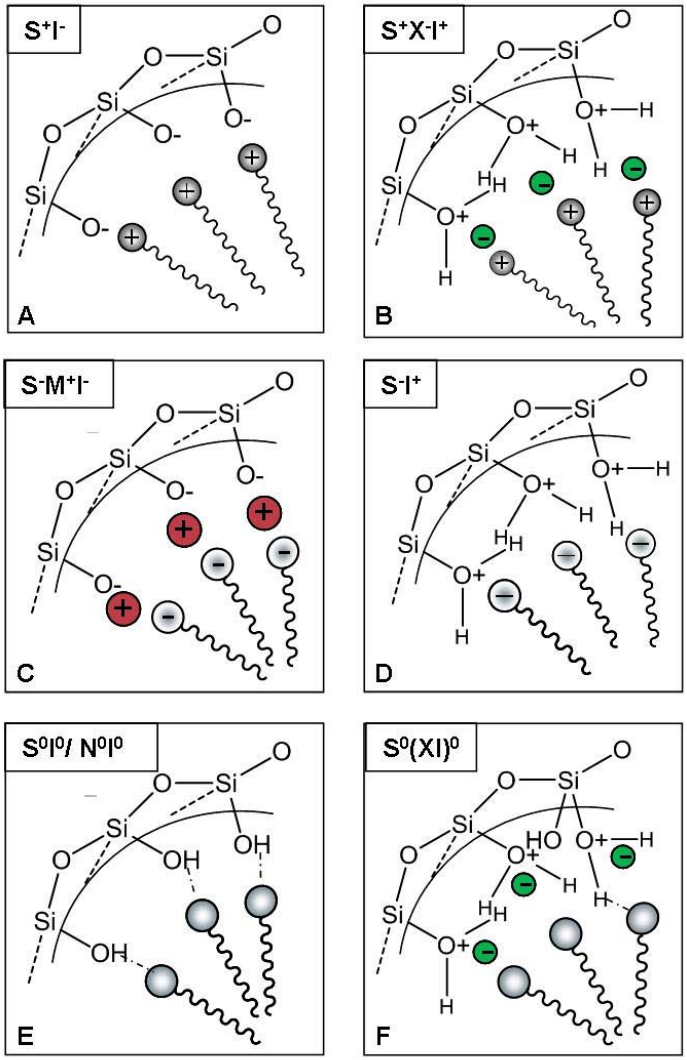

Figure 5 Interactions between the inorganic precursor species with the head group of ionic (A-D) or non-ionic (E-F) surfactants. The different possible paths for the organization of the nanocomposite depending on the pH of the media (acidic, basic or neutral, the electrostatic interactions are S^+I^-, $S^+X^-I^+$, $S^-M^+I^-$, S^-I^+ and the formation of hydrogen bonds S^0I^0, N^0I^0, $S^0(IX)^0$).[18]

For the description of the influence, Israelachivili developed the concept of the packing parameter P.[83]

$$P = \frac{V_M}{d \cdot l} \qquad \textit{Equation 1}$$

The packing parameter is directly proportional to V_M, the volume of the surfactant molecule, and indirectly to the product of its length l and the cross section d of the polar terminal

group.[83] Depending on the size of P, a different situation can be observed for the self-organisation process of the surfactant:

$P < 1$:	Conical packing, here two cases have to be distinguished:
$P < \frac{1}{3}$:	The amphiphilic surfactant is conically packed and forms a spherical micelle in aqueous solution.
$\frac{1}{3} \leq P \leq \frac{1}{2}$:	The amphiphil is packed in form of a truncated cone, which results in the conversion into a cylindrical micelle in water.
$P \approx 1$:	Planar packing, which leads to the formation of a lamellar structure
$P > 1$:	Inverse frustum packing, which forms an inverse micellar structure

Many different analysis techniques such as SAXS / XRD and cryo-TEM as well as NMR have been applied to investigate the evolution of the mesostructure, which is to follow different mechanisms.[84-87]

True Liquid Crystal Templating (TLCT) Mechanism. The starting point for the TLCT mechanism is the presence of a high surfactant concentration, beyond the critical micelle concentration (cmc), in which agglomerations of the surfactant molecules form lyotropic liquid crystalline (LC) phases. The cmc marks the surfactant concentration above which no further decrease in the surface tension can be observed as micelles are adsorbed at the air-liquid interphase and supramolecular surfactant aggregates are formed. Depending on the temperature, concentration, solvent, pH, etc. these supramolecular aggregates self-assembly to lyotropic liquid crystalline phases without the presence of a network-forming precursor.
Figure 6 shows the phase diagram of P123 in aqueous solution with the evolution of the LC phases in the presence of ethanol at room temperature. As seen in the diagram, minor concentrations of ethanol are already detrimental to the formation of the liquid crystalline phase, which has to be considered when tetraethylorthosilicate (TEOS) is employed as inorganic precursor, as the release of ethanol during hydrolysis and condensation disturbs the self-organisation of the surfactant micelles.

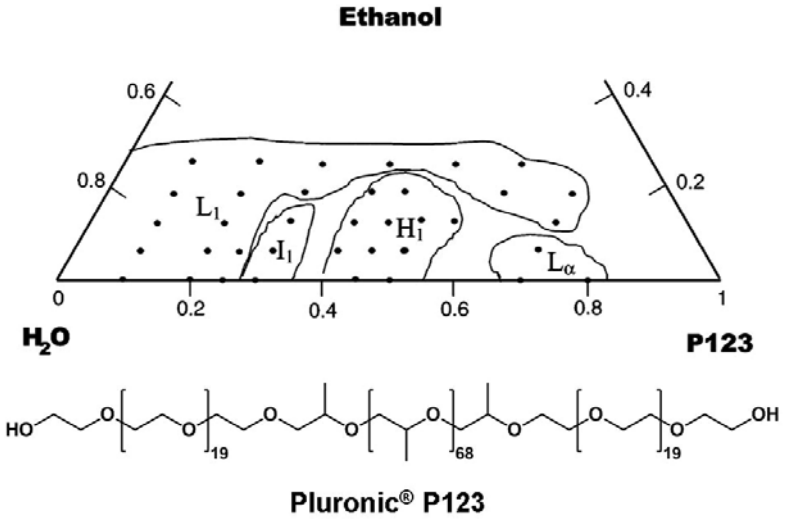

Figure 6 Phase diagram of Pluronic® P123 in aqueous solution in the presence of increasing quantities of ethanol. (Picture was adopted from literature [88])L1 marks the isotropic liquid phase. The phase I1 reveals hexagonally as well as cubic arranged micelles, whereas H1 are solely hexagonally assembled micelles. L_α marks the region of a lamellar structured phase.

Figure 7 shows the schematic TLCT mechanism as it was proposed by Kresge and Beck of Mobil Oil Corporation for an ionic surfactant.

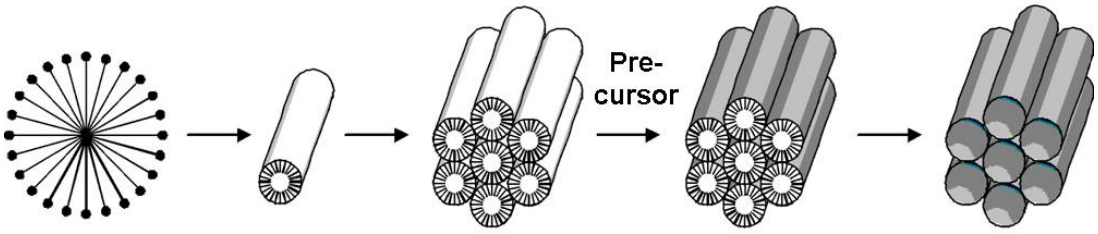

Figure 7 Schematic depiction of the TLCT mechanism as postulated by Kresge and Beck.[15, 16]

With increasing surfactant concentration first spherical and cylindrical micelles are formed, these self-assembly to a 2D-hexagonally ordered array of surfactant micelles. It is assumed that with the addition of the inorganic network-former no structural changes occur, thus hydrolysis and condensation reactions proceed at the hydrophilic domains of the assembled micelles replicating the surfactant mesostructure. By removing the template phase, an inorganic mesostructured material is obtained, which pores directly correspond to the diameters of the cylindrical micelles. It is widely assumed that for high surfactant

concentrations the TLCT mechanism is appropriate, however, there are results from investigations that exhibit discrepancies with this assumption. For instance if the liquid crystalline phase of sole P123 in 1 M HCl at 25°C is analyzed by SAXS, the SAXS pattern reveals a co-existence of hexagonally arranged and cubic arranged micellar arrays.[89] However, after the conversion of the same phase with tetrakis(2-hydroxyethyl)orthosilicate (EGMS), a purely 2D-hexagonally meso-structured silica material is obtained, which is not consistent with the TLCT mechanism.[48]

Co-operative Mechanism. This mechanism is also known as surfactant-templating co-assembly with inorganic oligomers or nanoparticles. Here no prior self-assembly of the surfactant is assumed, but the formation of the 3D-ordered nanocomposite proceeds as consequence to the interactions between the organic template phase and the inorganic precursor species.

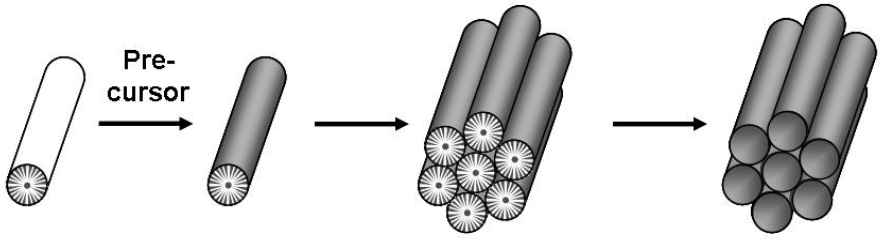

Figure 8 Schematic depiction of the co-operative mechanism according to Stucky and co-workers.[82]

The inorganic oligomers or nanoparticles either can be preformed from the original precursor molecule or can be generated *in-situ* during the assembly. According to Stucky et al. the condensation reactions of the silicate species at the interphase to the organic moieties change the charge density of the oligomers and therefore govern the arrangement of the organic species.[81, 82] The assembly procedure for a non-ionic surfactant with an uncharged precursor is most probably analogue to the S^0I^0/N^0I^0 formation of figure 5E. The positive interactions are even fortified by additional hydrogen bondings.

1.3.3. Design of the Macroporous System

For a number of applications, besides an ordered mesoporous system, there is also the requirement for a well-defined continuous macroporosity, such as for chromatographic or catalytic devices, allowing for a high diffusion rate. As discussed in the former section about macroporous materials, macroporosity can be introduced into a material by various techniques such as macrotemplating with latex spheres or bacteria. However, for the creation of a continuous macroporous framework with a narrow pore size distribution and a high inter-connectivity, the most promising method is by polymerization-induced phase separation for alkoxy-derived sol-gel systems. Nakanishi and co-workers first presented the possibility to design the macroporous morphology by polymerization-induced phase separation accompanied by sol-gel transition (freezing of the resulting morphology).[39, 90, 91] The system they applied included a water-soluble, highly polar polymer such as PEO in acidic media, with TEOS or TMOS as silicon source by which hence a hierarchical porous materials with pores over different length scales were obtained. Even though, the resulting macroporous morphology could be tuned via temperature, ratio of solvent to precursor, pH, etc., the mesopores of the materials showed a random distribution with no uniform pore diameter nor a well-ordered mesopore arrangement as they were post-synthetically introduced by an aging procedure under basic conditions.[92] To achieve a mesoscopic ordering of the pores, Lindén and Nakanishi tuned the technique by incorporating an endotemplating approach with ionic or non-ionic surfactants parallel to the designing of the architecture of the macroscopic framework.[43, 93-95]

In the initial state of the sol-gel process, the binary mixture of a water-soluble polymer *e.g.* PEO or an amphiphilic surfactant, and a polymerizable, alkoxy-derived precursor such as TEOS exists as a single-phase system. However, as in the case of TEOS the polycondensation in for example acidic media progresses with time, the average molecular weight of the siloxane oligomers increases until an infinite polymer is formed and the gel point is accomplished. In the case of ethylene oxide units of the employed polymer, hydrogen bonds are formed between the oxygen atoms of the polyether and the silanol groups of the siloxane oligomers, emerging a phase rich in polymer and siloxane oligomers that additionally promotes phase separation.

According to the thermodynamics of solutions containing polymerizable species, the solubility of either constituent of a multi-component system decreases with gaining average weight of

the polymerizing species. By applying the equation for the Gibbs energy (equation 2), it is obvious, that in the course of the polymerization the entropy of mixing decreases and thus the free energy ΔG of the system increases implicating a destabilization of the mixture.

$$\Delta G = \Delta H - T\Delta S \qquad \textit{Equation 2}$$

The moment the free energy becomes positive ($\Delta G > 0$), the phase separation is induced. The polycondensation of the polymerizable alkoxy-derived precursor climaxing in the sol-gel transition, can be seen as "chemical cooling", as the momentary situation in the constitutions of the components within the miscibility window and therefore different macroporous morphologies are frozen.[92, 96] (Figure 9)

There are two different mechanistic pathways for the induction of the phase separation depending on the deviation of system from the equilibrium.
The first route is the spinodal decomposition (figure 9A), which occurs in the unstable region of the phase diagram (between the spinodal boundaries). Here infinitesimal fluctuations of the compositions ratio leads to an amplification of energy and induces a spontaneous phase separation. The initially resultant phase domains are highly interconnected and exhibit diffuse interfaces. However, in the course to reduce interfacial energy of the phase domains re-organization processes occur, which in consequence cause a coarsening of the morphology. (Figure 9B)
The other mechanistic possibility to introduce heterogeneity into a homogeneous system is by nucleation and growth. In contrary to the spinodal region, fluctuations in the metastable region (between binodal and spinodal boundaries) consume energy and therefore activation energy is required to generate phase separated domains. In the initial stage of phase separation small sections of dispersed domains are formed, which are called nuclei. These nuclei grow by diffusion controlled agglomerations of molecules to the nuclei. The resultant phase domains show sharp interfaces of a dispersed phase in a matrix phase, generating particles of random size and distribution. [24, 97] (Figure 9B)

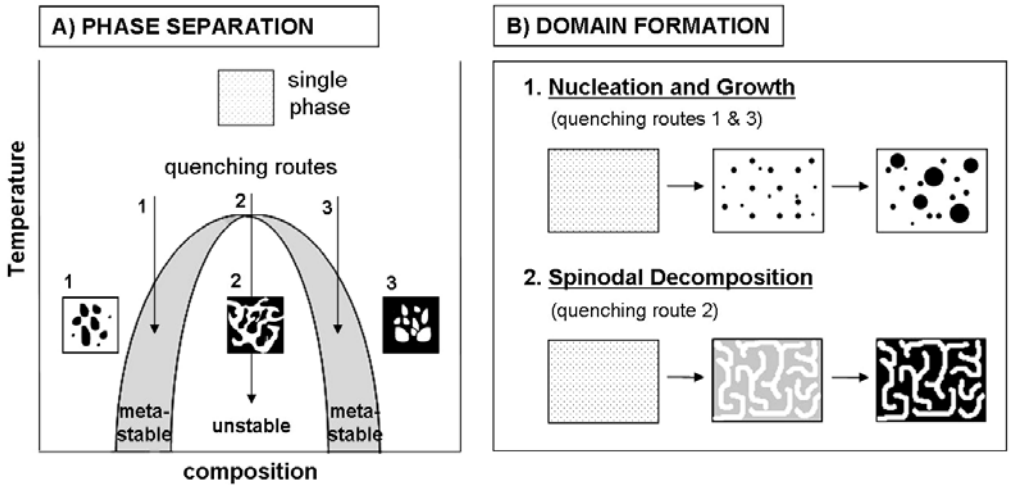

Figure 9 Phase separation and domain formation.**A –** Schematic depiction of the phase separation of a diluted polymerizable system for different quenching routes, **B –** schematic presentation of the different mechanistic routes for the phase separation and the resultant phase domains.[92, 96]

Parallel to the phase separation the sol-gel transition occurs, which can be seen as "chemical cooling" (figure 9), as the proceeding polymerization leads to the freezing of the momentary situation of the phase separated system and therefore of the resulting macroporous morphology. As phase separation and the sol-transition are competitive processes in the sol-gel system, the resulting morphology of the domains strongly depends on the onset of phase separation relative to the sol-gel transition. Therefore, for a spinodal decomposed system for an early onset of phase separation a co-continuous structure is obtained, while with evolving time for the phase separation coarsening of the domain phases are observed which results in the fragmentation of the structure into isolated domain fractions and sedimentation occurs.

1.3.4. Surface Modification

Amorphous and especially mesoporous silica frameworks are popular substrates in which organic functionalities are incorporated either within the matrix or on the pore wall surface *e.g.* by adsorption or chemical reaction. The combination of a thermally stable inorganic framework with variable organic moieties, which provide the desired characteristics, opens up the field for new of applications *e.g.* for heterogeneous catalysis. The fabrication of these hybrid materials can be achieved by different synthesis strategies.

1.3.4.1. Post-Synthetic Grafting

By the post-synthetic treatment of a mesoporous or even mesostructured silica material, the original mesoporous network is preserved during the introduction of organic functionalities. The modification is based on the reaction of accessible silanol groups at the pore walls with the functionalization agent such as organosilanes of the type $(R^1O)_3SiR$ or silazanes of the type $H_2N(SiR_3)$[47] or in some cases chlorosilanes ($ClSiR_3$, Cl_2SiR_2, etc.)[98] with R^1 = -methyl, -ethyl, etc. and R = -alkyl substituents such as octadecyl-[99], or 3-aminopropyl-[47, 100] and 3-mercaptopropyl-[47]. The application of chlorosilanes and in particular chlorotrimethylsilane (TMCS) as silylation agent has proven to be a convenient procedure for the drying of monolithic silica materials as an alternative to the supercritical drying with CO_2.[14, 47] Furthermore, investigations showed that by hydrophobization of the silica monolith with TMCS the template phase is extracted and the resultant hydrophobic monolith can be dried under ambient conditions as cracking of the monolithic body and the collapse of the porous structure are avoided (reduced loading of silanol groups on the surface).[47, 49]

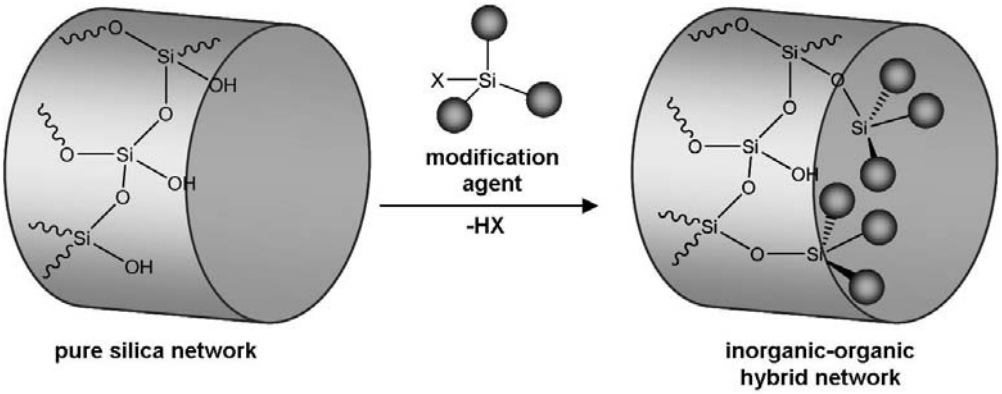

Figure 10 Schematic drawing of the post-synthetic modification approach towards a hybrid inorganic-organic silica network.

However, one disadvantage of the post-synthetic grafting is the inhomogeneous loading with functional groups, as the silanol sites at the pore entrances are the first to react. Depending on the size and functionality of the organic substituents, these reacted sites can impede the diffusion of further molecules into the pores resulting in low and inhomogeneous loading.[18]

1.3.4.2. Direct Functionalization (Co-condensation)

To achieve a homogeneous distribution of organic functionalities within the matrix, the direct functionalization approach by co-condensation of a tetraalkoxy-derived silane $(RO)_4Si$ with an organically modified trialkoxy silane $R^1Si(OR)_3$ is a promising approach. By this technique, organic functionalities are directly connected to the silica framework by a hydrolytically stable covalent Si-C bond and protrude into the pores. Here diffusion processes do not govern the loading and therefore no pore blocking occurs.

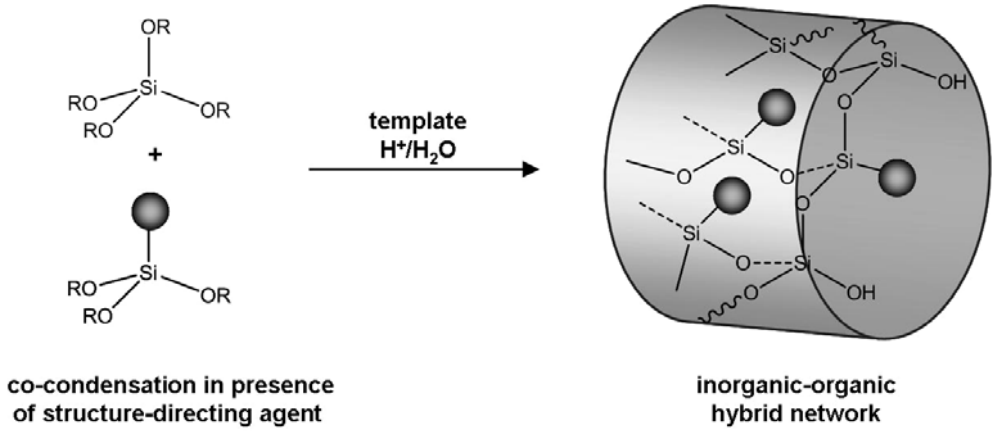

Figure 11 Schematic drawing of the *in-situ* modification via co-condensation to obtain a hybrid inorganic-organic silica network.

However, for the co-condensation, there are several restrictions for the synthesis of mesoscopically ordered hybrid silica materials. First with increasing ratio of the organically modified silane to the tetraalkoxy silane, the mesostructuring decreases, thus in most cases no ordering for the pores can be obtained above 40 mol % $R^1Si(OR)_3$.[18] Additionally this value is, however, strongly dependent on the nature of the organic group, especially on the polarity of the organic moiety, as the change in polarity affects the network architecture. Another restriction is that the resulting loading of terminal organic groups on the pore walls is lower than theoretically expected. This is due to the different hydrolysis and condensation rates of $R^1Si(OR)_3$ and $(RO)_4Si$ leading to the favouring of homo-condensation at the expense of networking co-condensation. In analogy to the altering of the network architecture with increasing amount of $R^1Si(OR)_3$, a reduction of the homogeneous distribution of the organic functionalities in the resulting material is also observed with increasing content of $R^1Si(OR)$ due to the preferred homo-condensation.

Therefore, the direct synthesis is an appropriate technique in the lower range of contents for the $R^1Si(OR)_3$ to fabricate mesoscopically ordered hybrid silica materials with a homogeneous, however, quite low loading of organic functional groups.

1.3.5. Requirements for HPLC

High Performance Liquid Chromatography (HPLC) has become one of the mostly applied analysis and separation methods for mixtures and the determination of their compounds.
There has been a lot of progress on the fine-tuning of the particle-packed silica gel columns with uniform spherical porous particles in the range of 3 – 5 μm during the last 30 years. The size and the distribution of the particles determine the separation efficiency leading to the conclusion that with decreasing size a higher packing of the particles can be achieved and thus a greater separation performance. However, along with decreasing size of the particles, the interparticular voids are reduced and limit the permeability of the solvent resulting in a high back pressure for the packed column.[2, 101]
By employing hierarchically organized monoliths including a co-continuous macropore system as stationary columns, the permeability and the performance can be controlled independently from each other. The permeability is determined by the macropore size distribution of the co-continuous macropore network, while the shape and the size of the mesopores establish the performance of the column.
The separation efficiency of a chromatographic column is expressed by its number of theoretical plates N, which can be determined from the resultant chromatogram.

$$N = 16\left(\frac{t_R}{w}\right)^2 = 5.54\left(\frac{t_R}{w_{0.5}}\right)^2 \qquad \textit{Equation 3}$$

The retention time t_R represents the time interval between the injection of the sample and its emersion point. Depending on the interactions between the stationary phase and the chemical components of the sample, each component has a different retention time t_R and hence can be separated from each other. $W_{0.5}$ is the full width at half-maximum of the maximum observed in the chromatogram.

Theoretically, the signals of a chromatogram exhibit a symmetrical Gaussian profile, however, in consequence to dead volumes within the column or to adsorption of analyte molecules at the stationary phase, a tailing of the signal can emerge. Therefore, another approach for the evaluation, the van Deemter model has to be applied in order to take the broadening factors such as diffusion and mass transfer into account.[102]

$$H = A + \frac{B}{u} + C * u \qquad \textit{Equation 4}$$

The term u represents the linear flow velocity and H is the height equivalent of a theoretical plate. The term A accounts for the diffusion term in dependency of the particle size and of the deviance from the ideal spherical shape, while term B considers the longitudinal diffusion of the sample molecules along the direction of the flow. The parameter C consists of two further terms and represents the mass transfer during the separation between the mobile and the stationary phase.

$$C = C_s + C_m \qquad \textit{Equation 5}$$

C_m is the mass transfer of the mobile phase, a diffusion perpendicular to the flow direction; which is hindered by the viscosity of the mobile phase and the packing of the particles. C_s takes the time for the intrusion and the emersion of the sample for the stationary phase into account. Depending on the flow rate of the HPLC system, the three parameters are of differing significance. For high flows the C parameter dominates the pattern of the van Deemter curve, while for small flows the B term plays the dominant role.[102]

By employing small spherical particles (d ~ 3 μm) for the column packing, both the term A and the diffusion path length within the particles can be reduced, leading to a greater column efficiency than for larger particles. However, as consequence of the small particle diameter a high back pressure results hindering the flow of eluent. Hence, small silica particles can only be employed in short HPLC columns limiting the number of theoretical plates N. Investigations of Tallarek et al. exhibited that by the use of monolithic silica columns the flow permeability was comparable to a packed column with particles of 11 μm.[103] The direct comparison of monolithic and conventional packed columns of Cabrera at Merck KGaA[2] revealed, that the separation efficiency of the monolithic columns were equivalent to the columns packed with

3.5 μm beads. While the maximum linear flow velocity u_{max} within the beads packed column was reached at approximately 7 mm/s, the monolithic column could be operated at velocities as great as 10 – 11 mm/s.

Chapter 2

Hierarchically Organized Silica (Hybrid-)Monoliths by Employing Ethylene Glycol-Modified Precursors

2.1. Purely Inorganic Silica Monoliths

2.1.1. Motivation

Six years ago Hüsing et al. presented the synthesis of hierarchically organized silica monoliths combining a macroporous framework with pores in the range of 200 – 800 nm with hexagonally arranged mesopores exhibiting diameters of 8 nm from purely aqueous solution.[72] The gel synthesis was performed by employing an ethylene glycol-modified silane (EGMS) as inorganic network-builder in the presence of a preformed liquid crystalline phase of the amphiphilic co-polymer Pluronic™ P123 in water.[72] Brandhuber extended this approach by a random variation of the nominal pH in the range from neutral to -0.7 and the composition ratio whereas the EGMS content was also varied.[104] The resulting macroporous morphologies as well as the obtained mesostructures of the silica gels indicate a strong dependency of the

macrophase separation and the formation of a mesoscopic ordering of the pores on these parameters.

Therefore, one motivation of this work is to refine the above described approaches to establish a trend within the formation of the hierarchical silica network in order to tailor the pore size regimes for their possible application as HPLC columns. Initially the focus is on the influence of the type of acid and its concentration on the resulting network architecture, therefore a stepwise variation has been chosen, in the range from 10^{-6} to 1 M HCl and the resulting gels were not only investigated with respect to their pore size regimes but also to their shrinkage behaviour during drying. (Section 2.1.3.) To complete the investigations of the sol-gel system of EGMS and Pluronic™ P123 in dilute HCl, composition ratios of P123 to HCl are varied and in an adjacent investigation, the affect of a reduced Si content on the structure formation is tested. (Section 2.1.4.)

In order to examine the influence of the acid's anion on the development of the bimodal network domains, HCl is substituted by some selected acids such as nitric acid, sulphuric acid, etc. in the sol-gel processing of the silica monoliths, while all other synthesis parameters are kept constant. (Section 2.1.5.) As the gelling as well as the aging temperature and the aging times are key parameters in the formation of the mesoporous arrangement as well as the macrophase separation and thus the macroporous morphology, the affect of the variations of these parameters is also a subject of this thesis. (Section 2.1.6.)

Besides the optimization of the sol-gel system for the synthesis of the hierarchical silica monoliths, another focus of this thesis is on the investigation of the influence of the container material on the surface boundary region. For HPLC columns, a homogeneous macroporous framework is greatly important to allow for a continuous flow of the eluent within the column and thus the best possible separation efficiency. However, in the synthesis of monolithic silica columns, densifications in the surface region of the gel body are an often observed phenomenon. In order to avoid this densified region, the influence of different container materials on the development of the macroporous framework close to the surface was investigated. (Section 2.3.)

2.1.2. Synthesis of the Gels

The ethylene glycol-modified silane (EGMS) has been synthesized according to the procedure of Mehrotra et al. via a transesterification reaction of ethylene glycol with tetraethylorthosilicate (TEOS) in the stoichiometric ratio of 4:1.[67]

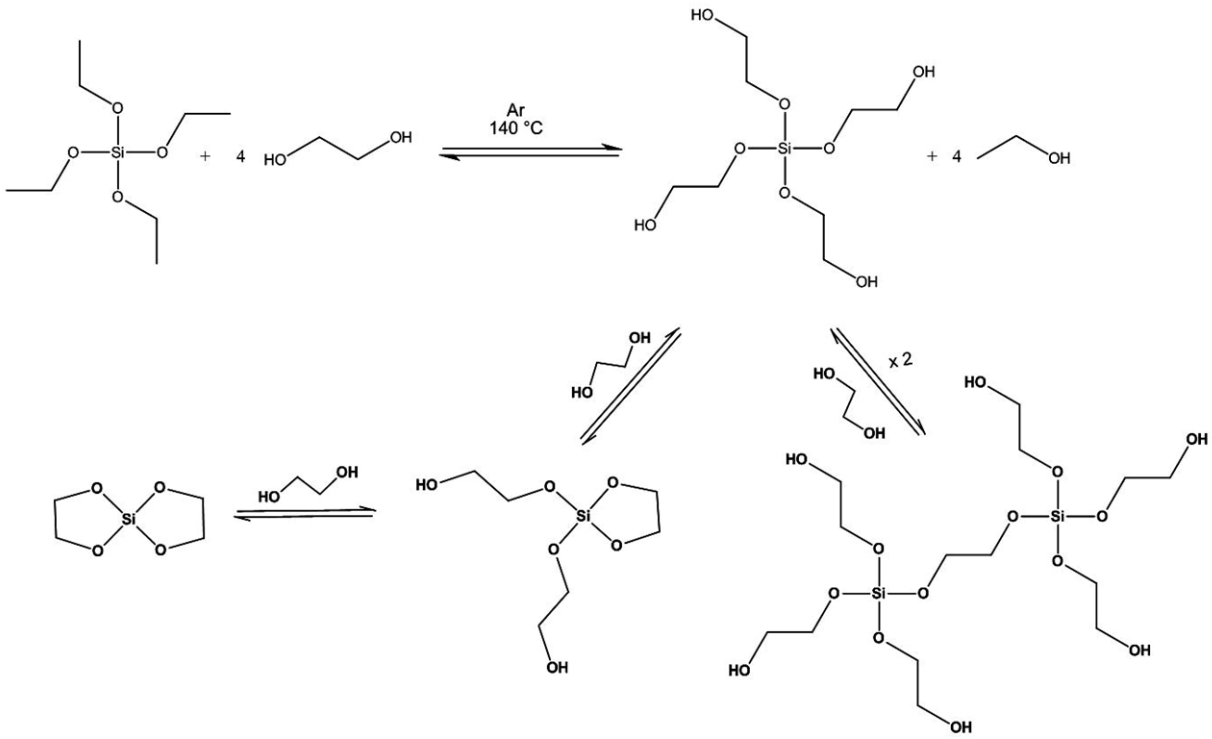

Figure 12 Reaction scheme of the EGMS synthesis; EGMS is in equilibrium with various bridged and chelated species.

The reaction requires no additional solvent, however, the synthesis has to be conducted in inert atmosphere as the resultant product is highly sensitive towards hydrolysis. The purity of the resultant product is controlled by spin-lock ^{29}Si-NMR, which diagram exhibits a peak at -81.86 – -82.45 ppm for the single molecule and at -88.61 ppm for an either chelated or bridged equilibrium species. As can be seen from the reaction scheme in figure 12, EGMS is not existent as a single molecule, but various chelated and bridged species are present that are at equilibrium with the single molecule. Additionally, ^{1}H-NMR spectroscopic measurements are performed in order to estimate the residual ethanol, which can shift the equilibrium towards the educt site. The Si content of the EGMS is calculated from the results of thermogravimetric analysis, which is 9.6 wt %Si (theoretical: 10.4 wt %, yield: 92%).

All hierarchically organized silica gels presented in the following sections are synthesized via the sol-gel route with EGMS as sole precursor and Pluronic™ P123 as structure-directing agent. For the different investigations, several changes of parameters are adopted. Based on the work of Hüsing and Brandhuber, the initial composition of Si / P123 / x M HCl or pure water is 8.4 / 30 / 70 by weight. After EGMS and the P123 phase have been homogenized with a Vortex, the sol is transferred into moulds, in which the system is allowed to gel and age at 40°C for 7 days. The synthesis procedure for the gel preparation is illustrated in figure 13.

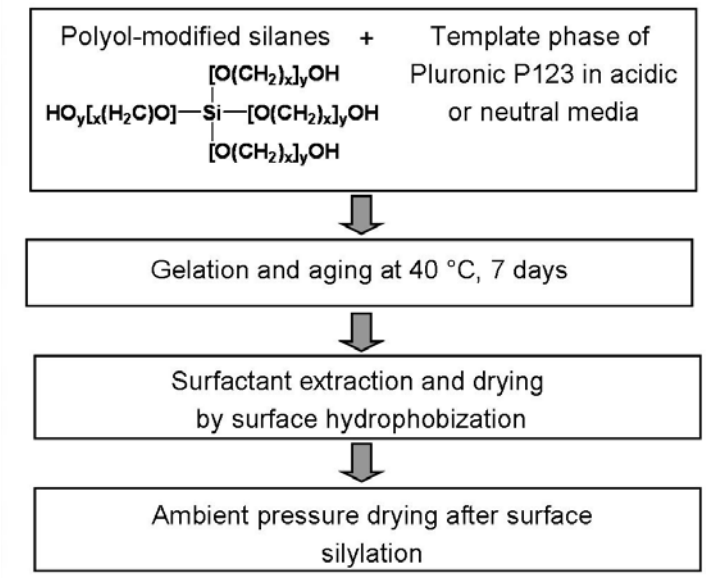

Figure 13 Schematic depiction of the silica gel synthesis.

Based on this synthesis route, parameters for the sol-gel process are varied in order to optimize the system for the synthesis of the hierarchically organized silica monoliths. (Table 3) Per every single investigation, only one parameter is varied, while the others are kept constant.

Table 3 Listing of the investigations and their varied parameters.

investigation	*varied parameters*	*section*
influence of the nominal pH	concentration of HCl	section 2.1.3.
influence of the composition of the template phase	variation of surfactant-solvent ratio	section 2.1.4.
effect of the corresponding acid anion	variation of the acid	section 2.1.5.
impact of the gelling (T_g) and aging temperature T_{age} and time t_{age}	variation of T_{age} , T_g and t_{age}	section 2.1.6.
impact of the mould on the macroporous morphology	variation of container material	section 2.3.

Subsequent to the aging, the gels are cured in an ethanol-HCl mixture under reflux to complete the acid-catalyzed condensation reactions between adjacent unreacted silanol moieties. The additional siloxane bonds enhance the mechanical strength of the silica network and thus the preservation of the monolithic shape. However, the monolithic shape is still susceptible and can easily be destructed by evaporation processes during drying as a consequence of high surface tensions of the solvent and capillary forces within the pores. Therefore, alternative drying procedures such as supercritical drying with CO_2 or surface hydrophobization reactions have to be employed in order to preserve the monolithic shape. Here the surface hydrophobization via a silylation reaction with chlorotrimethylsilane (TMCS) is chosen resulting in trimethylsiloxane groups on the pore walls. A positive add-on in this procedure is the simultaneous extraction of the organic template phase from the porous systems, which renders the calcination step, the usual technique to eliminate the organic phase, unnecessary. In an attached washing procedure, unreacted silane species and the generated HCl are removed from the monoliths before they are dried via a slow heating program up to 200°C. Theoretically, these monoliths therefore belong to the class of hybrid silica monoliths. However, as the surface is only post-synthetically modified with minor trimethylsiloxane moieties in order for a careful drying procedure, they will be referred to as pure silica

monoliths in the following sections to distinguish them from the real hybrid silica monoliths prepared by co-condensation.

2.1.3. Influence of the HCl Concentration

For the investigation of the influence of the HCl concentration on the formation of the hierarchical organization of the pore systems, silica gels were prepared by employing lyotropic phases of Pluronic P123 in dilute HCl in the concentration range from 1 – 10^{-6} M as structure-directing agents. The compositions of the initial sols were kept constant with Si / P123 / x M HCl = 8.4 / 30 / 70 by weight.
Investigations of the gelation times for the different HCl concentrations revealed, that the sol-gel transition, thus the gelation, can be seen as a function of the concentration at a certain temperature.

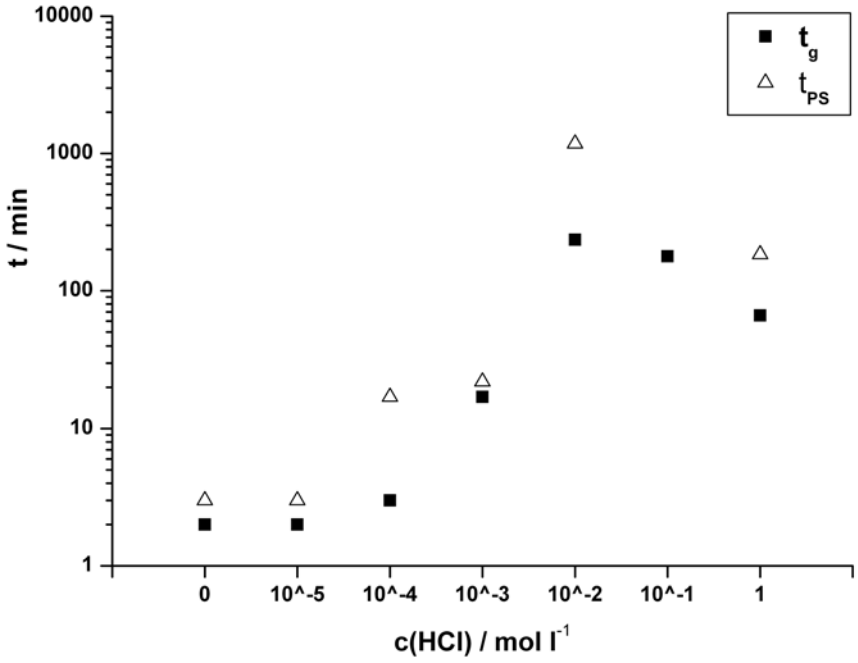

Figure 14 Time intervals of the sol-gel transition (t_g) and the phase separation (t_{PS}) as a function of the acid concentration c(HCl) at 40°C.

The gelation time (t_g) is defined as the time interval between homogenization and the moment, when the fluidity of the system is lost, which was determined by tilting the vessel. In analogy,

the time for the phase separation (t_{PS}) is defined as the time interval between homogenization and the moment, the gels turns turbid. As can be seen from figure 14, both t_g as well as t_{PS} depend on the acid concentration. At lower acid concentrations up to pure aqueous solution, the sol-gel transition as well as the phase separation occurs within few minutes. (As in alkaline media silica precipitates resulting in amorphous particles, these investigations were abandoned.)

With increasing concentration of HCl, the gelation times reach maxima around concentrations of 10^{-2} to 10^{-1} M that coincide with the point of zero charge for silica at which a minimum in the condensation rate occurs. In accordance, the times for the phase separation at these concentrations also reach maximum values, which can be related to the fact that due to the slow polycondensation rate, the system is miscible over a longer time scale and the introduction of the phase separation is delayed. It is well known from literature that the concentration of the acid catalyst affects the gelation time of TEOS and TMOS due to its impact on hydrolysis and condensation rates[59] and therefore the onset of the phase separation which is the basis for the formation of a well-defined macroporous morphology. Investigations by Nakanishi and co-workers exhibited, that the phase separation is induced by the presence of a polar, hydrophilic polymer such as PEO or the amphiphilic block co-polymer Pluronic™ P123[40, 92]. By the formation of hydrogen bonds between preformed oligomeric silica species, which do not carry surface charges in the pH-range of 2 – 6, and the hydrophilic ethylene oxide blocks (N^0I^0-mechanism) the polycondensation reactions can be forced. (section 1.3.2.2.) Due to this aggregation, silica oligomers are drawn together and the formation of new siloxane bonds and therefore the polycondensation reactions are accelerated leading to a shorter gelation time and therefore according to Nakanishi to the phase separation.

An important issue in the synthesis of hierarchically organized silica monoliths as HPLC columns, is the shrinkage of the monolithic gel bodies during the drying procedure. Figure 15 shows the degree of shrinkage of the silica monoliths prepared with the different HCl concentrations. These values obtained for the shrinkage of the monoliths give an impression of the magnitude of the shrinkage and are given as arithmetic means.

Interestingly, the silica gels at higher HCl concentrations ($c(HCl) = 1 – 10^{-2}$ M) are more stable towards mechanical stress than the monoliths prepared with lower HCl concentrations and therefore more monoliths can be preserved during the drying procedure. Despite the fact of a higher resistance towards mechanical stress, the silica monoliths prepared at $c(HCl) < 10^{-2}$

M shrink to a larger extend with up to 14% for the diameter and 6% for the length than the gels synthesized at c(HCl) = 10^{-2}, 10^{-4}, and 10^{-6} M. These monoliths exhibit shrinkages in length of ΔL = 3 – 5% and in diameter of ΔD = 0 – 8%. Among the silica monoliths prepared at c(HCl) = 10^{-3} M and 10^{-6} M not enough monoliths could be preserved during the drying procedure for the determination of the shrinkage which can be related to a high amount of unreacted silanol groups due to the early sol-gel transition.

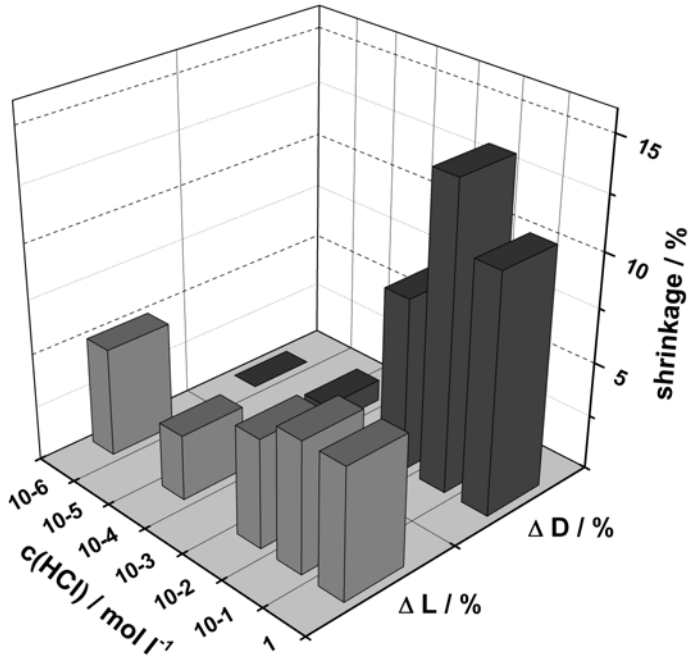

Figure 15 Diagram representing the percentage of shrinkage of the silica monoliths for the diameter and the length related to the dimensions after aging.

2.1.3.1. Influence on the different pore size regimes

When silica gels exhibiting pore size regimes over different length scales ought to be synthesized, the time for the sol-gel transition and the phase separation are key issues in the design of the porous architectures.

Table 4 Physicochemical data of the silica gels prepared from different HCl concentrations.

samples		*SAXS*	*N_2-sorption*			*Hg-Porosimetry*	
	c_{HCl} /mol l^{-1}	d_{10} /nm	S^{BET} /m^2 g^{-1}	D_{BJH} /nm	t_{wall} /nm	R^{Hg} /μm	V^{Hg} /cm^3 g^{-1}
P1-1	1	11.2	1023	6.3	6.7	0.3	3.0
P1-2	10^{-1}	11.2	908	5.4	7.5	0.3	3.0
P1-3	10^{-2}	11.2	944	6.9	6.0	-	-
P1-4	10^{-3}	11.5	939	6.9	6.4	0.1	0.8
P1-5	10^{-4}	11.8	972	3.6	10.1	0.3	2.7
P1-6	10^{-5}	11.6	940	6.9	6.5	-	2.8
P1-7	10^{-6}	11.9	1102	6.9	6.8	-	2.5

d_{10} represents the repeating unit calculated for a 2D-hexagonal pore array, S^{BET} is the specific surface area, D^{BJH} corresponds to the pore diameter distribution, t_{wall} represents the pore wall thickness which is calculated from SAXS and nitrogen sorption data as followed: $t_{wall} = \frac{2d_{10}}{\sqrt{3}} - D^{BJH}$, R^{Hg} corresponds to the macropore radii distribution; V^{Hg} is the calculated cumulative volume.

The data presented in table 4 show high surface areas of around 1000 m²/g throughout the variation series of c(HCl) and values for the d_{10} repeating units of 11.2 – 11.9 nm. However, small angle X-ray scattering (SAXS) experiments revealed, that with decreasing catalyst concentration, the degree of the mesoscopic ordering of the pore arrangement gradually diminishes. (Figure 16)

This development is consistent with the gradually decreasing interactions between the siliceous species and the hydrophilic blocks of Pluronic P123. At high acid concentrations, thus below the point of zero charge (PZC) of silica (pH < 2), protonated cationic silica species enhance the formation of hexagonally arranged silica / organic template assemblies by additional hydrogen bonds (see also figure 5 F, $S^0(XI)^0$). With decreasing acid concentration above the point of zero charge of silica (pH ≥ 2), the silica species exhibit only silanol groups on the

particle surface, that still form hydrogen bondings with the organic structure-directing agent, however, the formation of the assembly is less pronounced compared to the cationic species.[21] Furthermore, the condensation rate is higher at lower acid concentration for the silica system, leading to shorter gelation and phase separation times that are reached within only few minutes. This period is too short for the system to evolve a highly periodically arranged template-silica nanocomposite according to the N^0I^0-mechanism that after template extraction results in a mesoscopically ordered pore network.

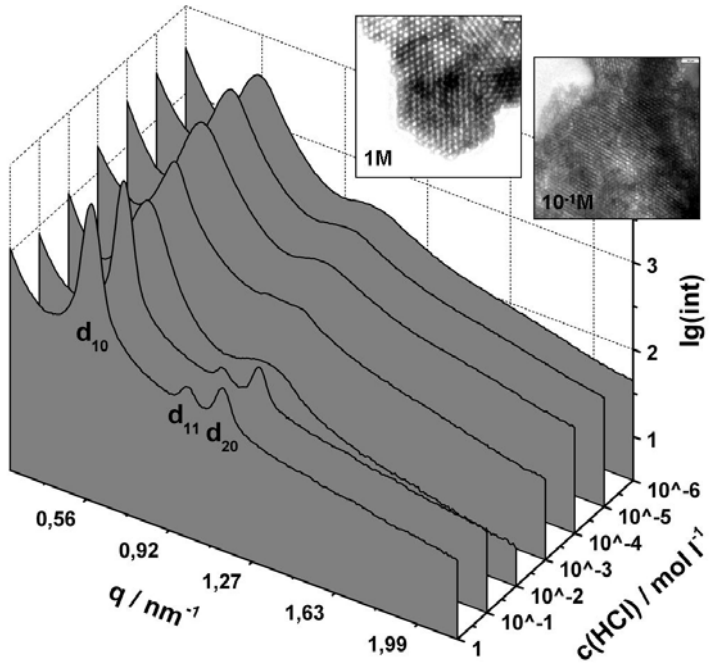

Figure 16 SAXS pattern of the dried silica monoliths prepared at different HCl concentrations.

This trend can also be tracked for the evolution of the macroporous morphology. (Figure 17) For high acid concentrations the macroporous network is formed by rod-shaped silica strands, which enclose the macropores (1 and 10^{-1} M).

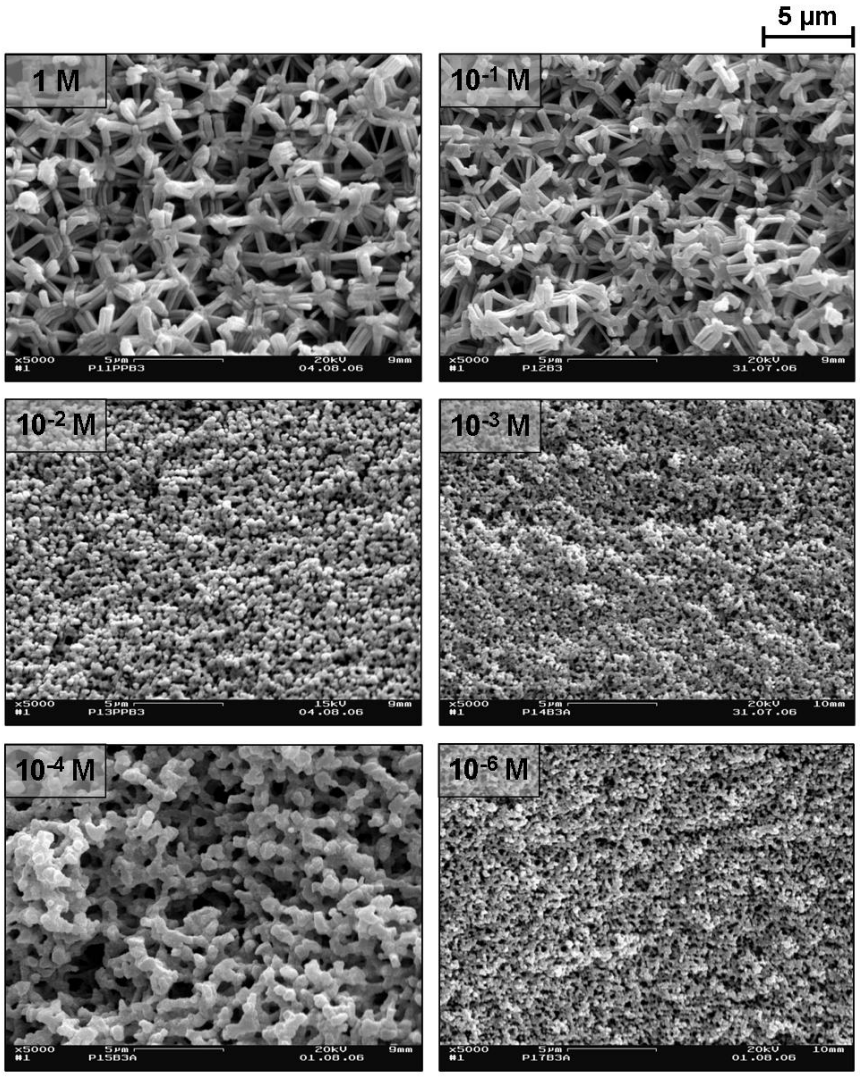

Figure 17 SEM images of the silica gels prepared with different HCl concentration.

Even though the gelation time and the delayed on-set of phase separation indicate the nucleation and growth mechanism for the evolution of the macroscopic domains, the high interconnectivity and the well-ordered arrangement of silica rods are characteristics for spinodal decomposed materials.

In order to investigate the evolution of the macropore size domains during aging, silica gels (Si / P123 / 1 M HCl = 8.4 / 30 / 70) were quenched via silylation with chlorotrimethylsilane (TMCS) in petroleum ether directly after the gelation and after 1, 2, and 23 h of aging. The quenching of the aging process inhibits further condensation reactions and re-arrangement processes. The resultant macroporous morphologies are presented in figure 18.

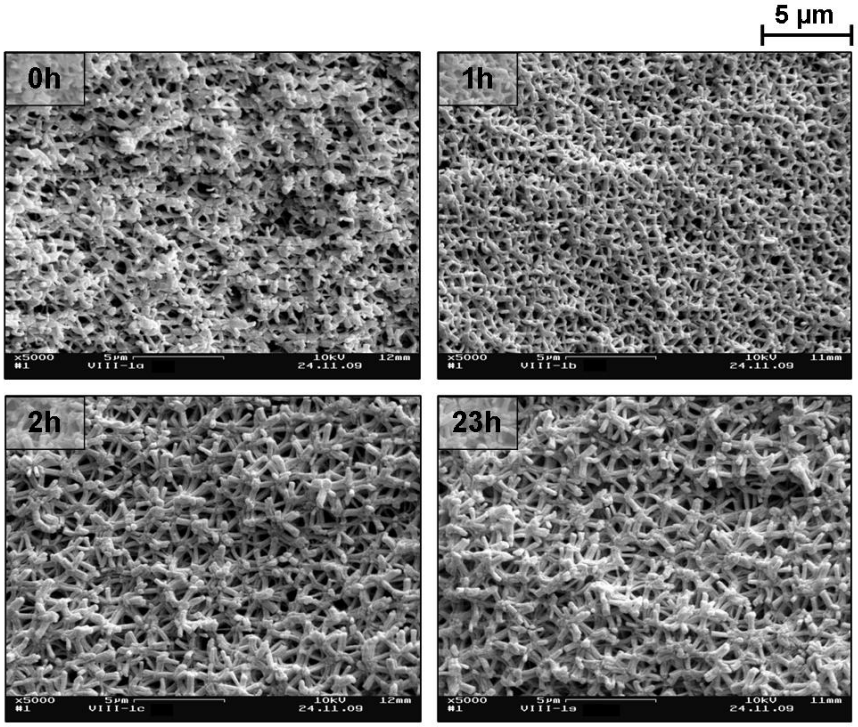

Figure 18 Evolution of the macroporous morphology of the silica gels quenched immediate (0 h), 1, 2, and 23 h after gelation. The composition of the gels were constant with
Si / P123 / 1M HCl = 8.4 / 30 / 70 by weight for all presented silica gels.

As seen in figure 18, the quenching immediately after the gelation results already in a co-continuous macroporous morphology, which is formed by silica strands. Due to the weakly cross-linked silica network shortly after the gelation, the quenching with TMCS causes a strong shrinkage and deformation of the monolithic gel body, which is also obvious from random agglomerations and deformations within the macroporous framework.

After 1 h of aging, an ordered interconnected macroporous framework is obtained with macropores of uniform size. With further aging for 2 h and 23 h, coarsening of the macropore network occurs in order to reduce interfacial energies. The silica strands consist of agglomerated silica rods that form the interconnected macroporous framework. According to Nakanishi et al., the early existence of the interconnected macroporous framework is an indication for the spinodal decomposition.[105] The resultant macroporous morphology is strongly dependent on the time interval between the on-set of phase separation and the sol-gel transition. If gelation and phase separation occur in quick succession, aging processes such as Ostwald ripening are limited resulting in a fine macroporous network. This phenomenon can be seen for the macroporous morphology of the silica monoliths prepared at 10^{-3} and 10^{-6} M

HCl presented in figure 17. For these sol-gel systems, gelation and phase separation occur almost concomitantly as can be seen from figure 14 ($t_g(10^{-3}$ M) = 17 min and $t_{PS}(10^{-3}$ M) = 22 min; $t_g(10^{-6}$ M) = 2 min and $t_{PS}(10^{-6}$ M) = 3 min), resulting in macroporous networks with diffuse interfaces. The enclosed macropores possess a relatively broad pore radii distribution in the range of 0.1 μm as can be seen from figure 19.

With increasing time interval between sol-gel transition and phase separation, aging processes such as Ostwald ripening cause a coarsening of the macroporous framework in order to reduce interfacial energies. The Ostwald ripening is a thermodynamically driven process, in which large particles (energetically favoured due to the low ratio of surface to volume) grow at the expense of small particles.

The coarsening of the macroporous structure is observed for the silica gels prepared at 1, 10^{-1} and 10^{-4} M HCl, which in accordance exhibit delayed time intervals for the phase separation. As presented in figure 14, the macroscopic sol-gel transition of the gels prepared at 1 and 10^{-1} M HCl occurs after 66 min and for the latter at 178 min, whereas the phase separation takes 184 min at 1 M HCl. For comparison, the sol-gel system at 10^{-4} M HCl is already gelled after 3 min and the phase separation occurs after 17 min. For all three HCl concentrations, sharp interfaces of the macropore domains are observed (as can be seen from figure 17) exhibiting uniform macropores with radii of R^{Hg} = 0.3 μm. (Figure 19)

The time for the coarsening procedure is only limited to a certain period which finally disrupts and results in the fragmentation of the structure and sedimentation occurs. Due to the exceptional time interval between the onset of phase separation (t_{PS} = 1179 min) and the sol-gel transition (t_g = 235 min) observed for the system at 10^{-2} M HCl in combination with the resulting particulate macroscopic morphology of the gels, the evolution of the macroporous network cannot be assigned to either spinodal decomposition or to the nucleation and growth mechanism. The resultant macroporous framework is no longer formed by rod-shaped silica strands, but consists of sintered particles, which enclose randomly distributed macropores of nonuniform size as can be seen from figure 17 and 19.

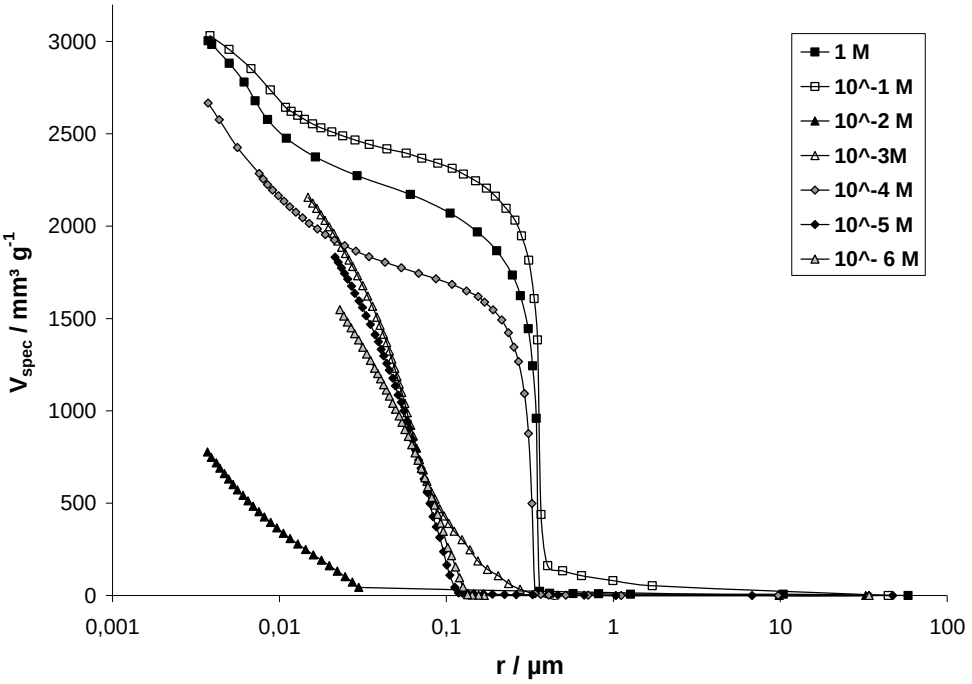

Figure 19 Macropore radii distribution of the silica gels prepared at varying HCl concentrations.

The macroscopic morphology of the silica gels prepared at 1 and 10^{-1} M HCl highly resembles SBA-15 materials with rod-shaped silica strands. These materials are normally synthesized by either employing fluoride or high salt concentrations to enhance the ionic strength of the system.[106-108] In comparison, the silica monoliths prepared with EGMS as sole precursor in presence of high concentrations of Pluronic P123 in strong acidic aqueous solution, do not require further additives in order to evolve the rod-like morphology. It is known from literature, that the ratio of water / silicon alkoxide is crucial for the final silica network architecture. For low water contents (water / silicon alkoxide ≤ 2) silica gels with a low degree of cross-linking are formed resulting in a rather high amount of unreacted alkoxy groups in the gel network which makes these systems adequate candidates for the synthesis of fibres and coatings. In contrary, a high water content (water / silicon alkoxide ≥ 4) results in silica networks with a high degree of cross-linking. These systems allow for the synthesis of monolithic materials in which silanol groups dominate the surface behaviour of the gels.[92] Due to the high acid concentration, the ratio of Si / water is theoretically reduced for the EGMS-derived sol-gel systems at 1 and 10^{-1} M, however, as an excess of water was employed (water / EGMS ~ 12) the reduction is negligible.

Investigations of other diol-modified silanes with longer alkyl chains as precursors for the preparation of monolithic silica materials exhibited, that EGMS is the only precursor, which

produces rod-shaped silica strands. The employment of the propylene glycol-modified silane already results in a particulate morphology consisting of spherical particles. This observation indicates that the polarity of the released ethylene glycol during hydrolysis and condensation reactions has a high impact on the formation of the silica rods.

2.1.4. Composition of the Template Phase and the Si-Content

The investigations of the influence of the HCl concentration have indicated, that both the formation of a well-organized mesoporous arrangement as well as the evolution of the macroscopic framework are very sensitive towards changes within the synthesis parameters. To examine the impact of changes in the composition for the resultant silica monoliths, the composition of the template phase as well as the content of Si are varied. Based on the experiments in section 2.1.3., the influence of the HCl concentration was also taken into account. For the investigations of the impact of the template composition, the ratio of P123 to HCl has been varied from 10 / 90 up to 40 / 60 by weight, whereas EGMS has been employed as sole precursor and the Si content has been kept constant with 8.4 wt %. Higher quantities of the block co-polymer resulted in an inhomogeneous template phase at 40°C, and have therefore not been taken into account. For all samples' series, the HCl concentration has been changed in the range from 1 – 10^{-4} M. The container material of the used vessels is poly(methyl methacrylate) (PMMA) and all silica gels have been cured in a mixture of ethanol-HCl after aging for 7 days at 40°C. In table 5 the physicochemical characteristics of the different silica monoliths synthesized with 1 and 10^{-1} M HCl are presented. The data of the silica monoliths prepared with 10^{-2} – 10^{-4} M HCl are listed in the experimental section.

Table 5 Physicochemical characteristics of the silica gels prepared with varied composition of the template phase and at different HCl concentrations.

samples		SAXS	N_2-sorption			Hg-Porosimetry	
	c_{HCl} /mol l^{-1}	d_{10} /nm	S^{BET} /m^2 g^{-1}	D_{BJH} /nm	t_{wall} /nm	R^{Hg} /μm	V^{Hg} /cm^3 g^{-1}
P10-90-0	1	11.2	831	3.4	9.5	1.3	3.1
P20-80-0	1	11.3	905	5.3	7.7	0.3	3.7
P30-70-0	1	11.5	891	6.2	7.1	0.2	3.3
P40-60-0	1	12.1	1085	5.2	8.8	-*	-
P10-90-1	10^{-1}	11.6	731	4.0	9.4	0.4	3.7
P20-80-1	10^{-1}	11.3	924	4.2	8.8	0.4	3.6
P30-70-1	10^{-1}	11.2	912	4.9	8.0	0.5	3.4
P40-60-1	10^{-1}	11.3	800	3.7	9.4	0.5	2.6

* no uniform pore size distribution was obtained for this sample.

Investigations of the shrinkage exhibit in analogy to the precedent section, that the shrinkage of the length linearly decreases for the silica monoliths prepared below 10^{-1} M for all compositions. (Figure 20) Among the composition variation, the length of the silica monoliths is more affected for high P123 contents with values up to 15% of shrinkage at 10^{-1} M HCl than for the ones synthesized with lower quantities of P123. For P132 / 10^{-4} M HCl = 30 / 70 and 40 / 60, the gelation has occurred too fast so that these sol-gel systems did not allow for the transfer into the PMMA vessels. The trend of the shrinkages for high P123 quantities is also observed for the shrinkage of the monoliths' diameter along with the HCl variation. Interestingly, the silica monoliths prepared with Si / P123 / 1 M HCl = 8.4 / 10 / 90 show an uncommon high shrinkage of 19% compared to the gels prepared with lower HCl concentrations (4 – 6%). This deviation can be related to the macroporous morphology of the resultant silica monoliths. The SEM pictures of these monoliths exhibit (Figure 22), that the macroporous framework is not formed by regular arranged well-defined silica strands like at Si / P123 / 1 M HCl = 8.4 / 20 / 80 or 8.4 / 30 / 70. In addition, the enclosed macropores are larger with R^{Hg} = 1.3 μm than for the gels prepared with the higher P123 contents (of 20 and 30 wt %, R^{Hg} = 0.2 – 0.3 μm).

Furthermore, the monolith synthesized with the composition of 8.4 / 10 / 90 at 10^{-1} M HCl exhibits a less coarsened macroscopic morphology with smaller macropores (R^{Hg} = 0.4 μm) as can be seen from figure 24 and the resultant shrinkage is reduced to 5%.

Investigations of the shrinkage behaviour of EGMS-derived silica gels by the group of Hoffmann exhibited shrinkages of 44 – 47% when sols of 50 wt % and nominal pH-values of 0 and 1 were employed. For the gels prepared from pure water shrinkages of 30% were obtained. These gels were synthesized without the employment of a structure-directing agent and were supercritically dried with CO_2.[109] In order to reduce the shrinkage of the gel bodies, a new approach was chosen by adding small quantities of the cationic precursor *N*-[(trimethoxysilyl)proyl]-*N*,*N*,*N*-trimethylammonium chloride to the glycol-modified silane resulting in gels with ionic charges within the silica network.[110] By this approach the shrinkage of the wet gels (prepared at the nominal pH 7) could be drastically reduced due to the repulsive interactions of the positive charges within the SiO_2 network, however, the shrinkage during the drying procedure was even enhanced with values up to 50%.[109, 110]

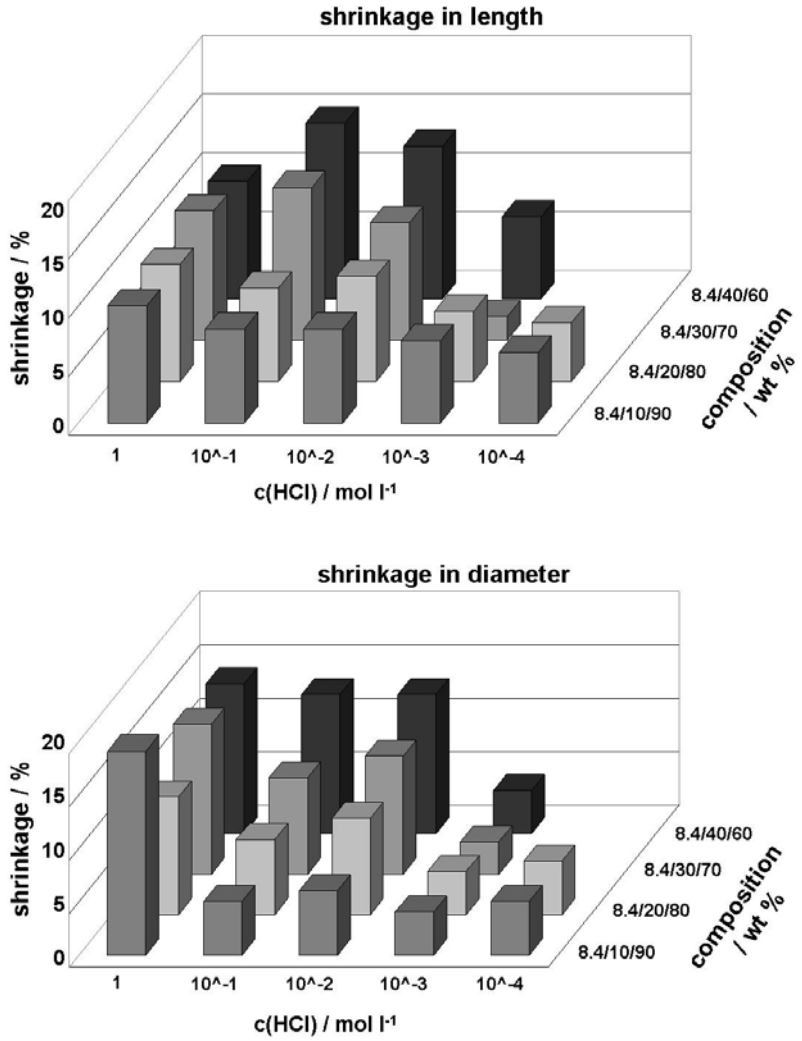

Figure 20 Diagrams illustrating the shrinkage in length and diameter at varying template compositions and HCl concentrations.

SAXS experiments on the silica monoliths prepared with 1 M HCl show (figure 21), that all samples possess a 2D-hexagonal mesopore arrangement with values for the repeating unit d_{10} of 11 – 12 nm. The composition Si / P123 / 1 M HCl = 8.4 / 10 / 90 exhibits the smallest repeating unit distance with d_{10} = 11.2 nm which increases to d_{10} = 12.1 nm for the highest content of P123 (40 wt %). The diffraction pattern of the silica gels prepared at low contents of P123 (10 and 20 wt %) exhibit the reflections for the (10), (20) and the (21) diffractions at q_{10} = 0.6 nm^{-1}, q_{20} = 1.1 nm^{-1} and q_{21} = 1.5 nm^{-1}. The sample synthesized with 30 wt % does not exhibit the signal for the (21) diffraction, however, besides the diffraction peaks for the (10) and the (20) diffraction, the signal for the (11) reflection is present indicating the 2D-hexagonal array of the mesopore system (q_{10} = 0.6 nm^{-1}, q_{11} = 1.0 nm^{-1}, q_{20} = 1.1 nm^{-1}). At 40°wt % a loss of the long-range ordering is observed and the resolution of the diffraction pattern is reduced to two broad diffraction peaks which can be related to the (10) and the (20) diffractions at q_{10} = 0.5 nm^{-1} and q_{20} = 1.1 nm^{-1}.

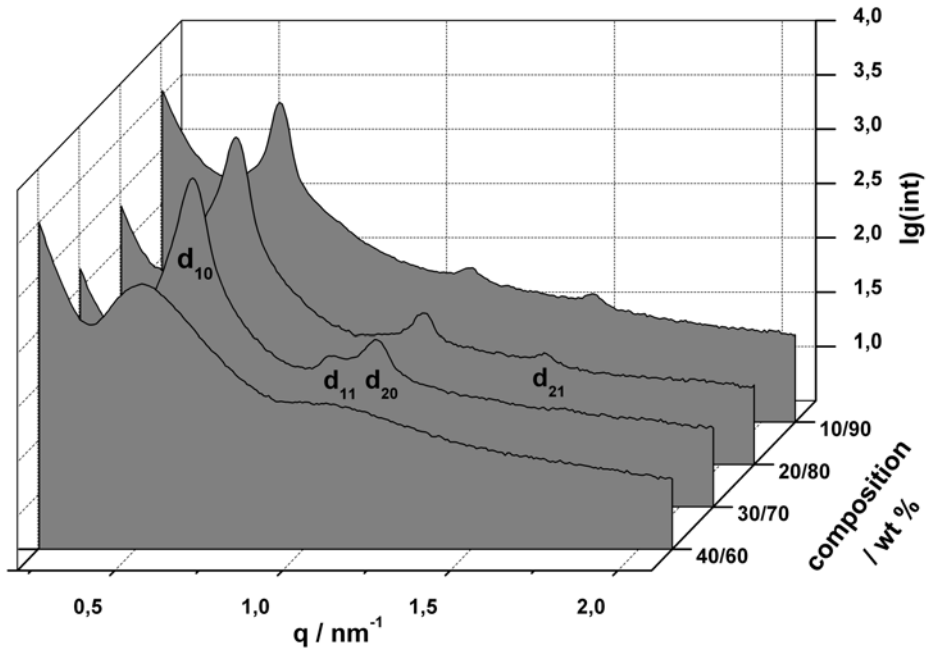

Figure 21 SAXS pattern of the resulting mesostructure of the silica monoliths prepared with different template compositions at 1 M HCl. The composition itemized at the y-axis refers to the ratio of P123 / 1 M HCl, whereas the Si-content was constant with 8.4 wt %.

As mentioned above, the macroporous morphology of the silica monoliths of the composition Si / P123 / 1 M HCl = 8.4 / 10 / 90 differs from the other samples. (Figure 22) The samples of the composition 8.4 / 20 / 80 and 8.4 / 30 / 70 show the well-arranged macroporous

framework formed by rod-shaped silica strands, however, with reduced P123 content, a coarsened morphology with macropores of 1.3 μm in radius result which is also affirmed by mercury intrusion measurements as can be seen from figure 23. In contrast, by increasing the ratio of P123 / 1 M HCl above 30 / 70, the rod-like morphology is replaced by a particulate and densified macroporous framework with pores of non-distinct size. (Figures 22 and 23) The gelation times t_g for the gels of all composition are alike with about 60 min. However, while the sol-gel transition of the silica monoliths of the compositions 8.4 / 10 / 90 to 8.4 / 30 / 70 occur concomitantly with the phase separation, the gels of 8.4 / 40 / 60 turn turbid after 180 min. This time interval allows for a longer particle growth period at expense of the rod-like morphology and the narrow macropore size distribution.

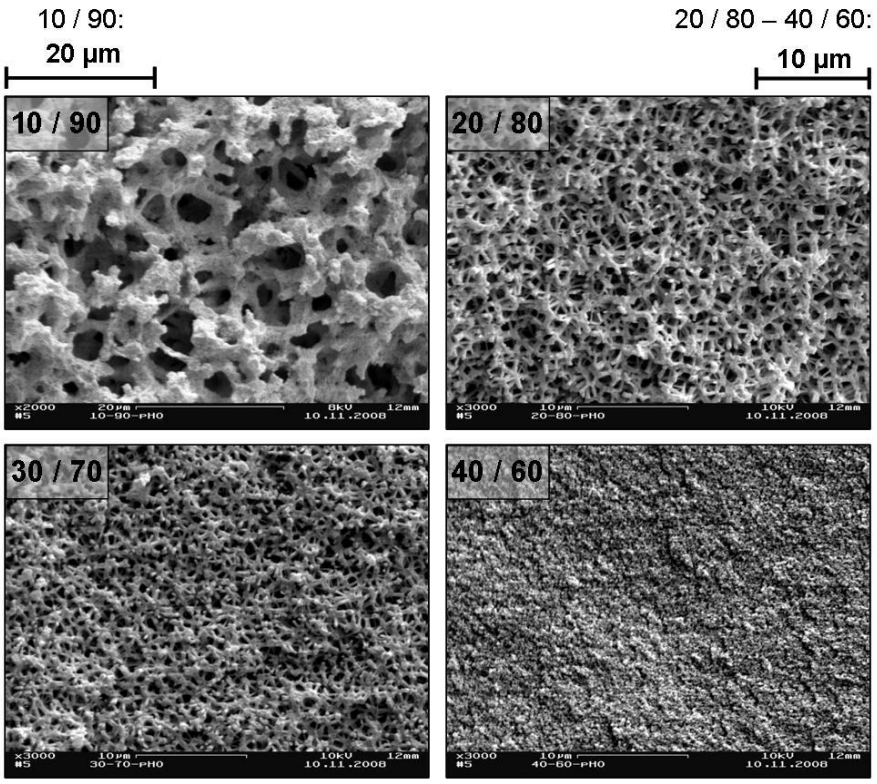

Figure 22 SEM images presenting the macroporous morphology of the silica monoliths prepared with varied template composition at 1 M HCl. The SEM image of the sample 10 / 90 (top, left) has been taken with 2000-times magnification (20 μm scale bar); all other images have been recorded with 3000-times magnification (10 μm scale bar).

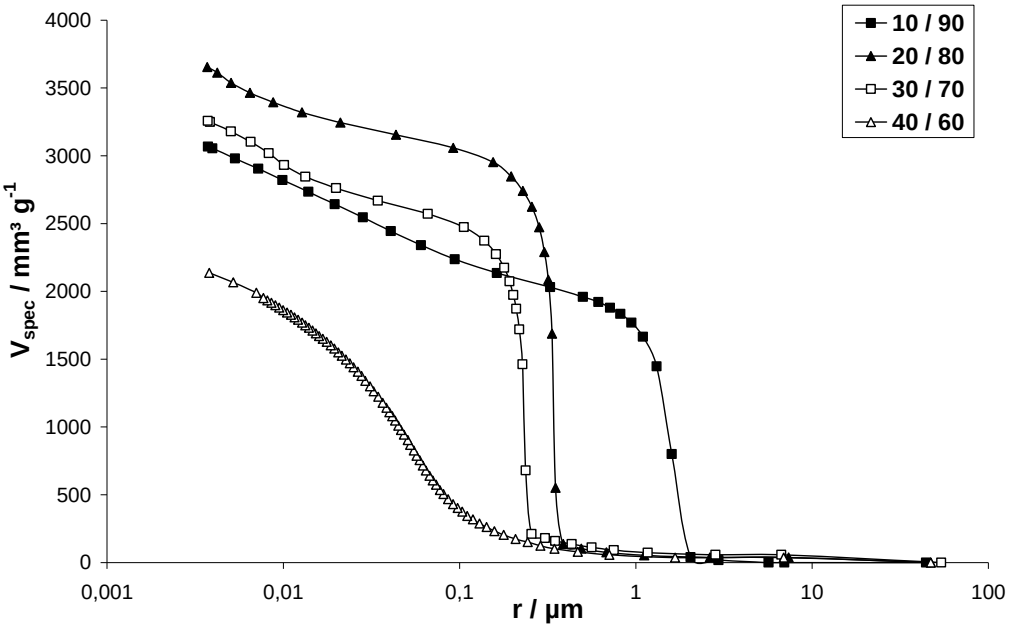

Figure 23 Macropore radii distribution of the silica gels derived from varied template composition at 1 M HCl.

In accordance to the gel series at 1 M HCl, all silica monoliths prepared with 10^{-1} M HCl exhibit 2D-hexagonally arranged mesopore networks with repeating units for the (10) diffraction in the range of d_{10} = 11 – 12 nm as can be seen from figure 24. With increasing content of P123 from 10 to 30 wt %, the SAXS pattern reveal a evolution of the 2D-hexagonal arrangement in the long-range ordering. The SAXS curve of the sample synthesized with 10 wt % P123 exhibits only one pronounced diffraction peak for the (10) diffraction at q_{10} = 0.5 nm^{-1} and two minor reflections for the (20) and the (21) diffractions at q_{20} = 1.1 nm^{-1} and q_{21} = 1.4 nm^{-1} resulting in a repeating unit distance of d_{10} = 11.6 nm. At 20 wt % the corresponding diffraction peaks at q_{10} = 0.6 nm^{-1}, q_{20} = 1.1 nm^{-1} and q_{21} = 1.5 nm^{-1} are more prominent compared to the resolution of the diffraction pattern observed at 10 wt % P123. The silica gel obtained from 30 wt % exhibits additional to the signals for the (10), (20), and (21) diffractions also the reflection for the (11) diffraction (q_{10} = 0.6 nm^{-1}, q_{11} = 1.0 nm^{-1}, q_{20} = 1.1 nm^{-1} and q_{21} = 1.5 nm^{-1}). In analogy to the observations made for the silica gels obtained at 1 M HCl, the SAXS pattern of the silica gels synthesized with 40 wt % exhibit a reduction of the mesoscopic ordering with only two pronounced reflections for the (10) and the (20) diffractions at q_{10} = 0.6 nm^{-1} and q_{20} = 1.1 nm^{-1}.

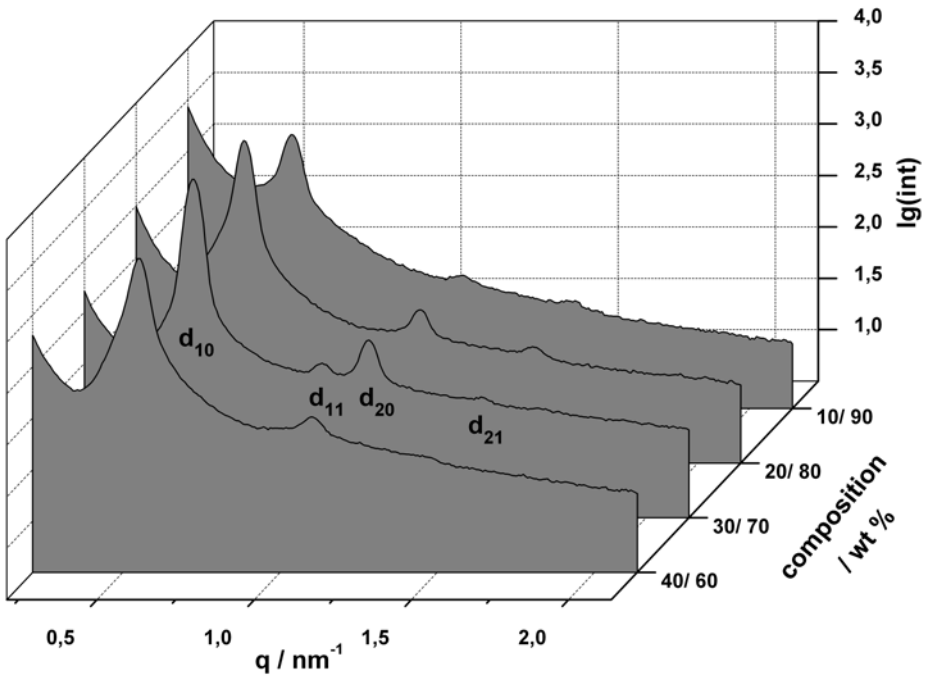

Figure 24 SAXS pattern illustrating the evolution of the mesoscopic ordering for a varied template composition at 10^{-1} M HCl. The composition itemized at the y-axis refers to the ratio of P123 / 10^{-1} M HCl, whereas the Si-content was constant with 8.4 wt %.

Unlike the gel series at 1 M HCl, the sol-gel transition of the gels prepared at 10^{-1} M HCl occurs after few hours directly accompanied by the phase separation in the macroscopic range. All silica gels prepared at this HCl concentration exhibit a well-defined macroscopic architecture resulting in a narrow pore size distributions with pores of 0.4 – 0.5 μm in radius as can be seen from figures 25 and 26.

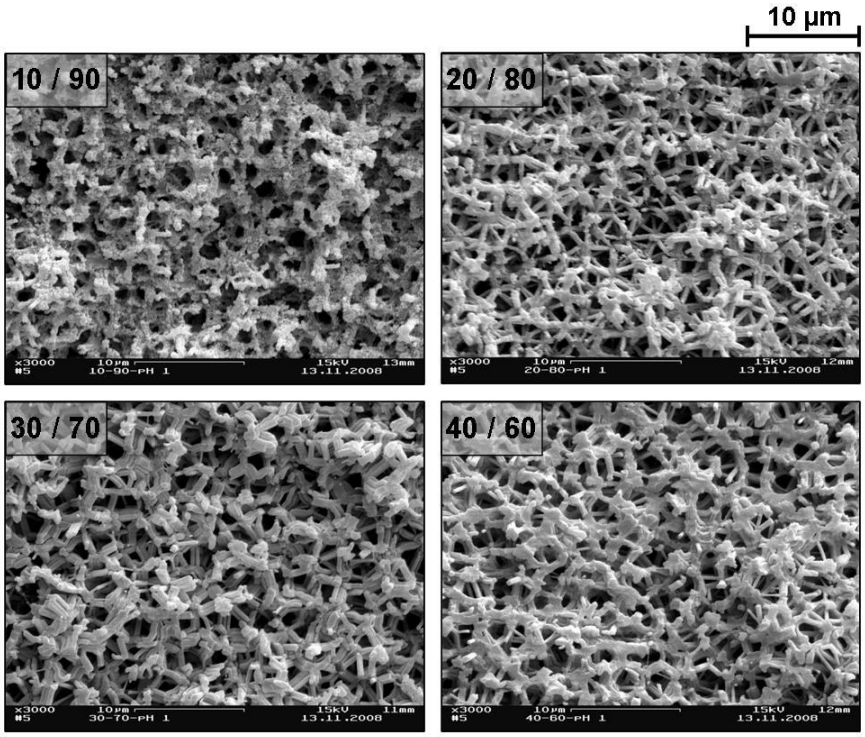

Figure 25 SEM images presenting the evolution of the macroporous morphology with varying template composition at 10^{-1} M HCl.

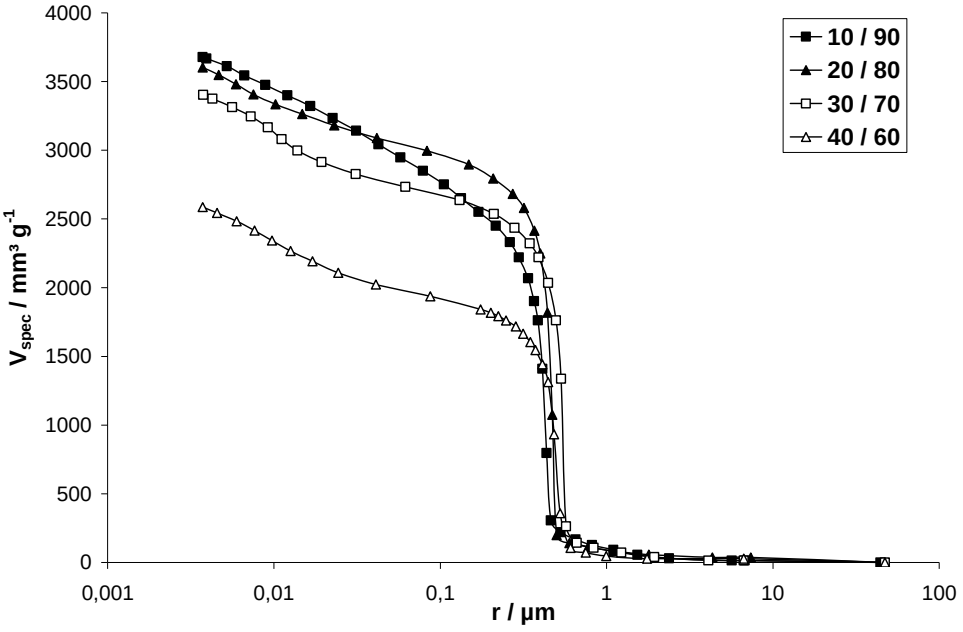

Figure 26 Macropore radii distribution of the silica gels prepared with varying composition of the template phase (P123 / 10^{-1} M HCl = 10 / 90 – 40 / 60 wt %).

In the here employed system, the ethylene glycol-modified silane (EGMS) acts as silicon source. During hydrolysis and condensation reactions, ethylene glycol is released which leads to the dilution of the template phase. In order to avoid a further dilution of the system, the influence of lower Si contents has been subject to investigation.

For the synthesis of the gel series, the HCl concentration as well as the composition of the template phase have been constant with c(HCl) = 1 M and the ratio of P123 / 1 M HCl = 30 / 70. Instead of PMMA vessels, smaller polyethylene moulds have been chosen. All silica gels were dried via surface hydrophobization with TMCS before they were heated up to 200°C.

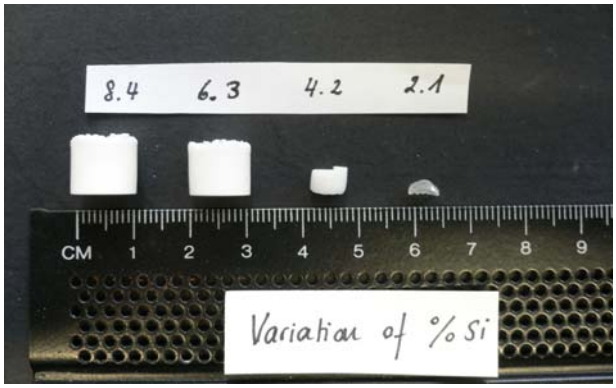

Figure 27 Photo of the resultant silica monoliths prepared with different Si contents in the range of 8.4 to 2.1 wt %(from left to right). The HCl concentration has been kept constant at 1 M.

As can be seen from figure 27, starting from %Si = 4.2 wt % the gels lose the turbidity with further decreasing content of Si. This trend indicates that the system loses its tendency to phase separate with decreasing Si content. This effect is a result of a lower degree of cross-linking of the siloxane polymers / oligomers resulting in a high amount of unreacted terminal silanol groups and hence in the inhibition of the induction of the phase separation due to the missing gradient in polarity between the polar solvent-rich phase and the silica-rich phase. This trend can also be observed from the gelation times. The silica gels prepared with Si-contents of 8.4 and 6.3 wt % are gelled after 79 min and 56 min (for the latter) and the phase separation occurs after 224 and 221 min. The gels synthesized with Si-contents of 4.2 wt % already exhibit longer gelation times with 110 min and a drastically delayed time for the phase separation of 1715 min. By even further reduction of the Si-content to 2.1 wt %, the sol-gel transition is only reached after 303 min and no phase separation is induced. Table 6 gives the

physicochemical data obtained by SAXS, nitrogen sorption and mercury intrusion measurements.

Table 6 Physicochemical characteristics of the silica gels prepared with varied Si content at the constant ratio of P123 / 1 M HCl = 30 / 70.

		SAXS	*N_2-sorption*			*Hg-Porosimetry*	
samples	*%Si*	d_{10}	S^{BET}	D_{BJH}	t_{wall}	R^{Hg}	V^{Hg}
	/wt %	*/nm*	*/m² g⁻¹*	*/nm*	*/nm*	*/µm*	*/cm³ g⁻¹*
P1-01q	8.4	10.9	759	5.7	6.9	0.2	2.4
P30-01	6.3	9.5	871	3.5	7.5	0.3	2.3
P31-01	4.2	10.6	715	3.3	8.9	-	-
P32-01	2.1	-	670	3.2	-	-	-

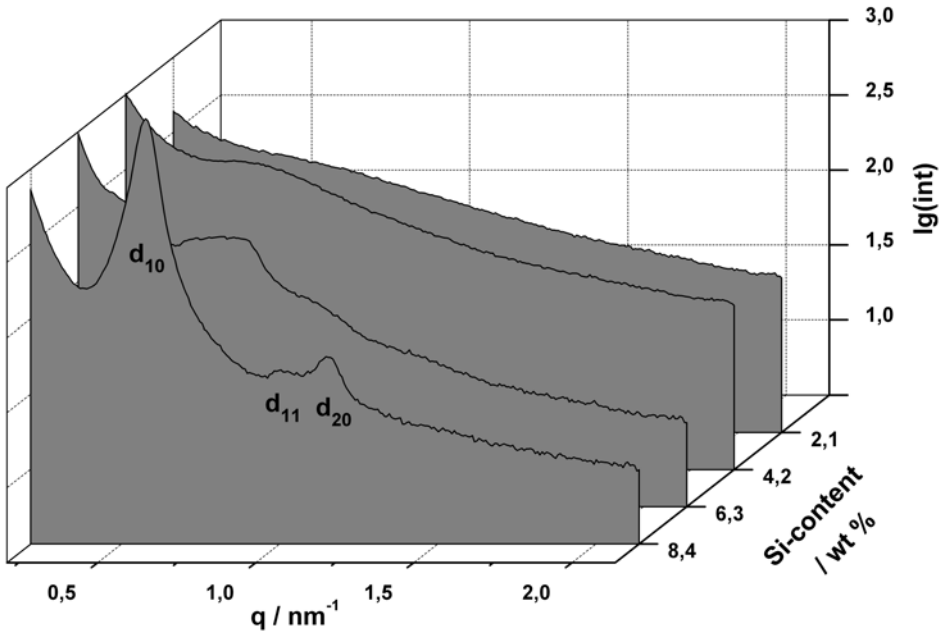

Figure 28 SAXS pattern of the development of the periodical with decreasing Si-content. From front to back, the Si-content was decreased from 8.4 to 2.1 wt %, while the ratio of P123 / 1 M HCl was constant at 30 / 70 by weight.

SAXS and SEM investigations (figures 28 and 29) confirm the trend of a decreasing development of the hierarchical pore size domains. The formation of a well-defined mesopore arrangement in the resultant silica gels is already impaired at %Si = 6.3 wt %. At %Si = 8.4 wt %, the SAXS diagram shows the diffraction peaks of the (10), (11), and (20)

diffractions at q_{10} = 0.6 nm^{-1}, q_{11} = 1.0 nm^{-1}, and q_{20} = 1.2 nm^{-1} resulting in a repeating unit distance of d_{10} = 10.9 nm. However, already at a Si-content of %Si = 6.3 wt % the SAXS curve does not allow for an explicit indexing to a symmetrical pattern, as the primary diffraction peak is very broad and its decreasing slope exhibits a shoulder indicating the presence of another type of arrangement.

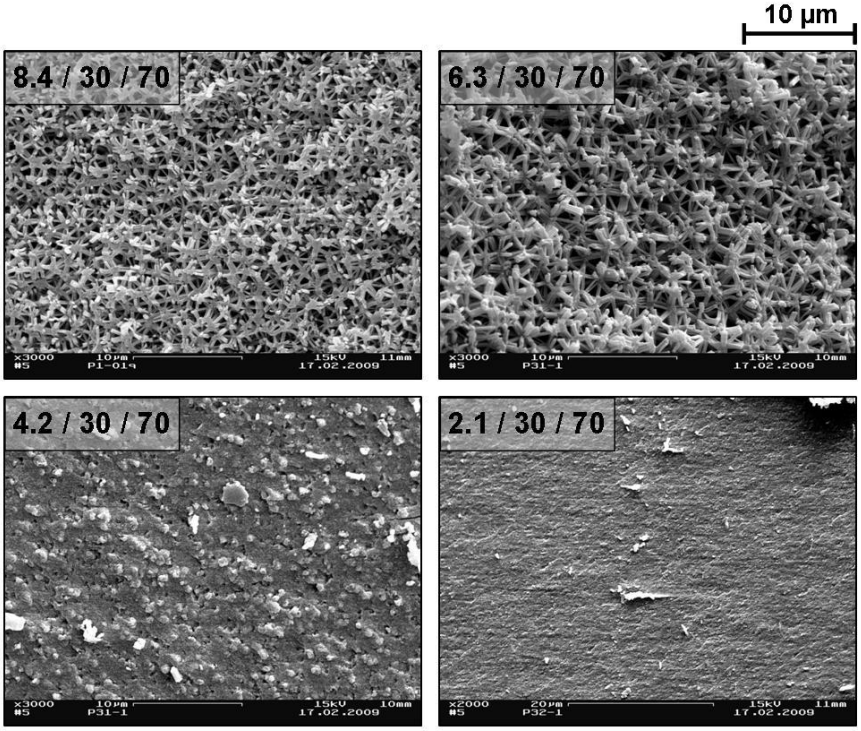

Figure 29 SEM pictures presenting the decreasing distinctive macroporous morphology of the silica monoliths with reduced Si content. All samples were prepared with P123 / 1 M HCl = 30 / 70 by weight.

The SEM images in figure 29 reveal that until %Si = 6.3 wt % the macroscopic framework is still formed by rod-shaped silica strands which enclose interconnected macropores of 0.2 to 0.3 μm in radius. Below a Si-content of 6.3 wt % no macropore network is formed, but a smooth surface is reached at %Si = 2.1 wt % on this length scale.

2.1.5. The Acid Anion

The hierarchical ordering of the different pore regimes for high HCl ($c(HCl) \geq 10^{-1}$ M) concentrations indicates that the formation of the mesoporous structure proceeds according to the $S^0(XI)^0$ mechanism (see also section 1.3.2.2.) with an enhanced tendency to form hydrogen bonds between the cationic silica species and the hydrophilic EO units of the EO_{20}-PO_{70}-EO_{20} block co-polymer. As the silica species is positive charged at $c(HCl) \geq 10^{-1}$ M, it is assumed that the counterion, the acid anion, acts as charge equalizer between the cationic silica species and the amphiphilic block co-polymer. To examine the influence of the counterion, different inorganic acids such as HCl, HNO_3, H_2SO_4, $HClO_4$ and the organic acid CF_3COOH were employed and all systems were adjusted to pH 1. Again, the composition of the sol-gel system was kept constant with Si / P123 / acid = 8.4 / 30 / 70 and EGMS was used as sole precursor. All silica gels were subsequently surface silylated with TMCS before they were dried at 200°C. The gelation times for the different gels varied with $CF_3COOH \approx H_2SO_4 < HNO_3 \approx HCl < HClO_4$ from 130 min up to 280 min, which is in accordance with the acidic strengths (listed in table 7), which increase from CF_3COOH to $HClO_4$ considering the two-step dissociation of H_2SO_4.[111]

Table 7 pKa-values of the acids and the observed times for the gelation and the phase separation for the particular acid employed.

sample	*acid*	*pKa-values* [111] *acid in H_2O*	t_g */min*	t_{PS} */min*
P1-2-a	HCl	-8.0	175	>360
P1-2-b	HNO_3	-1.3	160	>360
P1-2-c	H_2SO_4	-3.0, 1.99*	130	>300
P1-2-d	$HClO_4$	-10.0	280	>270
P1-2-e	CF_3COOH	-0.25	130	>240

*determined for the first and the second dissociation step.

Table 8 lists the analytical results obtained from nitrogen sorption and mercury intrusion experiments as well as SAXS investigations for the silica gels prepared with the different acids.

Table 8 Physicochemical data of the silica gels prepared with different acids at the nominal pH 1.

samples	acid	SAXS	N_2-sorption			Hg-Porosimetry	
		d_{10} /nm	S^{BET} /$m^2\,g^{-1}$	D_{BJH} /nm	t_{wall} /nm	R^{Hg} /μm	V^{Hg} /$cm^3\,g^{-1}$
P1-2-a	HCl	10.9	890	5.0	7.6	0.3	0.9
P1-2-b	HNO_3	8.8	984	-	-	0.4	1.5
P1-2-c	H_2SO_4	10.8	1045	3.5	9.0	0.5	1.9
P1-2-d	$HClO_4$	9.0	686	3.2	7.2	0.4	1.8
P1-2-e	CF_3COOH	8.2	610	3.4	6.1	0.6	1.6

Interestingly, the formation of the macroporous morphology is not affected by the change of the counterion. As can be seen by the SEM images in figure 32 all silica gels exhibit a co-continuous macroporous silica network formed by rod-shaped silica strands. Results from mercury intrusion measurements confirm that the enclosed macropores exhibit a narrow pore radii distribution in the range of 0.3 – 0.6 μm as can be seen from figure 31. However, the resultant mesoscopic ordering is highly affected by the change of the acid anion. The SAXS pattern of the silica gels reveal that only the sample prepared with H_2SO_4 exhibits the same *d* spacing ($d_{10} \approx 10.8$ nm) for the (10) reflection as usually obtained with HCl. (Figure 30)

The employment of HCl results in silica gels exhibiting the highest degree of mesoscopic ordering with diffraction peaks for the (10), (11) and the (20) diffractions at $q_{10} = 0.6\ nm^{-1}$, $q_{11} = 1.0\ nm^{-1}$, and $q_{20} = 1.2\ nm^{-1}$. The SAXS curves of the silica monoliths synthesized by using H_2SO_4 as acidic catalyst show the reflections for the (10) and the (20) diffractions at $q_{10} = 0.6\ nm^{-1}$ and $q_{20} = 1.2\ nm^{-1}$, however, a shoulder is present in the pattern at $q \approx 0.7\ nm^{-1}$ indicating that besides the 2D-hexagonal arrangement of the mesopores a further structural array is present.

The employment of $HClO_4$, HNO_3, and CF_3COOH results in silica gels for which a decreasing degree of the 2D-hexagonal ordering is observed. Each reflection of the first ordering is shifted to larger values for the scattering vector q with $q_1(HClO_4) = 0.7\ nm^{-1}$, $q_1(HNO_3) = 0.7\ nm^{-1}$, and $q_1(CF_3COOH) = 0.8\ nm^{-1}$. Interestingly, the shift of the scattering vector coincides with the q-value of the shoulder observed when H_2SO_4 is used as catalyst indicating a change of the pore arrangement in the mesoscopic range. The loss of reflections within the SAXS pattern from H_2SO_4 to CF_3COOH is assumably related the loss

of the 2D-hexagonal array with a long-range ordering to a arrangement which only exhibits a certain degree of periodicity in the short-range.

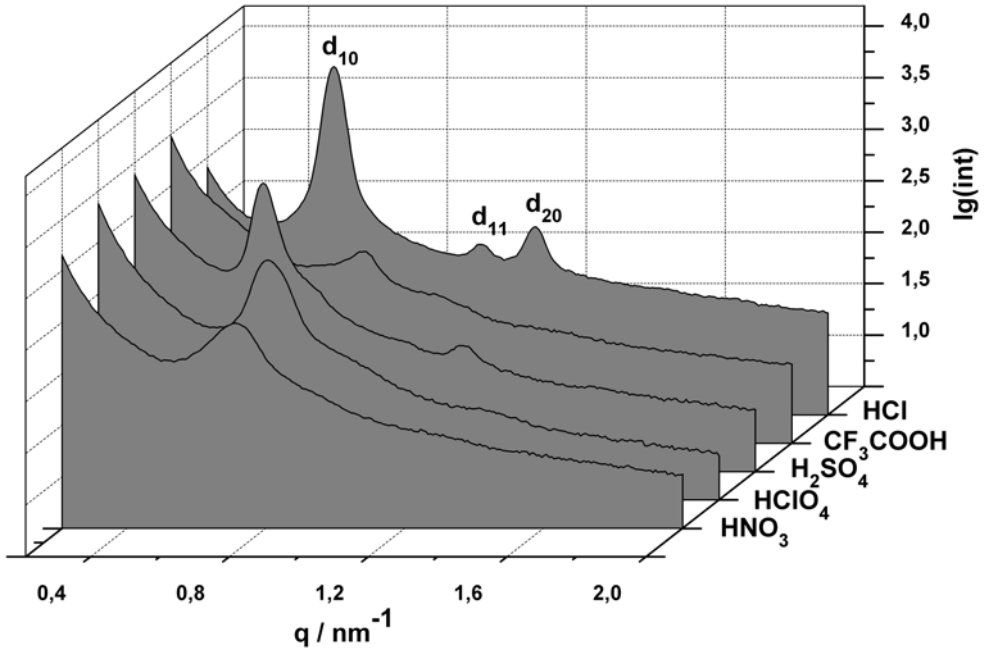

Figure 30 SAXS pattern for the mesoscopic ordering of the silica gels prepared with the different acids arranged from HNO_3, $HClO_4$, H_2SO_4, and CF_3COOH up to HCl.

The radius and the charge of the anion and the strength of the acid play important roles in the aggregation behaviour of the silica oligomers and the organic template phase. Zhao et al. proposed a $(S^0H^+)(X^-I^+)$ pathway for the assembly of the silica / polymer mesophase in acidic media (below pH 2) based on the combination of electrostatic, hydrogen bonding, and van der Waals interactions. The anion is assumed to be coordinated directly to the silicon atom through expansion of the silicon atom's coordination sphere.[21] It is known from literature, that the anion affects the self-assembly of the surfactant as well as the co-assembly of precursor / surfactant in solution.[112] For the anions Cl^- and SO_4^{2-} a positive contribution to the formation of the mesoscopical arrangement was found, while the presence of ClO_4^- and NO_3^- resulted in a less pronounced mesoporous ordering. The results for Cl^-, SO_4^{2-} and NO_3^- agree with the trend found for the morphology control of SBA-15 mesoporous silica by the group of Chao.[112] However, CF_3COO^- disturbs the formation of the 2D-hexagonal arrangement of the mesopores, which is probably caused by the hydrophobic CF_3-moiety of the acid anion, which favours the neighbourhood of the hydrophobic block of the

template / solvent assembly instead of the interphase between the silica species and the hydrophilic domains of the template / solvent assembly.

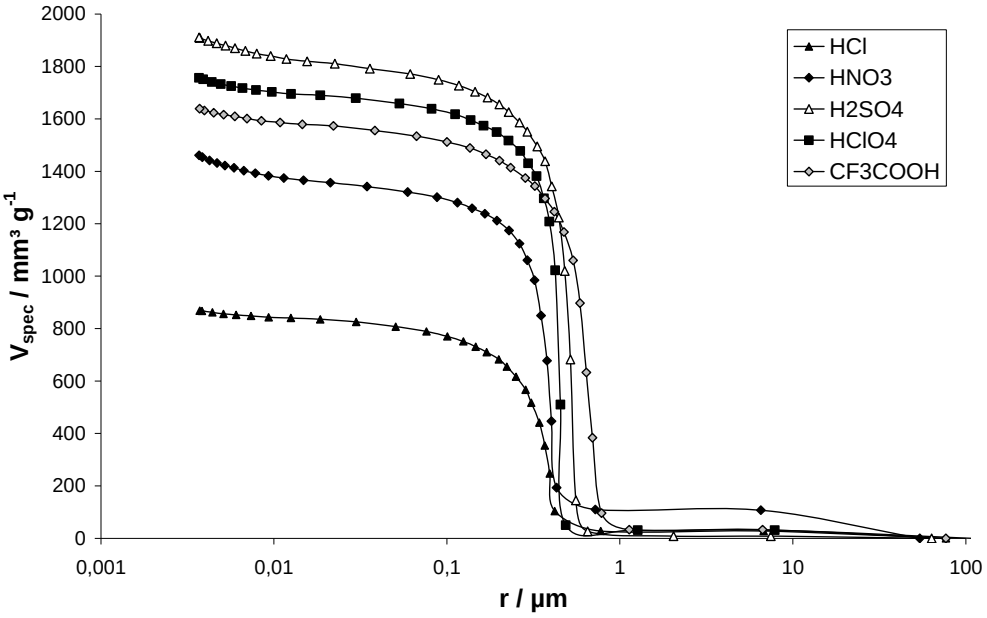

Figure 31 Macropore radii distribution of the silica gels synthesized from different acids at the nominal pH 1.

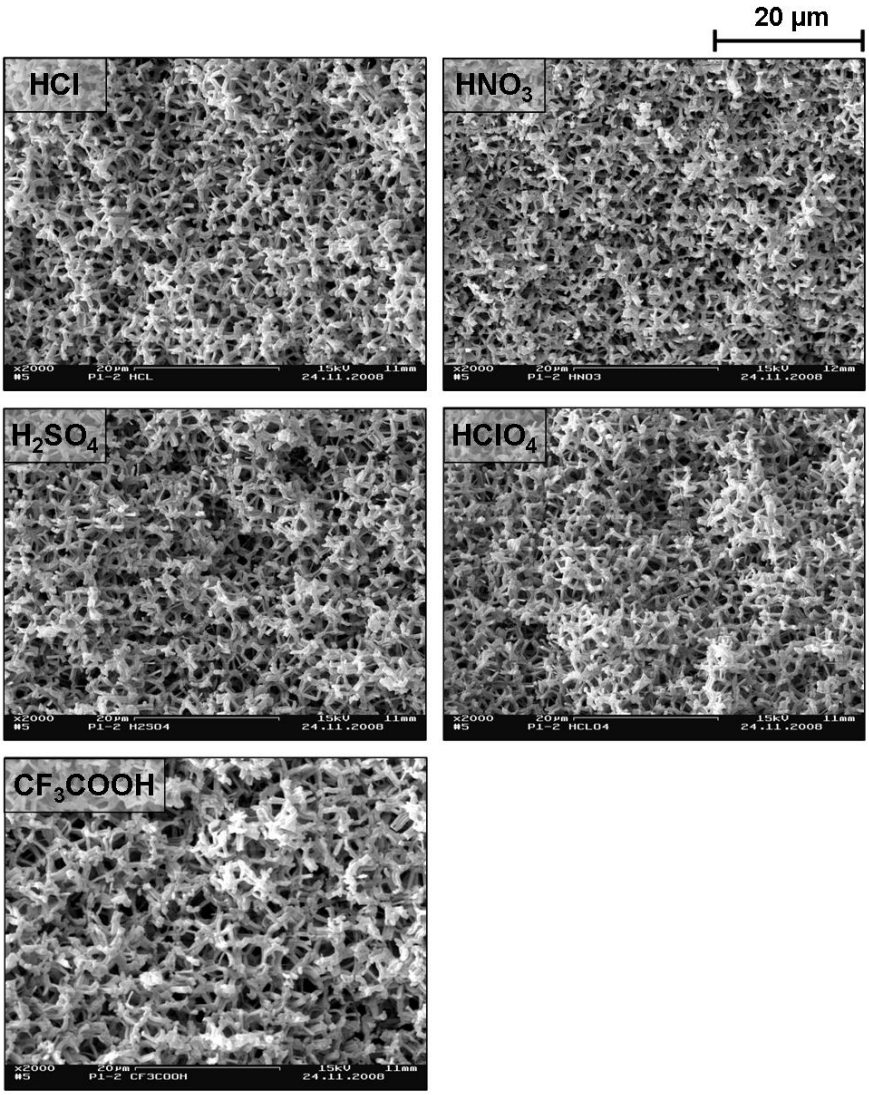

Figure 32 SEM images of the hierarchically organized silica monoliths prepared with the different acids at pH 1. Progressing from the top with HCl (left) and HNO_3 (right), to the middle positions with H_2SO_4 (left) and $HClO_4$ (right) to the last picture on the bottom with CF_3COOH.

2.1.6. Gelation / Aging Temperature and Time

The sol-gel systems are complex systems with many parameters affecting the interactions between the polymerizable siliceous species and the structure-directing agent, usually solutions of ionic or non-ionic surfactants. Besides the pH of the solution, also the nature of the acid anion as well as the composition of Si to surfactant phase, the temperature during gelation and aging is one prominent factor, which affects the evolution of the hierarchical arranged pore size regimes. Even though, a "solid" gel network is formed at the sol-gel transition, chemical reactions still take place within the gel system. On the one hand, residual sol is enclosed in the

pore systems providing condensable silica species and even monomers for further condensation reactions with the gel backbone. On the other hand, structural re-arrangement reactions occur during aging. Due to the flexibility of the gel network, silanol groups can react with other adjacent silanol groups or with unreacted Si-OR groups via condensation reactions resulting in a higher degree of cross-linking of the gel network. Furthermore, Ostwald ripening processes contribute to a further solidification of the gel network by transferring siliceous species from thermodynamically unfavourable sites to thermodynamically favourable sites such as pores, cracks and neck of pores where they are integrated again via condensation reactions.[14]

In order to reduce the aging time, the influence of higher gelation and aging temperatures on the resulting pore domains are examined. The temperature has been varied between 40 to 90°C and the aging time from 3 to 7 days. Due to the high temperatures, autoclavable polypropylene (PP) vessels have been used as container materials. The initial composition of all sols has been Si / P123 / 1 M HCl = 8.4 / 30 / 70 with EGMS as silicon source.

In table 9 the physicochemical data are listed for the resultant silica gels for all temperatures after 3 and 7 days of aging.

The diagram in figure 33 illustrates the influence of the temperature on the gelation time (t_g) and the time period for the phase separation (t_{PS}) of the silica monoliths. The trend of the recorded time intervals affirm the theoretical considerations, that with increasing temperature both t_g as well as t_{PS} are reduced as the polycondensation of the silica species is accelerated. The gelation time decreases from 66 min at 40°C to 23 min at 90°C. Below 60°C, the onset of phase separation occurs delayed to the gelation with 180 min at 40°C and 68 min at 50°C. However, at and above 70°C phase separation as well as the sol-gel transition almost emerge concomitantly after only 23 – 30 min.

Table 9 Physicochemical properties of the samples gelled and aged for 3 and 7 d at different temperatures in the range of 40 – 90°C.

samples			SAXS	N_2-sorption		
	T /°C	t /d	d_{10} /nm	S^{BET} /m² g^{-1}	D^{BJH} /nm	t_{wall} /nm
P1-40-3	40	3	10.6	441	4.9	7.3
P1-50-3	50	3	11.5	476	5.4	7.9
P1-60-3	60	3	11.2	490	3.7	9.2
P1-70-3	70	3	13.0	586	3.7	11.3
P1-80-3	80	3	-	730	-*	-
P1-90-3	90	3	-	708	-*	-
P1-40-7	40	7	10.5	438	4.9	7.2
P1-50-7	50	7	10.8	436	4.6	7.9
P1-60-7	60	7	11.4	529	3.7	9.5
P1-70-7	70	7	12.1	628	3.9	10.1
P1-80-7	80	7	-	732	-*	-
P1-90-7	90	7	-	661	-*	-

* D^{BJH} calculated for these samples resulted from nitrogen artefacts.

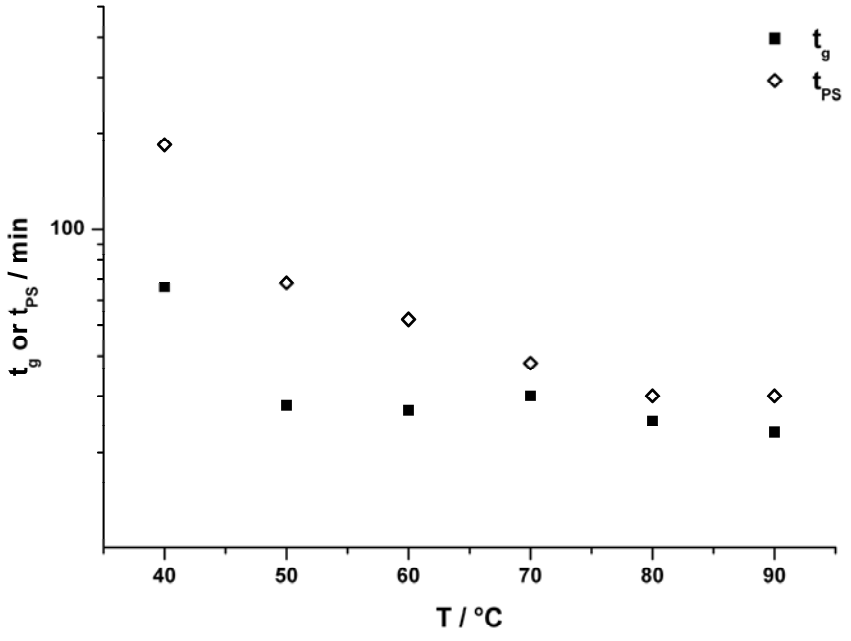

Figure 33 Diagram presenting the gelation times and the onset of phase separation as function of the temperature. The sol-gel system has been constant for this experiment sequence with Si / P123 / 1 M HCl = 8.4 / 30 / 70 and EGMS as sole precursor.

The SAXS experiments of the monolithic samples aged for 3 days at the different temperatures indicate that with increasing temperature the resultant degree of mesoscopic ordering is drastically reduced above 50°C, as the phase separation in the mesoscopic region emerges too fast for the evolution of a distinct periodical arrangement of the silica / template assemblies. (Figure 34) At 40 and 50°C the SAXS curves of the corresponding samples exhibit diffraction peaks for the (10) and the (20) diffractions at q_{10} = 0.6 nm^{-1} and q_{20} = 1.1 – 1.2 nm^{-1}. Already at 60°C the SAXS pattern only presents the signal for the (10) ordering and at 70°C only a weakly pronounced diffraction peak is observed at q_{10} = 0.6 nm^{-1}. This trend coincides with the decreasing time intervals for t_g and t_{PS}. Further SAXS and nitrogen sorption measurements exhibit, that an extension of the aging period does not affect the formation of the resulting ordering of the mesopores at each temperature. However, the handling of the silica monoliths indicates an increased resistance towards mechanical stress for the samples aged for a longer time period.

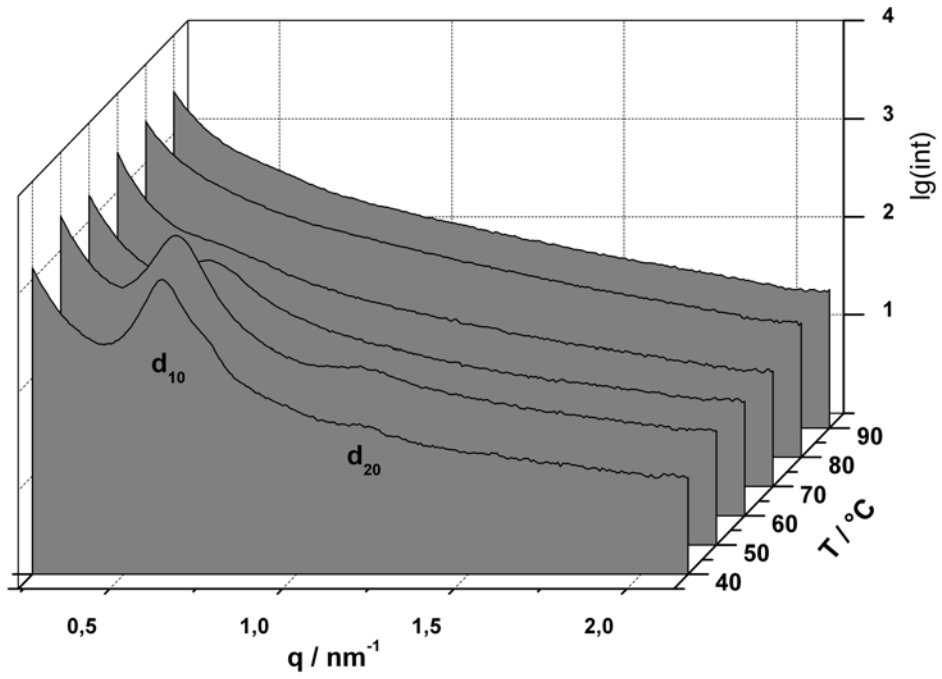

Figure 34 SAXS curves of the evolution of the mesoscopic ordering with increasing gelation and aging temperature after 3 d of aging.

Even though, the mesostructure of the silica gels gelled and aged at 50°C is well resolved after 3 d of aging, the SEM images of these samples display a not-well defined macroporous morphology. (Figure 35) With increasing temperature, the degree of densification of the

macroporous network is even enhanced. In contrary, the silica monoliths gelled and aged at 40°C, exhibit a well-defined macroporous morphology created of rod-shaped silica strands. The co-continuous macroporous framework exhibits no changes for the different aging times of 1 to 7 days as can be seen from figure 36. However, the stability towards mechanical stress such as the compressing of the monolith when picking up the monolith increases with increasing aging time at 40°C.

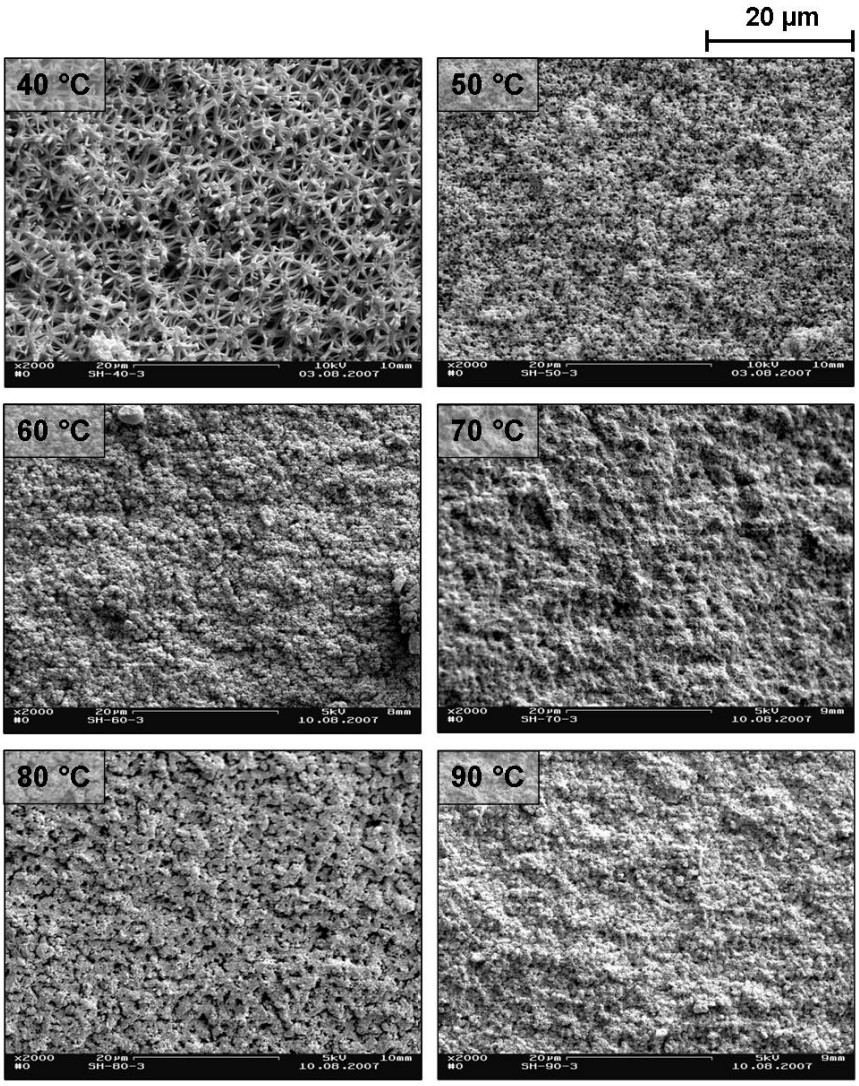

Figure 35 SEM pictures presenting the change of the macroporous morphology after aging for 3 d at different temperatures. All samples were prepared with Si / P123 /1 M HCl = 8.4 / 30 / 70.

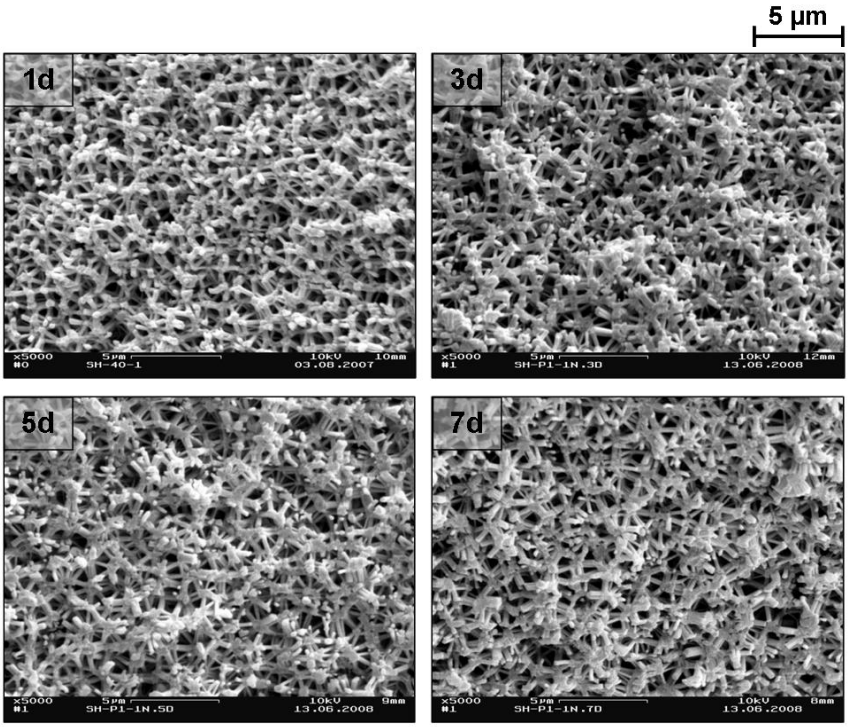

Figure 36 SEM images presenting the macroporous morphology of the silica monoliths aged for 1 – 7 d at 40°C. All samples were prepared with Si / P123 / 1 M HCl = 8.4 / 30 / 70.

2.2. Inorganic-Organic Hybrid Silica Monoliths

For some applications, such as reversed phase (RP) high performance liquid chromatography (HPLC), a non-polar surface of the stationary phase is required for the separation process. The functionalization of the surface of silica materials can be achieved via different synthesis procedures among which the post-synthetic grafting and the direct-synthesis by co-condensation are the most prominent techniques.

2.2.1. *In-situ* Modification by Co-condensation

The possibility to modify the pore walls of the silica network via the direct approach by co-condensing an organically functionalized trialkoxysilane with a tetraalkoxysilane was investigated. Two different organic moieties, methyl and phenyl, were selected as hydrophobic surface groups for the resulting inorganic-organic hybrid material.

2.2.1.1. Synthesis of the Inorganic-Organic Hybrid Silica Gels

Based on the synthesis of the ethylene glycol-modified silane (EGMS), trimethoxy-methylsilane and triethoxyphenylsilane were modified with ethylene glycol under inert atmosphere while the released alcohol was continuously removed from the reaction by distillation. (Figure 37 shows the reaction scheme for the transesterification reaction for the ethoxy-substituted educt.) The resulting ethylene glycol-modified methyl and phenyl silanes, which according to IUPAC are designated as tris(2-hydroxyethoxy)methylsilane and tris(2-hydroxyethoxy)phenylsilane, are referred to as MeGMS and PhGMS in the following sections. The purity of the resulting silanes was investigated by spin-lock ^{29}Si-NMR experiments in benzene-d_6. The resulting NMR spectra of MeGMS exhibited peaks with chemical shifts of δ(benzene-d_6) = -41.2 ppm and δ(benzene-d_6) = -49.3 ppm, indicating the presence of condensed species besides the monomer. The NMR spectra of PhGMS shows also two signals at different chemical shifts, at δ(benzene-d_6) = -56.1 – -58.0 ppm for the monomer and at δ(benzene-d_6) = -62.2 ppm for a condensed species. The Si content, determined by thermogravimetric measurements, of MeGMS and PhGMS was 9.9 wt % (theoretical: 12.5 wt %) and 9.3 wt % (theoretical: 9.8 wt %) respectively.

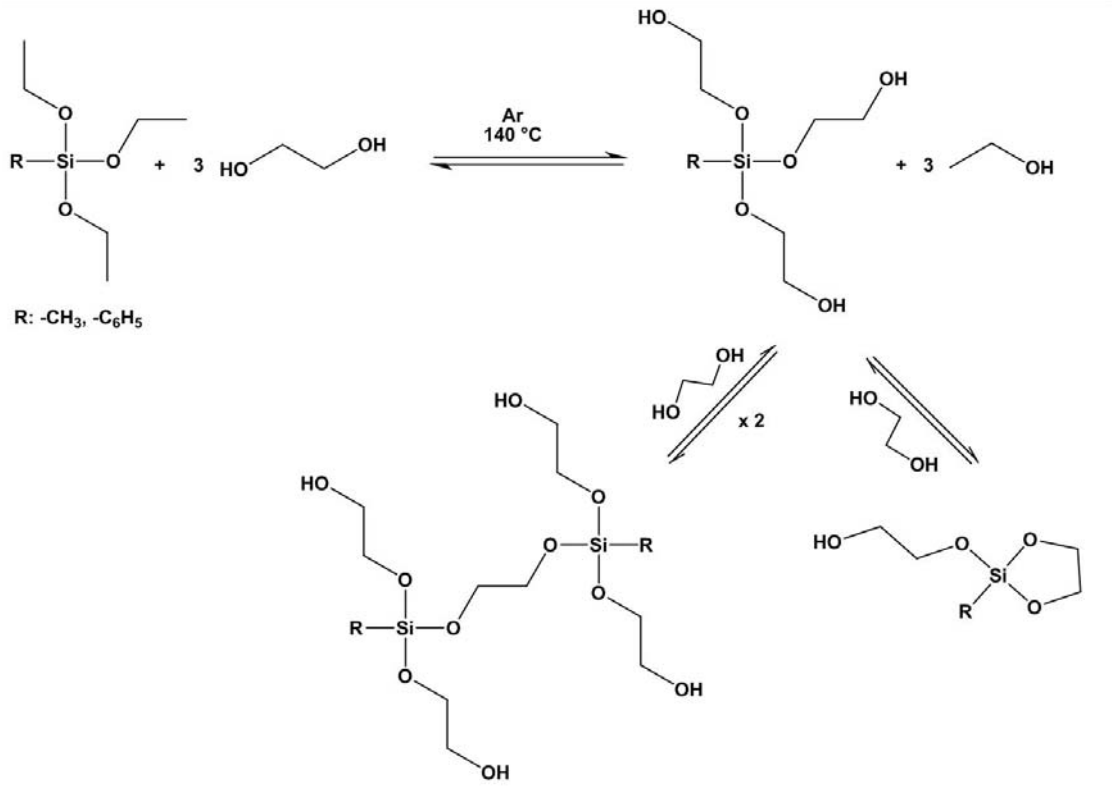

Figure 37 Reaction scheme of the synthesis of the tris(2-hydroxyethyl)organosilane (R: methyl or phenyl) from an ethoxy-substituted silane (educt).

In analogy to the pure silica gels prepared with EGMS as precursor, the inorganic-organic hybrid silica monoliths were also synthesized by employing a liquid crystalline phase of P123 in dilute HCl as endotemplate. The ratio of the organically functionalized silane to EGMS was varied in the range from 0 up to 100 mol % for MeGMS and for the system PhGMS to EGMS in the range from 0 to 30 mol % (PhGMS). This limitation for the PhGMS system was caused by the fact, that at contents of PhGMS higher than 30 mol % no homogeneous silica monoliths were obtained.

The total ratio of composition for all batches of Si / P123 / x M HCl was kept constant with 8.4 / 30 / 70 by weight, while the concentration of the employed acid catalyst was varied in the range from 1 M to 0.003 M. All hybrid silica gels were gelled and aged at 40°C for 7 d and were subsequently treated with chlorotrimethylsilane (TMCS) and dried in analogy to the pure inorganic gels in section 2.1.2.

For the investigation of the organic loading of the final monoliths, hybrid silica gels of varying MeGMS contents were synthesized at c(HCl) = 1 M and were dried by a supercritical drying procedure with CO_2 at T_C = 31°C and p_C = 73 bar.[14] These monoliths were heated to 200°C

in order to remove residual CO_2 from the pores by simultaneous preservation of the organic moieties, and were then investigated by IR-coupled thermogravimetric measurements in inert atmosphere.

In order to determine the average shrinkage of the hybrid silica monoliths, five gels were synthesized per series, which length and diameter were measured after each synthesis step.

2.2.1.2. Inorganic-Organic Hybrid Silica Monoliths

The synthesis of highly porous organically modified monoliths from pure silsesquioxane ($SiO_{1..5}$) *e.g.* by employing methyltrimethoxysilane (MTMS) is a challenging task and has only been reported by few groups among which Nakanishi, and Dong and Brennan are the most prominent representatives.[113, 114] Even though the phase separation is easily initiated by the employment of MTMS due to the hydrophobicity of the terminal Si-CH_3 groups resulting in defined macropore size domains, the final gels exhibit a high degree of mechanical flexibility. The missing rigidness is caused by a lower degree of cross-linking due to only three potential substitution sites for the network forming cross-linking reactions.[113, 114] However as described in section 1.3.4.2., the synthesis of hierarchically organized inorganic-organic hybrid silica monoliths via co-condensation also remains a challenging task as the hydrolysis and condensation rates of the organotrialkoxysilane and the tetraalkoxysilane differ from each other, which can result in the preference of homo-condensation reactions at the expense of network forming cross-linking reactions.[18, 49, 50]

For the investigation of the possibility to direct modification of the the pore walls of the silica monoliths by simultaneously preserving the hierarchy of the different pore size regimes, methyl and phenyl-modified hybrid silica monoliths are synthesized by co-condensing EGMS with MeGMS and PhGMS, respectively. In analogy to the inorganic silica monoliths, the shrinkage of the organically modified hybrid monoliths is also determined.

The shrinkage of hybrid silica monoliths does not significantly change with increasing content of MeGMS. The average shrinkage of the length is around 11% and of the diameter around 8% calculated for the gels after the heat treatment (200°C) in correlation to their initial length and diameter after aging. The same calculations for the PhGMS series resulted in a shrinkage of the diameter of 15% and 13% of the length. These results are surprising, as theoretically with increased content of the organically modified precursor a more flexible silica network and hence a decreasing degree of shrinkage is expected. Nakanishi and co-workers even reported a suppressed shrinkage of the methylsilsesquioxane monoliths which they related to the steric

hindrance of the condensation reaction of unreacted silanol groups by the methyl entities along with the fact that the hybrid silica network is more flexible and thus a higher degree of stress can be endured without the formation of voids.[115]

However, one has to keep in mind, that the hybrid inorganic-organic silica monoliths presented here are all subjected to the ambient pressure drying approach via surface silylation reaction with chlorotrimethylsilane (TMCS). Due to this modification, for all contents of MeGMS and PhGMS the resulting loading with unreacted silanol groups is low independently from the initial loading with organic entities and hence the shrinkage is moderate and similar among the hybrid gels synthesized with the particular precursor, MeGMS or PhGMS, respectively.

The results of the structural analysis of the hybrid silica monoliths, prepared with MeGMS of varying contents c(HCl) = 0.03 M according to the synthesis and the drying procedure with TMCS of the inorganic silica monoliths are listed in table 10.

Table 10 Physicochemical data of the inorganic-methyl hybrid silica gels prepared with a varied content of MeGMS at the nominal pH 1.5 (c(HCl) = 0.03 M).

samples		*SAXS*	*N_2-sorption*			*Hg-Porosimetry*	
	%MeGMS /mol %	d_{10} /nm	S^{BET} /$m^2\ g^{-1}$	D^{BJH} /nm	t_{wall} /nm	R^{Hg} /μm	V^{Hg} /$cm^3\ g^{-1}$
P2-1,5a	0	11.3	782	5.9	7.1	0.3	3.3
P4-1,5a	5	11.0	717	5.0	7.7	0.4	3.1
P6-1,5a	10	10.9	716	4.1	8.4	1.1	3.5
P8-1,5a	15	10.6	720	4.4	7.8	0.5	2.9
P10-1,5a	20	10.1	726	4.1	7.6	0.7	4.0
P11-1,5a	30	9.5	730	3.9	7.1	-*	4.5
P12-1,5a	40	8.7	766	3.9	6.1	-	-
P13-1,5a	50	-	658	3.7	-	-	-
P18-1,5a	100	-	651	3.6	-	-	-

* A nonuniform macropore radii distribution was obtained for this sample.

Figure 38 shows the SAXS pattern of the methyl-modified hybrid silica monoliths prepared with 0 – 100 mol % MeGMS at c(HCl) = 0.03 M. The SAXS curves of the gels exhibit for MeGMS contents below 40 mol % a 2D-hexagonal arrangement with a long-range ordering of the mesopores. The pronounced 2D-hexagonal arrangement of the mesopores is also affirmed

by transmission electron microscopy (TEM) investigations. Figure 39 shows the TEM images of the mesopore network of the gels prepared with 15 and 20% MeGMS.

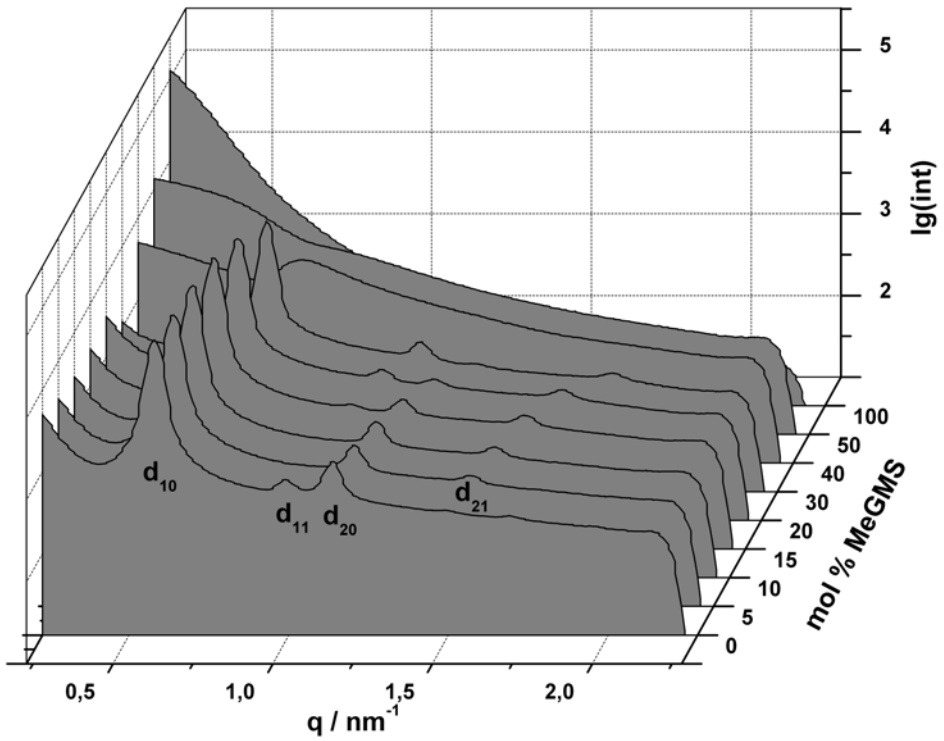

Figure 38 SAXS pattern of the evolution of the mesoscopic ordering with increasing content of MeGMS (at c(HCl) = 0.03 M).

The pure silica monolith exhibits the reflections for the (10), (11) and the (20) diffraction at q_{10} = 0.6 nm^{-1}, q_{11} = 1.0 nm^{-1}, and q_{20} = 1.1nm^{-1}. The (11) diffraction is not observed for the hybrid gels with 5 and 10 mol % MeGMS, instead the SAXS curves show the diffraction peak for the (21) diffraction at q_{21} = 1.5 nm^{-1} (besides the signals for the (10) and the (20) reflections). Only for contents of MeGMS of 15 mol % and more, the diffraction peak for the (11) diffraction re-appears. At 15 % an only minor pronounced reflection is resolved at q_{11} = 1.0 nm^{-1}. However, at 20 mol % the (11) reflection is more prominent while the intensity of the (20) diffraction is concomitantly reduced (q_{11}(20%) = 1.1 nm^{-1}, q_{20}(20%) = 1.2 nm^{-1}) until at 30 mol % the ratio of the intensities is even reversed compared to 15 mol % MeGMS (q_{11}(30%) = 1.1 nm^{-1}, q_{20}(30%) = 1.3 nm^{-1}). The increase in the ratio of the (11) / (20) reflections can be related to a favoured aggregation of the hybrid silica species along the (110) axis increasing the electron density, while the amount of the scattering objects along the (200) (or (100), respectively) stays rather constant.[85, 116]

Interestingly, parallel to the development of the (11) reflection, the repeating unit distance d_{10} is reduced from 10.9 nm (for 10 mol % MeGMS) to 9.5 nm (for 30 mol % MeGMS) indicating a contraction of the hybrid silica network. It can be assumed that the contraction is caused by a decrease in the electrostatic repulsion between the condensing aggregates due to the replacement of protonated silanol groups by Si-CH_3 entities.[116]

Above 40 mol % MeGMS a drastic reduction of the mesoscopic ordering is observed until at 70 mol % MeGMS no ordering is evolved at all. These results agree with the observations made by Fröba et al., who reported a decreasing mesoscopic ordering climaxing in a complete disordering in the final materials when the content of organic moieties exceeds 40 mol %.[18]

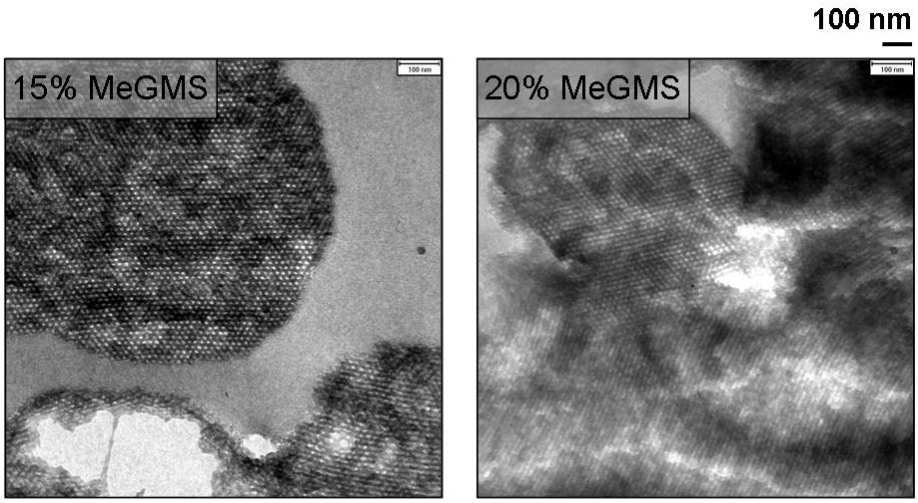

Figure 39 TEM images of the two selected hybrid silica gels prepared with 15 mol % and 20 mol % MeGMS at c(HCl) = 0.03 M.

Interestingly, with increasing content of MeGMS the macroscopic morphology is more affected than the mesostructuring of the hybrid silica gels. SEM images of the methyl-modified hybrid silica gels reveal that at 10 mol % MeGMS the resulting macroporous framework is no longer formed by rod-shaped silica strands (0 mol % MeGMS: $R^{Hg} = 0.3\,\mu m$), but of agglomerations of rod-shaped particles, which are connected by fragile silica strands forming larger pores with an average radius of $R^{Hg} = 1.1\,\mu m$. (Figure 40)

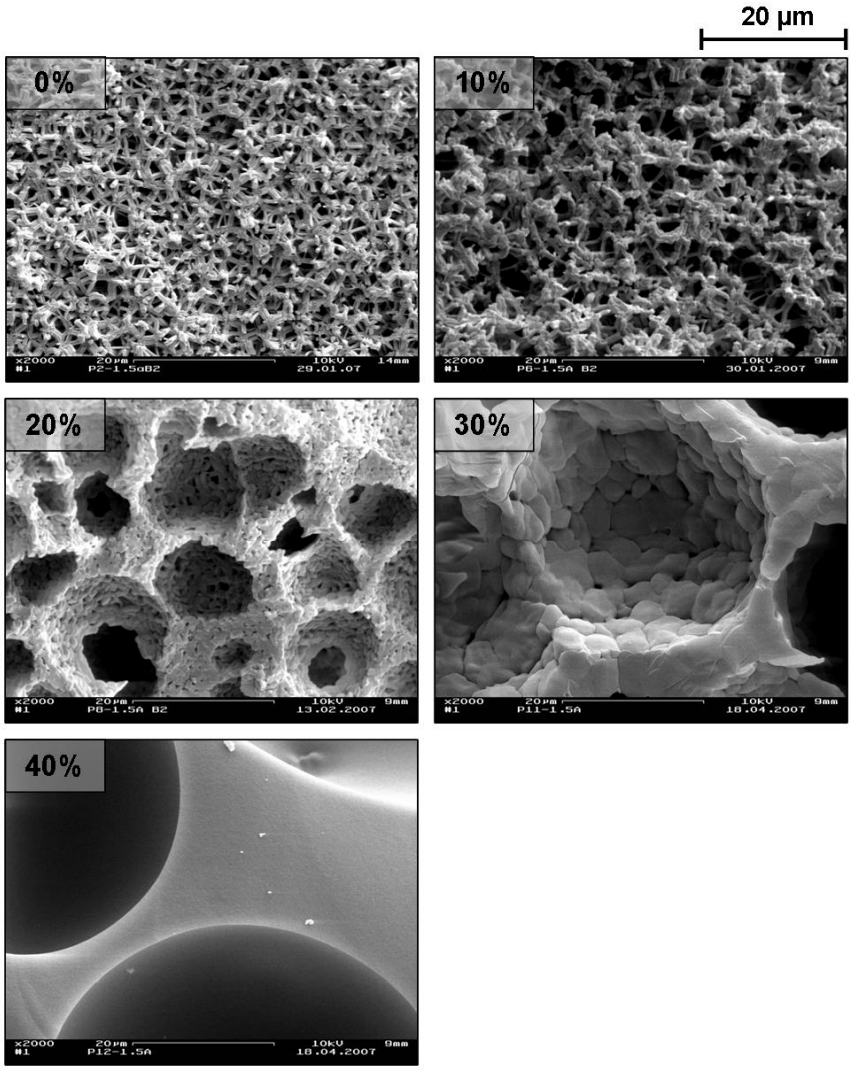

Figure 40 SEM images of the hybrid methyl-silica gels prepared with varied contents of MeGMS in the range of 0 – 40 mol % at c(HCl) = 0.03 M.

By increasing the MeGMS content, the bicontinuous macroporous morphology is no longer formed by rod-shaped silica strands but a densified cellular network is obtained at 20 mol % MeGMS in which distorted silica rods enclose spherical voids. At 30 mol % MeGMS, a further densification of the macroporous framework is observed, which is caused by the assembly of "rice grain"-like particles and results in isolated macropores of about 35 μm in diameter. Above 40 mol % MeGMS, the framework is no longer formed by particles nor strands, but by a densified bulk material which encloses large isolated pores with diameters of about 50 μm. These results indicate the influence of the decreasing polarity of the organic modified silica species on the phase separation in the macroscopic range until an emulsion is formed at contents of MeGMS of 30 mol % and higher, resulting in isolated macropores.

The group of Nakanishi as well as Dong and Brennan reported the successful synthesis of pure methylsilsesquioxane ($H_3CSiO_{1.5}$) monoliths for the application as RP-HPLC stationary phases via two different approaches. Nakanishi and co-workers applied a ternary sol system of MTMS, methanol / formamide and nitric acid which composition determined the resulting macroporous morphology. As can be seen from figure 41, by adjusting the composition ratio, morphologies ranging from nanoporous (figure 41b, top left) and co-continuous (figure 41b, top right) to isolated macropores (figure 41b, bottom left) and fragmented particulate domains can be obtained.[114, 115] Dong and Brennan chose a two-step acid / acid sol-gel process in which MTMS was first pre-hydrolyzed under weakly acidic conditions before in a second step a strong acid was applied to accelerate the condensation reactions. By this approach, methylsilsesquioxane monoliths were synthesized exhibiting an ordered cellular framework with a narrow macropore size distribution of 2.1 μm.[113] Even though both approaches proved to be adequate synthesis pathways for the preparation of hybrid silica monoliths exhibiting highly interconnected macroporous networks, the incorporation of an organized porosity on a different length scale (meso- or micropores) has not been achieved yet.[113-115]

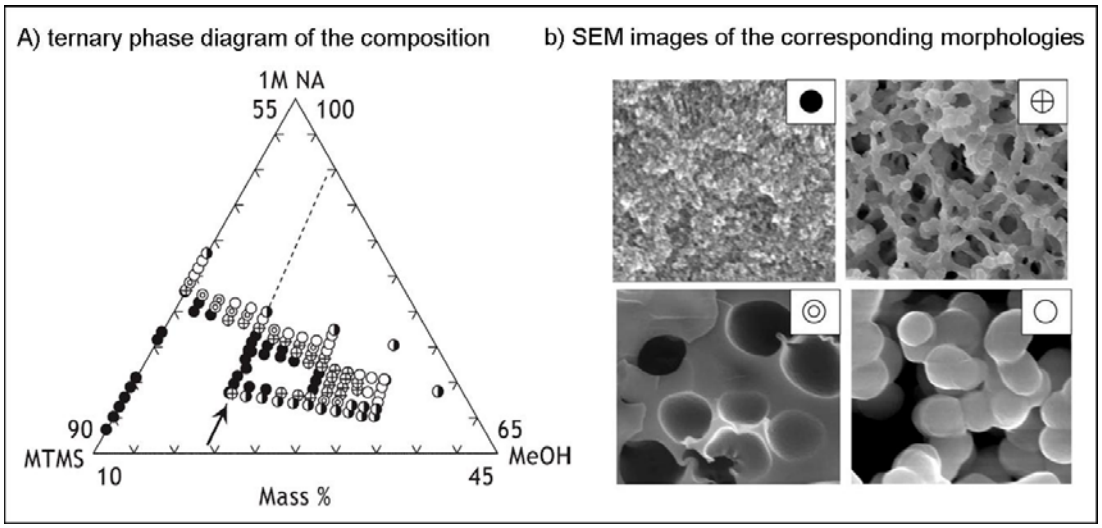

Figure 41 Relationship between the composition of the sol and the resulting macroporous morphologiesA) presents the ternary phase diagram consisting of methyltrimethoxysilane (MTMS), methanol (MeOH) and 1 M nitric acid (NA). B) shows the SEM images of the typical macroporous morphologies of the resulting methylsilsesquioxane monoliths: ● nanoporous; ⊕, ◑ co-continuous; ◎ isolated macropores; ○ particulate network. [114]

In contrary to the methyl-modified silica gels, no homogeneous hybrid silica monoliths can be obtained above 30 mol % of the phenyl-analogon (PhGMS). The physicochemical properties of the hybrid silica monoliths are listed in table 11.

Table 11 Physicochemical properties of phenyl-modified hybrid silica gels prepared with varying contents of PhGMS (0 – 30%) at c(HCl) = 0.03 M.

samples		*SAXS*	*N_2-sorption*			*Hg-Porosimetry*	
	%PhGMS /mol%	d_{10} /nm	S^{BET} /$m^2\ g^{-1}$	D^{BJH} /nm	t_{wall} /nm	R^{Hg} /μm	V^{Hg} /$cm^3\ g^{-1}$
sh-P19-1	0	11.5	936	3.9	9.4	0.4	3.2
sh-P21-1	5	10.8	1041	3.7	8.8	0.4	2.1
sh-P9-1	10	10.0	1027	3.7	7.8	0.4	2.2
sh-P24-1	15	9.2	846	3.7	6.8	-*	0.5
sh-P10-1	20	-	815	3.7	-	-*	0.9
sh-P11-1	30	-	370	3.2	-	-	-

* A nonuniform macropore radii distribution was obtained for this sample.

Structural investigations by SAXS experiments of the phenyl-modified monoliths reveal that already contents above 10 mol % PhGMS disturb the evolution of the mesostructure. As can be seen from figure 42, the reflections for the (10), (11), (20), and (21) diffractions are only pronounced for silica gels prepared with 0 and 5 mol % PhGMS which can definitely be related to a 2D-hexagonally arranged mesoporous network. (The corresponding q-values are determined to q_{10} = 0.6 nm^{-1}, q_{11} = 1.0 nm^{-1}, q_{20} = 1.1 – 1.2 nm^{-1}, and q_{21} = 1.5 – 1.6 nm^{-1} for 0 and 5 mol % PhGMS and the corresponding repeating unit distances are in the range of d_{10} = 11.5 – 10.8 nm.)

The SAXS curve of the hybrid network derived from 10 mol % PhGMS shows a less distinct pattern for the 2D-hexagonal arrangement with only one pronounced reflection for the (10) diffraction at q_{10} = 0.6 nm^{-1} and two minor pronounced signals for the (11) and (20) diffractions at q_{11} = 1.0 nm^{-1} and q_{20} = 1.3 nm^{-1}. The corresponding TEM investigations of this monolith (10 mol % PhGMS) confirm the existence of the 2D-hexagonal arrangement of the mesopores as can be seen from the left image in figure 43.

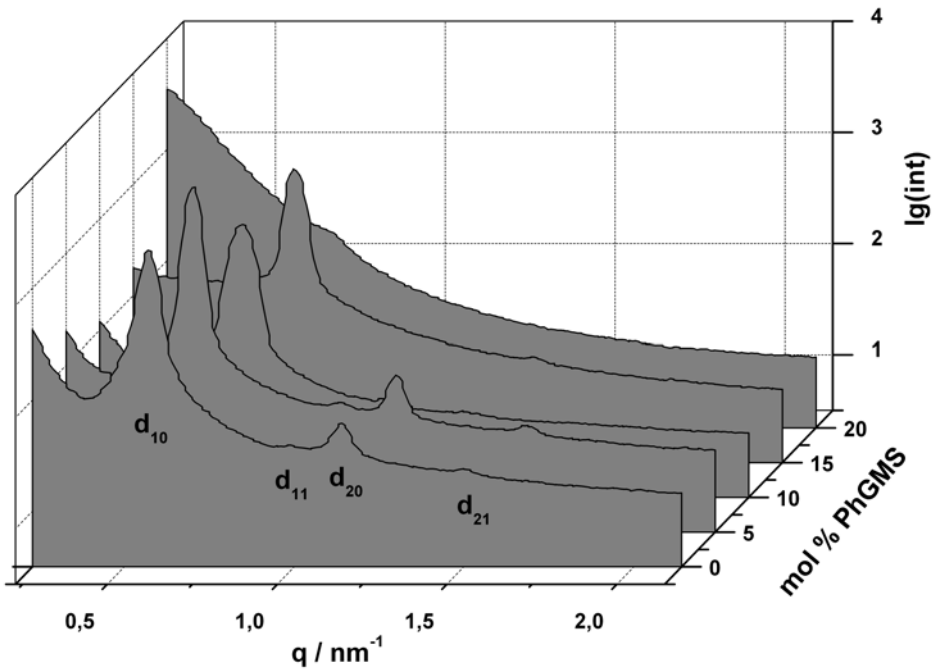

Figure 42 SAXS pattern of the evolution of the mesoscopic ordering with varying PhGMS content in the range from 0 – 20% (at c(HCl) = 0.03 M).

The TEM image of the hybrid silica sample prepared with 15 mol % PhGMS shows parallel pore channels with a spacing of about 9 nm (right image in figure 43). This spacing coincides with the repeating unit distances d_{10} and d_{20} calculated for the 2D-hexagonal ordering with the two diffraction peaks (10) and (20) at $q_{10} = 0.7\ nm^{-1}$ and $q_{20} = 1.4\ nm^{-1}$ ($d_{10} = 9.2$ nm and $d_{20} = 9.1$ nm).

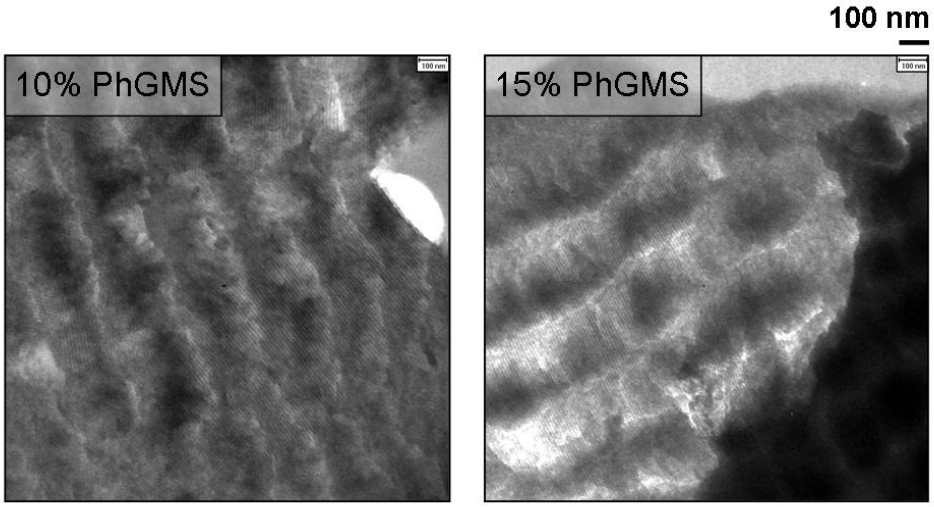

Figure 43 TEM images of the hybrid silica gels synthesized with 10 and 15 mol % PhGMS at c(HCl) = 0.03 M. The broad irregular lines result from the sample preparation.

In analogy to the development of the macroporous morphology of the methyl-modified hybrid silica monoliths, the increasing content of PhGMS also affects the formation of the macroporous framework. As can be seen from figure 44 the altering polarity of the sol-gel system with increasing content of PhGMS, results already in a more randomly arranged particulate framework at 5 mol % PhGMS compared to the well-defined rod-shaped morphology at 0 mol % PhGMS. Even though, the macroporous network at 5 mol % PhGMS appears to be densified compared to the corresponding network at 0 mol % PhGMS, both systems exhibit macropore radii of $R^{Hg} = 0.4\ \mu m$ (as can be seen from figure 45).

At 10 mol % PhGMS a coarsened macroporous framework is observed in which thick agglomerates of particles (width ~ 10 μm) form the macropore walls which are connected by fragile silica strands and the average macropore radii is determined as $R^{Hg} = 0.4\ \mu m$. The macroporous framework of the monoliths prepared with 20 mol % PhGMS consists of randomly distributed spherical macropores with diameters in the range of 40 – 100 μm which exhibit a rather low degree of interconnectivity.

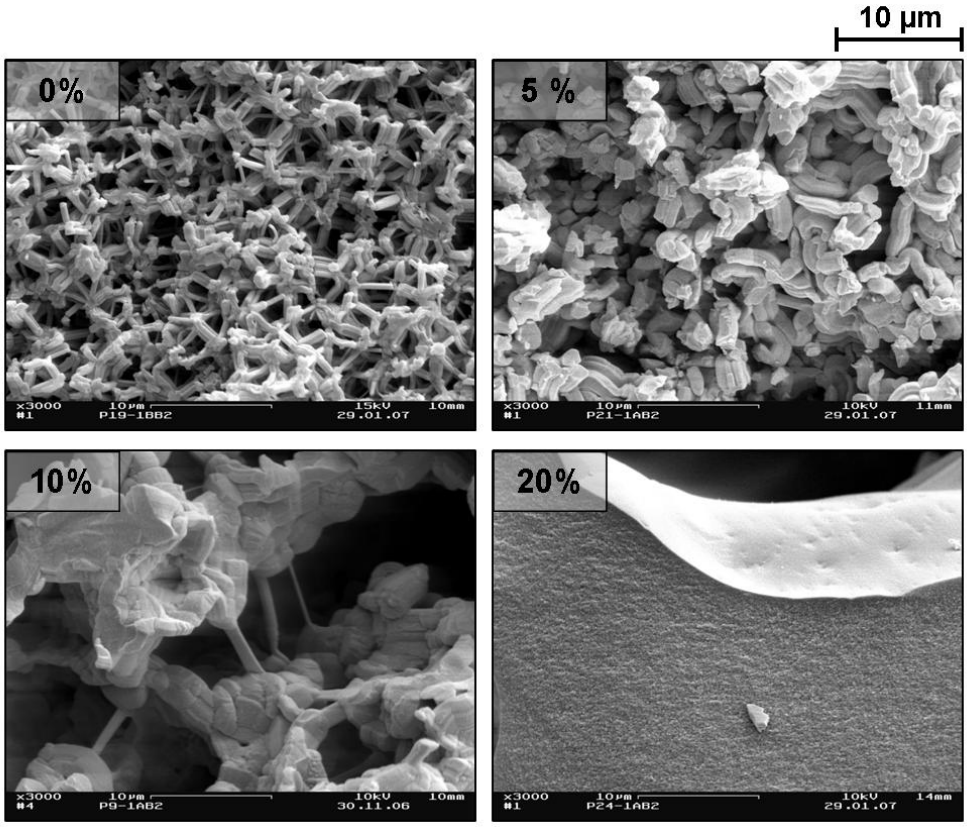

Figure 44 SEM images of the macroporous framework of hybrid silica gels with PhGMS contents of 0, 5, 10, and 20 mol % (prepared at c(HCl) = 0.03 M).

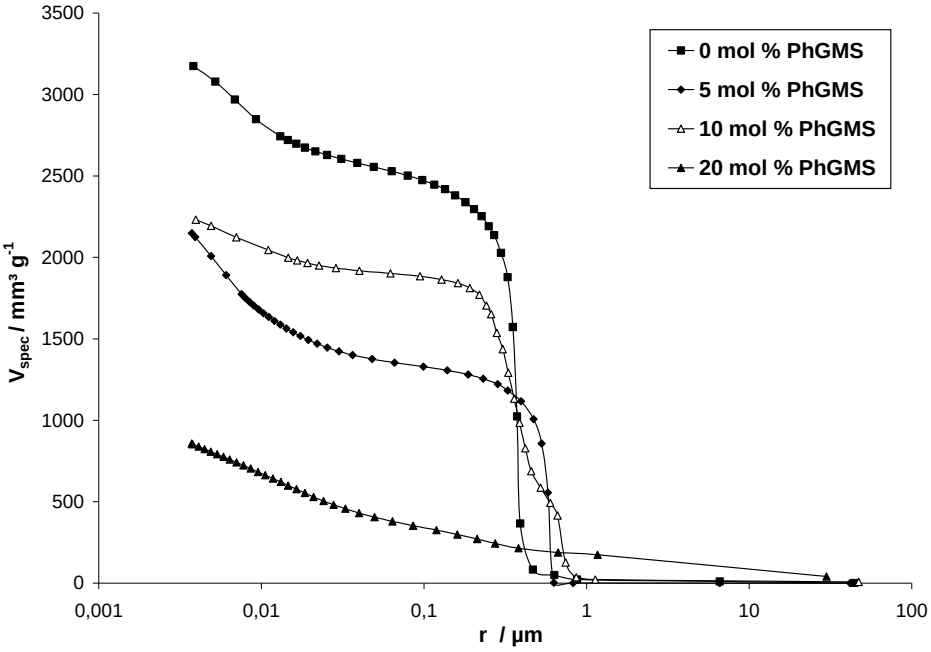

Figure 45 Macropore radii distribution of the phenyl-modified hybrid silica gels synthesized with varying contents of PhGMS of 0, 5, 10, and 20 mol %.

Interestingly, the comparison to directly synthesized phenyl-functionalized SBA-15 materials exhibits a similar impact of the phenyl-modified precursor on the formation of the macroporous morphology and the 2D-hexagonal ordering of the mesopore system. Wang et al. report that by co-condensing TEOS with varying molar ratios of trimethoxyphenylsilane (PTMS, maximum content: 23 mol %), the 2D-hexagonal ordering of the mesopore system is decreased with increasing content of PTMS. Parallel to the decreasing ordering in the mesoscopic range, the macroscopic morphology formed by arrays of cylindrical silica rods at (0 mol % PTMS) is changed. At 23 mol % PTMS a more particulate morphology is observed which is formed by particles of random shape and distribution.[117]

The effective loading of the inorganic-organic hybrid silica monoliths were investigated by IR-coupled thermogravimetric measurements of supercritically dried hybrid monoliths of varying MeGMS contents in inert atmosphere. During the thermal decomposition of the hybrid methyl-modified silica network, IR spectra were recorded of the released organic fragments in the gas phase.

Prior to the investigation, all monoliths were tempered at 200°C to eliminate residual CO_2 from the pores. Figure 46 shows the resulting pattern for the weight loss at different

temperatures for the selected hybrid silica gels prepared with 20, 50, 80, and 100 mol % MeGMS and the pure silica gel (0 mol % MeGMS) for comparison.

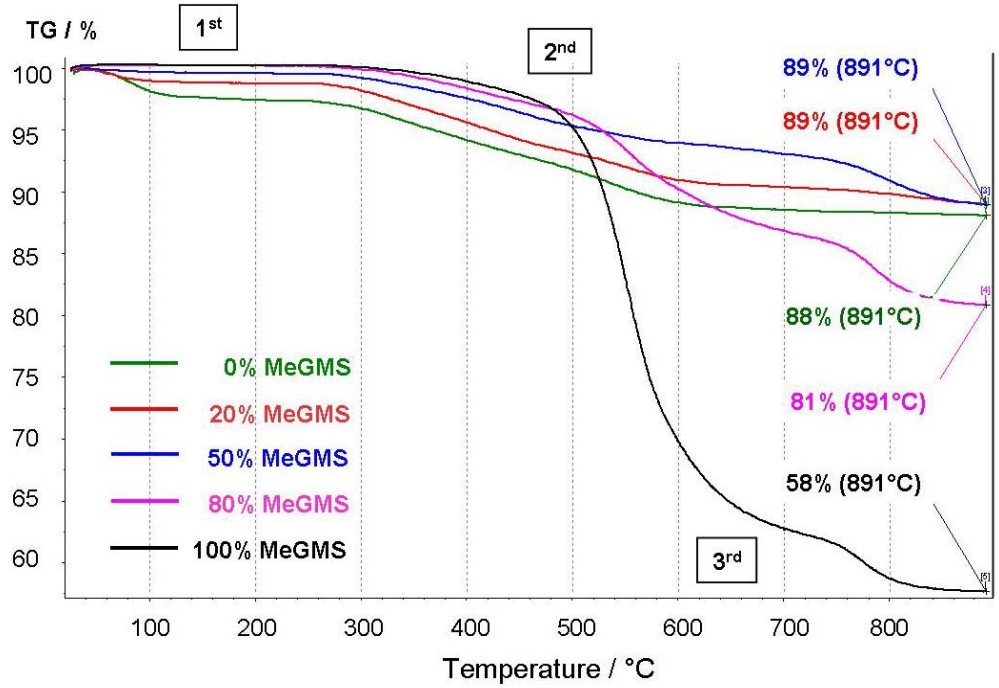

Figure 46 TG diagram of the mass loss of the different methyl-modified silica monoliths prepared with 0, 20, 50, 80, and 100 mol % of MeGMS at c(HCl) = 1 M in the range from 30 – 900°C.

As can be seen from the pattern of the TG curves, in general three major steps occur during the heat treatment of the different monoliths. The first step in the range from RT to approx. 120°C can be related to the evaporation of adsorbed water and / or ethanol on the surface. This step is only present for the monoliths prepared with low contents of MeGMS (0 – 50 mol %). This weight loss decreases from 0 – 50 mol % MeGMS in correlation with the increasing loading of methyl groups on the surface from Δm = 2.5% to Δm = 0.5%.

The second step of weight loss in the temperature range from 280 to 600°C is observed for all monoliths ranging from 8.6% for the pure SiO_2 gel up to 37.3% for the monolith synthesized with 100 mol % MeGMS. During this step a shift in the eliminated fragments occurs, as for the pure silica the weight loss results only from surface-bonded ethoxy groups. The presence of ethoxy groups is caused by employing ethanol as solvent, which is exchanged with CO_2 during the supercritical drying. However, substitution reactions of the surface hydroxy groups by ethoxy groups in ethanol occur, which remain during the ethanol-CO_2 exchange. With increasing loading of methyl entities, the number of substituted ethoxy groups is reduced, and

hence the weight loss is caused by a combined elimination of ethoxy and easily accessible methyl groups. The contribution of the easily accessible methyl moieties becomes predominant with further loading of methyl groups (20 mol % MeGMS: 8.2%, 50 mol % MeGMS: 5.5%) until for the samples prepared with 80 and 100 mol % MeGMS, the elimination of the methyl groups represents the majority of the weight loss with 10.3 and 37.3%.

During the last step above 680°C, only methyl moieties with a difficult accessibility, hence from the inner pores, are released.[113] The weight loss is rather small for the hybrid monoliths synthesized with low contents of MeGMS (Δm(20 mol % MeGMS) = 1.7%) and is pronounced for contents of MeGMS of 50 mol % and higher with Δm = 5 – 6%.

Coupled IR-spectra in this temperature region (680 – 830°C) show the corresponding vibration bands for the eliminated alkyl fragments at $\tilde{\nu}$ = 3014 – 3016 cm^{-1} for the symmetric stretching vibrations, while the bands at $\tilde{\nu}$ = 1302 – 1304 cm^{-1} and $\tilde{\nu}$ = 1130 cm^{-1} can be related to the asymmetric and the symmetric deformation modes.[113] (Figure 47) With increasing amount of the eliminated methyl fragments, the intensity and the number of evolved bands increase along with the cumulative MeGMS content, and thus with the loading of methyl moieties on the pore walls.

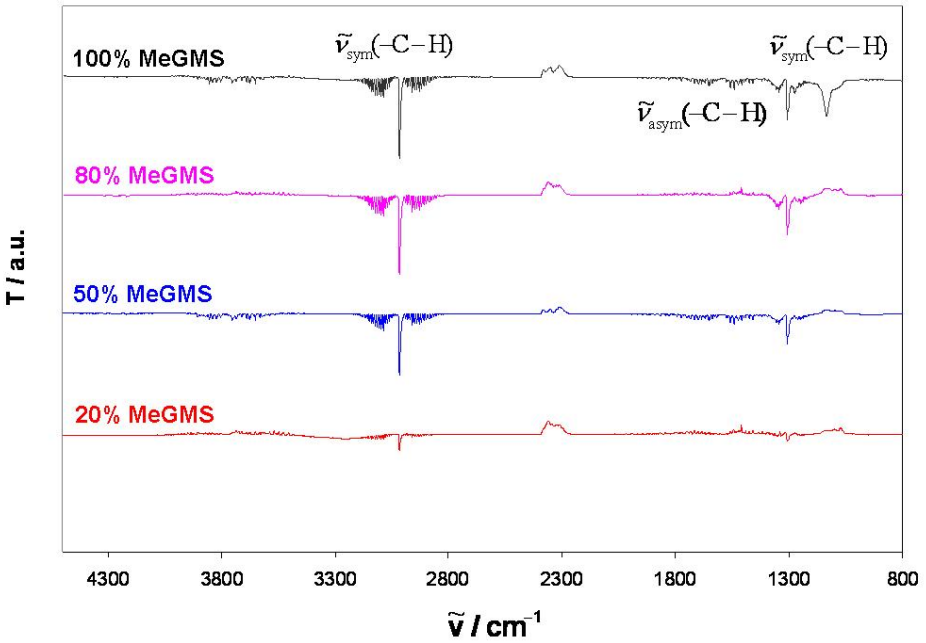

Figure 47 Coupled IR-spectra of the released alkyl fragments in the range from 680 – 830°C (measured in inert atmosphere). The y-axis represents the transmission and is abbreviated with T.

2.2.2. Surface modification by post-synthetic grafting

The surface functionalization via co-condensation by simultaneous preservation of the hierarchical pore organization only resulted in a low loading of the organic entities on the pore walls. In order to optimize the loading, achieving a higher degree of hydrophobization and thus a reduced shrinkage of the monolithic bodies during drying, the post-synthetic approach was chosen.

The hydrophobization reaction was conducted by employing either chlorododecyl-dimethylsilane (DDMCS) and chlorotrimethylsilane (TMCS) as sole functionalization agents or the combination of DDMCS and TMCS. By using a two-step silylation with a steric demanding substituted silane first, such as DDMCS, and a smaller silane species (such as TMCS) in a second step, a higher degree of loading of hydrophobic surface moieties ought to be achieved. This technique is also known as end-capping and the so-treated silica monoliths will be referred to as end-capped samples. (Figure 48)

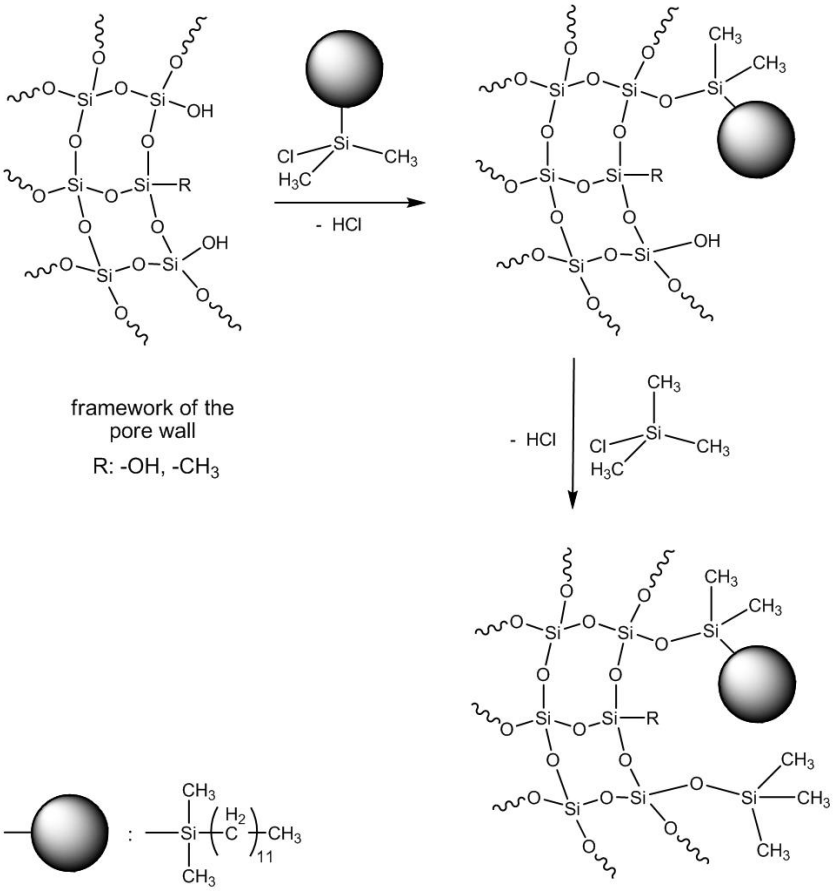

Figure 48 Schematic depiction of the surface modification reactions via the end-capping approach of either a pure silica network or a pre-modified hybrid network with a low loading of methyl groups.

For the investigation of the surface modification by post-synthetic grafting, both pure silica and hybrid silica monoliths, with a low loading of methyl groups (10 mol % MeGMS / 90 mol % EGMS) and hence exhibiting well-defined pore size domains, were selected.

All silica monoliths were prepared according to the procedure in the former sections with Si / P123 / 1 M HCl = 8.4 / 30 / 70 (by weight) with EGMS as sole precursor for the pure silica monoliths and with Si / P123 / 0.03 M HCl = 8.4 / 30 / 70 for the hybrid silica monoliths, whereas the Si-content was achieved by combining the adequate amounts of 10 % mol MeGMS and 90 mol % EGMS. According to the synthesis procedure in the former sections, the gels were gelled and aged at 40°C for 7 d. Prior to the surface modification, all silica monoliths were refluxed in an ethanol / HCl_{conc} mixture (50 / 50% v/v, 65°C) to strengthen the silica network by acceleration of the polycondensation of unreacted silanol groups and simultaneously to decompose and extract the organic template from the porous systems. For the silylation, the monoliths were either treated with a solution of DDMCS (5% v/v) or TMCS (10% v/v) in petroleum ether for 24 h. For the end-capping approach, the monoliths were first silylated in DDMCS / petroleum ether (5% v/v, 24 h) and after washing with petroleum ether, in TMCS / petroleum ether (10% v/v, 24 h). In order to preserve the organic functionalization of the surface, the monoliths were dried only at 200°C.

Besides the characterization of the resultant monoliths by SAXS, nitrogen sorption, and mercury porosimetry measurements, contact angle measurements were also conducted. The corresponding physicochemical data obtained from these investigations are listed in table 12 for the sole EGMS-derived silica gels and in table 13 for the MeGMS / EGMS-derived monoliths (10 mol % MeGMS).

Table 12 Physicochemical properties of the different silylated silica monoliths prepared with EGMS as sole precursor at c(HCl) = 1 M.

samples		*SAXS*	*N_2-sorption*			*Hg-Porosimetry*	
	silylation agent	d_{10} /nm	S^{BET} /$m^2\ g^{-1}$	D^{BJH} /nm	t_{wall} /nm	R^{Hg} /μm	V^{Hg} /$cm^3\ g^{-1}$
P1-1g1	TMCS	11.8	904	5.8	7.8	0.1	2.6
P1-1g2	DDMCS	10.5	943	5.4	6.7	0.1	2.3
P1-1g3	end-capped	11.6	771	6.3	7.1	0.2	2.9

Table 13 Physicochemical properties of the different silylated hybrid silica gels prepared with 10 mol % MeGMS and 90 mol % EGMS at c(HCl) = 0.03 M.

samples	silylation agent	SAXS	N_2-sorption			Hg-Porosimetry	
		d_{10} /nm	S^{BET} /$m^2\ g^{-1}$	D^{BJH} /nm	t_{wall} /nm	R^{Hg} /μm	V^{Hg} /$cm^3\ g^{-1}$
P6-1,5b1	TMCS	10.9	911	3.7	8.9	0.3	3.1
P6-1,5b2	DDMCS	10.1	654	3.6	8.1	0.2	2.3
P6-1,5b3	end-capped	10.9	768	3.7	8.9	0.3	3.3

SAXS investigations of all silylated silica gels exhibited a well-defined 2D-hexagonal pore arrangement. The SAXS diagram of the silica gels prepared from 100 mol % EGMS shows diffraction peaks for (10), (11) and (20). The values of the scattering vector coincide for the TMCS-modified and the end-capped silica gels with q_{10} = 0.5 nm^{-1}, q_{11} = 1.0 nm^{-1}, and q_{20} = 1.1 nm^{-1}, resulting in a repeating unit distance determined for the (10) diffraction of d_{10} = 11.8 nm for the TMCS-treated gel and d_{10} = 11.6 nm for the end-capped sample. (Figure 49) The gels silylated with DDMCS exhibit the analogue diffraction peaks, however, the q-values of the diffraction peaks are shifted towards higher values with q_{10} = 0.6 nm^{-1}, q_{11} = 1.0 nm^{-1}, and q_{20} = 1.2 nm^{-1}, resulting in a shorter repeating unit distance of d_{10} = 10.5 nm. This shift is also obtained for the DDMCS treated hybrid silica gels as can be seen from figure 50. The SAXS pattern of all silylated hybrid silica gels exhibit reflections for the (10), (20) and (21) diffractions. In analogy to the post-modified silica samples, the corresponding q-values of the TMCS-modified gels are consistent with the end-capped hybrid system (q_{10} = 0.6 nm^{-1}, q_{20} = 1.2 nm^{-1}, and q_{21} = 1.5 nm^{-1}) and show a repeating unit distance of d_{10} = 10.9 nm. In comparison, the DDMCS silylated gels synthesized with 10 mol % MeGMS possess higher q-values (q_{10} = 0.6 nm^{-1}, q_{20} = 1.3 nm^{-1}, and q_{21} = 1.7 nm^{-1}) and thus a shorter repeating unit distance with d_{10} = 10.1 nm.

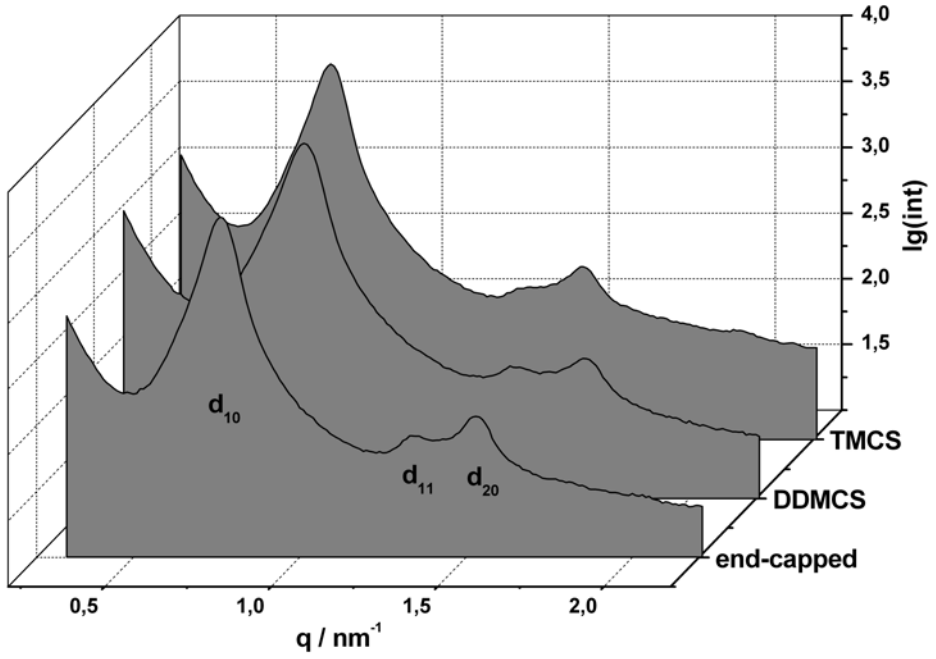

Figure 49 SAXS pattern of the silylated silica gels prepared with 100% EGMS at c(HCl) = 1 M.

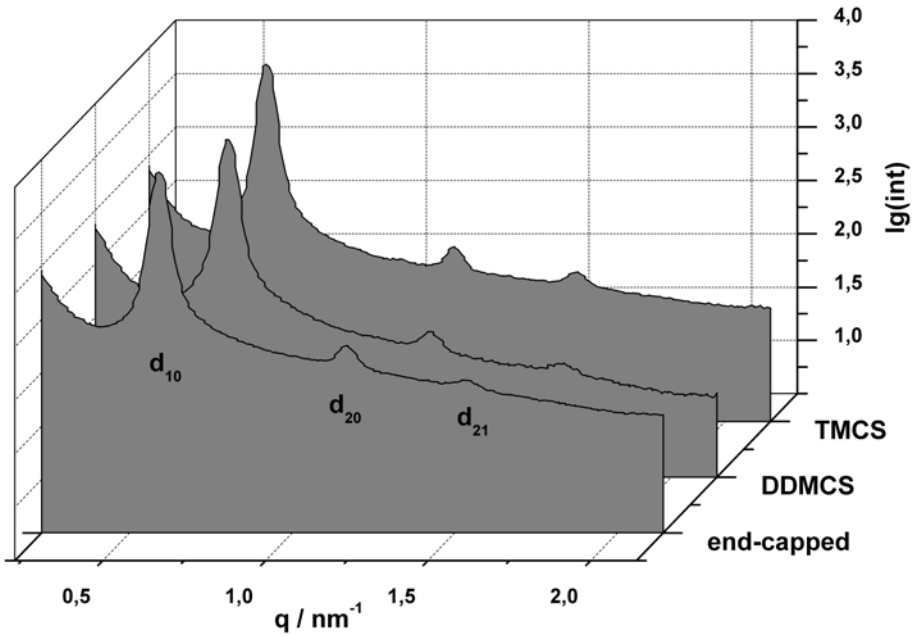

Figure 50 SAXS pattern of the silylated hybrid silica gels prepared with 10 mol % MeGMS and 90 mol % EGMS at c(HCl) = 0.03 M.

As can be seen from table 14, the shrinkage for the DDMCS-modified silica and hybrid silica gels is amplified with ΔL = 11 – 15% (ΔL: shrinkage in length) and ΔD = 8 – 9% (ΔD:

shrinkage in diameter) compared to the TMCS-modified and the end-capped silica and hybrid silica gels with $\Delta L = 4 – 7\%$ and $\Delta D = 3 – 4\%$.

Table 14 Determined shrinkage in length (L) and in diameter (D) of the silylated monoliths. The shrinkage is given in % for the final values after the heat-treatment at 200°C in relation to their initial values after aging.

sample	*silylation agent*	*mol % MeGMS*	*ΔL /%*	*ΔD /%*
P1-1g1	TMCS	0	7	3
P1-1g2	DDMCS	0	15	9
P1-1g3	end-capped	0	6	4
P6-1,5b1	TMCS	10	4	4
P6-1,5b2	DDMCS	10	11	8
6-1,5b3	end-capped	10	4	4

Furthermore, contact angle measurements with water droplets as polar measuring system reveal that all monoliths modified with DDMCS are hydrophilic. In contrary the silica gels silylated with TMCS or by end-capping possess high contact angles in the range from 127° – 135° (TMCS) and 137° – 139° (end-capping). The hydrophilicity of the silica gels silylated with chlorododecyldimethylsilane can be related to blocking of the pore entrances due to steric hindrance of the bulky C_{12} chain and hence the limitation of the diffusion of the silylation agent into the mesopore channels resulting in a high loading of silanol groups within the mesopores.[118]

The presence of a high amount of free silanol groups also explains the higher degree of shrinkage for the DDMCS-treated gels compared to the end-capped and trimethylsilylated gels with less free silanol groups on the surface.

Figure 51 shows photographs taken of the different silylated monoliths and their wetting behaviour towards a water / ink-droplet.

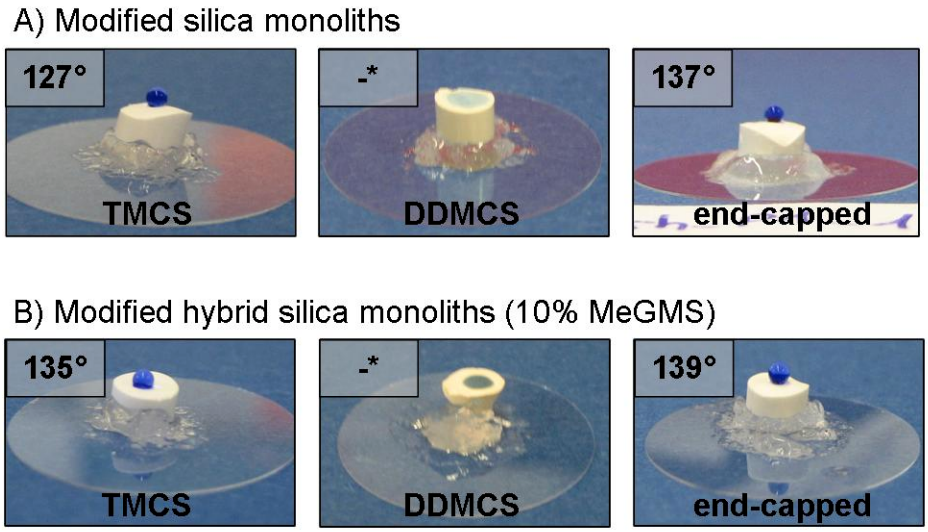

Figure 51 Photographs of the different modified monoliths and their wetting behaviour towards water (water-ink) droplets including their corresponding contact angles. * Due to the hydrophilicity of the DDMCS-modified monoliths, no contact angle was obtained.

In contrary to the surface modification via co-condensation, the formation of the macroporous network is not affected as the post-synthetic treatment has no influence on the macrophase separation and the SEM images resemble the corresponding images of figure 40 (10 mol % MeGMS at c(HCl) = 0.03 M, section 2.2.1.2.) and of figure 17 (100 mol % EGMS at c(HCl) = 1 M, section 2.1.3.1.).

2.3. Container Material

One major objective for the synthesis of monolithic HPLC columns is to create a homogeneous macroporous morphology with no densifications within the macroporous framework to guarantee a constant flow of the eluent and to avoid barriers adding to the back pressure during the separation. One explicitly sensitive region is the boundary region of the silica monolith at the interface between monolith and container wall which is especially susceptible to changes in the macroscopic morphology, *e.g.* to densifications of the macroporous framework.

As the heterogeneous regions are mostly observed close to the surface of the monolithic body, one can assume that the mould material and thus the interactions between the silica surface and the container have a major impact on the resulting boundary region.

Hence, in this section different container materials have been tested such as poly(methyl methacrylate) (PMMA), polyethylene (PE), poly(vinylidene fluoride) (PVDF, Polytetra) and polycarbonate (PC) in order to investigate the influence of the container material on the resulting morphologies. For this study, two different sol-gel systems were chosen. For once pure silica monoliths with the composition of Si / P123 / 10^{-1} M HCl = 8.4 / 30 / 70 with EGMS as sole precursor and hybrid silica monoliths with the composition of Si / P123 / 0.03 M HCl = 8.4 / 30 / 70, whereas the content of Si was established by employing 10 mol % MeGMS and 90 mol % EGMS. All silica gels were gelled and aged at 40°C for 7 d in the particular container. Prior to the heat treatment (200°C), the gels were first cured in EtOH / HCl_{conc} (6 h, 65°C) before they were subjected to a surface hydrophobization via silylation with TMCS / petroleum ether in order to preserve the monolithic body from cracking.

The physicochemical data obtained from nitrogen sorption experiments, SAXS and mercury intrusion analysis are given in table 15 for the silica monoliths and in table 16 for the inorganic-organic hybrid silica monoliths.

Table 15 Physicochemical data of the silica monoliths gelled and aged in different container materials (composition: Si / P123 / 10^{-1} M HCl = 8.4 / 30 / 70).

samples		*SAXS*	*N_2-sorption*			*Hg-Porosimetry*	
	container material	*d_{10} /nm*	*S^{BET} /$m^2\,g^{-1}$*	*D^{BJH*} /nm*	*t_{wall} /nm*	*R^{Hg} /µm*	*V^{Hg} /$cm^3\,g^{-1}$*
P1-2-1	PMMA	11.5	939	7.7	7.4	0.2	2.8
P1-2-3	PE	11.2	844	7.6	5.3	0.2	2.6
P1-2-5	PVDF	10.9	826	7.6	5.0	0.2	2.5
P1-2-8	PC	10.9	749	7.6	5.0	0.2	2.7

* D^{BJH} is calculated from the adsorption branch of the nitrogen sorption hysteresis.

Table 16 Physicochemical data of the hybrid monoliths gelled and aged in different container materials (composition: 10 mol % MeGMS / 90 mol EGMS and Si / P123 / 0.03 M HCl = 8.4 / 30 / 70).

samples		*SAXS*	*N_2-sorption*			*Hg-Porosimetry*	
	container material	d_{10} /nm	S^{BET} /$m^2\,g^{-1}$	D^{BJH*} /nm	t_{wall} /nm	R^{Hg} /μm	V^{Hg} /$cm^3\,g^{-1}$
P6-1,5.1a	PMMA	10.9	961	6.4	6.2	0.2	3.1
P6-1,5.3a	PE	10.5	975	6.4	5.7	0.2	3.2
P6-1,5.5a	PVDF	11.2	1000	7.5	5.4	0.3	3.7
P6-1,5.8a	PC	11.5	879	7.5	5.8	0.3	3.5

* D^{BJH} is calculated from the adsorption branch of the nitrogen sorption hysteresis.

The SEM images in figure 52 of the boundary regions of the silica gels (100 mol % EGMS) show that for PMMA, PE and PVDF vessels no heterogeneity within the macroporous framework can be observed, only close to the terminal edge of the monolith differences occur. Interestingly, the silica monolith synthesized in the PMMA container, exhibits silica strands that are parallel arranged, perpendicular to the edge. This peculiarity is not observed for the silica materials from the PE and PVDF moulds, where the macroporous framework is not changed adjacent to the edge.

The morphology of the silica samples synthesized within PC vessels does not resemble the observed morphologies for the monoliths described above. Here the resulting macroporous framework is less porous and disoriented compared to the periodically arranged silica-rods of the other silica monoliths. In contrary to PE, PMMA, and PVDF, PC is not stable against moisture for a longer time period, leading to cracks and crazes of the container.[119] Furthermore, the released ethylene glycol during hydrolysis and condensation reactions leads to glycolysis of the polycarbonate resulting in a partial decomposition of PC and in the release of bisphenol A.[120] This diol is less polar than ethylene glycol and disturbs the phase separation and hence, the evolution of the macroporous framework. However, as only small amounts of bisphenol A are produced at 40°C, the disturbing influence is restricted to a small area in the boundary region of the monolith (close to the container), which exhibits a distorted macroporous morphology.

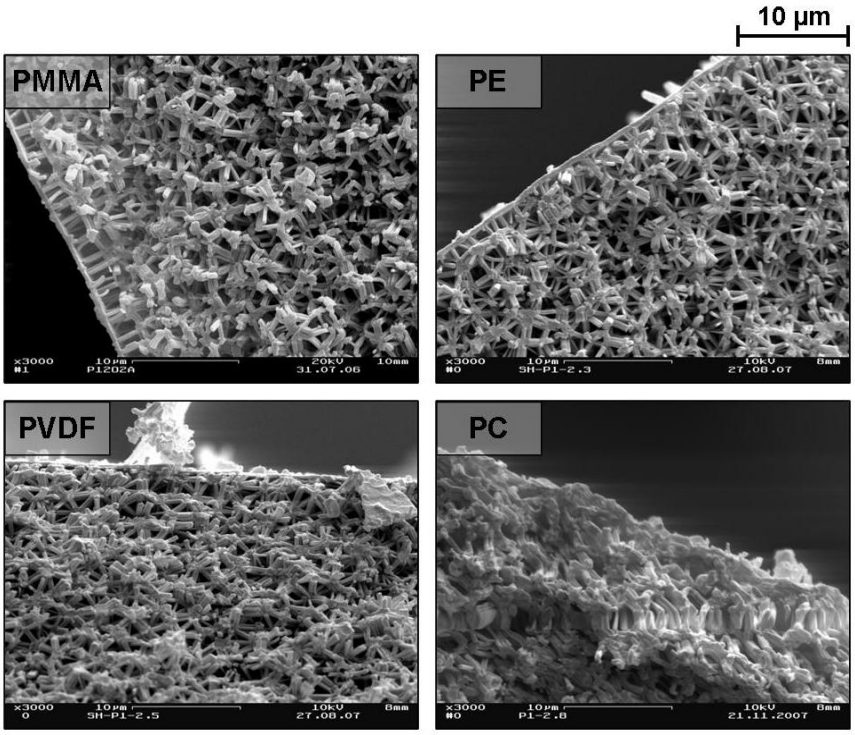

Figure 52 SEM images of the resulting macroporous morphologies in the boundary region of the SiO_2 monoliths for the different container materials.

Interestingly, the influence of the different container materials is not so pronounced for the hybrid silica monoliths (10 mol % MeGMS) as can be seen from figure 53. The boundary region of the hybrid silica monolith gelled and aged in PMMA, PE and PVDF moulds resemble the observation made for the pure SiO_2 monolith prepared in a PMMA vessel. While the bulk of the monoliths consists of regularly star-like arranged silica strands, the macroporous framework at the monoliths' edge is formed by parallel arranged silica strands which are oriented perpendicular to the monolith surface. These peculiarities can be explained by the already decreased polarity of the organically modified silica oligomers which interactions with the non-polar polyethylene and the poly(vinylidene fluoride) are stronger than for the non-modified silica oligomers resulting from the hydrolysis and condensation of sole EGMS. Furthermore, the boundary region of the hybrid silica monolith from the PC vessels does not exhibit the disoriented boundary region as the pure silica monolith. Instead, slight densifications of the boundary regions are observed indicating a reduced impact of the released bisphenol A on the formation of the methyl-modified hybrid silica network.

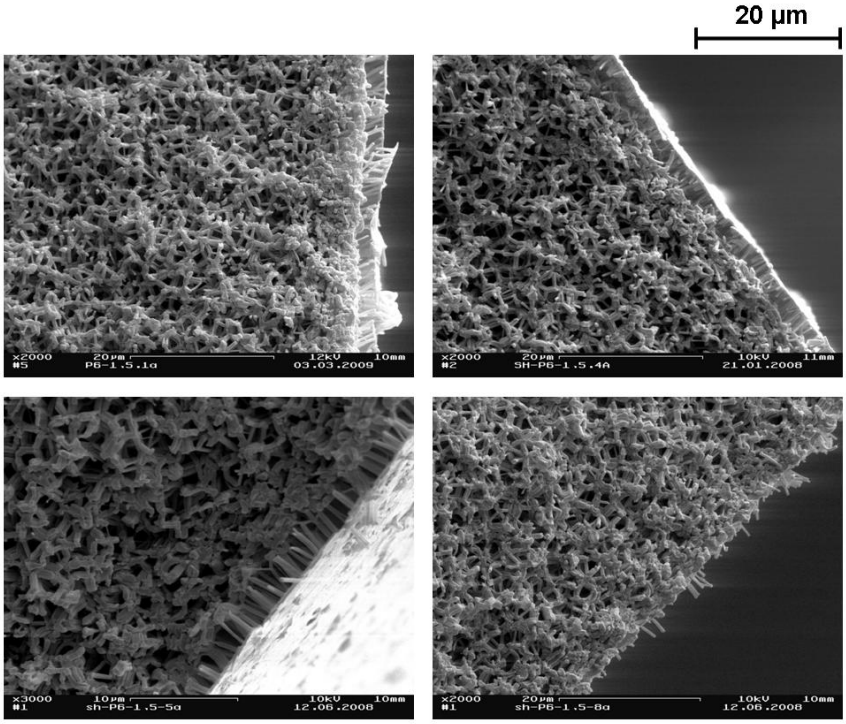

Figure 53 SEM images of the resulting macroporous morphologies in the boundary region of the hybrid silica monoliths (10 mol % MeGMS) for the different container materials.

2.4. Conclusion

Hierarchically organized silica monoliths with well-defined pore size regimes have been synthesized by the employment of an aqueous phase of Pluronic P123 as structure-directing agent and the ethylene glycol-modified silane (EGMS) as silicon source for the silica network. By adjusting the synthesis parameters such as the concentration of the acidic catalyst, the ratio of P123 to solvent, the Si content as well as gelling and aging temperature, etc. the resulting architecture of the hierarchical pore size domains can be fine tuned with respect to the desired properties. With regard to the application as HPLC columns, the silica monoliths synthesized with the composition ratio of Si / P123 / 1 and 10^{-1} M HCl = 8.4 / 30 / 70 (t_{age} = 7 d at 40°C) exhibit best results. The silica monoliths derived from these sol-gel systems possess the desired co-continuous macroporous framework with pores of uniform size (R^{Hg} = 0.3 μm) and a 2D-hexagonally arranged mesopore network with a narrow pore diameter distribution of D^{BJH}(1 M) = 6.3 nm and D^{BJH}(10^{-1} M) = 5.4 nm. (Figure 54)

For the application as Reversed Phase (RP) HPLC columns, a hydrophobic surface of the stationary phase is required. Therefore, inorganic-organic hybrid silica monoliths have been

synthesized via the direct-functionalization approach by co-condensing the organo-substituted ethylene glycol-modified precursor (methyl: MeGMS, phenyl: PhGMS) with EGMS, whereas the ratio of Si / P123 / 0.03 M HCl = 8.4 / 30 / 70 has been kept constant.

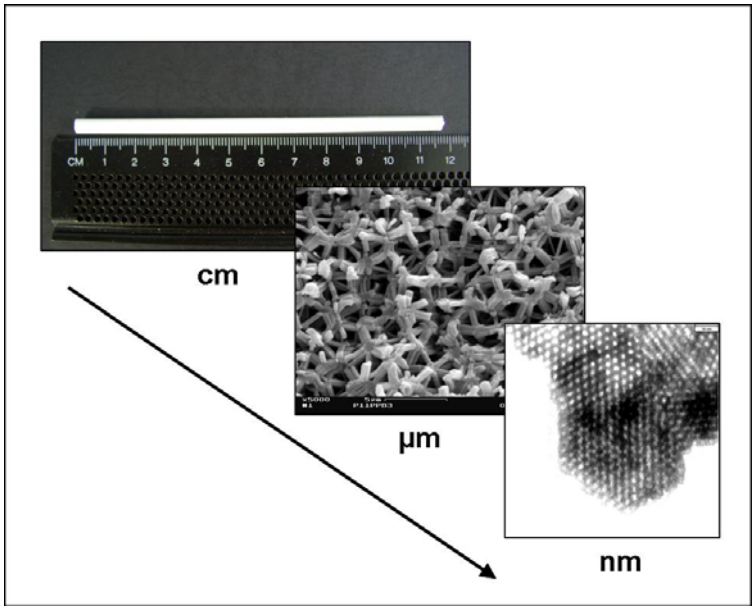

Figure 54 Hierarchically organized silica monolithprepared with the composition Si / P123 / 1 M HCl = 8.4 / 30 / 70. The monolith was aged at 40°C for 7 d in a PMMA vessel.

In analogy to the inorganic silica monoliths, the hierarchical architecture of the different pore size domains can also be adjusted by varying the synthesis parameters. However, the most crucial parameter for the preservation of the hierarchy is the ratio of the organically modified silane to EGMS. By employing MeGMS as co-precursor the 2D-hexagonally arranged mesopore network is obtained for contents of MeGMS up to 40 mol %, however, the interconnectivity of the macroporous framework is already decreased above 20 mol % MeGMS. For the employment of a PhGMS-derived sol-gel system, the 2D-hexagonal ordering in the mesoscopic range can only be obtained for a maximum content of 15 mol % PhGMS. In analogy to MeGMS, the preservation of a co-continuous macroporous network can only be achieved at even lower contents of PhGMS (contents of up to 10 mol % PhGMS). The best results for the inorganic-organic hybrid monoliths with respect to a homogeneous co-continuous macroporous framework, which skeleton exhibits a 2D-hexagonally arranged mesoporous network by simultaneous maximum loading of the organic moieties on the pore walls, have been achieved by employing 10 mol % MeGMS and by employing 5 mol %

PhGMS. (10 mol % MeGMS: R^{Hg} = 1.1 μm, D^{BJH} = 4.1 nm; 5 mol % PhGMS: R^{Hg} = 0.4 μm, D^{BJH} = 3.7 nm)

However, for the application as RP-HPLC columns, a hydrophobic surface of the silica monoliths is required. In order to improve the degree of loading of organic functionalities on the pore walls and concomitantly to inhibit destruction of the hierarchical organization, post-synthetic grafting has been applied to inorganic and inorganic-organic hybrid silica monoliths. The surface modification by employing pure chlorotrimethylsilane (TMCS) and an end-capping approach with chlorododecyldimethylsilane (DDMCS) and TMCS results in highly hydrophobic surfaces for both applied silica systems with contact angles in the range of 127 – 135° for TMCS and 137 – 139° for the end-capped monoliths. Concomitantly, the architectural features of the modified silica monoliths (prepared from 1 M HCl) and the modified hybrid monolith (10 mol % MeGMS at 0.03 M HCl) are not changed by the grafting procedure.

Investigations of the impact of the interactions between the container material and the condensed silica phase on the homogeneity of macroporous framework in the boundary region of the monolith have also be performed for the inorganic silica and the inorganic-organic hybrid silica sol-gel systems. Independently from the polarity of the employed sol-gel system, poly(methyl methacrylate) (PMMA), polyethylene (PE) and poly(vinylidene fluoride) (PVDF) proved to be adequate container materials causing no densifications and thus no severe changes of the macroscopic framework in the boundary region.

Chapter 3

New Diol-Modified Silanes as Precursors for the Sol-Gel Process

3.1. Motivation

The employment of an ethylene glycol-modified silane (EGMS) as precursor in the sol-gel process has proven to be a convenient method to synthesize hierarchically ordered monolithic silica materials. In combination with a lyotropic phase of Pluronic 123 ($EO_{20}PO_{70}EO_{20}$) in aqueous HCl as template and EGMS as silicon source, silica monoliths with a well-defined macroporous network and 2D-hexagonally arranged mesopores are obtained. As ethylene glycol, which is released during hydrolysis and condensation reactions, is a polar solvent, the formation of neither the hexagonally arranged mesopore system nor the phase separation, which causes the formation of the well-defined interconnected macroporous network, is suppressed during the sol-gel transition. The employment of tetraalkoxysilanes such as TMOS and TEOS in the sol-gel processing of hierarchically organized silica monoliths indicates that with decreasing polarity of the released alcohol additional polar agents such as poly(ethylene

oxide) (PEO) have to be applied for the initiation of phase separation in order to obtain a co-continuous macroporous framework.[92, 94]

When a diol-modified silane is employed as precursor, which impact has the polarity of the released diol on the formation of the different pore size regimes? When diols with different alkyl chain lengths are used, how does the change of polarity affect the ordering in the macroporous and mesoporous range?

3.2. Synthesis and Characterization of the Precursors

For the investigation of these questions, silanes were modified with 1,2-propane diol (PGMS), 2,3-butane diol (BDMS), and 1,2-hexane diol (HDMS) by a transalkoxylation reaction. In analogy to the synthesis of EGMS according to Mehrotra et al.[67], tetraethylorthosilicate (TEOS) was reacted with the particular diol in the molar ratio of 1:4. As EGMS is very sensitive towards hydrolysis reactions in the presence of water, all diols were pre-dried over Na_2SO_4 and were subsequently distilled from magnesium prior to the reaction. The transesterification reaction was conducted in inert atmosphere and the produced alcohol was continuously removed by distillation.

In analogy to EGMS, all diol-modified silanes were characterized by spin-lock ^{29}Si-NMR spectroscopic investigations in benzene-d_6 and by thermogravimetric measurements. The presence of residual alcohol *e.g.* ethanol was investigated by ^{1}H-NMR experiments in benzene-d_6 or $CDCl_3$.

Figure 55 depicts the reaction scheme as well as the equilibrium reactions between the diol-modified monomer and (inter- and intramolecular) condensed species.[48]

Spin-lock ^{29}Si-NMR spectra of all diol-modified silanes show peaks in the range of δ(benzene-d6) = -82 – -86 ppm. However, not a single but multiple peaks of almost identical chemical shifts are observed in each NMR spectrum indicating the presence of equilibrium bridged and intramolecular condensed species.

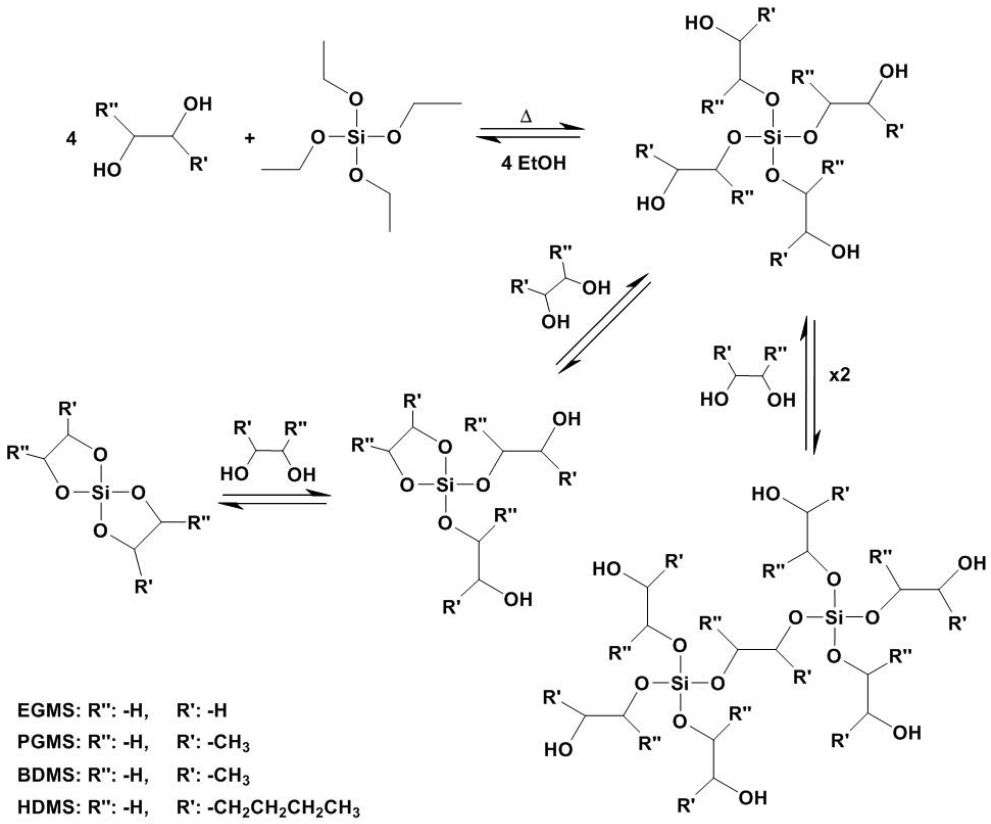

Figure 55 Schematic depiction of the synthesis and the equilibrium reactions of the different diol-modified silanes.

Thermogravimetric measurements of all diol-modified silanes were performed in the temperature range from 30 – 1000°C in air. (Figure 56) For EGMS three major weight losses are observed. The first weight loss of 23.5% from 30 – 210°C can be related to residual ethanol, unreacted tetraethylorthosilicate (bp: 168°C, p = 1.013 bar) and free ethylene glycol (bp: 198 – 199°C, p = 1.013 bar). In the second step, bonded ethylene glycol is eliminated under the formation of bridged and intramolecular condensed species. This elimination results in a weight loss of 43.4% in the temperature range of T = 210 – 450°C. In the course of the final weight loss (12.7%) between 450 – 1000°C oxidative decomposition to pure SiO_2 proceeds. Calculation of the Si-content from the residual mass of SiO_2 results in 9.7 wt % Si (theoretical: 10.4 wt %). In analogy to EGMS, resembling weight losses are also observed for PGMS. In the temperature range of T = 30 – 220°C residual ethanol, unreacted TEOS, and free propane diol (20.3%, bp of free 1,2-propane diol: 185 – 189°C) are released first, while between T = 220 – 300°C (35.7%) bonded 1,2-propane diol is eliminated, until between 300 – 1000°C the final oxidative decomposition to SiO_2 is observed (28.4%). The Si-content determined from the residual mass of SiO_2 is 7.4 wt % (theoretical: 8.6 wt %).

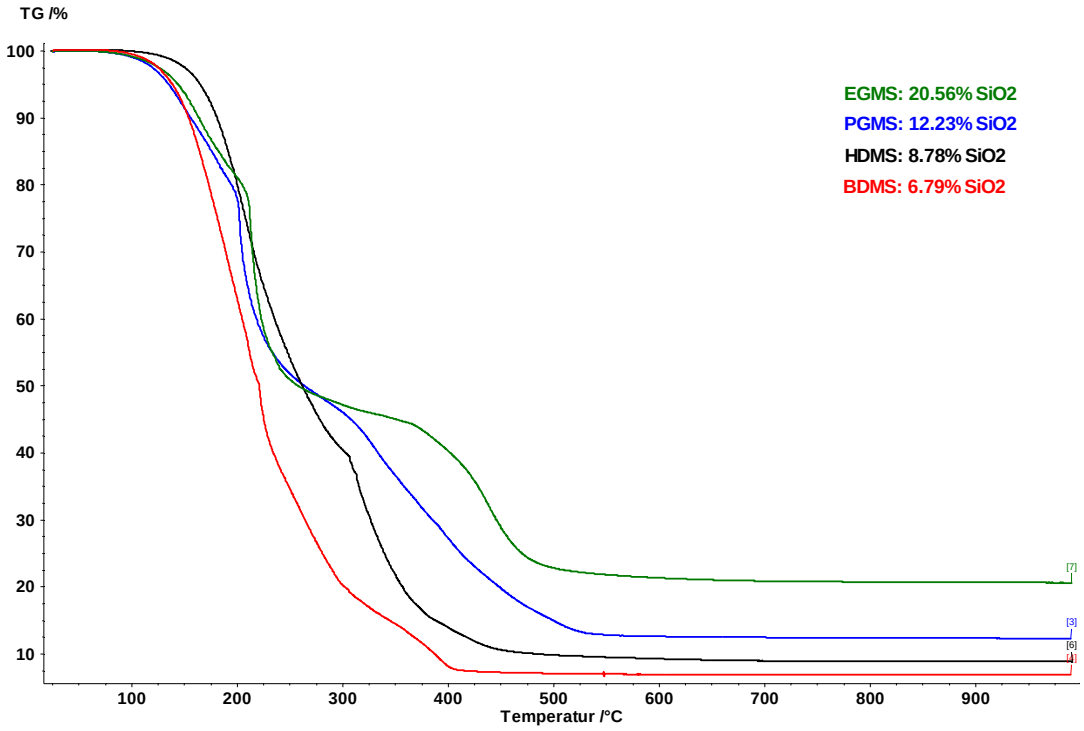

Figure 56 Thermogravimetric diagram of the thermo-oxidative decomposition of EGMS, PGMS, HDMS, and BDMS from 30 to 1000°C in air.

Interestingly, the TG curves of BDMS and HDMS show higher weight losses with 49.4% and 59.7% in the first step than observed for EGMS or PGMS, respectively. These weight losses indicate a high percentage of free 2,3-butane diol (bp: 183 – 184°C) and 1,2-hexane diol (bp: 214 – 215°C) and also unreacted tetraethylorthosilicate. Keeping in mind that from ethylene glycol to 2,3-butane diol and 1,2-hexane diol, steric effects of the increasing alkyl chain lengths hinder the substitution of all four substitution sites of the Si atom, the high percentage of free diol is not surprising.[67]

In the further course of the TG curves, BDMS shows a second weight loss of 30.3% in the range of 220 – 300°C for the elimination of bonded diol molecules, which is shifted to higher temperatures (300 – 390°C) for HDMS (25.3%). The oxidative decomposition to SiO_2 is observed between T = 300 – 1000°C for BDMS (13.5%) and from 390 – 1000°C for HDMS (6.3%), and the resulting Si-contents are determined as 3.2 wt % for BDMS (theoretical: 7.3 wt %) and 4.1 wt % for HDMS (theoretical: 5.7 wt %). The difference of the resultant SiO_2 contents and the theoretical determined silica contents can be related to the hindered substitution of the ethoxy groups by the 2,3-butane diol and the 1,2-hexane diol resulting in a high amount of unreacted TEOS compared to the substitution by ethylene glycol. The large

weight loss in the first step for BDMS and HDMS is an indication for the hindered substitution.

3.3. Influence of the Released Diol on the Hierarchy

All diol-modified silanes (PGMS, BDMS, and HDMS) are employed as sole precursors for the preparation of hierarchically organized silica monoliths, whereas EGMS is the reference system.

In analogy to precedent investigations, a lyotropic phase of Pluronic P123 in aqueous HCl is employed as supramolecular template in order to achieve a high degree of mesoscopic ordering. Concomitantly, P123 also induces a phase separation process in the macroscopic range. By varying the concentration of the acid catalyst in the range of c(HCl) = 1 - 10^{-6} M, the employment of P123 allows for the tuning of the hierarchical architecture of the pore size regimes (see also section 2.1.3.).

Starting from a ratio of Si / P123 / x M HCl = 8.4 / 30 / 70 (by weight) for EGMS and PGMS, the analogue compositions of the 2,3-butanediol- and 1,2-hexanediol-modified silanes result in silica gels with no hierarchical architecture. Hence, the Si content was reduced to 4.2 or 4.5 wt %, respectively, in order to limit the amount of the released diol which disturbs the formation of the different pore size domains due to the altered polarity.

In accordance with the prior investigations, all systems are gelled and aged at 40°C for 7 – 8 d. The template extraction from the pores and the simultaneous surface hydrophobization in order to preserve the monolithic body from cracking was achieved by treating the gels with TMCS in petroleum ether. Subsequent to the silylation, the gels are subjected to a washing procedure (petroleum ether, ethanol) before they are dried up to 200°C.

Prior to the synthesis of the silica gels, SAXS investigations were conducted to study the impact of each diol on the lyotropic phase of P123 (30 wt %) in 1 M HCl. Figure 57 shows the obtained SAXS curves for the different diols at 40°C, whereas the ratio of diol to template phase was varied from 0:1 to 0.75:1 by weight.

Even though, the employment of a sol consisting of P123 / 1 M = 30 / 70 as template and EGMS as precursor, results in silica gels with a 2D-hexagonally arranged mesopore structure (see also section 2.1.3.), the pure template phase does not exist as a single liquid crystalline phase but is a mixture of two different lyotropic phases.[121, 122] Figure 57 shows the structural development with increasing content of the particular diol.

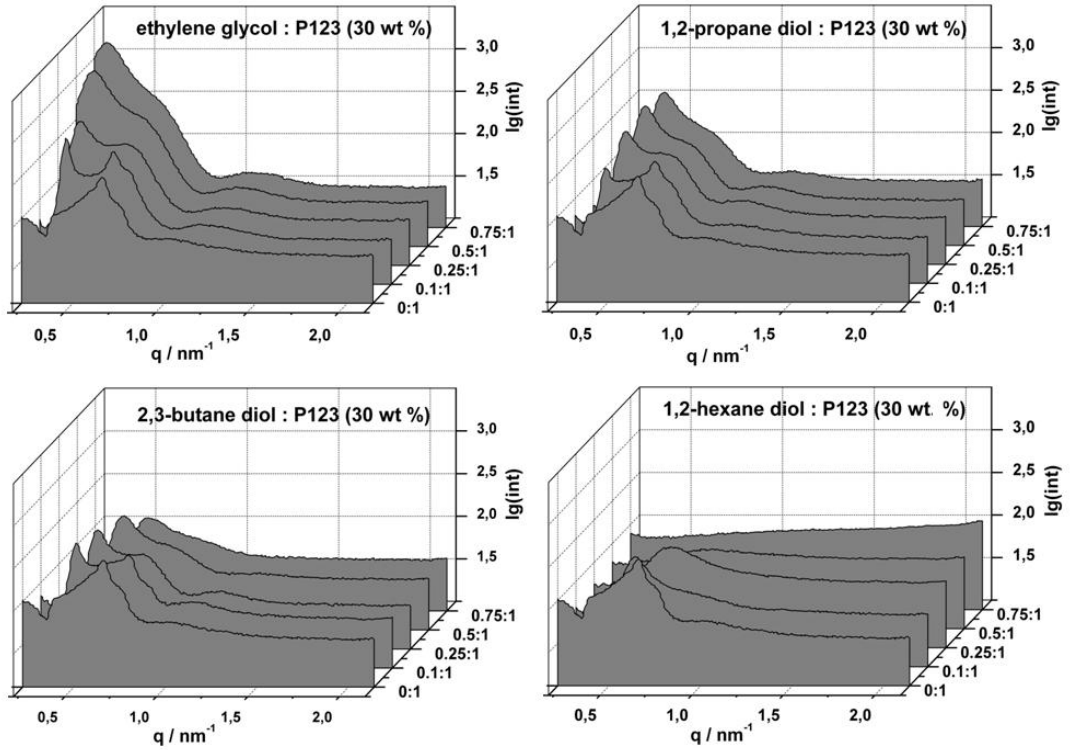

Figure 57 SAXS diagrams showing the influence of each diol on the lyotropic liquid crystalline phase of P123 (30 wt %) in 1 M HCl. The ratio of diol to the P123 template phase is given by weight.

The poor resolution of the diffraction peaks can be related to two problems involved with the measurement of liquid crystalline phases. As liquid crystalline phases are dilute systems with only few scattering objects being present within the reach of the X-ray beam, high initial intensities of the X-ray beam or long radiation times are required in order to obtain well-resolved scattering diagrams. The other problem is the fluidity of the P123 / 1 M HCl-system of 30 wt % at 40°C. Even though it is viscous, fluctuations within the system can cause a broadening of the resultant diffraction peaks.

However, it is known from former Synchrotron measurements of P123 in 10^{-2} M[121] and 1 M[122] HCl (30 / 70 wt %) at 40°C performed by Fritscher and colleagues, that the P123 phase in this concentration region is formed by cubic and hexagonally closed-packed spheres. Therefore, the diffraction peaks of the pure template phase can be related to a hexagonally closed-packed arrangement of spheres exhibiting the symmetry of P_{6_3mmc} and a cubic ordering of spheres of the symmetry F_{m3m}.

Table 17 Classification of the Bragg reflections of the various phase types; a: lattice constant, q: scattering vector, hkl: Miller indices, R^m: micelle radius.

phase	*position of Bragg reflections*	*sequence of Bragg reflections*	*micelle radius/ nm*
HCPS* (P_{6_3mmc})	$q_{hkl} = \frac{2\pi\sqrt{\frac{4}{3}(h^2+hk+k^2)+\frac{3}{8}l^2}}{a}$	(100), (002), (102), (110), (200), (112), ...	$R^m = \sqrt{2}/4\ a$
FCC (F_{m3m})	$q_{hkl} = \frac{2\pi\sqrt{h^2+k^2+l^2}}{a}$	(111), (200), (220), (311), (222), (400), ...	$R^m = a/2$

*HCPS: hexagonally close-packed spheres, FCC: face centred cubic.

The pattern of the pure P123 (30 wt %) in 1 M HCl shows a broad shoulder at q = 0.4 nm^{-1}. Despite the poor resolution, this diffraction peak can be related to P123 aggregates exhibiting a weak cubic close-packed ordering (F_{m3m}) as learned from the former Synchrotron experiments of a P123 phase of identical composition and measuring temperature.[122]

As can be seen from the SAXS diagram for the influence of free ethylene glycol in the top left corner of figure 57, this reflection evolves with increasing content of ethylene glycol. The corresponding q vector is shifted towards smaller values from q = 0.4 nm^{-1} (for 0% ethylene glycol) to q = 0.3 nm^{-1} for 75% ethylene glycol indicating an extension of the micellar radii from R^m = 9.6 nm to R^m = 13.7 nm (calculated for cubic closed-packed spheres). The inclusion of the polar ethylene glycol molecules (dipole moment μ = 2.26 D[123]) within the PEO shell results in swollen P123 micelles and thus to an increase of the lattice constant from a = 27.2 nm for the pure P123 phase up to a = 38.9 nm for the content of 75% ethylene glycol. This phenomenon was also observed for Pluronic P105 (EO_{37}-PO_{58}-EO_{37}). Alexandridis and co-workers reported the swelling of P105 micelles by addition of polar polyols such as glycerol (dipole moment μ = 2.68 D) resulting in larger lattice constants.[124, 125]

The addition of ethylene glycol (≥ 10%) and, thus the dilution of the system, results in an emerging (111) diffraction peak which indicates a shift from the HCPS arranged phase to a more cubic close-packed arranged phase. Thus, the number of HCPS arranged P123 aggregates is reduced and concomitantly a more pronounced arrangement of cubic close-packed spheres is obtained. In contrary, the enrichment of the template phase by addition of P123 at identical conditions results in the transformation of HCPS to hexagonally arranged cylindrical micelles,

which was affirmed by scattering experiments.[122] Parallel to the evolution of the (111) diffraction, the reflection at $q = 0.7\ nm^{-1}$ for the pure P123 (30 wt %) phase continuously diminishes. Above 25% ethylene glycol only a shoulder remains at $q \approx 0.6\ nm^{-1}$. Keeping in mind that the hydrolysis of EGMS theoretically produces four molecules of ethylene glycol, the employment of the composition of Si / P123 / x M = 8.4 / 30 / 70 results in a diluted sol system which is comparable to the dilution when the ratio of ethylene glycol / template phase = 0.75 / 1 is applied. (Figure 57) Despite this degree of dilution, the resulting silica monoliths possess a 2D-hexagonal ordering in the mesoscopic range indicating a self-assembly process of the polymerizing silica oligomers with the P123 micelles during the polycondensation, which is favoured by strong interactions between silanol groups and the hydrophilic shell of the P123 micelles.[96, 126]

The addition of 1,2-propane diol and 2,3-butane diol to the P123 mixture also results in the shift towards a phase of cubic close-packed spheres. In contrary to ethylene glycol, the increasing content of 1,2-propane diol only causes an insignificant shift of the peak for the (111) diffraction (q_{111} (0 – 75% PD) = 0.38 – 0.40 nm^{-1} , PD: 1,2-propane diol). The corresponding lattice constants are in the range of a^{fcc} = 27.2 – 28.6 nm indicating no insertion of 1,2-propane diol within the P123 micelles and thus no swelling of the micelle radii is observed (R^m = 9.6 – 10.1 nm).

The corresponding SAXS investigations of the impact of 2,3-butane diol and 1,2-hexane diol exhibit a contrary trend compared to ethylene glycol. The q-values for the (111) diffractions increase with addition of each diol (from q_{111}(0% diol) = 0.4 nm^{-1} to q_{111}(50% 2,3-butane diol) = 0.5 nm^{-1} and q_{111}(10% 1,2-hexane diol) = 0.5 nm^{-1}). The corresponding lattice constant a decreases from a = 27.2 nm to a = 23.2 nm for the butane diol (50%) diluted system and to a = 20.5 nm by addition of 10% 1,2-hexane diol. The corresponding SAXS diagrams of both systems in figure 57 show that by increasing the diol content above 10% for 1,2-hexane diol and above 50% for 2,3-butane diol the development of the SAXS pattern is reduced to one broad diffraction peak indicating a loss of periodicity of the arrangement of the micelles.
The reduction of the corresponding micelle radii from R^m (0% diol) = 9.6 nm to R^m = 8.2 nm for 50% 2,3-butane diol and R^m = 7.3 nm for 10% 1,2-hexane diol is caused by the contraction of the hydrophilic shell consisting of the PEO-blocks in order to reduce the unfavourable energetic interactions between the hydrophilic PEO shell and the non-polar diol.

The trends of the influence of the different diols are shown in figure 58, whereas the evolution of the lattice constant a is drawn in dependency of the diol content.

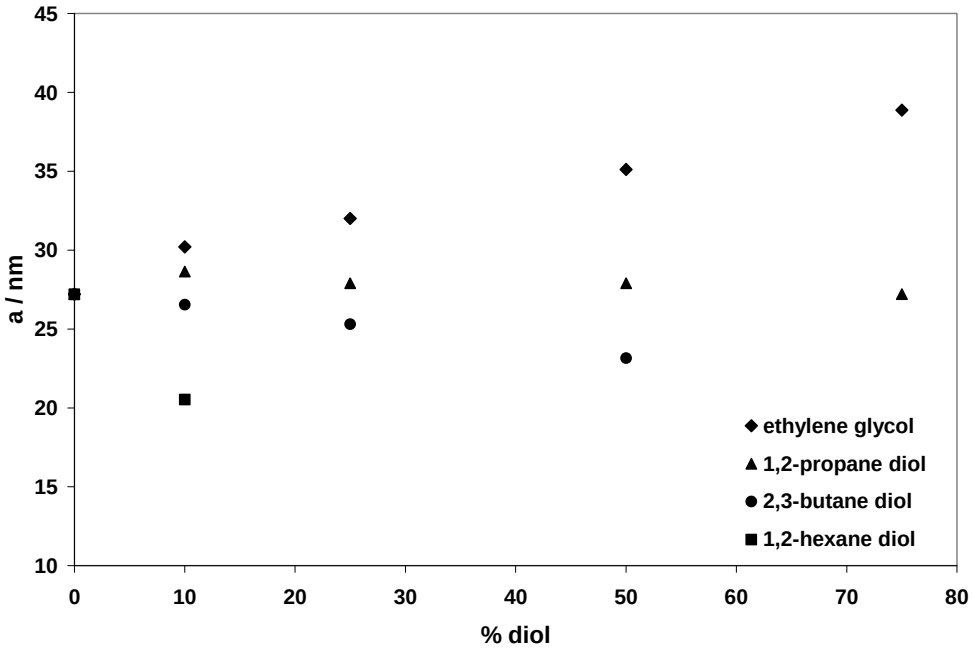

Figure 58 Correlation between the lattice constant a in dependency of the type and the content of the varied diols.

Investigations of the gelation times as a function of the acid concentration, show that the type of the released diol has an impact on the rates of hydrolysis and condensation and thus on the gelation times. As can be seen from figure 59, all diol-modified silanes show maximum values up to 40050 min at wt % Si = 8.4 for the sol-gel transitions between 10^{-1} and 10^{-2} M and minimum values at low concentrations (c(HCl) < 10^{-3} M), which is in accordance with the results reported by Brandhuber et al. for EGMS and the 1,2-propane diol-modified silane.[48]

Table 18 Gelation times of the silica monoliths prepared from the diol-modified silanes at different HCl concentrations and varying Si-contents at room temperature.

c_{HCl} /mol l^{-1}	*EGMS* 8.4 t_g/ min	*PGMS* 8.4 t_g/ min	*BDMS* 8.4 t_g/ min	*HDMS* 8.4 t_g/ min	*BDMS* 4.2 t_g/ min	*HDMS* 4.5 t_g/ min
1	300	600	5160	660	2125	2000
10^{-1}	670	6000	40050	4470	31255	22380
10^{-2}	1440	5520	32940	5940	24780	44640
10^{-3}	5	50	1100	50	420	75
10^{-4}	2	15	520	42	197	52
10^{-6}	<1	10	465	25	180	40

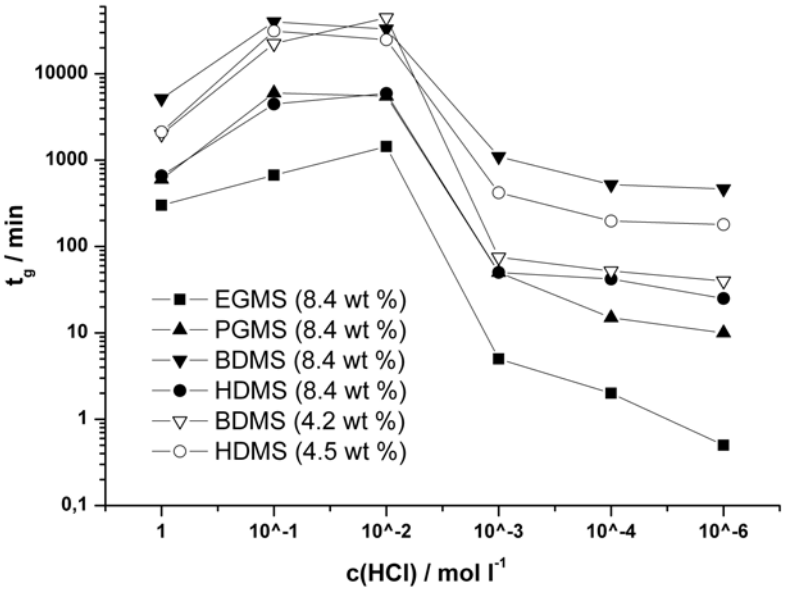

Figure 59 Diagram of the gelation times for the different diol modified silanes at room temperature.

At high acid concentrations (1 M) and Si-contents of 8.4 wt %, the gelation times increase from EGMS (t_g = 300 min) to PGMS (t_g = 600 min) to HDMS and BDMS, exhibiting a trend of t_g(EGMS) < t_g(PGMS) ≈ t_g(HDMS) < t_g(BDMS). Interestingly, the gelation time for HDMS almost coincides with PGMS with 660 min, whereas the BDMS-derived system takes 5160 min for the sol-gel transition. This delay results from the high dilution of BDMS with free 2,3-butane diol and the low Si-content (3.2 wt %) determined by TGA measurements.

This trend of t_g(EGMS) < t_g(PGMS) ≈ t_g(HDMS) < t_g(BDMS) is also observed for HCl concentrations of 10^{-1} and 10^{-2} M at which the gelation times vary from 670 min for EGMS to

40050 min for BDMS at 10^{-1} M and from 1440 min to 32940 min at 10^{-2} M for EGMS to BDMS. (The exact gelation times of the different diol-modified silanes are listed in table 18.)
As known from other alkoxy-derived silica systems, the point of zero charge of silica is around pH 2, indicating that the silica particles do not carry any charges, and hence condensation reactions sustain a minimum resulting in a significant increase of gelation times.[59] This trend corresponds to the results for the different diol-modified systems. Below 10^{-2} M HCl all diol-modified silanes exhibit decreasing gelation times and reach minimum values at 10^{-6} M at which the gelation of EGMS occurs in less than 1 min and the gelation of PGMS within 10 min.

Due to the disturbing effect of the amount of released diol on the macro- and mesophase separation for BDMS and HDMS, no hierarchical organized silica gels can be obtained, when Si-contents of 8.4 wt % are applied. Therefore, the Si-content for both diol-modified silanes is reduced to 4.2 wt % (BDMS) and 4.5 wt % (HDMS). The observed gelation times for the reduced Si-content of HDMS are delayed compared to the system with wt % Si = 8.4. At c(HCl) = 1 M the sol-gel transition occurs after 2000 min (for comparison t_g(8.4 wt %) = 660 min) and at c(HCl) = 10^{-2} M the gelation is only observed after 44640 min (t_g(8.4 wt %) = 5940 min). By decreasing the Si-content, fewer siliceous species are present for the polycondensation, leading to a lower degree of cross-linking which causes the extended gelation period. Interestingly, BDMS shows the opposite trend with reduced gelation times at wt % Si = 4.2. At c(HCl) = 1 M the sol-gel transition is accomplished after 2125 min, which is half the time the system takes with wt % Si = 8.4. Even though the reduced Si-content limits the degree of polycondensation (in analogy to HDMS), the reduced dilution of the sol-gel system by free 2,3-butane diol outweighs this effect, which results in an earlier sol-gel transition.

The silica gels synthesized with EGMS and PGMS at 1 M HCl as well as BDMS with 4.2 wt % Si, turn turbid after gelation. The silica gels prepared from HDMS stay transparent for all investigated Si-contents (8.4 – 4.5 wt %) at all HCl concentrations, indicating no macrophase separation and thus no evolution of a defined macropore domain. In addition, SAXS experiments as well as nitrogen sorption experiments exhibit no ordering of the pores in the mesoscopic range and hence the experiments of the HDMS-derived silica gels are excluded in the following presentation of the results.

In contrary, the employment of PGMS as precursor results in macrophase separated silica gels in the complete concentration range from 1 to 10^{-6} M.

The following tables 19 and 20 list the physicochemical data obtained from nitrogen sorption and SAXS measurements for the silica gels prepared with PGMS and BDMS at different HCl concentrations. The corresponding results for the silica gels obtained from EGMS are listed in table 5 of section 2.1.3.1.

Table 19 Physicochemical data of the silica monoliths prepared with PGMS as sole precursor at different HCl concentrations. The Si-content was kept constant with 8.4 wt %.

samples		*SAXS*	*N_2-sorption*			*Hg-Porosimetry*	
	c(HCl) /mol l^{-1}	d_{10} /nm	S^{BET} /m^2 g^{-1}	D^{BJH} /nm	t_{wall} /nm	R^{Hg} /μm	V^{Hg} /cm^3 g^{-1}
PG3-8.4-0-8	1	9.1	721	3.5	7.0	0.01	0.8
PG3-8.4-1-8	10^{-1}	8.2	455	3.0;4.2	6.5	-*	-*
PG3-8.4-2-8	10^{-2}	9.0	594	3.0;4.2	7.4	-	-
PG3-8.4-3-8	10^{-3}	10.3	1110	6.2	5.7	-	-
PG3-8.4-4-8	10^{-4}	10.1	1012	5.2	6.5	-	-
PG3-8.4-6-8	10^{-6}	10.5	975	5.3	6.8	-	-

* no uniform pore size distributions could be obtained.

Table 20 Physicochemical data obtained for the silica gels prepared with BDMS (4.2 wt %) at different HCl concentrations.

samples		*SAXS*	*N_2-sorption*			*Hg-Porosimetry*	
	c(HCl) /mol l^{-1}	d_{10} /nm	S^{BET} /m^2 g^{-1}	D^{BJH} /nm	t_{wall} /nm	R^{Hg} /μm	V^{Hg} /cm^3 g^{-1}
BD3-4.2-0-8	1	8.1	805	3.4	6.0	-*	0.5
BD3-4.2-2-8	10^{-2}	-	623	-*	-	-	-
BD3-4.2-3-8	10^{-3}	-	931	-*	-	-	-
BD3-4.2-4-8	10^{-4}	-	639	-*	-	-	-
BD3-4.2-6-8	10^{-6}	-	1015	-*	-	-	-

* no uniform pore size distributions could be obtained for the mesopore size calculation by the BJH method and the macropore size determination by mercury porosimetry experiments.

The direct comparison of the SAXS pattern of the silica gels prepared from EGMS, PGMS, and BDMS at c(HCl) = 1 M shows the impact of the polarity of the released diol on the formation of the mesoscopic ordering. (Figure 60) The reflections for the (10), (11), and (20) diffractions indicating a 2D-hexagonally arranged mesoporous structure are well resolved for the EGMS-derived system resulting in a repeating unit distance of 11.2 nm (calculated from q_{10} = 0.6 nm^{-1}). The corresponding SAXS pattern of the PGMS- and BDMS-derived silica gels, however, show a loss of long-range ordering of the mesopore arrangement. The SAXS curves of both systems exhibit only one broad reflection at q^1 = 0.7 nm^{-1} (PGMS) and q^1 = 0.8 nm^{-1} (BDMS). However, as a certain repeating pattern can be extracted, the repeating unit distances are determined as d^1 = 9.1 nm for PGMS and d^1 = 8.1 nm for BDMS.

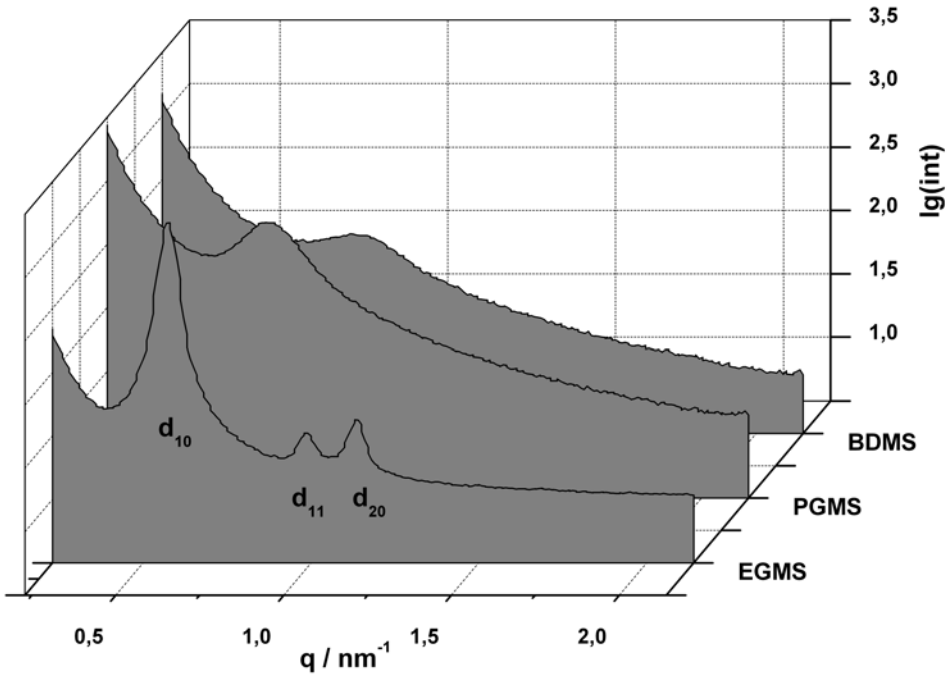

Figure 60 Direct comparison of the SAXS pattern of silica gels synthesized with EGMS (8.4 wt % Si), PGMS (8.4 wt % Si), and BDM (4.2 wt % Si) at c(HCl) = 1 M.

As can be seen in figure 61, TEM investigations of these samples show a change of the periodic arrangement of the mesopores from EGMS to BDMS. The TEM image of the EGMS-derived sample shows the honeycomb structure of the mesopores, which coincides, with the results of a 2D-hexagonal mesopore arrangement from the SAXS investigation. The TEM image of the silica gel prepared from PGMS exhibits pore channels that are arranged parallel indicating a 2D-hexagonal array of mesopores despite the poor resolution of the corresponding SAXS

pattern. The further decrease of the polarity to 2,3-butanediol results in the formation of a wormhole-like mesopore array.

The change in polarity of the released diol has not only a high impact on the development of the ordering in the mesoscopic range, but also on the evolution of the macroporous morphology. While the employment of EGMS at c(HCl) = 1 M favours the formation of a bicontinuous macroporous framework consisting of rod-shaped silica strands with a narrow pore radii distribution (R^{Hg} = 0.3 μm), the use of PGMS and BDMS result in a particulate morphology formed by spherical particles. (Figure 61) Interestingly, the employment of PGMS results in rather polydisperse particles with diameters in the range 1 – 7 μm, while in the BDMS-derived silica gel the particles are more monodisperse with diameters of 4 – 5 μm.

The phase separation in the macroscopic range is also strongly dependent on the polarity of the released diol or alcohols during hydrolysis reactions. Investigations by Nakanishi and Tanaka of TMOS-derived sol-gel systems showed that by introducing a polar additive such as formamide in the presence of either amphiphilic surfactants or polar polymers like PEO, the onset of phase separation and hence the resulting morphology can be adjusted.[45] In the process of polymerization, the polymerising siloxane oligomers loose polarity with increasing chain length and concomitantly the fluid phase depletes from polar water molecules caused by hydrolysis reactions.[127] In order to establish a gradient between the "non-polar" condensed silica species and the fluid phase, polar additives such as PEO are added and thus the formation of the macroscopic morphology can be controlled by adjusting the onset of phase separation, the spinodal decomposition.

As EGMS releases polar ethylene glycol during hydrolysis and condensation reactions, the gradient of polarity between the polymerising silica species and the solvent phase is established resulting in co-continuous macroporous morphologies in acidic media. By reducing the polarity of the released diol, the gradient between the silica polymers / oligomers and the fluid phase is reduced leading to a delayed phase separation and sol-gel transition compared to EGMS. The delay of the sol-gel transition causes a coarsening of the macroporous morphology until spheroidization and sedimentation occur resulting in a macroporous morphology formed by aggregation of spherical particles.

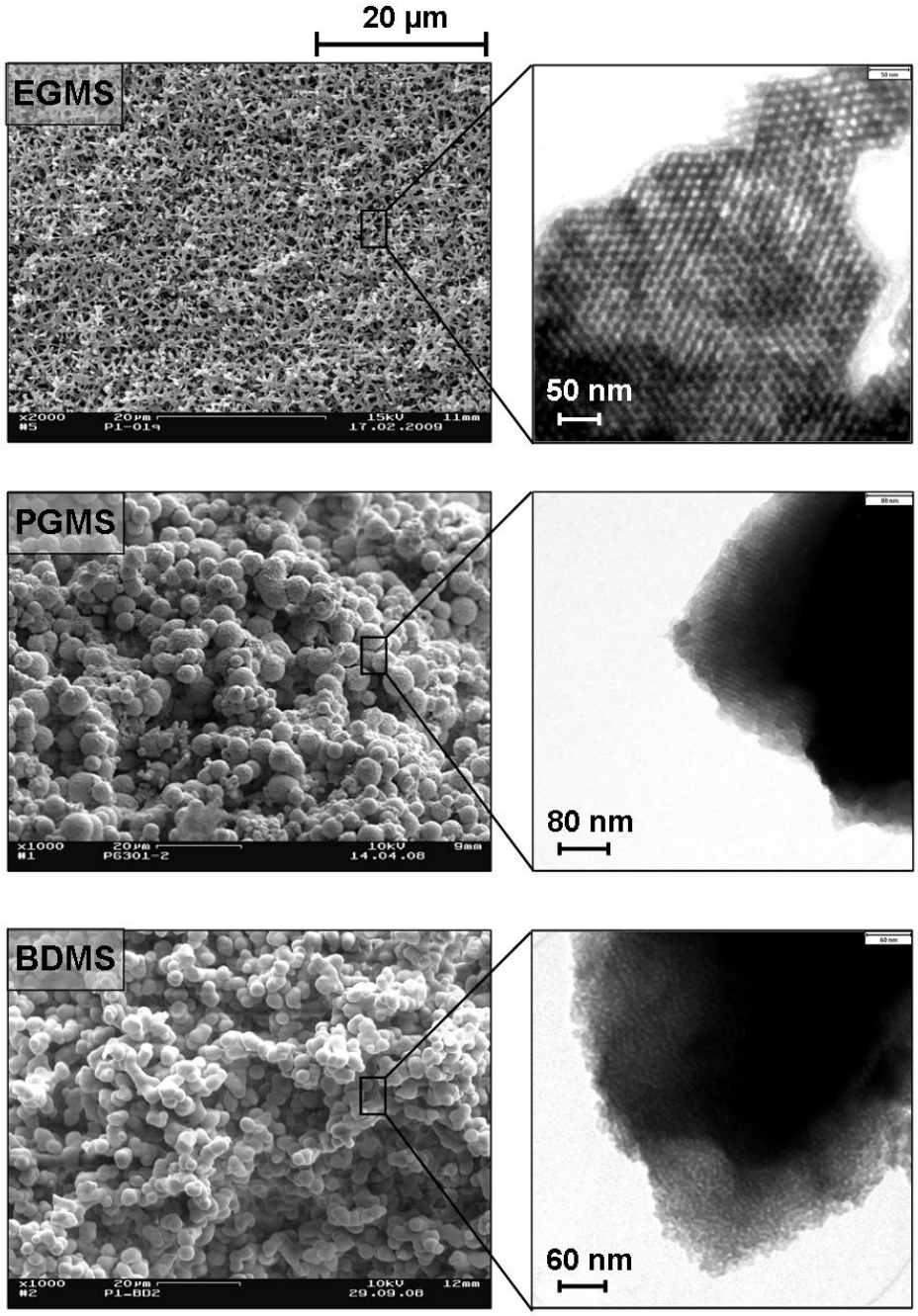

Figure 61 SEM and TEM images of the silica gels prepared with the different diol-modified silanes at c(HCl) = 1 M. From top to bottom: EGMS (8.4 wt % Si), PGMS (8.4 wt % Si), and BDMS (4.2 wt % Si)

3.4. Conclusion

The investigations of new diol-modified silanes such as PGMS (1,2-propane diol), BDMS (2,3-butane diol), and HDMS (1,2-hexane diol) as precursors for the synthesis of hierarchically organized silica monoliths have shown that the resulting architecture of the different pore size regimes is greatly influenced by the polarity of the diol which is released during hydrolysis and condensation reactions. Whereas the analogue EGMS-derived silica gels (at c(HCl) = 1 M) exhibit a co-continuous macroporous framework formed by regularly arranged silica strands and mesopores with a 2D-hexagonal ordering, the silica gels synthesized with PGMS by adapting the identical composition of Si / P123 / 1 M HCl reveal a particulate morphology in the macroscopic range formed by spherical silica particles and a reduced ordering for the mesoporous system. By adapting the identical composition for BDMS and HDMS no hierarchically organized silica monoliths can be obtained. Only by reducing the BDMS content to 4.2 wt %Si and hence the amount of released and free 2,3-butane diol molecules, hierarchical pore size domains can be achieved. The macroscopic morphology formed by spherical particles resembles the morphology observed for the PGMS-derived silica monoliths to a large extend. But in contrast to PGMS and EGMS, the influence of the released 2,3-butane diol on the phase separation in the mesoscopic range leads to wormhole-like arranged mesopores.

Chapter 4

Comparison of TEOS, Silicic Acid and Sodium Silicate to EGMS

4.1. Motivation

The employment of the ethylene glycol-modified silane (EGMS) as precursor in the sol-gel process results in hierarchically organized silica monoliths with tuneable pore architectures. By adjusting the synthesis parameters such as acid concentration, the composition of the Pluronic P123 template phase, a mesoporous network exhibiting a 2D-hexagonal periodic ordering and a co-continuous macroporous morphology can be achieved. Especially the employment of the composition of Si / P123 / 1 M and 10^{-1} M HCl of 8.4 / 30 / 70 wt % (in the case of EGMS) results in hierarchically organized silica monoliths with well-defined and distinctive pore size domains. However, the question arises whether the employment of a diol-modified silane is crucial in order to obtain hierarchically organized silica monoliths. Is it also possible to synthesize this kind of materials by employing commercially available silicon precursors, such as tetraethylorthosilicate (TEOS), sodium silicate, or silicic acid by employing equal synthesis

conditions? In the case of silicic acid, can hierarchically organized silica monoliths be prepared in purely aqueous solution?

4.2. Synthesis of the Gels

For the investigation of these questions, sol-gel experiments were performed in analogy to the synthesis of hierarchically organized silica monoliths by employing the ethylene glycol-modified silane (EGMS). As template and phase separation-inducing agent, Pluronic P123 in either HCl of varying concentration or for silicic acid also in purely aqueous solution was used. The P123 / solvent ratio of the template was varied in the range from 10 / 90 to 40 / 60 (wt %). For the direct comparison between TEOS and EGMS, the silicon content was kept constant with 8.4 wt %. However, in the case of silicic acid, the Si-content had to be lowered in order to avoid spontaneous gelation after the ion exchange and is adjusted to 4.2 wt %. (The H_4SiO_4 solution is only stable under 9 – 10 wt % SiO_2 at pH 2 for a certain period of time.[128]) In the case of the basic sodium silicate solution, the Si-content was varied from 8.4 to 4.2 wt %.

Prior to the monolith preparation, the template phases were homogenized at 40°C (with exception of P123 / x M HCl = 40 / 60 which was homogenized at 0°C), and were then mixed with the adequate amount of each precursor.

In the case of sodium silicate, almost immediate hydrolysis and condensation reactions occurred resulting in a slurry precipitation.

All sols were allowed to gel and age at 40°C. In contrast to EGMS-derived silica gels, due to incomplete gelation the aging time of 7 d had to be extended for TEOS as well as for silicic acid-derived batches. Samples from TEOS-derived gels were withdrawn after 7, 9, 12, or 14 d.

Similar to the sodium silicate batches, the silicic acid-derived systems exhibited phase separation resulting in a turbid gel phase. However, due to the reduced Si-content an only weakly cross-linked gel phase was formed and hence no monolithic gels could be obtained.

All obtained materials were further treated by an one-step template-extraction and surface hydrophobization via silylation reaction of the surface moieties with chlorotrimethylsilane (TMCS) in petroleum ether before they were washed (removal of residual HCl and unreacted silane species with petroleum ether and ethanol) and dried at 200°C.

4.3. Influence of the Type of Precursor

For the investigation of the influence of the silicon source on the resulting pore architecture, silica monoliths were synthesized by commercially available precursors such as tetraethylorthosilicate (TEOS) and sodium silicate as well as its protonated derivate, silicic acid.

4.3.1. TEOS as Sole Precursor in Comparison to EGMS

The employment of tetraethylorthosilicate (TEOS) as precursor for the synthesis of hierarchically organized silica monoliths were reported by Nakanishi and Lindén.[92, 94, 95] Both groups applied poly(ethylene oxide) polymers (PEO) as phase separation-inducing agents, which can be combined with for example an ionic surfactant such as cetyltrimethylammonium bromide (CTAB) as structure-directing agent as reported by Lindén.[94, 95]
In the case of the EGMS-derived hierarchically organized silica monoliths, the employment of an acidic 30 wt % P123 solution is adequate as structure-directing agent serving as simultaneous phase separation-inducing agent. Thus, the applicability of the P123 template was to be studied for TEOS as sole precursor.

The physicochemical data for the silica materials obtained by employing TEOS as precursor are listed in table 21. For comparison, the physicochemical data obtained for the corresponding EGMS-derived silica monoliths are listed in table 5 in section 2.1.4.

Table 21 Physicochemical data for the TEOS-derived silica monoliths obtained from nitrogen sorption and SAXS investigations.

samples				*SAXS*	*N_2-sorption*		
	composition	t_{age}	*c(HCl)*	d_{10}	S^{BET}	D^{BJH}	t_{wall}
	Si/P123/HCl	*/d*	*/mol l^{-1}*	*/nm*	*/m^2 g^{-1}*	*/nm*	*/nm*
10-90-0TS12	8.4/10/90	12	1	-	950	10.0	-
10-90-1TS7	8.4/10/90	7	10^{-1}	-	799	3.4	-
10-90-1TS12	8.4/10/90	12	10^{-1}	-	748	3.3	-
20-80-0TS7	8.4/20/80	7	1	-	1324	4.5	-
20-80-0TS12	8.4/20/80	12	1	-	940	3.7	-
20-80-1TS7	8.4/20/80	7	10^{-1}	-	820	3.4	-
20-80-1TS12	8.4/20/80	12	10^{-1}	-	781	3.3; 3.7	-
20-80-1TS14	8.4/20/80	14	10^{-1}	-	1002	4.5	-
30-70-0TS7	8.4/30/70	7	1	-	980	3.5	-
30-70-0TS12	8.4/30/70	12	1	-	809	3.5	6.9
30-70-0TS14	8.4/30/70	14	1	-	949	3.3; 4.0	7.1
30-70-1TS7	8.4/30/70	7	10^{-1}	-	755	-	-
30-70-1TS12	8.4/30/70	12	10^{-1}	-	857	3.9	-
30-70-1TS14	8.4/30/70	14	10^{-1}	-	787	2.1	8.3
40-60-0TS7	8.4/40/60	7	1	-	941	3.4	7.9
40-60-0TS12	8.4/40/60	12	1	-	844	-	-
40-60-0TS14	8.4/40/60	14	1	-	791	3.3	7.0
40-60-1TS7	8.4/40/60	7	10^{-1}	-	784	-	-
40-60-1TS12	8.4/40/60	12	10^{-1}	-	640	-	-
40-60-1TS14	8.4/40/60	14	10^{-1}	-	1119	-	-

In order to study the behaviour of TEOS as substitute precursor for EGMS under identical synthesis conditions, sols were prepared with TEOS at composition ratios of Si / P123 / 1 and 10^{-1} M HCl = 8.4 / 10 / 90 to 8.4 / 40 / 60 (by weight) and their gelation times at 40°C were recorded in analogy to the EGMS-derived sol-gel systems. The resulting gelation times for the TEOS sol-gel systems in comparison to the gelation times of EGMS-derived systems are presented in figure 63.

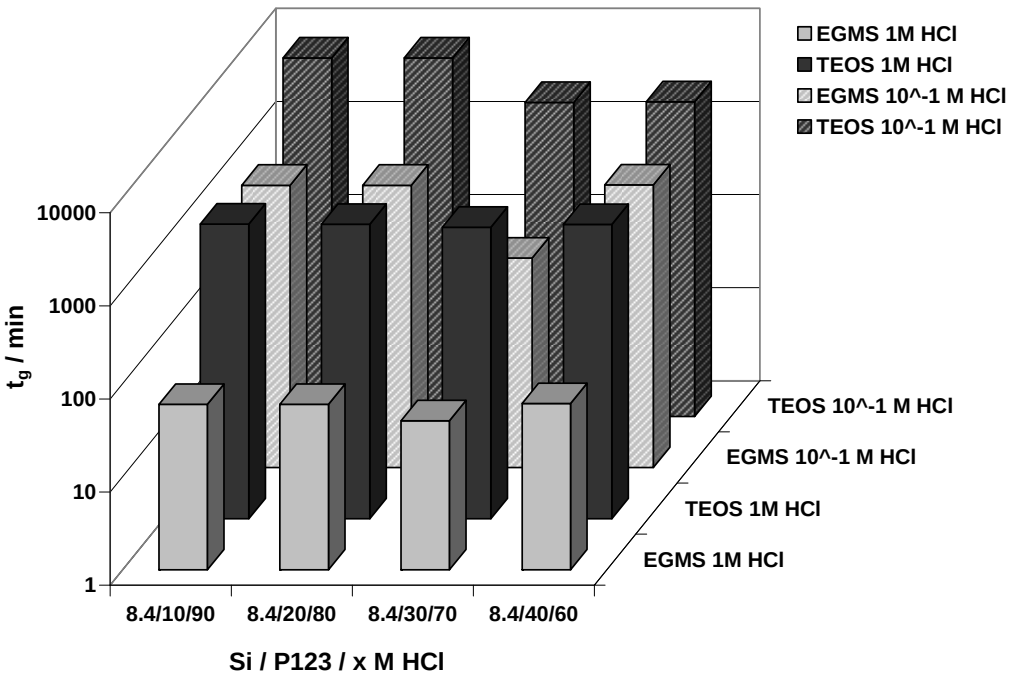

Figure 62 Comparison of the gel times at 40°C for the EGMS- and the TEOS-derived silica gels synthesized at 1 M and 10^{-1} M HCl.

As can be seen from the diagram in figure 62 the gelation times of the TEOS-derived silica gels at 1 M HCl vary in the range from 1350 min for Si / P123 / 1 M = 8.4 / 40 / 60 to 1462 min (~24 h) for Si / P123 / 1 M = 8.4 / 10 / 90. These time intervals for the sol-gel transition are significantly delayed compared to the gelation times of the EGMS-derived silica monoliths, which gelled within 40 to 61 min for the ratios of Si / P123 / 1 M = 8.4 / 30 / 70 and 8.4 / 40 / 60 (by weight). At c(HCl) = 10^{-1} M the hydrolysis and the condensation rates of the TEOS-derived sol-gel systems are even more reduced, resulting in extended gelation times of 1.6 d (2367 min for Si / P123 / 10^{-1} M HCl = 8.4 / 30 / 70) up to 5 d (7107 min for Si / P123 / 10^{-1} M HCl = 8.4 / 10 / 90). For comparison, the sol-gel systems of EGMS at the same conditions exhibit gelation times of approximately 3 h (178 min for Si / P123 / 10^{-1} M HCl = 8.4 / 30 / 70) to 18 h (1090 min for Si / P123 / 10^{-1} M HCl = 8.4 / 40 / 60). As known from literature, the hydrolysis rate of TEOS in acidic aqueous media strongly depends on the H_2O / TEOS ratio.[92]

Here an excess of water is employed resulting in a ratio of H_2O / TEOS = 13:1. It is assumed, that with an excess of water in the presence of high concentrations of an acidic catalyst (here 1 M and 10^{-1} M HCl), the hydrolysis rate greatly exceeds the condensation rate leading to the completion of the hydrolysis before condensation reactions take place.[59] After the sol is

depleted from monomers, the condensation of completely hydrolyzed siliceous species by particle-particle aggregation leads to the formation of a weakly branched silica network.

In contrast to the EGMS-derived sol-gel system, which is completely miscible with water, the initial system of TEOS in purely aqueous solution consists of two poorly miscible phases. This limitation of the sol-gel system is only annihilated, when a certain degree of hydrolysis is reached and a single phase is formed.[59, 129]

Unlike the EGMS-derived monoliths, the silica gels synthesized with TEOS are not subjected to phase separation in the macroscopic range resulting in transparent gels. (Figure 63) As described in chapter 3, the polarity of the released alcohol (or diol, respectively) greatly affects the induction of the phase separation. During the polycondensation of the siliceous oligomers, the polarity of the produced oligomeric / polymeric siloxane species decreases with increasing chain length. The hydrolysis of EGMS yields a considerable amount of ethylene glycol molecules (dipole moment $\mu = 2.26$ D[123]) which exhibit a limited miscibility with the "non-polar" polymeric siloxane species[127], but a good miscibility with the polar template phase of P123 in hydrochloric acid. These differing miscibilities cause a decomposition of the condensed silica species and the liquid phase resulting in phase separated gelled systems and hence in turbid gels. (Figure 64) In contrary, the hydrolysis of TEOS in acidic media releases ethanol that is known to be compatible with polar and non-polar systems. Thus, no gradient in polarity is established between the solvent / template rich phase and the polymeric silica phase and no phase separation occurs inhibiting the formation of a co-continuous macroporous framework. This phenomenon is observed for all compositions of the P123 template phase in the catalyst concentration range of $c(HCl) = 1 – 10^{-3}$ M.

The comparison of the densities of the silica monoliths prepared from either TEOS or EGMS show, that the non-phase separated silica gels possess a greater density than the phase separated monoliths. The density of the dried TEOS-derived gels (at 1 and 10^{-1} M HCl) is in the range of 0.7 – 0.8 g cm^{-3}, while the analogue EGMS-derived silica gels exhibit densities of $\rho = 0.2 – 0.3$ g cm^{-3}.

Despite the surface hydrophobization step with TMCS and the slow and careful drying procedure, most gel bodies of the TEOS-derived silica monoliths could not be prevented from cracking during the drying procedure as can be seen in figure 63.

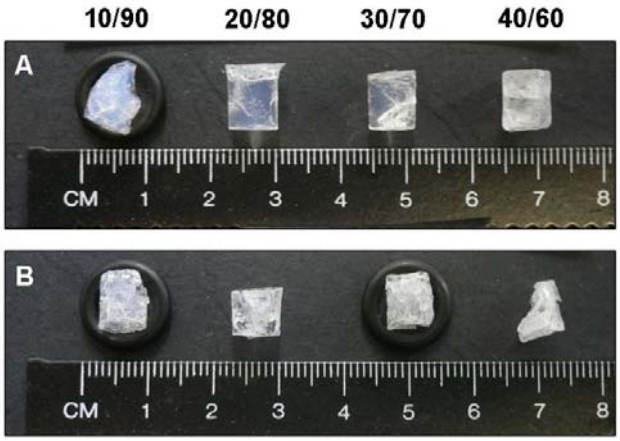

Figure 63 Photographs of the obtained silica monoliths prepared from TEOS and a varied template phase of Si / P123 / 1 M HCl (A) and 10^{-1} M HCl (B) in the range of 8.4 / 10 / 90 to 8.4 / 40 / 60.

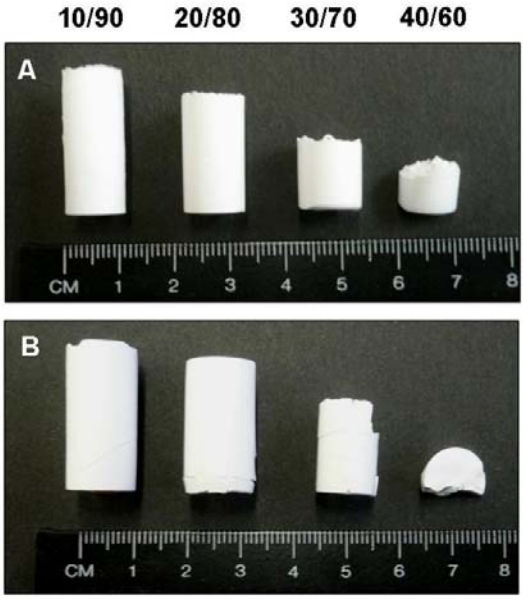

Figure 64 Photographs of the silica monoliths synthesized from EGMS and varied template phase of Si / P123 / 1 M HCl (A) and 10^{-1} M HCl (B) in the range of 8.4 / 10 / 90 to 8.4 / 40 / 60.

Figure 65 shows the SAXS pattern for the TEOS-derived silica gels synthesized at c(HCl) = 10^{-1} M with varying composition of the P123 template phase as representative example. The SAXS pattern of the analogue EGMS-derived silica gels can be seen in figure 24 in section 2.1.4.

For comparison, the Si-content was established to 8.4 wt % for both systems.

The SAXS diagram of the EGMS-derived silica gels show a periodic 2D-hexagonal arrangement of the mesopores with two pronounced reflections for the (10) and the (20) diffractions at minimum. In contrast, the scattering patterns of the TEOS-derived silica gels exhibit no periodic ordering of the mesopores, which is also affirmed by nitrogen sorption analyses. This result is not surprising, considering the fact that both the formation of a 2D-hexagonally arranged mesophase (figure 6 section 1.3.2.2.) and the induction of the phase separation is affected by the polarity of the released ethanol. In accordance to the formation of the co-continuous macroporous morphology, the formation of an organized mesopore network is based on the phase separation in the mesoscopic range resulting in sharp interfaces of the silica-rich / solvent-poor and the solvent-rich / silica-poor domains.

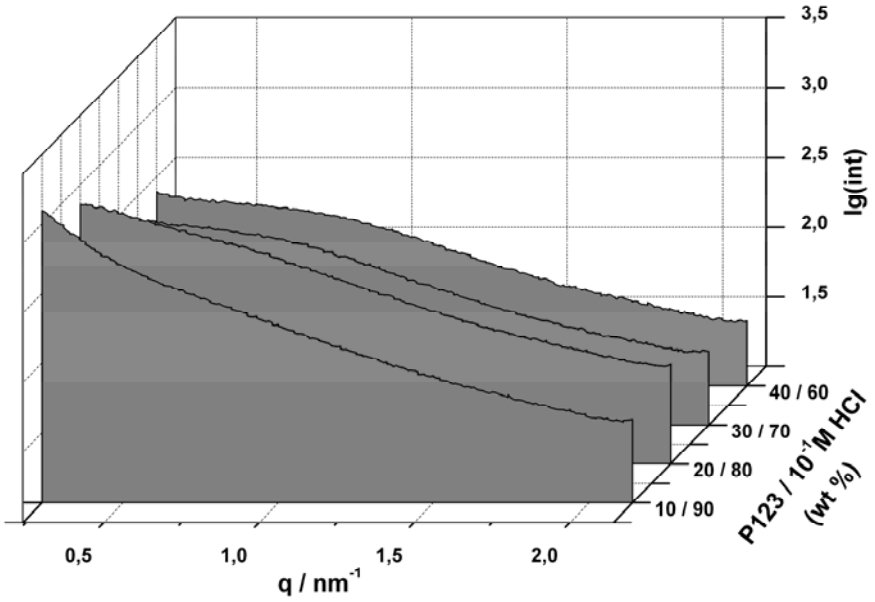

Figure 65 SAXS pattern of the TEOS-derived silica gels synthesized at P123 / 10^{-1} M HCl ranging from 10 / 90 to 40 / 60 (wt %).

4.3.2. Silicic Acid and Sodium Silicate as Precursors

The aim of this study was to investigate the possibility to synthesize hierarchically organized silica monoliths by substituting the ethylene glycol-modified silane (EGMS) by a commercially available precursor that can also be processed by water only.

Therefore, a sodium silicate solution, which was applied as purchased (27 wt % SiO_2, 8 wt % Na_2O) and its ion-exchanged derivative, silicic acid, were employed. Silicic acid was prepared

by first diluting the sodium silicate solution to 10 wt % SiO_2 followed by an ion-exchange reaction on an Amberlite IR-120 column, resulting in a H_4SiO_4 solution of pH 2.

For comparison, the synthesis parameters of the EGMS-derived silica monolith preparation were adapted for silicic acid with the pre-homogenized template phase of P123 / 1 – 0 M HCl = 30 / 70 and 40 / 60 (by weight). However, the Si-content of the silicic acid was limited to 4.2 wt % due to the prior ion-exchange step. (The employment of a more concentrated sodium silicate solution resulted in polycondensation of silicic acid on the column.)

For the investigation of the applicability of the basic sodium silicate solution (pH ~ 11), the Si-content was varied from 8.4 to 4.2 wt %, whereas a P123 template phases of P123 / 1 M HCl = 10 / 90 and 20 / 80 proved to be adequate systems for the introduction of an organized mesoporous network.

All silica gels were gelled and aged at 40°C (aging of 7 d) before they were subjected to the one-step template extraction / surface hydrophobization process by silylation of the gels with chlorotrimethylsilane (TMCS) in petroleum ether. In analogy to the EGMS and TEOS-derived silica gels, all gels were dried at 200°C by preservation of the hydrophobic surface.

The physicochemical data obtained from SAXS and nitrogen sorption experiments are listed according to the silicon source applied in the tables 22 to 24.

Table 22 Physicochemical data of the silica gels synthesized from silicic acid by employing P123 / 1 – 0 M HCl = 30 / 70 wt %.

samples				*SAXS*	*N_2-sorption*		
	composition	t_{age}	*c(HCl)*	d_{10}	S^{BET}	D^{BJH}	t_{wall}
	Si/P123/HCl	*/d*	*/mol l^{-1}*	*/nm*	*/m² g^{-1}*	*/nm*	*/nm*
30-70-0NW	4.2/30/70	7	1	10.9	725	3.7	8.9
30-70-1NW	4.2/30/70	7	10^{-1}	10.6	673	3.5	8.8
30-70-2NW	4.2/30/70	7	10^{-2}	9.9	649	3.5	7.9
30-70-3NW	4.2/30/70	7	10^{-3}	11.5	709	3.5	9.7
30-70-NNW	4.2/30/70	7	0	11.3	989	3.7; 6.7	9.4

Table 23 Physicochemical data of the silica gels synthesized from silicic acid by employing P123 / 1 – 0 M HCl = 40 / 60 wt %.

samples	composition Si/P123/HCl	t_{age} /d	c(HCl) /mol l^{-1}	SAXS d_{10} /nm	N_2-sorption S^{BET} /m^2 g^{-1}	D^{BJH} /nm	t_{wall} /nm
40-60-0NW	4.2/40/60	7	1	10.9	576	3.5	9.1
40-60-1NW	4.2/40/60	7	10^{-1}	11.9	809	3.5	10.2
40-60-2NW	4.2/40/60	7	10^{-2}	11.3	637	3.5, 5.8	9.5
40-60-3NW	4.2/40/60	7	10^{-3}	10.4	478	3.4	8.6
40-60-NNW	4.2/40/60	7	0	9.4	551	3.5	7.4

Table 24 Physicochemical data of the silica gels synthesized from basic sodium silicate solution by employing P123 / 1 M HCl = 10 / 90 and 20 / 80 wt %, whereas the Si-content was varied in the range from 8.4 – 4.2 wt %.

samples	composition Si/P123/HCl	t_{age} /d	c(HCl) /mol l^{-1}	SAXS d_{10} /nm	N_2-sorption S^{BET} /m^2 g^{-1}	D^{BJH} /nm	t_{wall} /nm
10-90-0NWG1	4.2/10/90	7	1	10.6	336	3.7, 8.0	8.5
10-90-0NWG2	6.3/10/90	7	1	10.3	475	5.7	6.2
10-90-0NWG3	8.4/10/90	7	1	-	240	3.7, 5.7	-
20-80-0NWG1	4.2/20/80	7	1	11.3	197	3.7, 15.5	9.3
20-80-0NWG2	6.3/20/80	7	1	11.0	380	7.6, 27.2	5.1

In contrast to the TEOS-derived silica monoliths, the silica gels synthesized from silicic acid are subjected to a phase-separation in the macroscopic range resulting in turbid gels. This effect is not surprising, as only H_2O (which is a polar solvent like ethylene glycol) is released during the condensation reactions resulting in a rapidly evolving gradient in polarity between the polar solvent-rich phase and the growing siloxane polymer which polarity decreases with growing polymer chain.

In addition, no hydrolysis step is required by employing silicic acid and hence the sol-gel transition occurs fast. Despite the short gelation time and the early on-set of phase separation, no silica monoliths could be preserved due to the low Si content resulting in an only weakly cross-linked silica network, which collapses during the drying procedure.

SEM investigations of the silica material synthesized from the ratio of Si / P123 / 10^{-1} M HCl = 4.2 / 40 / 60 (by weight) exhibit a filigree macroporous framework as can be seen from figure 66. The co-continuous macroporous network consists of large macropores which are enclosed by a net of fragile silica strands (0.3 – 1 μm). This morphology resembles the morphology of the framework observed for EGMS-derived silica gels synthesized with the composition of Si / P123 / 10^{-1} M = 8.4 / 30 / 70 (figure 17, section 2.1.3.1.) despite the absence of aggregates of assembled silica strands.

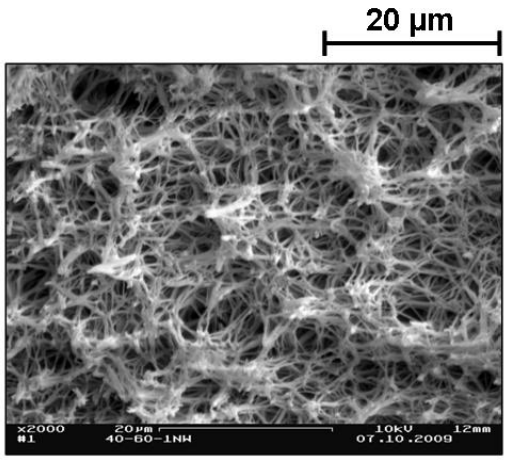

Figure 66 SEM image of the co-continuous macroporous framework of the silica gel prepared from silicic acid at the ratio of Si / P123 / 10^{-1} M HCl = 4.2 / 40 / 60.

In addition, SAXS investigations of the silica materials prepared with Si / P123 / 1 – 0 M HCl = 4.2 / 40 / 60 (by weight) exhibit a periodic arrangement of the mesopores as can be seen from figure 67. In analogy to the EGMS-derived silica gels, the SAXS patterns reveal a loss of ordering of the mesoporous network with decreasing concentration of the catalyst. The gels derived from silicic acid at concentrations of c(HCl) = 1 – 10^{-2} M exhibit diffraction peaks for the (10) and (20) diffractions at q_{10} = 0.5 – 0.6 nm^{-1} and q_{20} = 1.0 – 1.2 nm^{-1} which can be related to a 2D-hexagonal arrangement of the mesopores. The corresponding repeating unit distances determined for the (10) diffractions (d_{10} = 10.9 – 11.9 nm) agree with the repeating unit distances found for the EGMS-derived silica monoliths prepared with Si / P123 / 1 – 10^{-2} M HCl = 8.4 / 40 / 60 with d_{10} = 11.3 – 12.1 nm.

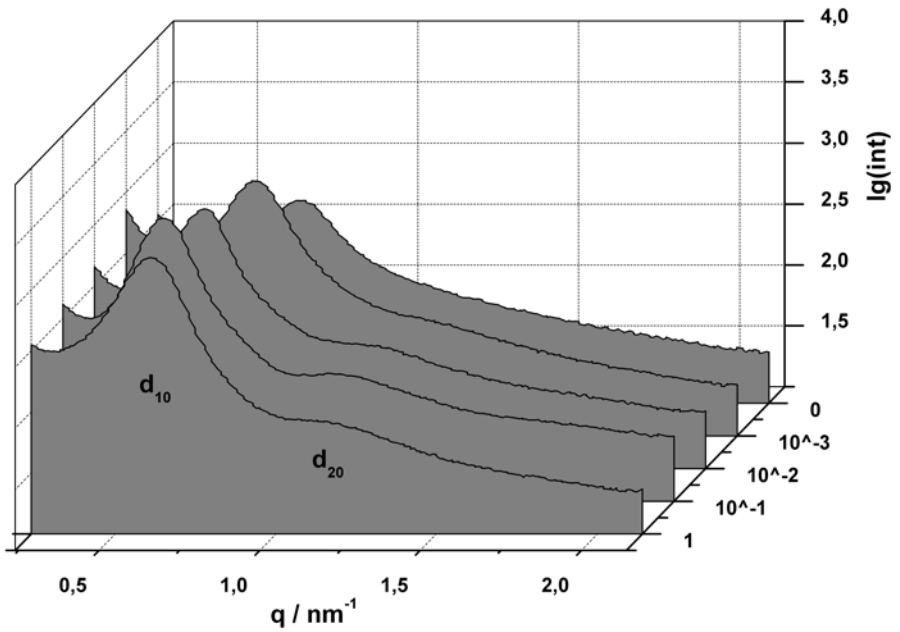

Figure 67 SAXS patterns indicating the mesoscopic ordering of the silica gels prepared with silicic acid at Si / P123 / 1 - 0 M HCl = 4.2 / 40 / 60.

By employing the basic sodium silicate solution as precursor, the addition of the highly acidic P123 template phase (P123 / 1 M HCl = 10 / 90 and 20 / 80 wt %) results in the immediate precipitation of SiO_2. Interestingly, during the aging process in sealed vessels at 40°C, the precipitated particles sinter and form heterogeneous bulk materials.

Structural investigations exhibit a 2D-hexagonally arranged mesoporous network of the silica materials synthesized with 6.3 and 4.2 wt % at P123 / 1 M HCl = 10 / 90 wt %, whereas the employment of 8.4 wt % (analogue Si-content of EGMS-derived silica gels) results in no periodic ordering of the mesopore system. (Figure 68) For 6.3 wt % Si, the best resolved SAXS pattern is obtained with reflections for the (10), (11), (20) and a broad signal for the (21) diffractions at q-values of q_{10} = 0.61 nm^{-1}, q_{11} = 1.08 nm^{-1}, q_{20} = 1.23 nm^{-1}, and approx. q_{21} = 1.66 nm^{-1}. The corresponding obtained repeating unit distance of d_{10} = 10.3 nm is smaller than the repeating unit distance determined for the EGMS-derived silica gel of the composition Si / P123 / 1 M = 8.4 / 10 / 90 (d_{10} = 11.2 nm). The SAXS curves for the gels prepared with Si / P123 / 1 M HCl = 4.2 / 10 / 90 and 6.3 / 20 / 80 exhibit two less pronounced signals which can be related to the (10) and the (11) diffractions.

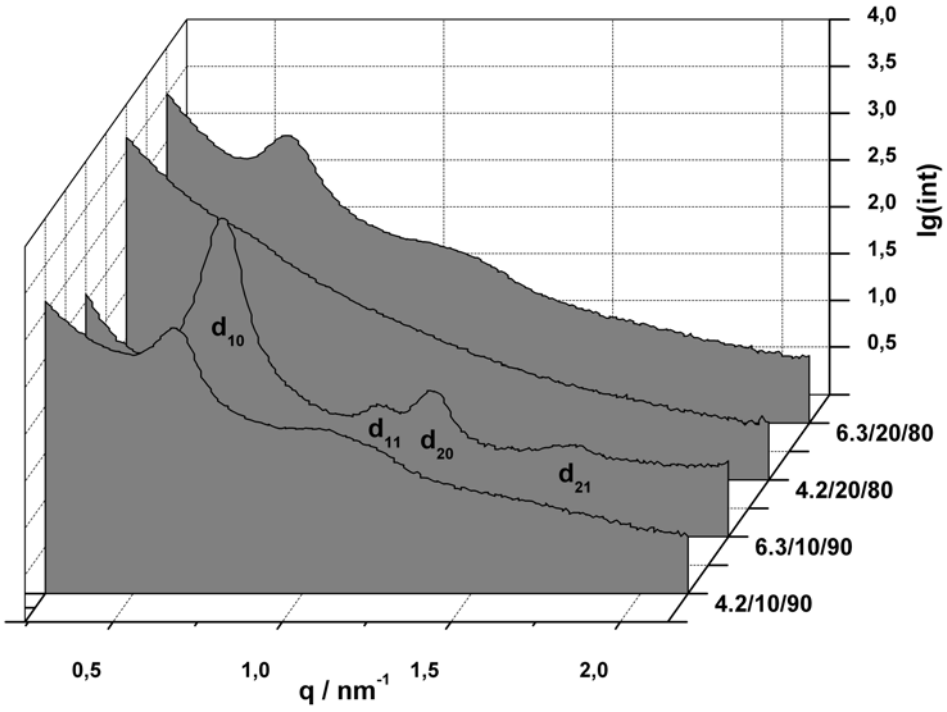

Figure 68 SAXS pattern of the silica gels derived from sodium silicate by employing P123 / 1 M HCl =10 / 90 and 20 / 80 wt % and Si-contents of 4.2 and 6.3 wt %.

The corresponding TEM image of the silica gel synthesized with Si / P123 / 1 M HCl = 6.3 / 10 / 90 (by weight) is presented in figure 69 confirming the 2D-hexagonal arrangement of the mesoporous system.

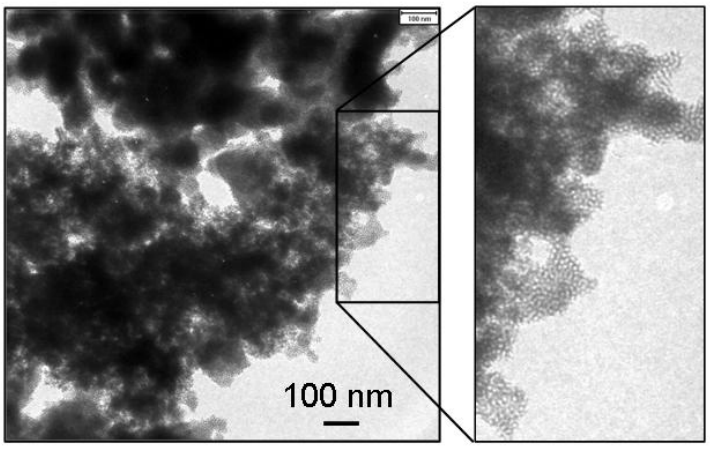

Figure 69 TEM image presenting the mesoporous system of the silica gel derived from sodium silicate (Si / P123 / 1 M HCl = 6.3 / 10 / 90).

4.4. Conclusion

The question whether it is possible to achieve hierarchically organized silica monoliths by substituting the ethylene glycol-modified silane (EGMS) by commercially available precursors such as tetraethylorthosilicate (TEOS), sodium silicate or silicic acid by employing an acidic P123 template phase was to be answered.
The investigations revealed that TEOS is not an adequate substitute for EGMS for the applied P123 / HCl system without employing a polar additive. The application of TEOS resulted in transparent, glass-like silica monoliths exhibiting no periodic ordering in the mesoscopic range for all compositions of Si / P123 / 1 – 10^{-3} M HCl = 8.4 / 10 / 90 – 8.4 / 40 / 60 (by weight).

In contrast, the employment of silicic acid resulted in hierarchically organized silica gels at the composition of Si / P123 / 10^{-1} M HCl = 4.2 / 40 / 60 exhibiting a highly interconnected filigree macropore network and a 2D-hexagonally arranged mesopore system. However, due to a poorly cross-linked silica network caused by the low Si-content, the monolithic shape could not be preserved during the drying procedure.

The employment of the basic sodium silicate solution in combination with the acidic P123 template phase resulted in immediate precipitation of SiO_2. The precipitated particles sintered during the aging process and formed a heterogeneous bulk material. The silica material synthesized at Si / P123 / 1 M HCl = 6.3 / 10 / 90 (by weight) exhibited a long-range ordering for the 2D-hexagonally arranged mesopore network; however, no ordered macroporous framework could be obtained.

These results indicate that for the synthesis of hierarchically organized silica monoliths by employing equal template phases of P123 in aqueous HCl as for the EGMS-derived systems, the presented commercially available precursors are no appropriate substitutes for EGMS.

Chapter 5

PDMS-Based Block Co-polymers as Structure-Directing Agents in the Synthesis of Hierarchically Organized Silica Monoliths

5.1. Introduction

Silicone surfactants have become a commercially important class of surfactants with a wide field of applications ranging from the synthesis of polyurethane foams[130, 131], as additives for coatings and paints to softening agents in cosmetic products, etc.[132-140] Especially amphiphilic siloxane surfactants containing a hydrophilic block, usually a poly(ethylene oxide) (PEO) block, and a hydrophobic block of *e.g.* polydimethylsiloxane (PDMS) have attracted attention as these surfactants have a strong surface activity in polar solvents such as aqueous solutions.[141-144] Due to the hydrophobic block of the co-polymers, they aggregate at the air-solvent interface with the hydrophobic block either being pushed out of the solvent (into the gas phase) or when the concentration of surfactant molecules is high enough to form micelles, into the micellar centre. Similar to amphiphilic hydrocarbon-based surfactants, *e.g.* poly(ethylene oxide)-poly(propylene oxide)-poly(ethylene oxide) (PEO-PPO-PEO) mem-

bers of the Pluronic group such as P123, linear amphiphilic siloxane co-polymers especially trisiloxane surfactants ($Me_3Si\text{-}OSiMe_2\text{-}OSiMe(CH_2)_x(OCH_2CH_2)_yOH$) can form lyotropic phases in aqueous solution.[141, 145-147] Even though there are various publications on the aggregation behaviour of siloxane surfactants in different solvents, they as far as we know are only barely used as templating agents in sol-gel processing.[148]

In contrast to purely hydrocarbon-based polymers, PEO-PDMS-PEO co-polymers offer the possibility to incorporate hydrophobic DMS segments inside a silica matrix by gradual degenerating the PEO blocks via a selective heat treatment. The combination of the ability of these surfactants to form lyotropic LC phases, which can be employed as supramolecular templates, and the opportunity to directly adjust the surface polarity of the resulting silica material, make them interesting candidates as structure directing agents in the synthesis of hierarchically organized silica materials with a tailored surface polarity.

Until today the emphasis of the synthesis of hierarchically organized monoliths is on the employment of either amphiphilic polyether-based surfactants *e.g.* Pluronic P123 and F127[40, 149-151],[47-50, 152],[51-54] or ionic surfactants such as cetyltrimethylammonium bromide (CTAB)[41] or tetradecyltrimethylammonium bromide (TTAB)[42] as supramolecular templates determining the arrangement and the size of the mesopores. Among the various syntheses pathways to create a well-ordered macroporous network for example by macrotemplating with polystyrene particles[35, 153] or foams[42, 154, 155], the manufacturing of an highly interconnected macroporous frameworks with pore sizes from 100 nm to 30 μm[40] by polymerization-induced phase separation accompanied by the sol-gel transition is a promising route towards these porous systems.

Depending on the synthesis conditions, amphiphilic polymers, such as P123 or ionic surfactants in combination with a polar agent like PEO can induce phase separation that precedes parallel to the polycondensation of the hydrolyzed siliceous species in acidic media. Thus, the resulting macroporous morphology is frozen in when the sol-gel transition is completed. This most prominent sol-gel procedure to introduce macroporous heterogeneity by polymerization-induced phase separation was studied in detail and reported by Nakanishi and co-workers.[39, 156]

The idea of the present work was to employ commercially available siloxane surfactants, as they can be easily purchased in large quantities at low costs. The surfactants used were linear ABA triblock co-polymers donated by Tego, Evonik Inc. Tego Glide 440 belongs to the

α,ω–terminated block co-polymers of the TEGOPREN 5 series (Figure 70) and is used as slip and flow additive in waterborne, radiation-curing formulations like industrial, wood, and furniture coatings in which they also enhance the scratch resistance.[157] LA-S 687 is isotype to Tegopren 5845, which also belongs to the TEGOPREN 5 product series.

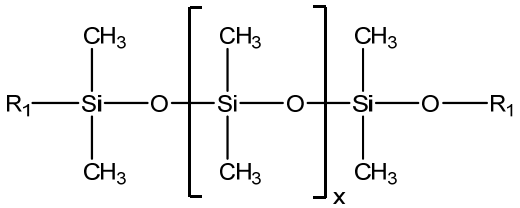

Figure 70 Scheme of the linear PEO-PDMS-PEO polymer of the Tegopren 5 Series.

5.2. Synthesis of the Gels

Silica gels were prepared by adding EGMS to a mixture of Tego Glide 440 or LA-S 687 and either aqueous hydrochloric acid (HCl) of varying concentration or purely aqueous solution. Based on the synthesis procedure described for the employment of Pluronic P123 as structure-directing agent, the ratio by weight of Si to surfactant phase was 8.4 / 100, whereas the composition of the surfactant to solvent phase was varied from 10 / 90 (wt %) up to 30 / 70 (wt %). In contrary to P123, the employment of the PEO-PDMS-PEO surfactants did not result in homogeneous sols at all compositions, but formed emulsions that were combined and homogenized with the precursor.

After gelling and aging at 40°C, some silica monoliths were dried via the template-extraction / surface-modification approach by silylation of the pore walls with chlorotrimethylsilane (TMCS) in petroleum ether (analogue conditions as described in the former sections). These so-treated monoliths were finally dried at 200°C.

To investigate the possibility of creating a hydrophobic surface by gradually degenerating the PEO chains of the ABA co-polymers, silica gels were supercritically dried with CO_2 followed by a selective heat-treatment up to 600°C, whereas samples at 200°C, 300°C and 400°C were withdrawn and analyzed.

5.3. Results and Discussion

The aim of this work was to prepare silica monoliths with a hierarchical structural organization comprising different levels of pore sizes. The idea was to employ commercially available amphiphilic siloxane surfactants as structure-directing agents for the formation of the mesoporous network, simultaneously acting as phase separation-inducing agents to obtain a macroporous framework. Hence, the first intention was investigate the aggregation behaviour of the surfactants by determining the particular critical micelle concentration (cmc).

5.3.1. Critical Micelle Concentration

Size exclusion chromatographic (SEC) experiments of Tego Glide 440 and LA-S 687 exhibited two broad distributions of the number average molecular weight indicating a high polydispersity for both co-polymers. In the ^{1}H-NMR spectrum of Tego Glide 440 the peaks at δ(benzene-d_6) = 0.44 – 0.45 ppm can definitely be assigned to the $Si(CH_3)_2O$- moieties of the polydimethylsiloxane block and the broad peak at δ(benzene-d_6) = 3.95 ppm to the (CH_2CH_2O)- groups of the polyether block.[143] As the exact number of spacer methylene groups between the PDMS and the PEO segments is not known and with respect to the fact that the surfactant exhibits a high polydispersity (from SEC measurements), the peaks at δ(benzene-d_6) = 0.93 – 0.94 ppm, 1.47 – 1.49 ppm and 1.91 – 1.95 ppm can only be related under reserve to the methylene groups. The signal at δ(benzene-d_6) = 3.71 – 3.73 ppm results from terminal $–OCH_3$ groups of the PEO block.

The spin-lock ^{29}Si-NMR spectrum of Tego Glide 440 affirms these results with peaks at δ(benzene-d_6) = 8.05 – 8.10 ppm for the terminal groups (M-units) for $–H_2CSi(CH_3)_2O–$ of the PDMS block and a broad distribution of peaks in the range of δ(benzene-d_6) = -19.31 – -22.35 ppm for the $–OSi(CH_3)_2O–$ (D-units) moieties.

Analogue conclusions can be drawn from the ^{1}H- and spin-lock ^{29}Si-NMR spectra of LA-S 687. The peaks for the $Si(CH_3)_2O$- groups (δ(benzene-d_6) = 0.43 – 0.44 ppm) and for the $–(CH_2CH_2O)$- groups (δ(benzene-d_6) = 3.96 ppm) can definitely be assigned, however, there is also no accurate correlation for the signals at δ(benzene-d_6) = 0.93 ppm, 1.48 – 1.49 ppm and 1.91 – 1.95 ppm to the spacer groups. In analogy to Tego Glide 440, the peak at δ(benzene-d_6) = 3.73 ppm can also be related to terminal OCH_3-groups. The spin-lock ^{29}Si-

NMR spectrum of LA-S 687 reveals also signals for the M-units of the terminal $H_2CSi(CH_3)_2O$ groups of the PDMS segment (δ(benzene-d_6) = 8.09 – 8.13 ppm) and for the D-units of the PDMS block (–$OSi(CH_3)_2O$–, δ(benzene-d_6) = -19.34 – -22.73 ppm).

For the investigation of the surface activity of the different siloxane surfactants in aqueous solution, surface tension measurements were performed with the ring method according to "du Noüy". The critical micelle concentration (cmc) marks the concentration of the surfactant in solvent above which no further reduction of the surface tension due to micelle formation can be observed. The tensiometry measurements of LA-S 687 in aqueous solution only result in a reduction of about 18 mN/m leading to a final surface tension of 48 mN/m. (Figure 71) The corresponding cmc is calculated as $c = 9.6*10^{-4}$ g/l. Tego Glide 440 exceeds these values up to 28 mN/m resulting in a surface tension of 44 mN/m as can be seen in figure 71 (corresponding cmc: $c = 1.2*10^{-3}$ g/l). It is known that siloxane surfactants *e.g.* trisiloxane surfactants can lower the surface tension up to 20 – 30 mN/m in comparison to hydrocarbon surfactants which achieve values of about 30 – 40 mN/m[142, 158] as the cohesion forces between the hydrophobic groups decrease from hydrocarbons to silicone oils. For a direct comparison, a 0.1% aqueous solution of Pluronic P123 possesses a surface tension of 34 mN/m at 25°C.[159] According to Hoffmann and Ulbricht the low effective reduction of the surface tension of the used surfactants cannot easily be related to the structure of the surfactants as it is rather independent of the size of the hydrophobic block but it increases with decreasing polarity of the hydrophilic block. As the here employed siloxane surfactants are amphiphilic surfactants with two terminal hydrophilic PEO blocks and the fact that they are polydisperse, the rather low effective surface activity compared to pure trisiloxane surfactant and even to a 0.1% aqueous solution of sole P123 is not surprising.

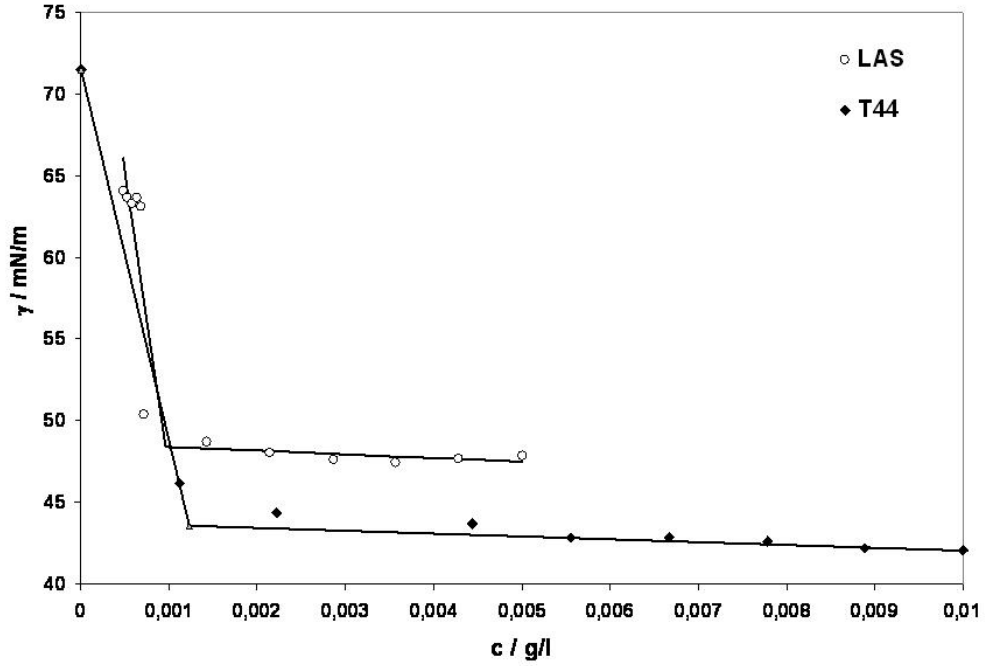

Figure 71 Pattern of the reduction of the surface tension for Tego Glide 440 (T44) and LA-S 687 (LAS). The surface tension is directly proportional to the maximal tractive force prior to the breakage of the lamella. The concentration of the surfactant is given in gram per litre.

5.3.2. Hierarchical Silica Gels

In analogy to the work of Brandhuber et al.[47, 48, 152] who reported the synthesis of hierarchically organized silica monoliths by employing Pluronic P123 as structure-directing agent with an ethylene glycol-modified silane (EGMS) as precursor, silica gels were prepared with LA-S 687 (LAS) and Tego Glide 440 (T44) as structure-directing agents in dilute HCl and purely aqueous solution. In contrast to P123, the employment of T44 (surfactant / solvent = 30 / 70 by weight) in purely aqueous solution results not in a homogenous solution but an emulsion. All silica samples presented in the next section were dried via a surface silylation reaction with trimethylchlorosilane (TMCS) prior to the heat treatment to preserve the monolithic shape of the silica gel during the drying procedure.

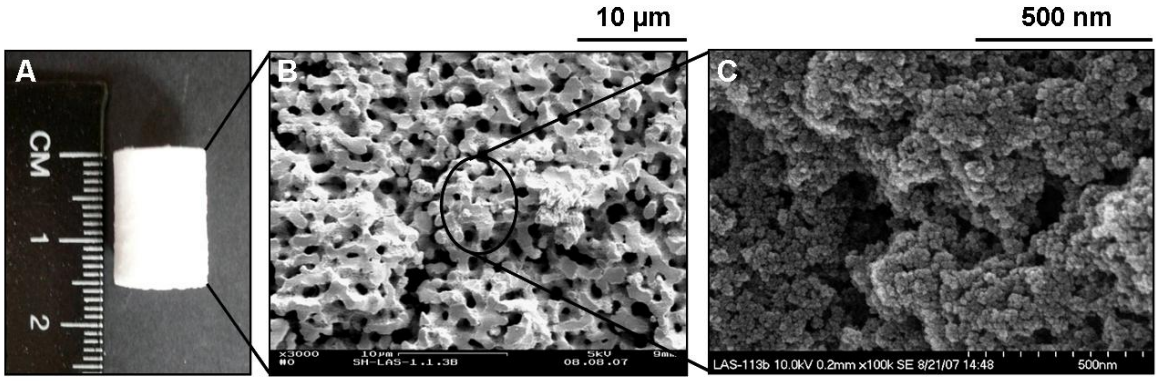

Figure 72 Silica monolith made with LA-S 687 in purely aqueous media exhibiting pores of different size domains: A) image of the silica monolith, B) interconnected macroporous network with pores of 0.6 μm in diameter (R^{Hg} = 0.3 μm); C) the silica strands of the macroporous network exhibit a porous morphology themselves resulting from interparticular voids.

Figure 72 shows the SEM images of a silica sample prepared with LA-S 687 (30 wt %) in purely aqueous solution. The macroporous morphology shows an interconnected macroporous network with pores of 0.6 μm in diameter, whereas the framework itself is formed by agglomerated silica particles (with size of about 30 nm). The hystereses of the corresponding nitrogen sorption measurements indicate the presence of mesopores; as can be seen from the hystereses of the type IV. Calculations according to the BJH model of the adsorption branch of the isotherm yield mesopores of about 7.6 nm. (Figure 73) This is also confirmed by SAXS investigations. The SAXS pattern for the silica gel prepared in purely aqueous solution (LAS-1.1.3) shows one distinct signal (q^1 = 0.6 nm^{-1}) and one less pronounced signal at (q^2 = 1.2 nm^{-1}) revealing a repeating unit distance of 11.0 nm (d^1, calculated for the first diffraction peak). Even though the shifts of these diffraction peaks are 1:2 relating to an organization in the mesoscopic range and in combination with the results from the nitrogen sorption measurements indicating an ordered mesoporous system, TEM investigations do not reveal a structuring in the mesoscopic range. However, as TEM images can only give information on a small sector of some hundred nanometres of a sample, the diffraction peaks in the SAXS pattern cannot exactly be assigned to an either 2D-hexagonal or lamellar structure.

Table 25 Data of the different silica monoliths prepared with LA-S 687 in different HCl concentrations.

samples	SAXS			N_2-sorption			Hg-Porosimetry
	c_{HCl} /mol l^{-1}	q^1 /nm^{-1}	d^{1}* /nm	S^{BET} /$m^2\ g^{-1}$	V_0 /$cm^3\ g^{-1}$	D_{BJH}** /nm	R^{Hg} /μm
LAS-1.1.3a	0	0.6	11.0	939	155.9	7.6	0.3
LAS-8.1.1a	10^{-6}	0.6	11.0	882	132.1	7.6	0.4
LAS-7.1.1a	10^{-5}	0.6	10.9	940	143.2	7.5	0.4
LAS-6.1.1a	10^{-4}	0.6	11.0	862	138.1	7.5	0.1
LAS-5.1.1a	10^{-3}	0.5	12.8	970	154.8	6.4	-

*d^1 represents the computated repeating unit distance for the first ordering. (Determined from q^1)

**The here presented pore diameter distributions were calculated from the adsorption branch of the sorption hysteresis.

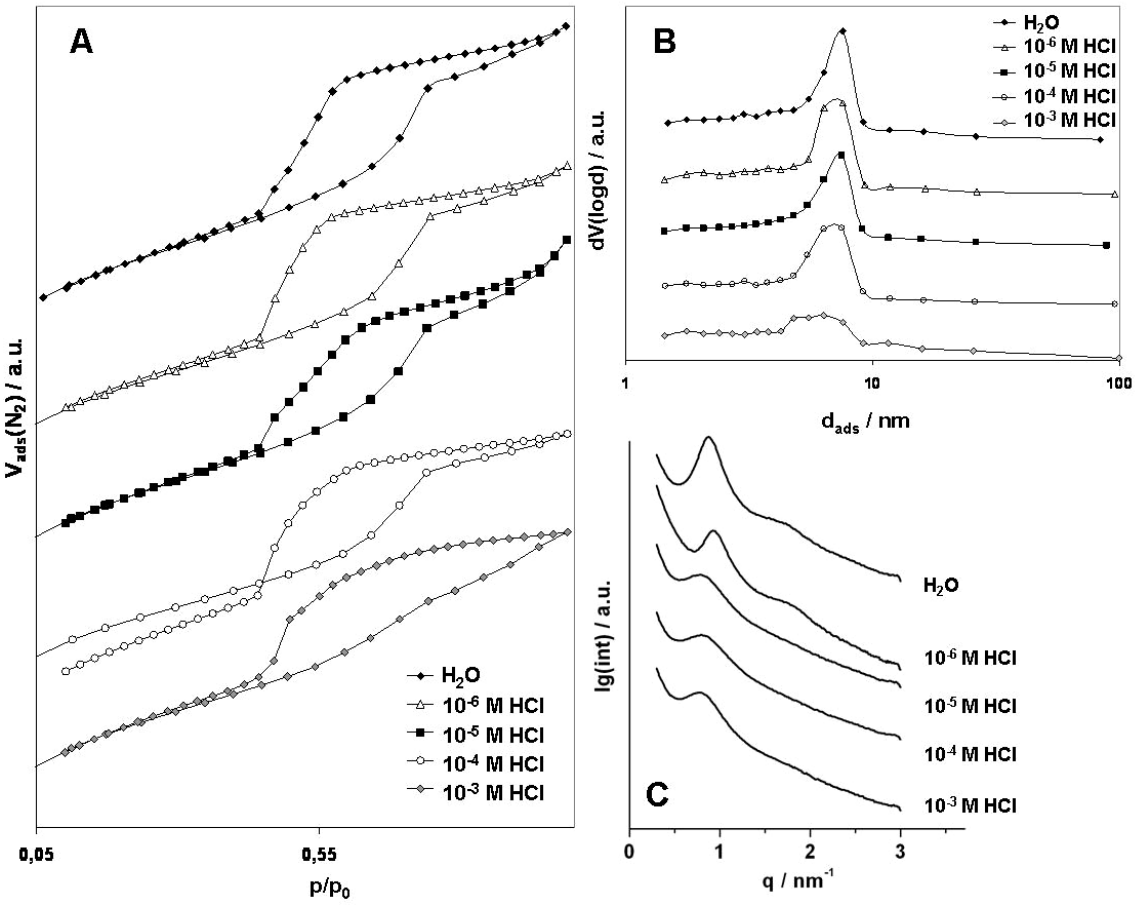

Figure 73 Investigations of the mesopore systems.A) Hystereses of the silica gels prepared from LA-S 687 in dilute HCl of varying concentrations. B) Pore diameter distributions calculated from the adsorption branch of the isotherm. C) SAXS patterns for the LAS silica gels. All presented silica gels were treated with TMCS and were subsequently heated up to 200°C.

In addition, high-resolution SEM images indicate that mesopores also result from interparticulate voids that are enclosed by agglomerated silica particles forming the macroporous framework.

Besides meso- and macroporosity, the sample also exhibits a third level of porosity. The high specific surface area (S^{BET} = 939 m^2 g^{-1}) and the high initially adsorbed nitrogen volume (V_0 = 155.9 cm^3 g^{-1}) indicate that the silica gel also comprises a significant amount of micropores. These results resemble the results from hierarchically organized silica gels prepared from a liquid-crystalline phase of Pluronic P123 in purely aqueous solution by employing EGMS as precursor. Besides an interconnected macroporous framework, the P123 templated silica gels comprise a 2D-hexagonally arranged mesostructure with pore diameters of about 7 nm (calculated from the desorption branch of the isotherm) and a repeating unit distance of 11.8 nm. In analogy, these gels also exhibit micropores resulting in a total specific surface area of about 930 m^2 g^{-1}, which resembles the value obtained for the hierarchically organized silica monolith prepared with LA-S 687.

With increasing concentration of the HCl (from 10^{-6} to 10^{-3} M) the interconnectivity of the macroporous network gradually vanishes (Figure 74) along with the mesoscopic ordering (Figure 73). This trend can not only be observed from the SAXS patterns for the silica gels prepared with different HCl concentrations, but is also evident from the development of the corresponding adsorption branches of the nitrogen sorption measurements and the resulting pore diameter distributions as shown in figure 73. However, the specific surface areas and the initially adsorbed nitrogen volumes as can be seen from table 25 are not affected by the lower degree of ordering for the meso- and macroporous networks. Therefore, it is assumed that the resulting microporosity is caused by the nature of the employed surfactant. It is known from literature that the application especially of amphiphilic polymers with hydrophilic PEO blocks as supramolecular templates, leads to silica materials with a considerable amount of micropores besides the mesopore formation. Smarsly et al. suggested the formation of a system for which a transition is accomplished starting from a three-phase system in which the inorganic siliceous phase is separated from the hydrophobic polymer blocks by PEO interlayer to a two-phase system where the hydrophilic PEO blocks are completely integrated within the siliceous phase.[160, 161] In this transition phase, PEO chains are dissolved in the inorganic siliceous phase, however, the limiting factor is the saturation that is responsible for the microphase separation resulting in a microporous system.

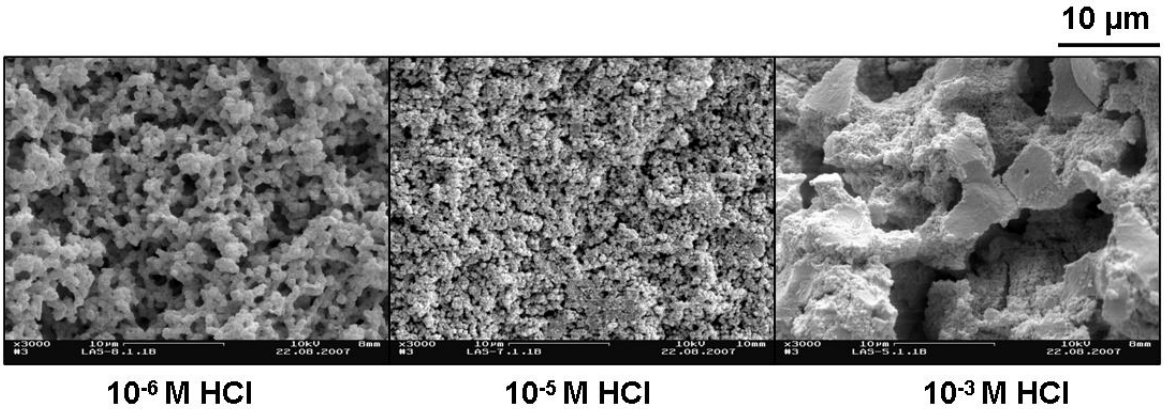

Figure 74 SEM images of silica gels prepared with LA-S 687 in dilute HCl of different concentrations. All presented silica gels were treated with TMCS and were subsequently heated up to 200°C.

The as-synthesized silica monoliths prepared with Tego Glide 440 (T44) differ from the gels prepared with LA-S 687. The T44 silica gels were also synthesized at different HCl concentrations and from purely aqueous solution. In contrary to LA-S 687 (30 wt %), the silica gels were obtained from an emulsion and not from a homogeneous sol at all employed HCl concentrations. After aging for 7 d at 40°C, all gels were treated with TMCS to extract the surfactant and simultaneously hydrophobize the silica surface to prevent the monolith from cracking. All samples were subsequently dried at 200°C to preserve the trimethylsilyl groups on the surface.

Table 26 Data of silica monoliths prepared with Tego Glide 440 at different HCl concentrations and heated up to 200°C; the pore radii marked with * showed a broad distribution.

samples	*SAXS*			*N_2-sorption*			*Hg-Porosimetry*
	c_{HCl} /mol l^{-1}	q^1 /nm^{-1}	d^1* /nm	S^{BET} /m^2 g^{-1}	V_0 /cm^3 g^{-1}	D_{BJH}** /nm	R^{Hg} /µm
T44-1.1.2a	0	0.6	10.9	932	139.8	7.6	0.4
T44-8.1.1a	10^{-6}	0.6	11.0	873	134.5	7.6	0.1“
T44-7.1.1a	10^{-5}	0.6	11.2	939	148.4	7.5	0.1“
T44-6.1.1a	10^{-4}	0.6	11.2	906	143.7	7.5	0.2
T44-5.1.1a	10^{-3}	0.6	11.0	860	139.5	7.6	1.0“

*d^1 represents the computated repeating unit distance for the first ordering. (Determined from q^1.)
**The here presented pore diameter distributions were calculated from the adsorption branch of the sorption hysteresis.
“ The mercury porosimetry measurements exhibited broad macropore radii distributions.

As can be seen from figure 75, the silica monoliths prepared from an emulsion of T44 in water (30 wt %) exhibit a structural hierarchy on multiple levels. In contrary to silica gels prepared with Pluronic P123 in purely aqueous solution exhibiting only a poorly pronounced macroporous morphology with a broad macropore size distribution, the macroporous network of the silica gels synthesized with T44 consists of two independent well-defined pore size regimes. As seen in figure 75B on the largest level of hierarchy, the macroporous network consists of isolated macropores in the range of 50 – 200 μm resulting from enclosed droplets during the sol-gel transition. The pore walls of these isolated macropores (approximate thickness: t = 5 – 10 μm) themselves consist of interconnected macropores with pore diameters in the range of 0.7 μm (R^{Hg} = 0.4 μm). (Figure 75C) As can be seen from figure 75D, the silica strands accommodate a third level of porosity.

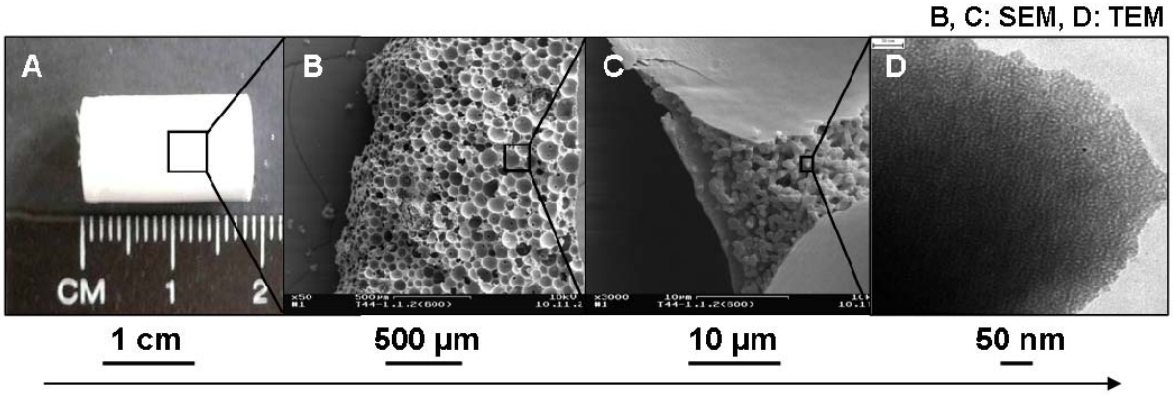

Figure 75 Silica monolith prepared with Tego Glide 440 in H_2O (A) exhibiting pore size regimes on different length scales: SEM image B shows isolated macropores in the range from 50 to 200 μm; C shows that the pore walls of the isolated pores reveal an interconnected macroporous network itself with macropores of 0.8 μm in diameter. The silica strands again hold a porous system with wormhole-like mesopores as can be seen in the TEM image D.

The corresponding SAXS curves and the pattern of the nitrogen hysteresis (figure 76) indicate the presence of a mesopore system exhibiting a periodic ordering with a repeating unit distance of d^I = 10.9 nm. The *d*-spacing is in the range of the repeating unit distance obtained for P123 in purely aqueous solution (d^{I0} = 11.8 nm). The corresponding TEM image shows that the mesoporous system is built-up of a wormhole-like aggregation of mesopores (figure 75D). Again, the TEM images give only insight into a small section of the total picture. The results from nitrogen sorption experiments and SAXS measurements indicate the presence of a periodic ordering over a larger length scale, as can be seen from the SAXS pattern in figure 76

with a distinct diffraction peak at $q^1 = 0.6\ nm^{-1}$ and a second less pronounced peak at $q^2 = 1.1\ nm^{-1}$.

In analogy to the silica gels prepared with LA-S 687 the samples prepared with Tego Glide 440 exhibit also a high amount of micropores ($V_0 = 139.8\ cm^3\ g^{-1}$), which contributes to the high specific surface area ($S^{BET} = 932\ m^2\ g^{-1}$).

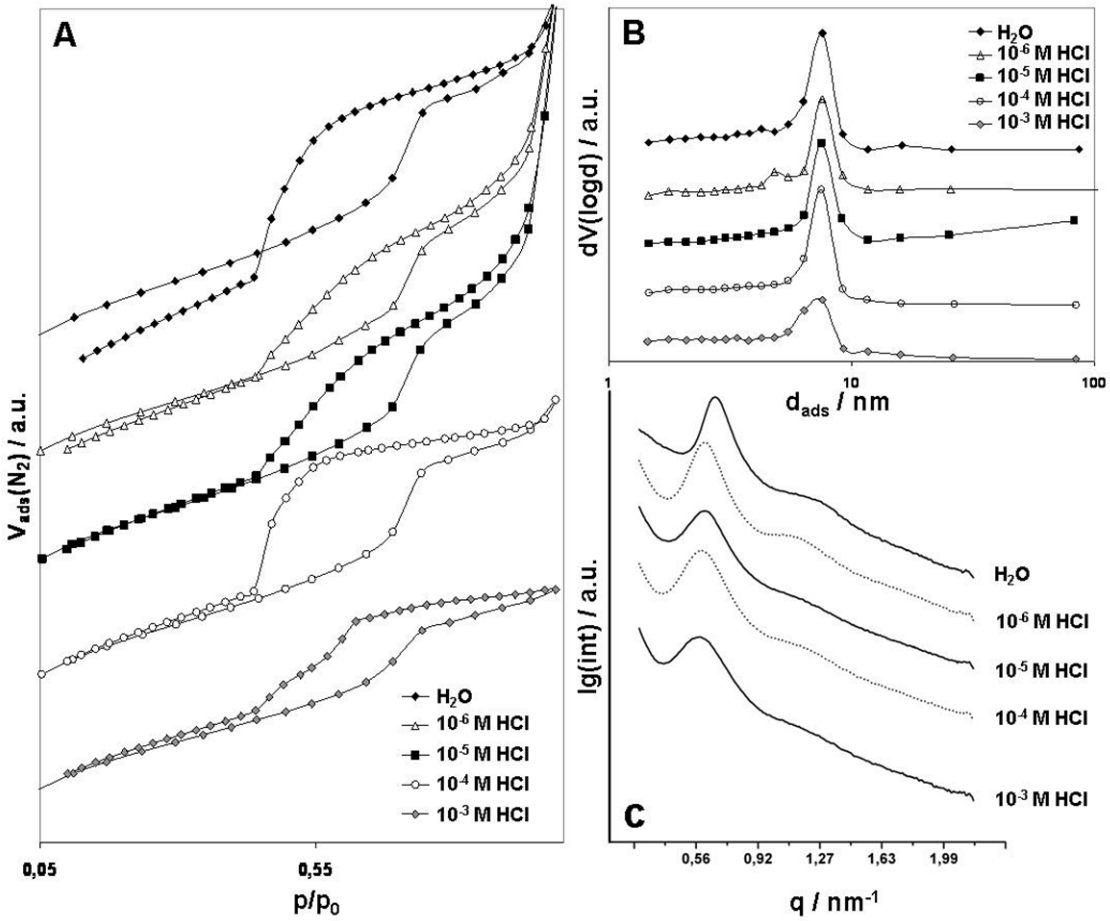

Figure 76 Structural investigations of the mesopore systems of the silica monoliths prepared with Tego Glide 440 (T44); all silica gels were treated with TMCS and subsequently heated up to 200°C. A) Hystereses of the T44 gels prepared in dilute HCl of varying concentrations. B) Pore diameter distributions calculated from the adsorption branches. C) SAXS pattern for T44 silica gels.

In analogy to the silica gels prepared with LA-S 687, the silica monoliths synthesized with Tego Glide 440 show a decreasing ordering of the mesopore system with increasing HCl concentration. However, this trend is not as pronounced for the employment of Tego Glide 440 as for LA S-687. Nitrogen sorption investigations and the SAXS measurements of the silica gels prepared from the different HCl concentrations are shown in figure 76.

In the pH-range from water (pH 5.5) to 10^{-4} M HCl (nominal pH 4) all silica gels exhibit an ordered mesoporosity which can be seen from the SAXS pattern with a well-resolved diffraction peak for the first ordering ($q^1(H_2O - 10^{-4}$ M HCl) = 0.6 nm^{-1}) and a broader signal for the second ordering ($q^1(H_2O - 10^{-4}$ M HCl) = 1.1 nm^{-1}). Only above a concentration of 10^{-3} HCl the mesoscopic ordering decreases as seen by the SAXS pattern and the nitrogen sorption hystereses, which slope for the adsorption branch, is less steep than for the other silica gels. The results for the corresponding SAXS measurements confirm this trend with a less pronounced diffraction peak for the first ordering.

SEM images in figure 77 of the corresponding silica gels show a reduction of the interconnectivity of the macropores with increasing HCl concentration. While the silica gels synthesized in 10^{-6} M HCl show a well-defined macroporous network with a pore radii distribution of 0.1 μm, the gels prepared in 10^{-5} M HCl already exhibit a coarser framework with isolated macropores in the range of 1 – 2 μm resulting in a broadening of the distribution of the macropores. The silica gels prepared with 10^{-3} M HCl exhibit macropore walls consisting of agglomerated silica particles. As seen in figure 77 the pores are not uniform in size, but are randomly distributed, leading to a broad pore radii distribution with a maximum at 1.0 μm (R^{Hg}).

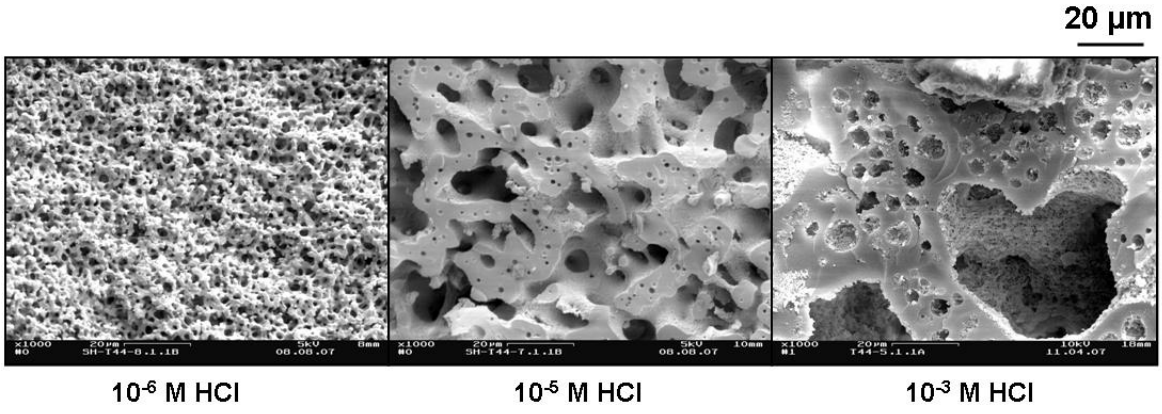

Figure 77 SEM images of silica gels prepared with Tego Glide 440 at different HCl concentrations and heated up to 200°C.

5.3.3. Silica Gels with a Tailored Surface

The tailoring of the surface polarity of silica materials is a major problem in order to meet the requirements for the different applications *e.g.* as catalysis, adsorption, or separation devices, etc. In the case of the hydrophobization of the surface, either post-synthetic grafting approaches are applied, such as the silylation of the surface silanol groups with silylation agents such as trimethylchlorosilane (TMCS), or the direct integration of the hydrophobic organic moieties *e.g.* by co-condensation of an organically functionalized silane (such as organo-trialkoxysilanes) with a tetraalkoxysilane. However, both approaches are subjected to limitations. The post-synthetic approach often results in a clogging of the mesopore entrances as consequence to steric effects of the organic groups and hence in a inhomogeneous distribution of the loading within the porous system.[18] The surface functionalization of a hierarchical organized material by co-condensation on the other hand, is also restricted due to the different hydrolysis and condensation rates of the organically modified silane and the tetraalkoxysilane resulting in an inhomogeneous distribution of the organic moieties for higher contents of the organically modified precursor. In addition, a higher content of the organically modified precursor, greater than 40 mol %, also causes changes in the evolution of the different pore size domains, leading to a reduced mesoscopic ordering and the loss of a well-defined co-continuous macroporous morphology.[18]

In order to achieve a homogenous distribution of hydrophobic groups within the pore systems and simultaneously to preserve the hierarchy of the silica monoliths, the idea was to generate the hydrophobic silica surface directly by a slow thermo-oxidative degradation of the PEO segments of the PEO-PDMS-PEO template phase within the pores resulting in a polydimethylsiloxane-modified surface.

To the best of our knowledge, the preparation of a PDMS-grafted mesoporous silica surface by a thermo-oxidative of PEO-PDMS-PEO co-polymers has never been reported in literature before. There are publications on the preparation of siloxane-modified mesoporous silica via post-synthetic grafting procedures, such as ultrasonic triggering of PDMS into a mesoporous host for drug release applications[162] or by the treatment of the silica matrix with cyanopropyl-methyl-phenyl-methyl-siloxane polymer.[163, 164] In addition, the direct synthesis of a polysiloxane-modified silica material by co-condensation of tetraethylorthosilicate (TEOS) with an oligomeric silanol terminated PDMS has also been described.[165, 166] However, the

direct approach via the gradual degeneration of the siloxane polymer-containing template has never been studied.

As known from literature, the thermo-oxidative degradation of sole PEO polymers strongly depends not only on the length of the chain but also on the excess of air. According to Han et al. the oxidation reactions of ethylene oxide units with oxygen generates peroxides that react with the PEO chains to low molecular weight oxygenated products. These degradation reactions are a reason for the broad temperature range necessary for the complete decomposition of PEO from below 100°C to temperatures higher than 350°C.[167, 168] Thermogravimetric investigations of hydrophobic PDMS polymers in air revealed, that the thermo-oxidative degradation of the DMS segments occurs in two steps. Like for PEO, Andrianov et al. postulated a free radical mechanism for the decomposition. In a first step, side-chain peroxides are formed and in a second step, side groups of the polymer are split off. These weight loss processes are observed at temperatures above 350°C for a pure polydimethylsiloxane.[169, 170] To investigate the possibility of incorporating the hydrophobic PDMS segment *in-situ* inside the porous systems by a selective thermo-oxidative degradation of the PEO-PDMS-PEO co-polymer, silica gels were synthesized with Tego Glide 440 in purely aqueous solution. All synthesis parameters were kept constant as described above with exception of the drying procedure with TMCS, which was replaced by supercritical drying with CO_2. The resulting gels were gradually heated to 600°C, whereas samples were withdrawn at 200, 300 and 400°C.

All gels, which were tempered at 200 and 300°C exhibited hydrophobic surfaces, whereas the sample at 400°C possessed a macroscopically hydrophilic surface. (Series of Photographs in figure 78) However, solid-state CP-MAS ^{29}Si-NMR investigations verified that even after a heat-treatment of 400°C, there were still T- and D-units present in the ^{29}Si-NMR spectra as can be seen from figure 78B. The D-units result from silicon atoms with two organic substituents (figure 78D) that can be related to the dimethylsiloxane (DMS) moieties, while T-units represent silicon atoms with only one organic substituent. These T-units result from oxidative degraded dimethylsiloxane segments (elimination of one methyl group) which can form a bonded to the silica surface via reaction with silanol groups. The silica gels calcined at 600°C (figure 78C) show neither T- nor D-units anymore, but only Q-units indicating a purely inorganic silica network.

For comparison, thermogravimetric analyses were conducted. The thermogravimetric measurement of sole Tego Glide 440 surfactant exhibits a gradual mass loss with three pronounced steps. The first mass loss of 71% is in the range of 30 – 410°C, which can be related to the defragmentation of the PEO segments (DTA: exothermic transition at 360°C). The second step (410 – 470°C) with a mass loss of 6% and the third step (470 – 990°C) exhibiting also a mass loss of 6% can be assigned to the two-step defragmentation of the PDMS segment with DTA exothermic maxima at 493°C and 593°C.

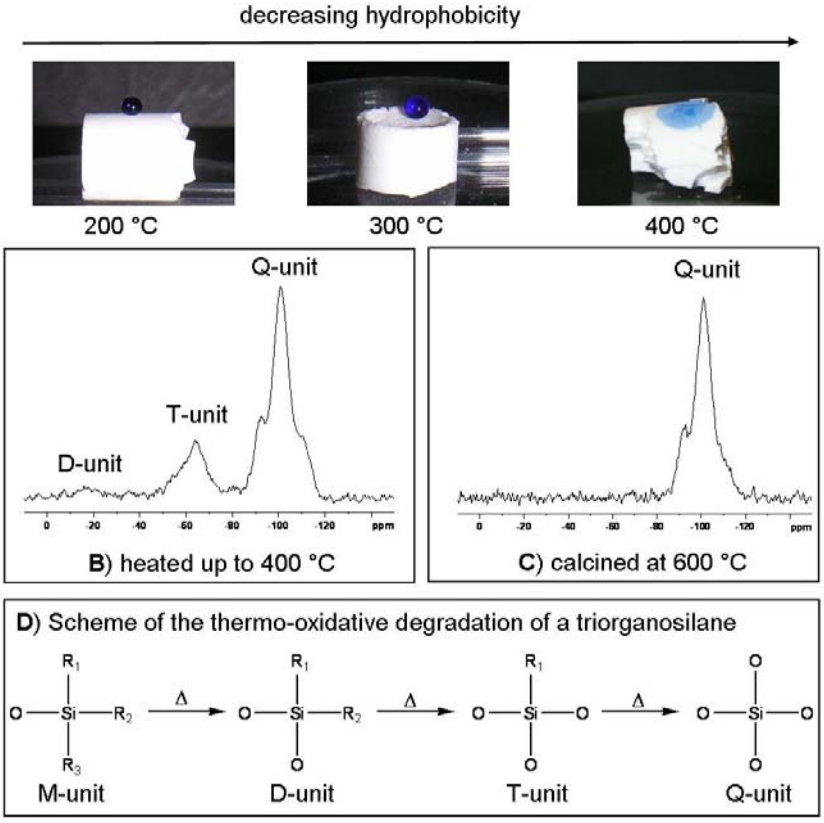

Figure 78 Silica monoliths supercritically dried with CO_2 and subsequently heated to 400 or 600°C, respectively. A) Blue ink droplets indicate the decreasing hydrophobicity of the silica surface from 200 to 400°C. B) presents the CP-MAS ^{29}Si-NMR spectra of the silica gel dried at 400°C and C) shows the CP-MAS ^{29}Si-NMR spectra of the corresponding silica sample calcined at 600°C.

The silica monoliths heat treated at 200°C and 300°C exhibit an additional mass loss in the region of 30 – 230°C of 3% and for the latter 230 – 340°C of 2%, which can be referred to adsorbed water and already fragmented volatile PEO segments as the corresponding DT analysis exhibits no maximum indicating a molecular decomposition process. The TGA diagram (in figure 79) of the 200°C tempered sample shows a mass loss of 14% in the

temperature range from 230 – 410°C, which can be related to the decomposition of PEO segments as the corresponding DTA curve shows an exothermic transition at 348°C. The last mass loss above 410°C results from the decomposition of present PDMS segments.

For the 300°C tempered sample the mass loss at 340 – 460°C of 4% results from the defragmentation of PEO and PDMS segments, which is affirmed by the DTA exothermic maxima at 389°C (PEO) and at 451°C (PDMS) respectively. The reduced mass loss in this temperature region indicates that by tempering up to 300°C, PEO segments are decomposed. In contrary, the DTA curve of the 400°C tempered silica sample shows no transitions in the temperature range from 200 – 460°C and the mass loss constitutes only 1%. Except for the calcined silica gel (600°C), the defragmentation of the PDMS blocks is induced at approx. 410°C. The respective DTA curves show exothermic maxima in the range of 451 – 471°C and a second transition at 526 – 529°C.

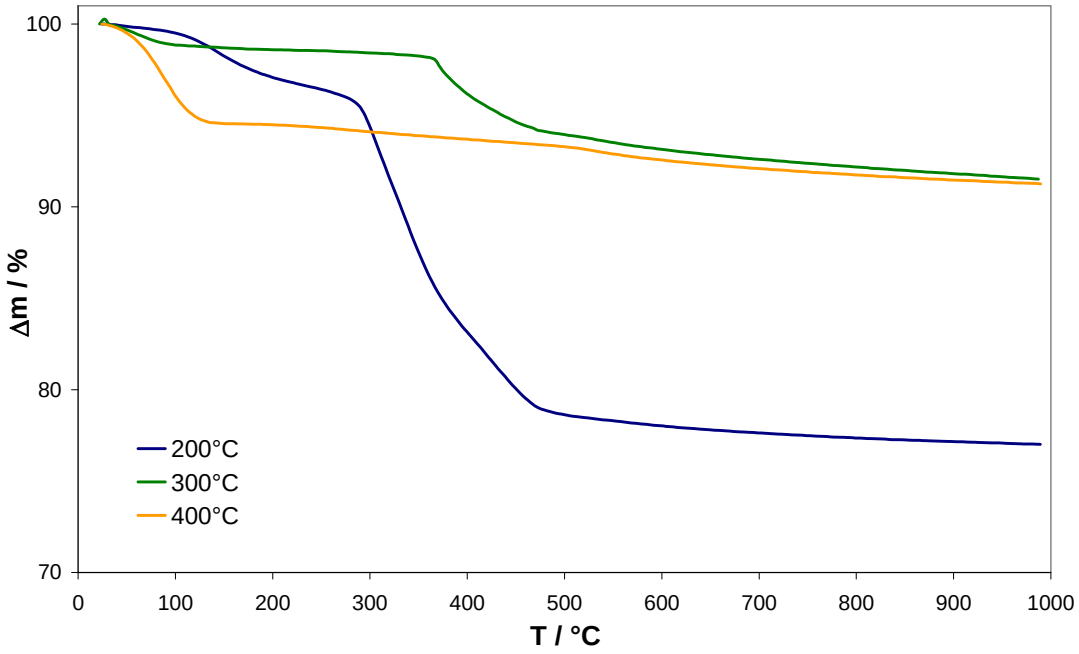

Figure 79 TGA curves presenting the thermal decomposition of the surfactant Tego Glide 440 within the pore systems of the silica gels. The silica monoliths were dried supercritically and subsequently heated to either 200, 300, 400, or 600°C.

5.4. Conclusion

Hierarchically organized silica monoliths were obtained via sol-gel processing by employing the commercially available linear PEO-PDMS-PEO surfactants Tego Glide 440 and LA-S 687 as structure-directing agents and an ethylene glycol-modified silane (EGMS) as precursor. In contrary to amphiphilic hydrocarbon-based surfactants *e.g.* Pluronic P123, the employment of especially Tego Glide 440 has opened up new perspectives in the synthesis of hierarchically organized silica monoliths as the templating from an emulsion gives access to the introduction of additional pore size regimes over larger length scales. Furthermore, the resulting well-defined co-continuous macroporous framework and the periodically ordered mesopore network showed that the macroscopic phase separation as well as the phase separation in the mesoscopic range is also induced in this emulsion-based sol-gel system.

In addition to the tuneable pore sizes, the employing of a PEO-PDMS-PEO co-polymer also offers the possibility to tailor the surface polarity directly by a gradual thermo-oxidative degradation of the hydrophilic PEO blocks resulting in hydrophobic silica monoliths with integrated siloxane moieties within the porous system.

Chapter 6

Application of Hierarchically Organized Silica Monoliths as HPLC Columns

6.1. Motivation

When in the year 2000, Merck KGaA company launched monolithic silica columns, known as Chromolith™, as stationary phases for HPLC applications, on to the market, the chromatographic separation was brought to a new level. Until then packed particulate columns consisting of silica beads or organic polymers such as polystyrene-divinylbenzene co-polymers were applied as stationary phases for which the separation efficiency is strongly dependent on the quality of packing and the average particle size.

One of the major problems of particulate columns is the fact that optimum separation efficiencies are obtained by employing small, uniform particles (*e.g.* 3 – 5 μm). However, as high back pressures arise during analysis, the flow rate of the mobile phase is limited and thus the analysis time is extended resulting in a reduction of the separation quality.[2]

In contrary, hierarchically organized monolithic columns exhibit lower back pressures due to their high permeability of their interconnected macroporous framework (with macropores of

2 μm in diameter for the Chromolith™). In combination with the mesoporous system being located within the silica skeleton and high specific surface areas, the application of monolithic columns allows for a high separation efficiency at a minimum separation time.[2, 171] Furthermore, due to their rigid skeleton, monolithic columns exhibit a higher durability than packed particulate columns.

The hierarchically organized silica monoliths, prepared from diol-modified silanes, resemble the pore architecture of the Chromolith™ columns, such as the well-defined co-continuous macroporous framework which silica strands exhibit mesopores with a narrow pore size distribution. In addition, the here presented monolithic systems, *e.g.* the EGMS-derived and also the MeGMS / EGMS-derived (≤ 30% MeGMS) gels, show a pronounced long-range ordering of the mesopores. The combination with high specific surface areas resulting from the different incorporated pore size domains and narrow pore size distributions in the meso- and the macroscopic range, make the EGMS- and MeGMS / EGMS-derived silica gels interesting candidates as potential HPLC columns.

In a collaboration, the silica and the hybrid inorganic-organic silica monoliths were subjected to extensive Normal Phase (NP) and Reversed Phase (RP) HPLC experiments at Merck KGaA, Darmstadt.

6.2. Application as HPLC Columns

For the investigation of the applicability as HPLC columns, silica and inorganic-organic hybrid silica monoliths were selected exhibiting pronounced hierarchical ordering.

The applied silica gels were synthesized from sole EGMS as precursor in the ratio of Si / P123 / 1 - 10^{-4} M HCl = 8.4 / 30 / 70 (per weight). The methyl-modified hybrid silica monoliths were prepared by applying an analogue composition of the template phase at c(HCl) = 0.03 M, whereas the Si-content of 8.4 wt % was achieved by employing EGMS and MeGMS with contents of MeGMS of 5 – 30 mol %.

The detailed synthesis procedure of the silica gels are given in section 2.1.2. and of the methyl-modified hybrid monoliths in section 2.2.1.1.

It has to be mentioned, that all silica and hybrid silica monoliths were post-synthetically modified with trimethylsilyl groups. This grafting was achieved via silylation reaction of the

accessible surface silanol groups with chlorotrimethlysilane (TMCS) and the hydrophobic surface was preserved throughout the drying procedure.

The monoliths had diameters of 4 – 5 mm and were truncated to lengths of 5 – 10 cm before they were enclosed in a polyaryletheretherketone (PEEK) cladding.

All monoliths were tested in Normal Phase (NP) standard (Si Standard Test) and in Reversed Phase (RP) tests at room temperature at flow rates of 2.0 mL min^{-1} for the NP standard experiments and at 1.0 mL min^{-1} for the RP tests.

The parameters and the composition of the mobile phase as well as of the analyte mixtures chosen for these tests are given in table 27.

Table 27 Testing parameters of the applied HPLC tests. All investigations were conducted at room temperature.

	NP standard test	*RP test*
mobile phase (flow rate)	*n*-heptane / dioxane (95 / 5% v/v) (2.0 mL min^{-1})	water / acetonitrile (40 / 60% v/v) (1.0 mL min^{-1})
pressure	≤ 200 bar	≤ 200 bar
UV-detection	254 nm response fast	254 nm response fast
injection volume	5 μL	5 μL
sample composition	toluene (0.47 mg mL^{-1}) nitrobenzene (0.04 mg mL^{-1}) 2-nitroanisol (0.15 mg mL^{-1})	thiourea (0.13 mg mL^{-1}) biphenyl-2-ol (0.06 mg mL^{-1}) progesterone (1.1 mg mL^{-1}) 1-phenyl-1-hexanone (0.137 mg mL^{-1}) anthracene l (0.1 mg mL^{-1})

In order to determine the performance of each tested column, the number of theoretical plates N (according to equation 3 in section 1.3.5.), the retention factor k′, the selectivity α as well as the resolution R are elucidated from the corresponding chromatograms.

As described in section 1.3.5. the separation efficiency is expressed by the number of theoretical plates N which is dependent on the retention time[102].

For the evaluation of the chromatograms and for the comparison of the performance of the different columns, the retention times are no adequate parameters, as they strongly depend on the flow velocity u of the mobile phase and the length L of the column. Hence the retention factor k' is introduced which is independent of these two parameters.

$$k' = \frac{t_R - t_0}{t_0} \qquad \textit{Equation 6}$$

t_R: retention time of the substance
(time period between injection and detection of the signal)
t_0: time interval required by the pure mobile phase or an unretained species to pass the column

The retention factor has to differ for each chemical component of the analyte mixture in order to obtain a separation and ought to exhibit values between 1 and 5 ($k' < 1$: can result in insufficient separations, $k' > 5$: can cause elongated analysis times).[102]

Determined in dependency of the retention factors (equation 7), the selectivity α for a given pair of analytes of the HPLC system is a prominent parameter in order to describe the separation selectivity of a system. For a separation of two analytes, α has to exceed 1. If α = 1, the retention times of two substances will be equal, and hence no separation is performed.

$$\alpha = \frac{k'_2}{k'_1}, \text{ with } k'_2 > k'_1 \qquad \textit{Equation 7}$$

k'_2: retention factor of component 2
k'_1: retention factor of component 1

A further quality factor of a separation is the resolution R of two adjacent peaks, which is determined according to equation 8.

$$R = \frac{2(t_2 - t_1)}{w_2 + w_1}$$ *Equation 8*

$t_{1(2)}$: retention time of substance 1(2)
$w_{1(2)}$: peak width at base of the signal of substance 1(2)

Another possibility to express R is in dependency of the retention factor k' (if $k'_2 >> k'_1$), the number of theoretical plates N and the selectivity α.

$$R = \frac{1}{4}\frac{(\alpha - 1)}{\alpha}\sqrt{N}\frac{k'_2}{1 + k'_2}$$ *Equation 9*

The monoliths exhibiting the best performance of each series in the initial NP and RP tests, were subjected to further experiments such as the investigation of the selectivity of the monolith for different analyte mixtures as NP as well as RP stationary phase. In addition, van Deemter curves were also recorded for these monoliths to identify the optimum linear flow velocities and thus establishing the maximum separation efficiency of each column.

6.2.1. EGMS-derived Silica Monoliths

For the investigation of the applicability as HPLC columns, silica monoliths derived from sole EGMS in acidic media (c(HCl) = $1 - 10^{-4}$ M) were selected. These silica monoliths exhibited hierarchically organized pore size domains consisting of a co-continuous macroporous framework and a 2D-hexagonally arranged mesopore system located within the macroporous skeleton.
The detailed monolith synthesis procedure is described in section 2.1.3. and the physico-chemical properties of the monoliths are listed in table 5 (section 2.1.3.1.).

The chromatographic data obtained from the NP HPLC standard tests and from the RP tests including the length of each monolith, the arising backpressure, and the corresponding specific surface area (determined from nitrogen sorption measurements) are listed in tables 28 and 29.

The selectivity α and the resolution R are determined for the last pair of peaks and the retention factor k′ is calculated for the last peak.

Figure 79 shows the resulting Normal Phase (NP) chromatograms of the EGMS-derived silica columns for the separation of toluene, nitrobenzene and 2-nitroanisole by employing *n*-heptane / dioxane (95 / 5% v/v) as mobile phase.

Table 28 Chromatographic data obtained from Normal Phase (NP) Si standard tests at RT.

	Si standard test								
samples	*c(HCl)* /mol l^{-1}	*L* /cm	*N/m*	T_{USP}	*k'*	α	*R*	*p* /bar	S^{BET} /m^2 g^{-1}
P1-1e Nr.2	1	5	23480	1.69	0.59	2.87	2.41	103	1023
P2-0a	1	5	48980	1.91	1.48	3.65	6.69	120	927
P1-2b	10^{-1}	5	36000	-	1.63	4.00	6.21	103	908
P1-3	10^{-2}	5	-	-	-	-	-	167	944
P1-5	10^{-4}	5	18180	-	2.06	4.13	5.01	88	1066

The tailing T is determined according to the USP (United States Pharmacopeia) as $T_{USP} = \frac{a+b}{2a}$ at 5% peak height. S^{BET} is determined from nitrogen sorption measurements.

Table 29 Chromatographic data obtained from Reversed Phase (RP) tests at RT.

	RP standard test								
samples	*c(HCl)* /mol l^{-1}	*L* /cm	*N/m*	T_{USP}	*k'*	α	*R*	*p* /bar	S^{BET} /m^2 g^{-1}
P1-1e Nr.2	1	5	61080	-	2.54	1.11	1.01	61	1023
P2-0a	1	5	-	-	1.22	1.09	0.42	94	927
P1-2b	10^{-1}	5	-	-	1.34	1.09	0.29	64	908
P1-3	10^{-2}	5	-	-	-	-	-	60	944
P1-5	10^{-4}	5	5560	-	1.01	1.37	0.56	26	1066

The tested hierarchically organized silica monoliths possess different macroporous morphologies. However, all monoliths exhibit a 2D-hexagonal arrangement of the mesopores whereas the determined mesopore diameter varies in the range of D^{BJH} = 3.6 – 6.9 nm for the different applied HCl concentrations.

The silica monoliths synthesized at c(HCl) = 1 M (P1-1e Nr.2, P2-0a) and c(HCl) = 10^{-1} M (P1-2b) exhibit a highly interconnected macroporous framework formed by rod-shaped silica strands which enclose macropores of uniform size (R^{Hg} = 0.3 μm). Their corresponding mesopore diameters resulting from nitrogen sorption experiments are determined to D^{BJH} (P1-1e, P2-0a) = 6.3 nm and D^{BJH} (P1-2b) = 5.4 nm. The silica monolith synthesized at c(HCl) = 10-4 M (P1-5) also exhibits a highly interconnected macroporous framework, however, the silica strands are no longer rod-shaped. The enclosed macropores show a narrow pore radii distribution with R^{Hg} = 0.1 μm. The integrated mesopore system shows the smallest pore diameter distribution with D^{BJH} (P1-5) = 3.6 nm.
For comparison, a monolith of reduced hierarchical ordering is also tested. P1-3 (synthesized at (HCl) = 10^{-2} M) exhibits an interconnected macroporous framework, however, the macropores are of random shape and size, whereas the ordering of the mesopores (D^{BJH} (P1-3) = 6.9 nm) is retained.

The results of the HPLC testing of the different hierarchically organized silica monoliths in the Normal Phase mode are presented in figure 80.

The chromatogram of the silica monolith P1-3 (c(HCl) = 10^{-2} M) shows only one broad signal indicating no separation of the mixture of toluene, nitrobenzene and 2-nitroanisole. Keeping in mind, the low degree of organization and uniformity of the macroporous framework, this result is not surprising. Despite the well-defined macroporous morphologies with narrow macropore radii distributions of the silica monoliths P1-2b and P1-5 (prepared at c(HCl) = 10^{-1} and 10^{-4} M), the corresponding chromatograms exhibit insufficient separation qualities for the separation of the standardized analyte mixture.

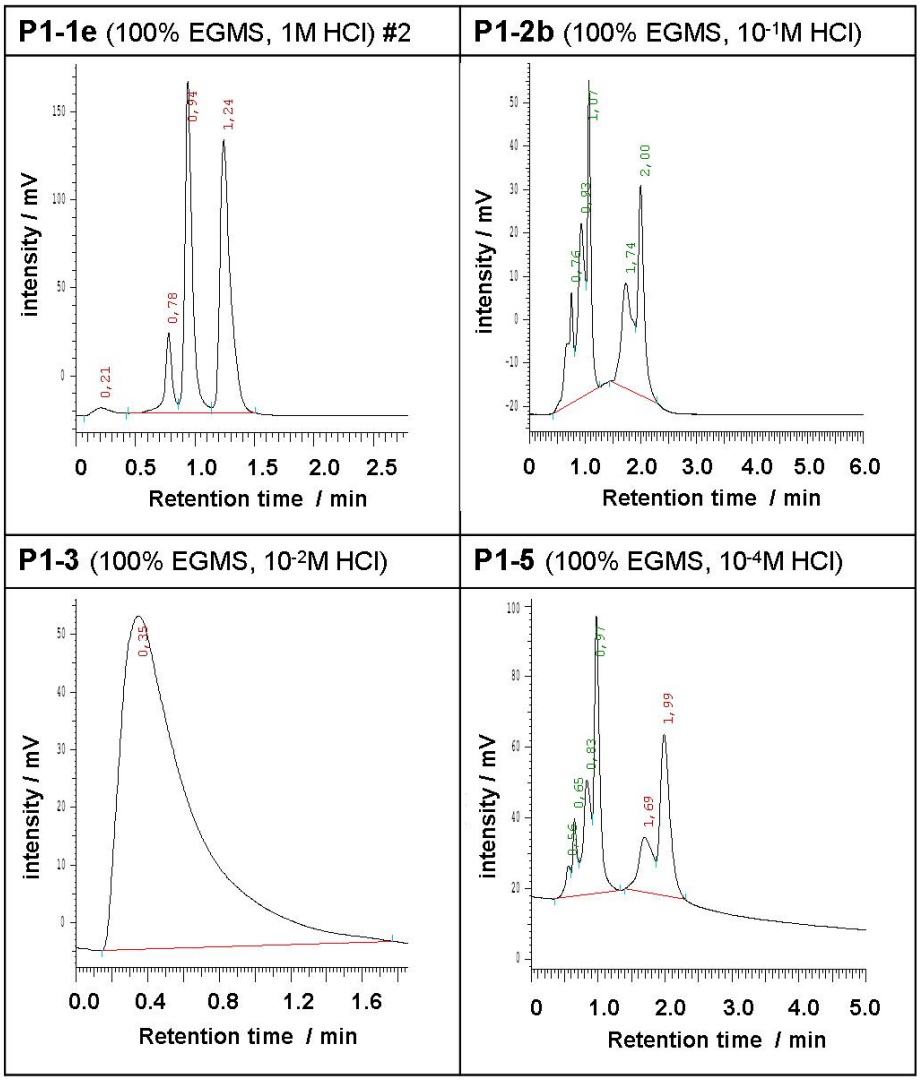

Figure 80 Chromatograms of the separation of toluene, nitrobenzene, and 2-nitroanisole with *n*-heptane / dioxane (95 / 5% v/v) by the different silica columns derived from EGMS sol-gel systems at different acid concentrations.

In contrast, the silica monolith P1-1e prepared at c(HCl) = 1 M exhibits a good performance as stationary phase with nearly baseline separated peaks indicating an efficient separation of the analyte mixture and an only low degree of tailing with T_{USP} = 1.69.

For comparison, the chromatogram of the analogue HPLC experiment for the Chromolith™ Performance (pure SiO_2) with macropores of 2 μm in diameter and mesopores of 13 nm in diameter is presented in figure 81.

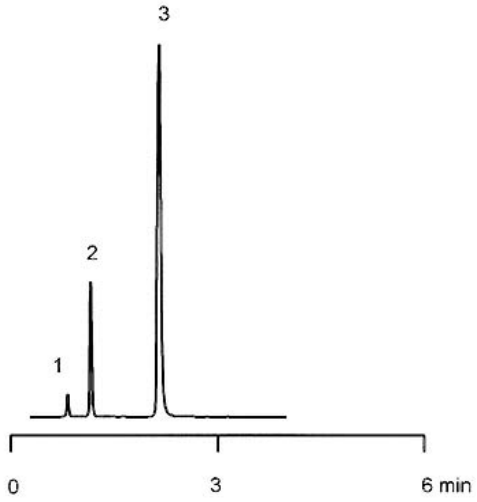

Figure 81 Chromatogram obtained by applying Chromolith™ Performance Si (100-4.6 mm) for the separation of toluene (1st), nitrobenzene (2nd), and 2-nitroanisole (3rd) with *n*-heptane / dioxane (95 / 5% v/v) as eluent and a flow rate of 2 mL min^{-1}.[172]

The determined selectivity $\alpha = 2.87$ in combination with the resolution $R = 2.41$, all determined for the last pair of peaks, affirm the good performance of P1-1e as stationary phase. The performance is in line with the structural and morphological properties of the monolith exhibiting well-organized pore size regimes with narrow pore size distributions of the mesopores $D^{BJH} = 6.8$ nm (determined from the desorption branch of the nitrogen hystereses) and the macropores ($D^{Hg} = 0.6\ \mu m$). (Figure 82)

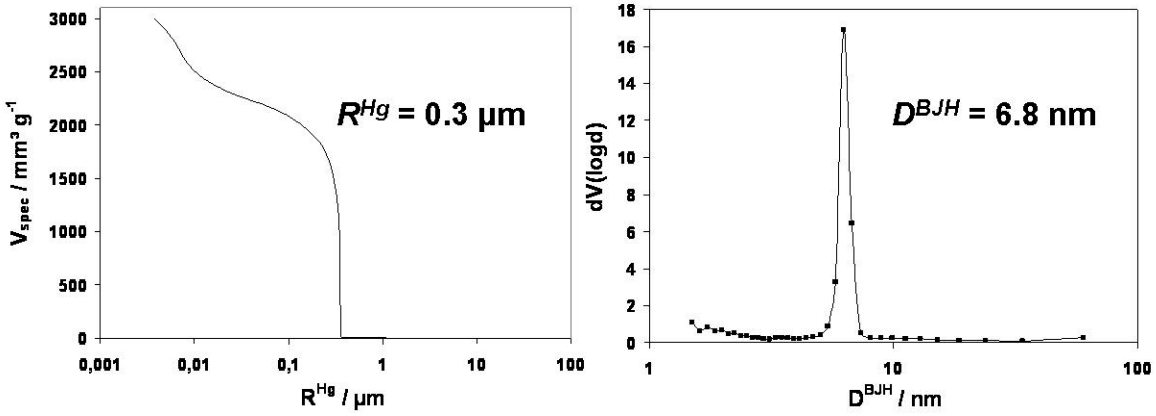

Figure 82 Pore size distributions of the macropores (left) and the mesopores (right) of P1-1e (prepared from 100 mol EGMS at 1 M HCl).

For further investigations of the applicability of P1-1e (100 mol % EGMS, 1 M HCl) in the NP mode, van Deemter diagrams were created for nitrobenzene and 2-nitroanisole in the range

of u = 0.27 – 4.39 mm s^{-1} (back pressure p = 9 – 138 bar) (Figure 83). Minimum values for H (height equivalent to a theoretical plate) for nitrobenzene (H = 40.19 μm) and 2-nitroanisole (H = 47.48 μm) are obtained at u = 0.8 mm s^{-1} indicating the optimum separation efficiency of the column per analyte. (N_{max}(nitrobenzene) = 1244 and N_{max}(2-nitroanisole) = 1053, each determined for a 5 cm column)

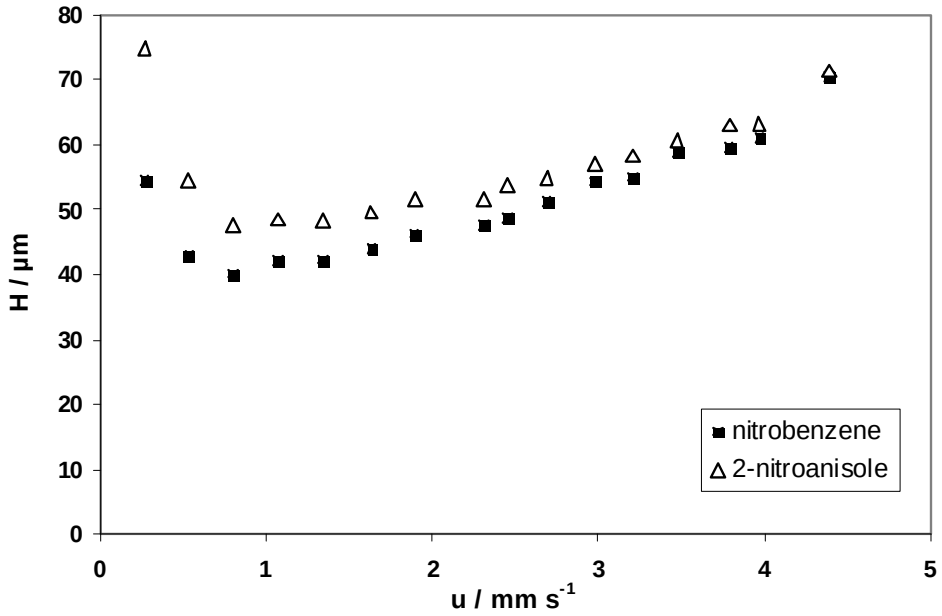

Figure 83 Van Deemter curves for the silica column prepared at 1 M HCl of nitrobenzene and 2-nitroanisole at RT.

The application of the same EGMS-derived monoliths as stationary phases in the RP mode, reveals a surprising result. As can be seen in figure 84, P1-1e also shows a good performance as RP-HPLC column. The separation of a mixture of thiourea, biphenyl-2-ol, progesterone, 1-phenyl-1-hexanone, and anthracene results in a chromatogram in which only the last two peaks are not completely resolved (R = 1.01). The separation quality is also affirmed by the determined retention factor $k' = 2.54$ and the selectivity $\alpha = 1.11$.

This result is rather unusual as for a certain surface polarity, hence either hydrophobic or hydrophilic properties, sufficient separation efficiencies and especially selectivities can usually only be obtained for either the NP mode (hydrophilic such as Chromolith™ Performance Si) or the RP mode (hydrophobic such as Chromolith™ RP-18 end-capped, which is grafted with octadecyl moieties).

However, one has to keep in mind that the silica monoliths were surface modified with TMCS resulting in the silylation (-Si-O-Si$(CH_3)_3$) of the accessible silanol groups on the surface. As

the trimethylsilyl moieties are rather small, a high degree of loading in combination with a rather homogeneous distribution of the organic groups within the pores can be achieved. The loading is affirmed by contact angle measurements, which exhibit a hydrophobic surface with a contact angle of 127° (see also section 2.2.2., measured for an as-synthesized monolith). If compared to the modification with octadecyl moieties, the loading of the silica surface with small trimethylsilyl groups results in a low shielding of unreacted silanol groups enabling the application as stationary phase for NP-HPLC experiments.

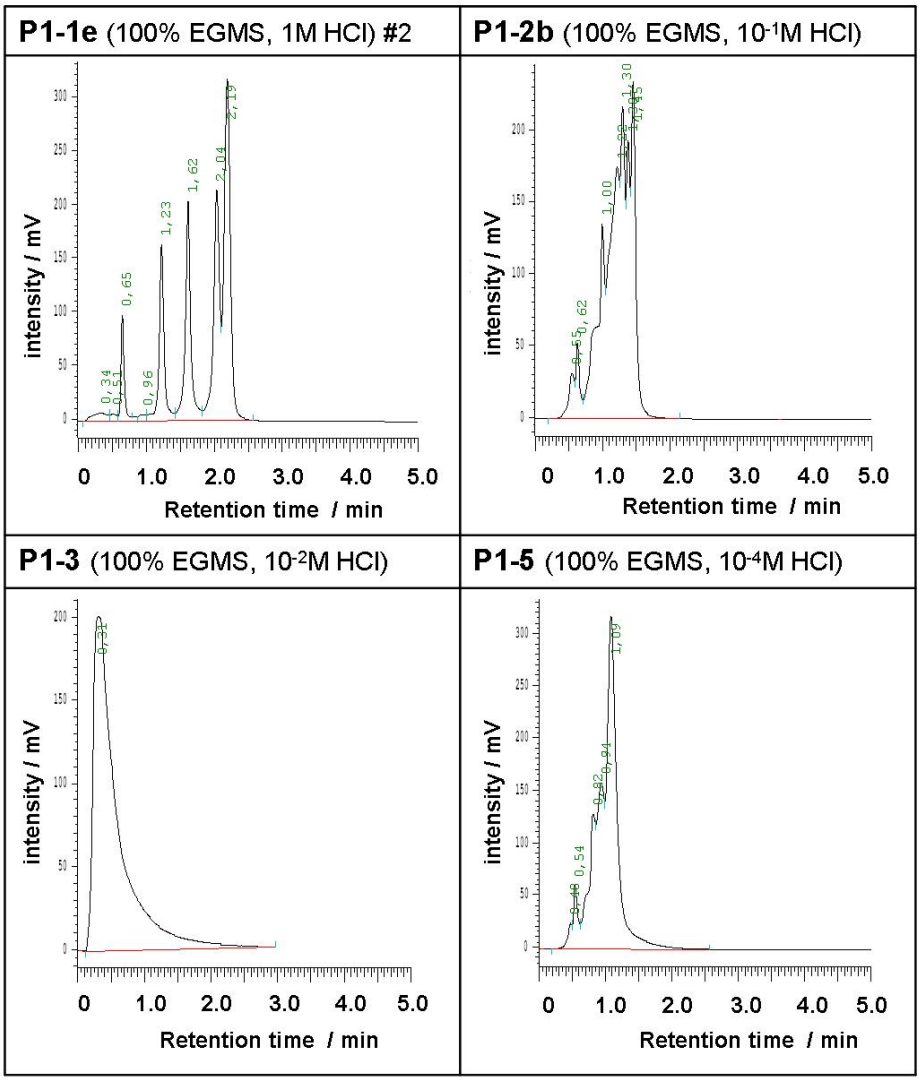

Figure 84 Chromatograms of the separation of thiourea, biphenyl-2-ol, progesterone, 1-phenyl-1-hexanone, and anthracene for the different silica columns derived from EGMS at different c(HCl).

In contrast to P1-1e, the silica monoliths P1-2b and P1-5 (c(HCl) = 10^{-1} and 10^{-4}M HCl) showed no separation in the RP mode (analogue to the NP mode). It is assumed that the ineffectiveness of these monoliths results from inhomogeneities within the hierarchical pore size domains. Especially, inhomogeneities of the pore sizes cause diffusion pathways of differing lengths and a limited mass transfer resulting in a broadening of peaks and even to the coincidence of multiple peaks.

In analogy to the investigations in the NP mode, van Deemter curves were also recorded for the RP tests with anthracene and progesterone as testing systems. The resulting diagram is presented in figure 85. The minimum plate height for progesterone is H_{min} = 20.01 μm at a linear flow velocity of u = 0.65 mm s^{-1} indicating the best efficiency with N = 2499 (per 5 cm column) for progesterone. Unlike particulate silica columns, the van Deemter curve of monolithic columns exhibits a gentle slope of the curve in the minimum's region. The value of the plate height is almost constant with increasing linear flow u due to the favourable mass transfer properties of the hierarchical pore size domains of the monolith. Here, this region is found at linear flows of u = 0.65 – 1.67 mm s^{-1} in which the optimum separation efficiency for progesterone can be achieved for P1-1e. The optimum efficiency N = 1296 (per 5 cm column) for anthracene is obtained with H_{min} = 38.58 μm at a linear flow velocity of u = 1.32 mm s^{-1}.

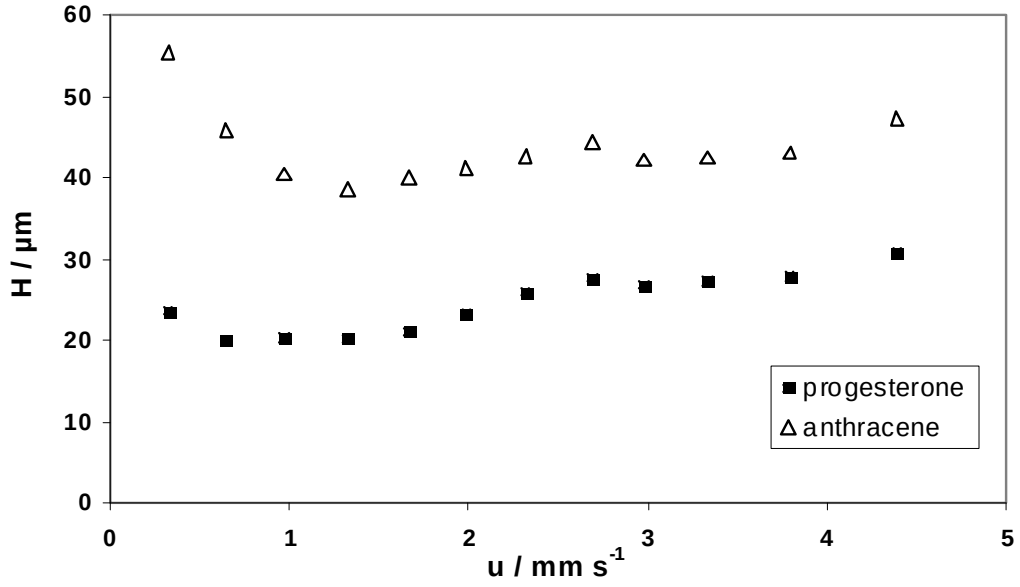

Figure 85 Van Deemter curves of the RP-system for the EGMS-derived silica column prepared at 1 M HCl of progesterone and anthracene at RT.

In order to study the selectivity of P1-1e (100 mol % EGMS, 1 M HCl), a variety of separation experiments in the NP and the RP mode were conducted. In accordance with the results from the standard tests, P1-1e exhibits greater selectivities in the RP-HPLC investigations than in the NP tests. Figure 85 shows the chromatograms of the selectivity tests exhibiting the best separation performances. The corresponding experimental conditions including each analyte mixture are given in table 30.

Table 30 Listing of the RP separation experiments performed on the P1-1e column. All experiments were conducted at RT; the sample volume was 10 μl and the flow velocity 1 ml min^{-1}.

experiment	*eluent*	*composition of the analyte mixture*
Tanaka 2	methanol / water (30 / 70% v/v) (isocratic)	uracil (1.0 mg) caffeine (2.5 mg) phenol (10.1 mg)
Acids	methanol / 20 mM Na-phosphate buffer 2,0 (30 / 70% v/v) (isocratic)	thiourea (1.83 mg) 2-nitrobenzoic acid (2.4 mg) salicylic acid (26.35 mg) benzoic acid (26.4 mg)
Complexing Agents	methanol / 20 mM Na-phosphate buffer 2,0 (70 / 30% v/v) (isocratic)	uracil (0.3 mg) purpurine (5.6 mg) quinizarin (1.5 mg)

Even though, the surface of the EGMS-derived silica monolith is only loaded with trimethylsilyl moieties, the separation performance for the mixtures (presented in figure 86) is qualitatively high with a complete separation of the mixtures within a maximum of 10 min (L(P1-1e) = 5 cm). The fastest separations within a 3 min period are obtained for the system Tanaka 2, a mixture of uracil, caffeine, and phenol, and for the Complexing Agents consisting of uracil, purpurine and quinizarin. The separation of more complex mixtures such as the Acid mixture (mixture of thiourea, 2-nitrobenzoic acid, salicylic acid, and benzoic acid) requires a longer time period of up to 10 min.

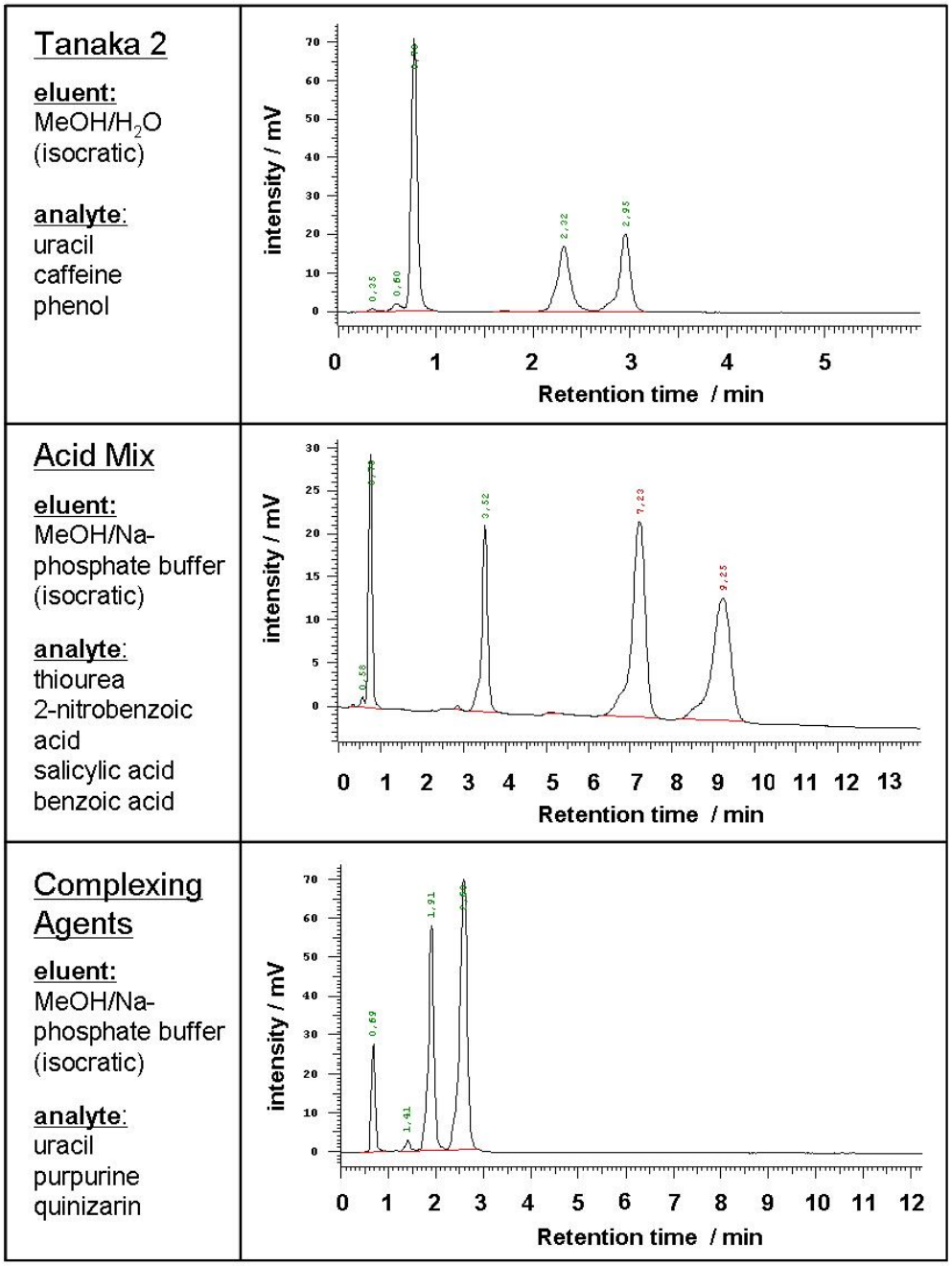

Figure 86 Chromatograms of the investigations of the selectivity of P1-1e (100 mol % EGMS, 1 M HCl) as RP column for different analyte mixtures.

6.2.2. MeGMS / EGMS-derived Hybrid Silica Monoliths

In analogy to the investigations of the silica monoliths derived from sole EGMS, inorganic-organic hybrid silica monoliths being synthesized via co-condensation of the ethylene glycol-modified methylsilane (MeGMS) and EGMS in which the molar content of MeGMS was varied in the range of 5 – 30 mol % were also investigated as HPLC columns. As described in section 2.2.1.2., the maximum homogeneous loading of organic groups, which can be achieved by simultaneous preservation of the hierarchical architecture of the pore size domains, is restricted by the different condensation rates of MeGMS and EGMS. As above 30 mol% MeGMS, the hierarchy cannot be preserved, the resulting loading with methyl moieties is low and hence an additional post-synthetic grafting is desirable.

In analogy to the EGMS-derived silica monoliths, the post-synthetic grafting was performed via silylation reaction of accessible surface silanol groups with chlorotrimethylsilane (TMCS) resulting in an additional loading with hydrophobic trimethylsilyl moieties on the surface.

The different hybrid methyl-modified silica monoliths were synthesized at 1 and 0.03 M HCl. The system chosen for the presentation of the Normal Phase (NP) and Reversed Phase (RP) tests are the monoliths prepared at 0.03 M HCl with a varied molar content of MeGMS (5 – 30 mol %). The chromatographic parameters obtained from the Si standard tests (NP) and from the RP mode are given in the tables 31 and 32. The corresponding testing parameters including the composition of the eluent phase as well as the composition of the analyte mixtures are given in table 27.

Table 31 Chromatographic data obtained from Normal Phase (NP) Si standard tests for the hybrid methyl-modified silica monoliths at RT (gels prepared at 0.03 M HCl).

	Si standard test								
samples	*%MeGMS /mol %*	*L /cm*	*N/m*	T_{USP}	*k'*	α	*R*	*p /bar*	S^{BET} /$m^2\ g^{-1}$
P4-1,5a	5	10	41800	2.29	2.29	3.82	11.82	102	973
P5-1,5a	7.5	10	34140	2.08	2.22	3.74	10.80	109	976
P6-1,5a	10	5	22120	1.65	2.29	3.72	4.83	78	1017
P7-1,5a	12.5	10	15010	1.42	2.38	3.69	6.87	79	1069
P8-1,5a	15	10	5650	0.95	2.21	3.70	4.12	74	1095
P9-1,5a	17.5	10	4120	1.75	2.22	3.71	3.42	93	1032
P10-1,5a	20	10	6490	1.09	2.03	3.62	4.12	67	1034
P11-1,5a	30	5	1760	1.16	1.83	3.67	1.50	46	1015

Table 32 Chromatographic data obtained from Reversed Phase (RP) standard tests for the hybrid methyl-modified silica monoliths at RT (gels prepared at 0.03 M HCl).

samples	RP standard test								
	%MeGMS /mol %	L /cm	N/m	T_{USP}	k'	α	R	p /bar	S^{BET} /$m^2\ g^{-1}$
P4-1,5a	5	10	-	-	1.54	1.07	0.49	76	973
P5-1,5a	7.5	10	-	-	1.37	1.1	0.79	76	976
P6-1,5a	10	5	-	-	-	-	-	39	1017
P7-1,5a	12.5	10	-	-	-	-	-	42	1069
P8-1,5a	15	10	-	-	-	-	-	36	1095
P9-1,5a	17.5	10	-	-	-	-	-	51	1032
P10-1,5a	20	10	-	-	-	-	-	29	1034
P11-1,5a	30	5	-	-	-	-	-	9	1015

Figure 87 shows the chromatograms of the HPLC experiments in the NP mode of the hybrid methyl-modified silica monoliths.

Interestingly, all monoliths synthesized with 5 – 30% MeGMS at 0.03 M HCl, exhibit well-resolved chromatograms for the separation of toluene from nitrobenzene and 2-nitroanisole. While with increasing content of MeGMS the tailing is reduced from T_{USP} = 2.29 (5 mol % MeGMS) to T_{USP} = 1.09 (20 mol % MeGMS), the selectivity α almost remains constant with values of about 3.7. The comparison of the equally long monoliths P4-1,5a to P10-1,5a (L = 10 cm) show that the required time periods for the separation of the analyte mixture are fast with 1.5 to 3.2 min, whereas the fastest separation is observed for P6-1,5a (10 mol % MeGMS). This result is not surprising as P6-1,5a exhibits the largest macropore sizes with narrow radii distributions of R^{HG} = 1.1 μm among the hybrid methyl-modified silica monoliths (5 – 30 mol % MeGMS) allowing for the most efficient mass transfer.

The retention factor decreases from P4-1,5a (5 mol % MeGMS) and P6-1,5a (10 mol % MeGMS) with k′ = 2.29 to P11-1,5a (30 mol % MeGMS) with k′ = 1.83. Despite a relatively pronounced tailing (in particular for the last peak), the best performances are found for P4-1,5a (N/m = 41800) and P6-1,5a (N/m = 22120).

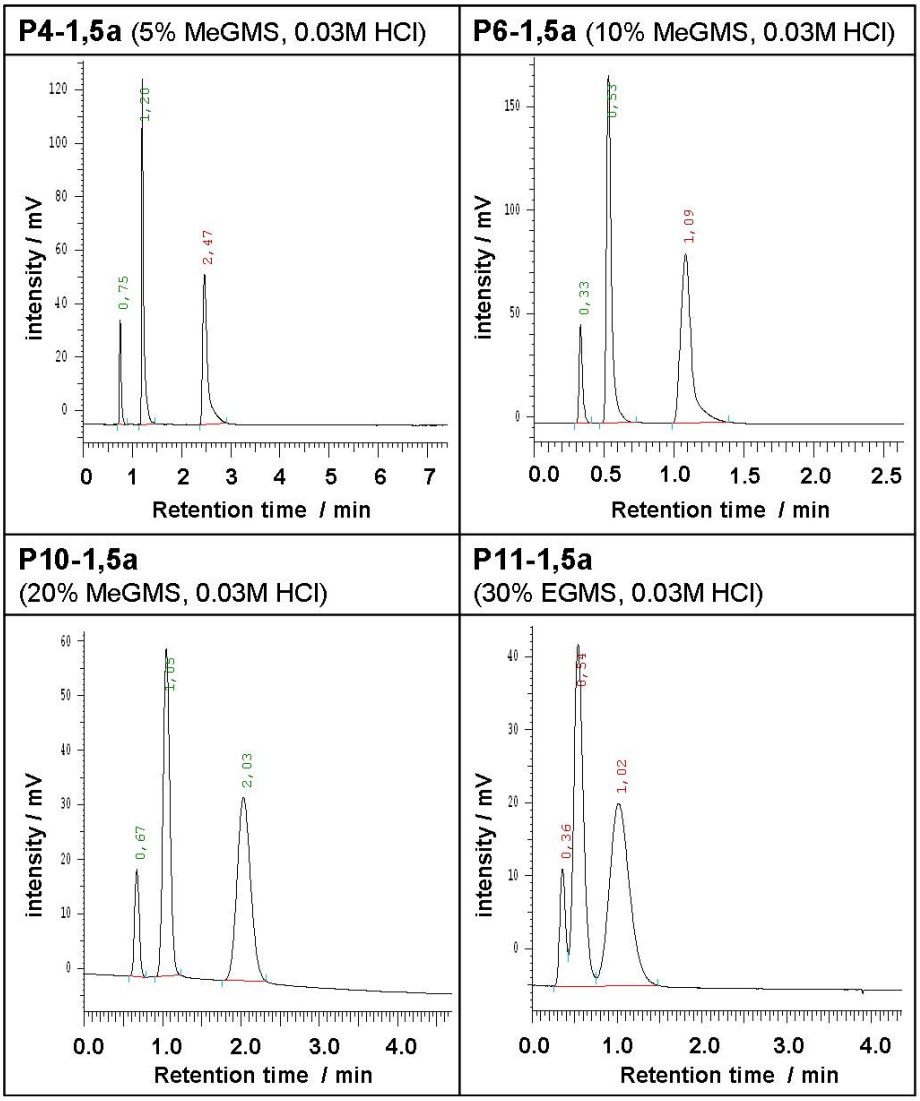

Figure 87 Chromatograms of the separation of toluene, nitrobenzene, and 2-nitroanisole of the different hybrid methyl-modified silica columns derived from EGMS / MeGMS sol-gel systems of varied contents of MeGMS in the range of 5 – 30 mol % at 0.03 M HCl (eluent: *n*-heptane / dioxane (95 / 5% v/v)).

As the column prepared with 5 mol % MeGMS exhibits one of the best performances, van Deemter diagrams were created for nitrobenzene and 2-nitroanisole in order to investigate the separation efficiency of the column with increasing linear flow velocity of the mobile phase in the range of u = 0.30 – 4.63 mm s^{-1}. (Figure 88) For nitrobenzene the optimum separation efficiency (N = 6085 determined for L = 10 cm) with the corresponding minimum plate height of H_{min} = 16.43 μm is observed at a linear flow velocity of u = 1.54 mm s^{-1}. For 2-nitroanisole, the maximum separation efficiency (N = 3312 per L = 10 cm, H = 30.19 μm) is even shifted to a larger linear flow velocity of u = 2.45 mm s^{-1}. The corresponding

backpressures at these velocities are moderate with 56 and 88 bar. Interestingly, the values of the plate height of 2-nitroanisole stays rather constant with values of about 31 μm in the linear flow range of u = 1.54 – 4.39 mm s^{-1}. This phenomenon does not occur for particulate columns, which exhibit steeper slopes and a rapidly increasing backpressure with increasing linear flow velocity.

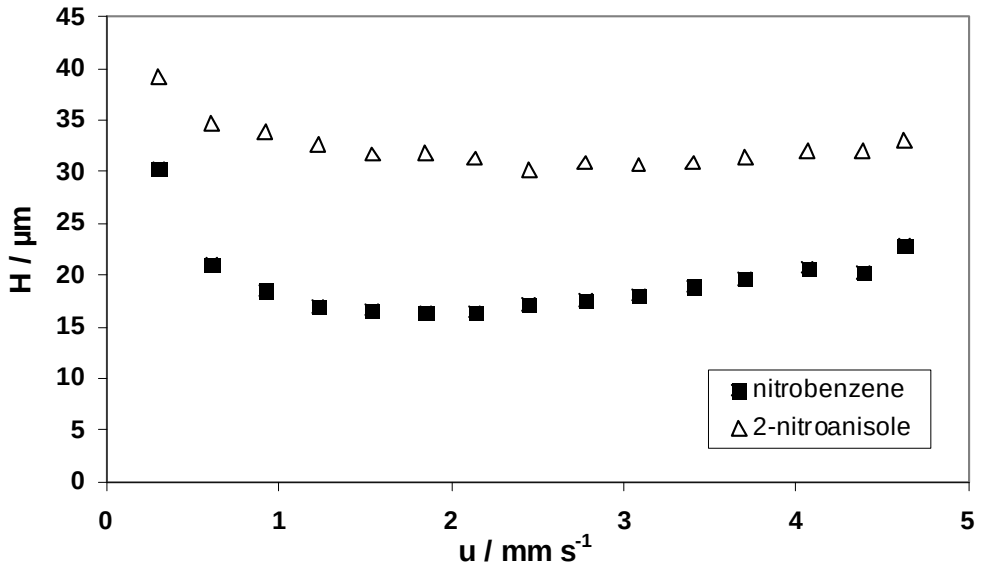

Figure 88 Van Deemter curves for the hybrid silica column prepared with 5 mol % MeGMS at 0.03 M HCl of nitrobenzene and 2-nitroanisole at room temperature.

Subsequent to the NP Si standard tests, the hybrid silica monoliths were also tested as stationary phases for the separation of thiourea, biphenyl-2-ol, progesterone, 1-phenyl-1-hexanone, and anthracene in the RP mode. (Experimental conditions are given in table 27.)
Despite the fact of a theoretically higher loading of methyl groups on the surface compared to the EGMS-derived silica monolith (P1-1e), the methyl-modified hybrid silica gels exhibit an insufficient performance for the RP mode. The chromatograms of the RP mode experiments of the hybrid silica monoliths are presented in figure 89.

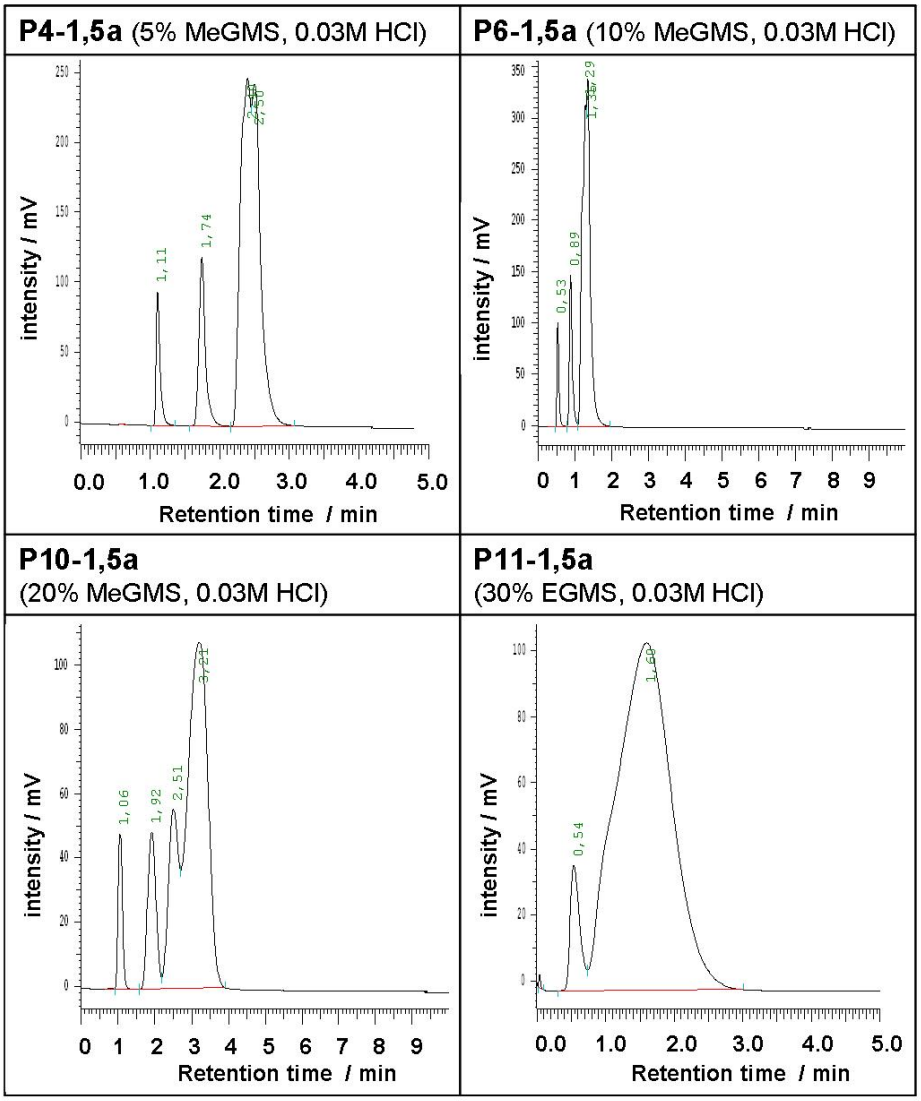

Figure 89 Chromatograms of the separation experiments of thiourea, biphenyl-2-ol, progesterone, 1-phenyl-1-hexanone, and anthracene for the different methyl-modified hybrid silica columns prepared with varied MeGMS contents in the range of 5 – 30 mol % at 0.03 M HCl.

Subsequent to the RP mode testing, the hybrid silica monoliths were re-tested in the NP mode (Standard Si experiment, see table 27). Even though, the determined number of theoretical plates N/m of each monolith is reduced compared to the first experiments (with exception of P8-1,5a), the resultant chromatograms show well-defined separations of toluene, nitrobenzene and 2-nitroanisole for the monoliths prepared with 5 – 20 mol % MeGMS. (Figure 90)

The corresponding chromatographic data are listed in table 33. For comparison, the initially determined number of theoretical plates N_0/m for each monolith is also listed in table 33.

Table 33 Chromatographic data obtained from the re-testing (NP-Si standard tests) of the hybrid silica monoliths at RT (prepared with 0.03 M HCl).

samples	Si standard test							
	%MeGMS /mol %	L /cm	N/m	N_0/m*	k'	α	R	p /bar
P4-1,5a	5	10	30510	41800	2.58	3.98	11.22	90
P5-1,5a	7.5	10	30020	34140	2.47	3.94	9.69	91
P6-1,5a	10	5	16320	22120	2.54	3.92	5.37	48
P7-1,5a	12.5	10	13630	15010	2.70	3.98	7.13	51
P8-1,5a	15	10	9000	5650	2.44	3.90	5.53	45
P9-1,5a	17.5	10	4180	4120	2.46	3.84	3.61	61
P10-1,5a	20	10	5080	6490	2.22	3.72	3.80	37
P11-1,5a	30	5	1020	1760	1.80	3.88	1.13	20

* N_0/m: number of theoretical plates determined in the first measurements.

The retention factors k′ of the monoliths prepared with 5 – 20 mol % MeGMS are in the optimum range with values between 2.2 and 2.7 and also the observed selectivities with values of $\alpha = 3.7 – 4.0$ affirm the good performance of these columns. In contrast, P11-1,5a (30 mol % MeGMS) exhibits a drop of performance for the re-testing with overlapping signals in the chromatogram.

The retention times resemble the times obtained at the first Normal Phase tests and thus, the separation of the analyte mixture is completed within three minutes for the hybrid monoliths synthesized with 5 – 20 mol % MeGMS.

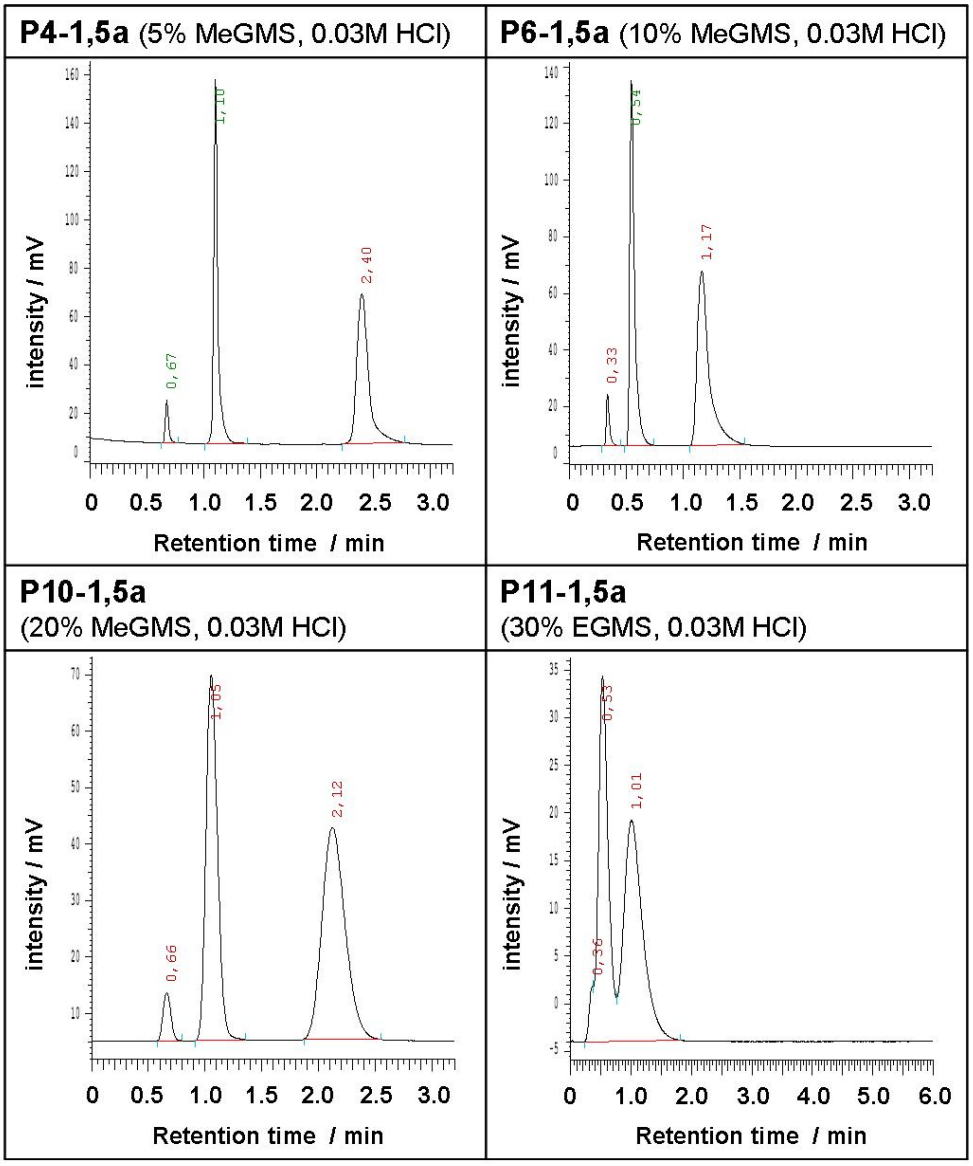

Figure 90 Chromatograms of the re-testing of the separation of toluene, nitrobenzene, and 2-nitroanisole of the different hybrid methyl-modified silica columns derived from EGMS / MeGMS sol-gel systems of varied contents of MeGMS in the range of 5 – 30 mol % at 0.03 M HCl (eluent: *n*-heptane / dioxane (95 / 5% v/v)).

6.3. Conclusion

Hierarchically organized silica and methyl-modified hybrid silica monoliths synthesized from EGMS and by co-condensation of MeGMS and EGMS have been investigated as stationary phases for Normal Phase (NP) and Reversed Phase (RP) HPLC experiments.

The hybrid silica monoliths prepared at c(HCl) = 0.03 M with 5 – 20 mol % MeGMS proved to be promising candidates as stationary phases in the NP mode. The best performance with

respect to separation quality was observed for P4-1,5a (5 mol % MeGMS) and P6-1,5a (10 mol % MeGMS).
Additional van Deemter experiments of nitrobenzene and 2-nitroanisole revealed that by application of P4-1,5a as stationary phase, it is possible to increase the flow rate without a considerable reduction of the separation efficiency in order to obtain shorter analysis times.

HPLC experiments of the EGMS-derived silica monoliths have shown, that P1-1e (c(HCl) = 1 M) exhibits a good performance as HPLC column in the RP mode and concomitantly a sufficient separation quality in the NP mode (for the separation of toluene, nitrobenzene and 2-nitroanisole with n-heptane / dioxane = 95 / 5% v/v).
Additional RP investigations of the selectivity α indicate the applicability of P1-1e as adequate column for the separation of more complex analyte systems such as a mixture of complexing agents consisting of uracil, purpurine and quinizarin.

These results exhibit that the EGMS- and MeGMS / EGMS-derived hierarchically organized (hybrid) silica monoliths are promising candidates for the application as stationary phases in HPLC. However, additional HPLC experiments of calcined EGMS-derived silica monoliths are required for a closer investigation of the applicability as stationary phases in the NP-mode.
With regard to the long-term ambition, the direct synthesis within the HPLC tubes, the synthesis parameters and the container material have to be optimized in order to inhibit formation of heterogeneous regions within the meso- and the macroporous networks.

Chapter 7

Experimental

7.1. Analytical Methods

7.1.1. Nitrogen Sorption

Today, the measurement of adsorption and desorption of nitrogen at 77 K (-196°C) is the preferred method to determine the specific surface area, the pore volume and shape, and the pore size distribution of porous and especially mesoporous materials with pore sizes in the range of 2 – 50 nm.[173] The base for this analysis method is the assumption that the adsorption of nitrogen is by physisorption, where only weak van-der-Waals interactions between the adsorbent (solid phase) and the adsorptive (gas phase) occur.

The adsorption mechanism is mostly determined by the pore size of the porous solid, thus three different processes can be distinguished:

1. monolayer-multilayer adsorption
2. micropore filling
3. capillary condensation.

By plotting the adsorbed gas volume as a function of the relative pressure p/p_0 (p: gas pressure above the adsorbent, p_0: the saturation pressure of the adsorbent) adsorption and desorption isotherms are obtained. Depending on the pattern of the isotherms, different classes can be distinguished according to IUPAC.

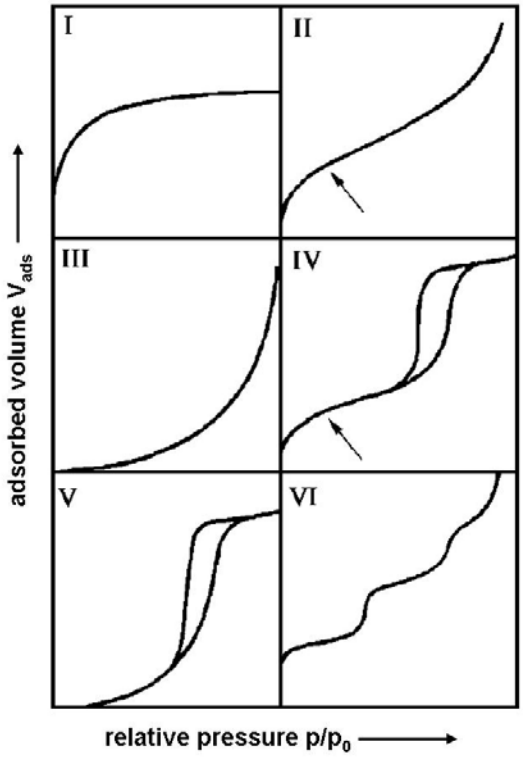

Figure 91 Classification of the different isotherms according to IUPAC.[174]

The type I isotherms are characteristic for microporous materials, as a significant volume of gas is adsorbed at low pressures. The maximum adsorbed volume is determined by the accessible micropore volume and not by the specific surface. Macroporous and non-porous materials often show isotherms of the types II and III, where a smooth transition of a mono- to multimolecular adsorption layer is present. While strong interactions between the adsorbent and adsorptive dominate for the type II isotherm, only small interactions occur between the

adsorptive and the adsorbent of materials showing isotherms of the type III. (The arrow in II indicates the region, in which the curve temporarily transforms into a linear slope.)

The isotherms of the type IV and V are characteristic for mesoporous solids with the maximum adsorbed gas volume at high relative pressures. In contrary to the former described types of isotherms, here hysteresis loops are observed which are caused by capillary condensation within the mesopores and thus desorption is temporarily delayed and only occurs at lower relative pressures compared to the adsorption. (Figure 91: lower branch – adsorption, upper branch – desorption) In analogy to the types II and III, the difference in the slopes for the isotherms for type IV and V are also caused by differentially pronounced interactions between the adsorptive and the adsorbent that are less prominent for isotherms of the type V.

Isotherms of the type VI are seldom. Some activated carbons show this certain type of isotherm. The individual steps are induced by a gradual multi-layer adsorption on the adsorbent with the height of the step being an indication of the capacity of each layer.

The isotherms of the type IV can feature different patterns of the hysteresis loops, depending on the pore shape and the pore size distribution. (Figure 92)

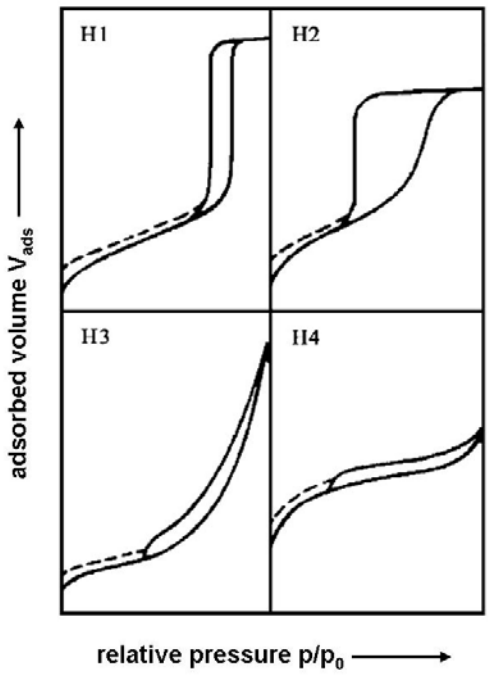

Figure 92 Classification of the different hysteresis loops.[174]

The ideal hysteresis type H1 is found for mesoporous solids with a monomodal and narrow pore size distribution e.g. easily accessible cylindrical pores as found in MCM-41 and SBA-15. In contrary, the hystereses of materials exhibiting mesopores of non-uniform size and also materials exhibiting drop-shaped mesopores, often show hystereses loops of the type H2. Materials formed by plate-like particles or exhibiting slit-shaped pores show hystereses loops of the type H3. The type H4 is also found for solids with slit-shaped pores, however, the course of the isotherms indicate a microporous system.

Determination of the specific surface area according to Brunauer, Emmett and Teller[173, 175]

The adsorption theory according to Brunauer, Emmett and Teller (BET) was originally the multilayer extension of the Langmuir kinetic model. The assumption for the Langmuir concept is a monolayer adsorption on the surface of the solid, wherein all adsorption sites are identical. The extension of this model includes the formation of multilayer adsorption wherein according to the BET model the molecules of each layer can act as potential adsorption sites for the next layer.

By applying the BET theory, measurements of the specific surface area of porous materials are possible, as they allow the prediction of the number of required adsorbate molecules in order to generate a single monolayer on the solid surface. When the size of the molecular cross-section of the adsorbate or the effective area covered with one adsorbate molecule is known, the specific surface area can be calculated as the product of the effective molecular cross-sectional area of one adsorbate molecule and the number of molecules of the monolayer.

Even though, a single monolayer is never present in real systems, it is possible to experimentally determine an approximation of the specific surface area of porous materials in the lower range for the relative pressure p/p_0 ($p/p_0 = 0.05 – 0.3$) by applying the linear form of the BET equation.

$$\frac{p/p_0}{n(1-p/p_0)} = \frac{1}{n_m C} + \frac{C-1}{n_m C}(p/p_0) \qquad \textit{Equation 10}$$

n amount of adsorbed gas molecules

n_m monolayer capacity

C empirical constant

The empirical constant C is a substrate specific constant, which is exponentially related to the net molar energy of adsorption (E_1-E_L), is thus linked to the adsorption energy of the first adsorption layer E1, and can be described by the following simplified equation.

$$C \approx \exp[(E_1 - E_L)/RT] \qquad \textit{Equation 11}$$

R	molar gas constant (R = 8.314 J mol^{-1} K^{-1})
T	absolute temperature
E_1	adsorption energy of the first layer
E_L	energy of condensation

The value of the constant C provides an indication of the adsorbent-adsorptive interactions and therefore for the polarity of the adsorbent. In the case of N_2 as adsorptive at 77 K, C > 100 indicates relatively strong interactions such as between a polar adsorbent surface and the adsorptive. For many amorphous and non-microporous solids, the C value is often in the range of 100.

For the determination of the surface area several steps have to be taken. From the BET plot the value of n_m is derived as it is indirectly proportional to the sum of the y axis intercept ($i = 1/n_m$) and the slope of the straight line ($s = [(C-1)/n_m C]$). (The validity is only given for a limited linear segment of the adsorption isotherm at low relative pressures p/p_0 and is in most cases only appropriate for type II or IV isotherms. For adsorbents such as silica, alumina, non-porous amorphous carbons and porous glasses linearity of the BET plot is only given in the range of $p/p_0 \approx 0.04 – 0.25$.)

In a second step the specific surface area S^{BET} is calculated from the molecular cross-section area σ of the adsorptive gas, the monolayer capacity n_m and the Avogadro constant N_A ($N_A = 6.022 * 10^{23}$ mol^{-1}). Calculations by Brunauer and Emmett yielded $\sigma(N_2) = 0.162$ nm^2 for the cross-section of a single adsorbed nitrogen molecule.

$$S^{BET} = \sigma(N_2) N_A n_m \qquad \textit{Equation 12}$$

Determination of the pore size distribution according to Barrett, Joyner and Halenda (BJH)[173, 176, 177]

For the determination of the mesopore size distribution different mathematical models based on the Kelvin equation can be employed assuming that initially multilayer adsorption occurs on the pore surface, which results in capillary condensation of the adsorptive within the pores until all pores of a given size are completely filled with nitrogen.

$$\ln\left(\frac{p}{p_0}\right) = -\frac{2\gamma\nu^1}{r_K RT} \qquad \textit{Equation 13}$$

r_K radius of the meniscus (Kelvin radius) (for cylindrically shaped pores)

γ surface tension

ν^1 molar volume of the condensate

Barrett, Joyner, and Halenda extended this approach by assuming that all pores are cylindrically shaped. The adsorptive is kept at the surface via two different mechanisms, the physisorption at the pore surface and the capillary condensation in the inner capillary volume. By application of these two assumptions, the Kelvin equation is simplified. As within the micropores with pore diameters smaller than 2 nm no nitrogen can be adsorbed and for macropores with diameters larger than 200 nm a multilayer adsorption of nitrogen can not be assumed, the determination of the pore size distribution according to the BJH-model can only be employed for mesoporous and macroporous materials with diameters below 200 nm. By employing the BJH-model, the total pore volume can be evaluated from the adsorbed volume of nitrogen $V_{N_2 ads}$.

$$V_P = \frac{p_{N_2(l)} \cdot V_{N_2 ads} \cdot \nu_{N_2}}{R \cdot T_{N_2(l)}} \qquad \textit{Equation 14}$$

p_{N_2} pressure of $N_{2(l)}$

T_{N_2} temperature of $N_{2(l)}$

ν_{N_2} molar volume of $N_{2(l)}$

Besides the BJH model, there is a variety of calculation methods, such as the density functional theory (DFT) for the determination of the pore size distribution. In analogy to the BJH computation model, all these methods are based on desorption of the condensed adsorptive from the pores and represent only approximations as they depend on theoretical assumptions.

For this thesis the adsorption-desorption isotherms were obtained from measurements on a NOVA 4000e and a QUADRASORB SI (Quantachrome Instruments, Boynton Beach, USA) devices. Prior to analysis, all samples were out gassed for 3 h at 100°C in vacuo. The specific surface area (S^{BET}) was determined according to the BET model using adsorption data in the relative pressure range $p/p_0 = 0.05 – 0.3$. The mesopore size distribution was calculated according to the BJH model using the data from either adsorption or desorption branch.

7.1.2. Mercury Porosimetry[178, 179]

In the field of the analysis of porous materials, mercury porosimetry has become one of the most applied techniques for the determination of pore sizes in the range of 4 nm to 500 μm with the main focus on macropores (> 50 nm).
Mercury porosimetry is based on the principle that non-wetting liquids such as Hg recede in capillaries (convex shaped meniscus, resulting in a capillary depression), thus the penetration of the capillary / pore has to be forced by applying pressure. Therefore, the larger pores are filled at low pressures ($p \leq 1$ bar, pores ≥ 7.4 μm are penetrated), while the smaller pores are only filled when the pressure is increased.

During the measurement, the penetration of Hg into the pores (intrusion) and the extrusion of Hg out of the pores are plotted against the pressure, resulting in a hysteresis. It has to be mentioned, that the intrusion and the extrusion branches never meet at low pressures as mercury is trapped within the pores.

The applied pressure p for the intrusion and the pore size R^{Hg} are connected by the Washburn equation.

$$p = \frac{-2\gamma\cos\theta}{R^{Hg}}$$ *Equation 15*

γ	surface tension of Hg (480 mN/m at 20°C)
θ	contact angle of Hg (140° at 20°C)
R^{Hg}	pore radius (assumption: cylindrical pore)
p	applied pressure

The corresponding cumulative pore volume can be determined as function of the obtained pore size distribution with regard to the pore geometry.

The mercury porosimetry experiments were performed on a Macropore Unit 120 (Fisons Instruments) for the characterisation of macropores ≥ 7.4 μm in the pressure range from vacuum to ambient pressure (~1 bar). The investigation of the pores with radii ≤ 6 μm was performed on a Porosimeter 2000 (Fisons Instruments) in the pressure range from 1 – 2000 bar. All samples were evacuated for 15 min at room temperature prior to analysis. The pore size distribution as well as the cumulative pore volume distribution was calculated for a cylindrical system.

7.1.3. Small Angle X-ray Scattering (SAXS)[180, 181]

For mesoporous silica gels with pore diameters in the range of 2 – 50 nm small angle X-ray scattering (SAXS) experiments represent a convenient method for the investigation of the mesoscopic structuring of these gels. As the material is formed by particles and their agglomerates, which are not in the same magnitude as the wavelength of the incident X-ray beam, the rays are elastically scattered at the surrounding electron clouds. Based on the fact, that every electric dipole is a starting point of a scattered wave, interference of the scattered X-rays occurs resulting in a scattering pattern with minima and maxima. (In order to obtain a maxima, the path difference between the waves has to be an integral multiples of the wavelength λ.)

The size of scattering particle is reciprocal related to the scattering angle, hence, with increasing size of the scattering object the scattering angle is reduced. As the electron density

within the mesopores of a periodically arranged silica network is drastically decreased, the pore distances and therefore the spacing of the repeating units (*d*) can be derived from the scattering pattern, if the conditions of the Bragg's law are fulfilled.

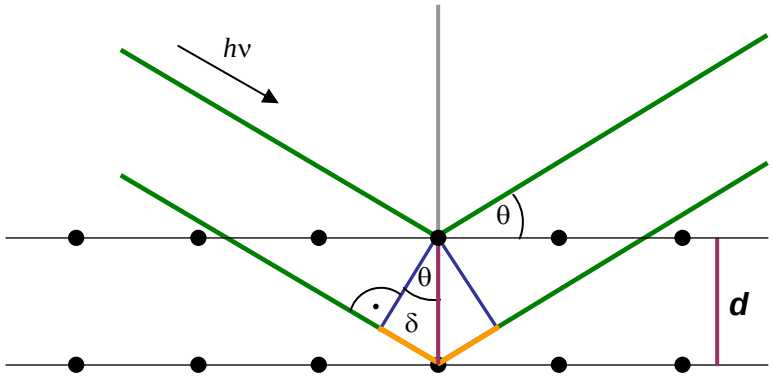

Figure 93 Schematic drawing of Bragg's Law for the scattering of X-rays at a periodic lattice of pores, points, etc. with the repeating unit distance *d*[182]

$$2d_{hkl}\sin\theta = n\lambda$$ *Equation 16*

d_{hkl}	repeating unit distance defined by the respective Miller indices *hkl* for the structure
θ	scattering angle
n	integer
λ	wavelength of the incident beam ($\lambda(\mathrm{Cu}_{\mathrm{K}\alpha}) = 0.154\mathrm{nm}$)

In SAXS experiments, the distribution of the intensity is measured as a function of the scattering vector $\vec{q}$, which represents the difference of the wave vectors of the incoming wave $\vec{k}$ and the scattered wave $\vec{k}'$.

$$\vec{q} = \vec{k} - \vec{k}'$$ *Equation 17*

Therefore, the magnitude of the scattering vector is determined as follows:

$$\left|\vec{q}\right| = q = \left(\frac{4\pi}{\lambda}\right)\sin\left(\frac{2\theta}{2}\right) \qquad \textit{Equation 18}$$

The repeating unit distances d_{hkl} can be determined in a first approximation from the maximum q values from the scattering diagram according to

$$d_{hkl} = \frac{2\pi}{q_{max}} \qquad \textit{Equation 19}$$

In combination with the corresponding lattice constant a, the exact repeating unit distances d_{hkl} can be calculated for the dedicated structure. (Some selected structure samples including the corresponding equations and their sequences of Bragg reflections are listed in table 34)

Table 34 Selected samples of possible structures including the corresponding equations for the determination of the position of the Bragg reflections and their sequence of Bragg reflections.[88]

structure	*position of Bragg reflections*	*sequence of Bragg reflections*
2D-hexagonal (P_{6m})	$q_{hk} = \frac{2\sqrt{h^2 + hk + k^2}}{a\sqrt{3}}$	(10), (11),(20), (21),(30),(22), …
lamellar	$q_h = \frac{2\pi h}{a}$	(100), (200), (300), …
cubic (F_{m3m})	$q_{hkl} = \frac{2\pi\sqrt{h^2 + k^2 + l^2}}{a}$	(111), (200), (220), (311), (222), (400), ...

In combination with the pore diameter distribution resulting from the BJH determination, the thickness of the pore wall t_{wall} can be calculated for a hexagonally structured mesoporous material according to the following equation.

$$t_{wall} = \frac{2d_{10}}{\sqrt{3}} - D^{BJH} \qquad \textit{Equation 20}$$

For this thesis, all SAXS patterns were obtained by measurements on a Nano-STAR instrument (Bruker AXS, Karlsruhe) equipped with a HI-STAR area detector. The X-ray emitting device was operated at 40 kV and 35 mA. The incident X-ray beam

($\lambda(Cu_{K\alpha}) = 0.154$ nm) was mono-chromated by a Ni-plate and the distance between sample and detector was about 105 cm on which scattering curves in the q-range of 0.2 to 2.1 nm^{-1} were obtained.

7.1.4. Electron Microscopy

7.1.4.1. Scanning Electron Microscopy (SEM)

Scanning Electron Microscopy (SEM) is a convenient technique to investigate the morphology of a macroporous network.
Electrons are accelerated to 2 – 60 keV and are then focussed via electronic lenses. This electron beam scans the sample surface generating secondary electrons and X-ray photons up to 5 nm in depth. For the creation of the image, the secondary electrons and the X-ray photons are collected and intensified in a detector.
The majority of the images for this thesis were taken on a Zeiss DSM 962 microscope (Carl Zeiss AG, Jena). Prior to the investigation, all silica and hybrid silica samples were sputtered with an Au-Pd layer of 20 nm thickness in order to avoid electrostatic charging of the samples' surface during the measurement. The applied acceleration voltage was in the range of 5 to 10 keV.

7.1.4.2. Transmission Electron Microscopy (TEM)

In contrary to SEM, the transmission electron microscopy (TEM) provides information of the mesoporous structure. Even though, both techniques employ a similar set-up, the type of imaging is different. Here the electron beam transits the sample and the resulting image is magnified and projected on a luminescent screen. The resultant image is the negative of the original structure, as only transmitted electrons reach the luminescent screen.

The investigation of selected samples were performed on a Philips EM 400 transmission electron microscope with a tungsten filament operating at 80 keV.

7.1.5. Nuclear Magnetic Resonance Spectroscopy (NMR)

The purity of the employed diol-modified silanes was investigated by liquid ^{1}H- and spin-lock ^{29}Si-NMR spectroscopy experiments.

The ^{1}H-NMR spectroscopy investigations provided information about residual ethanol in the precursor, which promotes the back reaction and thus shifts the equilibrium towards the educt site.

The spin-lock ^{29}Si-NMR spectroscopy experiments gave information about the type of present diol-modified silanes, either isolated, in a condensed form or if educt silane species were still existent. As ^{29}Si-nuclei are seldom and possess long relaxation times, the Si-NMR spectra were performed by applying the spin-lock technique. The spin-lock method is based on the principle that dipolar coupling nuclei can conduct a transfer of magnetization from a frequent sensitive nucleus, such as a ^{1}H-nucleus, to an insensitive nucleus, such as a ^{29}Si-nucleus. The spin of the proton is deflected of 90° by a pulse of fitting length and a so-called spin-lock field is applied on both nuclei, which results in the transfer of the polarisation from the ^{1}H-nucleus to the ^{29}Si-nucleus. In order to provide a reservoir of protons for the polarisation transfer, a solvent is required for the NMR experiments with a higher number of protons such as deuterated benzene-d_6 or dimethylsulfoxide-d_6.

The spin-lock ^{29}Si-NMR and ^{1}H-NMR spectra of the diol-modified silanes were all performed on a Bruker AMX 400 spectrometer (Bruker BioSpin, USA). The ^{1}H- and the spin-lock ^{29}Si-NMR spectra were recorded with 400.1 MHz and 79.5 MHz, respectively.

7.1.6. Thermogravimetric Analysis (TGA)

The Si-content of the resulting diol-modified silanes was determined by thermogravimetric analysis (TGA). Each sample was heated from room temperature to 1000°C with a constant heating ramp of 10°C min^{-1} in air, wherein the gradual mass loss was registered by a balance. For the determination of the content of organic compounds in the hybrid inorganic-organic silica gels, TG-IR (thermogravimetric device coupled with an infrared spectrometer) measurements were conducted under inert gas (N_2), in order to correlate the resulting

vibrational bands in the IR spectra of the released organic fragments in the gas phase with the eliminated organic moities.
All TG analyses were performed on a STA 449C Jupiter® (Netzsch Gerätebau GmbH, Selb). The TG-IR measurements were conducted on a Bruker TENSOR 27 TGA-IR device (Bruker Optics, USA).

7.2. Sample Preparation

7.2.1. Materials

Diols. Ethylene glycol (BDH Prolabo ≥ 98%), 1,2-propane diol (Merck > 99%), 2,3-butane diol (Merck ≥ 98%), and 1,2-hexane diol (Aldrich 98%) were all predried over Na_2SO_4 (Merck) and subsequently distilled from Mg.

Silanes. Tetraethylorthosilicate (TEOS, Merck 98%), trimethoxymethylsilane (MTMOS, Merck ≥ 98%), and triethoxyphenylsilane (PhTEOS, Merck ≥ 98%) were all employed as purchased. For comparison, sodium silicate (Merck, 7.5 – 8.5% Na_2O, 25.5 – 28.5% SiO_2) and silicic acid (obtained by protolysis of the diluted sodium silicate solution over the acidic Amberlite IR 120 cation exchange resins resulting in silicic acid with 8.3 wt % SiO_2) were also employed as precursors for sol-gel processing.
The silylation agents chlorotrimethylsilane (TMCS, Merck ≥ 99%) and chlorododecyl-dimethylsilane (DDMCS, Aldrich 97%) were used as received.

Surfactants. The surfactant poly(ethylene oxide)-poly(propylene oxide)-poly(ethylene oxide) co-polymer Pluronic™ P123 (EO_{20}-PO_{70}-EO_{20}) (Aldrich, M_{av} = 5800) as well as the siloxane surfactants Tego Glide 440 and LA-S 687 (Evonik Tego Chemie GmbH), both ABA block co-polymers (PEO-PDMS-PEO), were applied as purchased.

Solvents and Acids. Ethanol, petroleum ether (PE) and hydrochloric acid (HCl) were obtained from BDH Prolabo and were applied without further purification. Sulphuric acid (H_2SO_4), nitric acid (HNO_3), perchloric acid ($HClO_4$), and trifluoroacetic acid (CF_3COOH) were purchased from Merck and used as received.

7.2.2. Synthesis of the Precursors

The diol-modified silanes were synthesized via transesterification reactions based on the work of Mehrotra et al.[67] Prior to the substitution reaction, all diols were pre-dried over Na_2SO_4 and for further purification were then distilled over magnesium. For the synthesis of the diol-modified silane, such as the ethylene glycol-modified methylsilane (MeGMS), the silane was reacted at 140°C under Ar-atmosphere with the corresponding stoichiometric equivalent of the silane, i.e. for MeGMS ethylene glycol was reacted with the trimethoxymethylsilane in the molar ratio of 3:1. (The molar ratios of diol to silane for the synthesized precursors are listed in table 35 including the respective Si-content of the obtained products.) The monovalent alcohol, which was released during the transalkoxylation reaction, was continuously removed from the equilibrium by distillation over a Vigreux column. When no more progress of the distillation could be observed, the residual alcohol was removed *in vacuo* (at RT). The Si-content of the resultant diol-modified silanes was determined by thermogravimetric analyses (given in table 35).

Table 35 Listing of the different synthesized diol-modified silanes.

denotation	*silane*	*diol*	*molar ratio*	*content of Si / wt % (theoretical yield)*
EGMS	tetraethyl-orthosilicate	ethylene glycol	1/4	9.6 (10.4)
PGMS	tetraethyl-orthosilicate	1,2-propane diol	1/4	7.4 (8.6)
BDMS	tetraethyl-orthosilicate	2,3-butane diol	1/4	3.2 (7.3)
HDMS	tetraethyl-orthosilicate	1,2-hexane diol	1/4	4.1 (5.7)
MeGMS	trimethoxy-methylsilane	ethylene glycol	1/3	9.9 (12.5)
PhGMS	triethoxy-phenylsilane	ethylene glycol	1/3	9.3 (9.8)

The obtained Si-contents agree with the theoretical calculated yields. For all synthesized diol-modified silanes, ^{1}H- and spin-lock ^{29}Si-NMR spectra were recorded in benzene-d_6. The chemical shifts for the protons and the chemical shifts for the Si species are listed in table 36

Table 36 Listing of the data from ^{1}H- and spin-lock ^{29}Si-NMR of the diol-modified silanes, R represents the respective diol substituents.

Precursor	*schematic depiction of the structure*	*^{1}H-NMR /ppm*	*spin-lock ^{29}Si-NMR /ppm*
EGMS	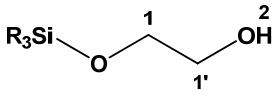	1.32 - 1.39 (CH_3CH_2OH) 3.77 - 3.82, 4.04 – 4.08 (**1, 1'**) 5.14 (**2**)	-81.6
PGMS	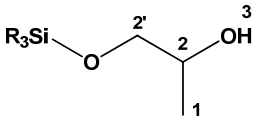	1.37 (CH_3CH_2OH) 1.90 – 1.95 (**1**) 3.82 – 4.32 (**2, 2'**) 5.15 (**3**)	-81.5
BDMS	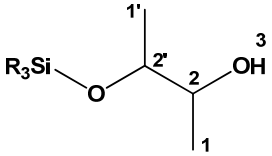	1.21 (broad signal, **1, 1'**) 3.59 – 3.72, 4.14 (**2, 2'**) 4.81 – 4.82 (**3**)	-85.7
HDMS	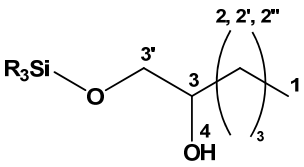	0.86 – 0.90 (**1**) 1.29 – 1.40 (**2, 2', 2''**) 3.57 – 3.70 (**3, 3'**) 4.03 – 4.04 (**4**)	-83.4
MeGMS	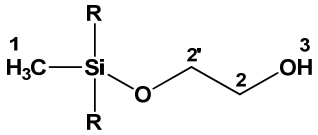	0.041 (**1**) 3.48 – 3.68 (**2, 2'**) 4.36 (**3**)	-41.2, -49.3
PhGMS	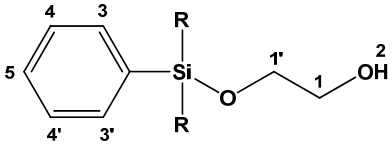	3.61 – 3.68, 3.90 – 3.96 (**1, 1'**) 4.15 – 4.20 (**2**) 7.35 – 7.37, 7.65 (**3, 3', 4, 4', 5**)	-56.1 - -58.0, -64.2

7.2.3. Preparation of the Monoliths

7.2.3.1. Preparation of Pure Silica Monoliths with Pluronic P123

The silica gels were synthesized by addition of the silicon source precursor to a homogeneous phase of Pluronic P123 in acidic or purely aqueous media. The P123 phase was employed as structure-directing and phase separation inducing agent in order to obtain hierarchically organized monoliths exhibiting a periodically organized mesopore system and a well-defined co-continuous macroporous framework.

For all variations of the synthesis parameters, which will be discussed in the following section, the underlying synthesis procedure was kept constant. Prior to the gel synthesis, the particular quantity of P123 was dissolved in the corresponding volume of acid or water at low temperatures and subsequently stored in the refrigerator at 0°C for a complete homogenization. For the synthesis, these template phases (with exception of P123 / x M HCl = 40 / 60 wt % employed at 0°C) were warmed-up to 40°C and homogenized, before the adequate amount of the precursor was added to the calculated quantity of the template phase. (The batch sizes are given for each experiment series in the corresponding section.)

The mixture was homogenized at RT with a Vortex stirrer for 1 – 5 min and the resulting sol was then transferred into vessels. In contrary to the small, wide PE vessels, all long vessels such as the PMMA, PC, PVDF moulds, had to be filled by injection via syringes. The filled long vessels were then centrifuged at low rotation speeds for 5 min to eliminate air cavities within the sol before the vessels were sealed. All systems were gelled and aged at a particular temperature for a certain period of time.

After aging, the monoliths were removed from the vessels. The tall monoliths with a small diameter and for comparison some small monoliths were refluxed in ethanol / HCl_{conc} (50 / 50% v/v) for 6 h at 65 °C to strengthen the silica network (by further condensation reaction of unreacted silanol species) and to degrade the template phase within the pores. Residual template phase and HCl was removed from the pore systems by washing the monoliths with ethanol (12 h) and petroleum ether (8 h).

All silica monoliths (both cured and not cured) were subjected to surface hydrophobization reactions with chlorotrimethylsilane (TMCS) in petroleum ether (10 / 90% v/v, 24 h). (Figure 94) By silylating the accessible silanol groups on the surface, the interactions between the Si-OH groups are reduced and hence the monolithic shape is preserved from cracking during the drying procedure.

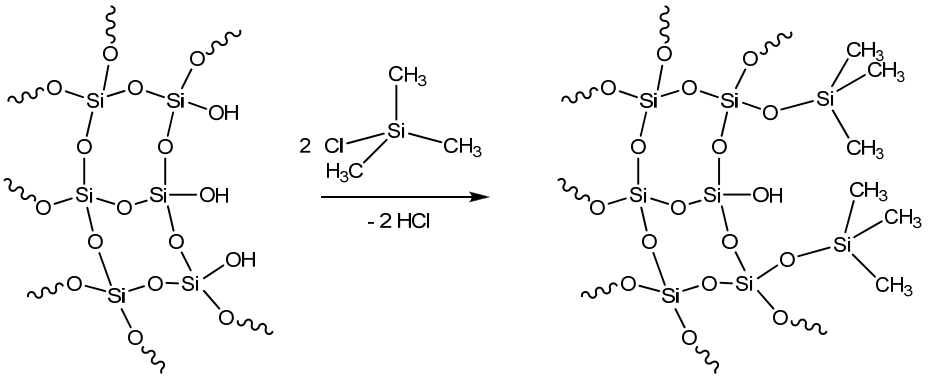

Figure 94 Schematic depiction of the surface hydrophobization via silylation with chlorotrimethylsilane (TMCS).

In addition to the hydrophobization of the silica surface, the treatment with TMCS also extracts residual template phase from the pores. For the removal of unreacted silane species and produced HCl, the silica monoliths were subjected to a washing procedure with PE (24 h) and ethanol (24 h).

In a final step, the silica gels were dried via a slow heating program at temperatures from 30°C up to 200°C within 5 d in a drying cabinet with ventilation.

Variation of the HCl concentration

For the investigation of the influence of the acid concentration on the formation of the hierarchical pore regimes, the HCl concentration was varied in the range from 1 – 10^{-6} M. The composition of the sol-gel system was kept constant with Si / P123 / x M HCl = 8.4 / 30 / 70. The template phases of each acid concentration was prepared prior to the gel synthesis by adding 6 g P123 to 20 g of the corresponding acid. The weight portions of the employed EGMS and each template phase are listed in table 37 including the Si-content of the employed EGMS. The size of the sol batches was reduced from 20 g to 2.0 g template phase at c(HCl) ≤ 10^{-5} M, due to the rapid hydrolysis and condensation reactions of EGMS in this pH-range.

Table 37 Applied weight portions of the template phase P123 / 1 – 10^{-6} M HCl = 30 / 70 and the precursor EGMS. The Si-content of EGMS and the respective HCl concentration are also given per series.

series	c_{HCl} */mol l^{-1}*	*Si-content of EGMS /wt %*	*m(EGMS) /g*	*m(template phase) /g*
P1-1	1	9.7	17.4	20.0
P1-2	10^{-1}	9.7	17.4	20.0
P1-3	10^{-2}	9.7	17.4	20.0
P1-4	10^{-3}	9.7	17.4	20.0
P1-5	10^{-4}	9.7	17.4	20.0
P1-6	10^{-5}	9.7	1.7	2.0
P1-7	10^{-6}	9.7	1.7	2.0

For the determination of the average shrinkage of the gels six long poly(methyl methacrylate) (PMMA) vessels (diameter x length: 4.5 x 170 mm) and three small polyethylene (PE) moulds (diameter x length: 12.1 x 50 mm) were filled with the sol per each series. All gels were gelled and aged at 40°C for 7 d.

The particulate gelling times t_g as well as the times for the onset of phase separation are listed in table 38. The corresponding diagram is presented in figure 14 in section 2.1.3.

Table 38 Time intervals for the sol-gel transition (t_g) and the phase separation (t_{PS}) for the different HCl concentrations at 40°C.

samples	c_{HCl} */mol l^{-1}*	*T /°C*	*Si /wt %*	*P123 /wt %*	*HCl /wt %*	t_g */min*	t_{PS} */min*
P1-1	1	40°C	8.4	30	70	66	184
P1-2	10^{-1}	40°C	8.4	30	70	178	-
P1-3	10^{-2}	40°C	8.4	30	70	235	1179
P1-4	10^{-3}	40°C	8.4	30	70	17	22
P1-5	10^{-4}	40°C	8.4	30	70	3	17
P1-6	10^{-5}	40°C	8.4	30	70	2	3
P1-7	0	40°C	8.4	30	70	2	3

The shrinkage of length and the diameter of the silica monoliths synthesized in PMMA vessels are shown in figure 15 in section 2.1.3.1.; the corresponding data are for the PMMA and PE vessels are given here in table 39.

Table 39 Shrinkage in diameter and the length of the silica monoliths.

samples	c_{HCl} /mol l^{-1}	$\Delta L(PMMA)$ /%	$\Delta D(PMMA)$ /%	$\Delta L(PE)$ /%	$\Delta D(PE)$ /%
P1-1	1	6	11	9	8
P1-2	10^{-1}	6	14	10	9
P1-3	10^{-2}	5	8	9	7
P1-4	10^{-3}	-	-	5	2
P1-5	10^{-4}	3	1	4	2
P1-6	10^{-5}	-	-	0	1
P1-7	10^{-6}	5	-1	0	2

Variation of the Composition of the Template Phase and the Si-Content

The dependency of the resulting meso- and macroporous networks on the composition of the template phase as well as on the Si-content was investigated.

In a first series of experiments, the ratio of P123 / x M HCl was varied from 10 / 90 wt % up to 40 / 60 wt % (template phases of higher contents of P123 could not be homogenized) and the HCl concentration, respectively, was varied in the range from 1 to 10^{-4} M, whereas the Si-content was kept constant with 8.4 wt %.

The gel series of Si / P123 / 1 – 10^{-2} M HCl = 8.4 / 10 / 90 – 8.4 / 40 / 60 were prepared by employing 17.6 g EGMS (EGMS: 9.6 wt % Si) and 20 g template phase of each composition. The gels of Si / P123 / 10^{-3} – 10^{-4} M HCl = 8.4 / 10 / 90 – 8.4 / 40 / 60 were synthesized by employing 15.9 g EGMS (EGMS: 10.6 wt % Si) calculated with respect to 20 g template phase. For the determination of the average shrinkage of the gels six long PMMA vessels (diameter x length: 4.5 x 170 mm) were filled with the sol per batch. All gels of these series were gelled and aged at 40°C for 7 d.

The template compositions of the series at each acid concentration are given in table 40 as well as the resultant average shrinkage of the diameter and the length of the particular monoliths.

Table 40 Composition, c(HCl), aging temperature, and the obtained average shrinkage in diameter and length of the silica gels prepared from EGMS at varied compositions.

samples	c_{HCl} /mol l^{-1}	*T* /°C	*Si* /wt %	*P123* /wt %	*HCl* /wt %	Δ*L* /%	Δ*D* /%
P10-90-0	1	40°C	8.4	10	90	10	19
P20-80-0	1	40°C	8.4	20	80	10	11
P30-70-0	1	40°C	8.4	30	70	11	14
P40-60-0	1	40°C	8.4	40	60	10	14
P10-90-1	10^{-1}	40°C	8.4	10	90	8	5
P20-80-1	10^{-1}	40°C	8.4	20	80	8	7
P30-70-1	10^{-1}	40°C	8.4	30	70	13	9
P40-60-1	10^{-1}	40°C	8.4	40	60	15	13
P10-90-2	10^{-2}	40°C	8.4	10	90	8	6
P20-80-2	10^{-2}	40°C	8.4	20	80	9	9
P30-70-2	10^{-2}	40°C	8.4	30	70	10	11
P40-60-2	10^{-2}	40°C	8.4	40	60	13	13
P10-90-3	10^{-3}	40°C	8.4	10	90	7	4
P20-80-3	10^{-3}	40°C	8.4	20	80	6	4
P30-70-3	10^{-3}	40°C	8.4	30	70	2	3
P40-60-3	10^{-3}	40°C	8.4	40	60	7	4
P10-90-4	10^{-4}	40°C	8.4	10	90	6	5
P20-80-4	10^{-4}	40°C	8.4	20	80	5	5

The physicochemical characteristics of the silica gels prepared with 1 and 10^{-1} M HCl are listed in table 5 in the section 2.1.4. The data for the silica gels synthesized with 10^{-2} – 10^{-4} M HCl are given here in table 41. Due to the fast gelation of the compositions Si / P123 / 10^{-3} and 10^{-4} M HCl = 8.4 / 30 / 70 and 8.4 / 40 / 60, no silica monoliths could be synthesized from one large batch. Therefore, these series are not further discussed.

For the investigation of the impact of the Si-content on the hierarchical architecture, silica gels with Si-contents of 2.1, 4.2, 6.3, and 8.4 wt % were prepared. For this series the ratio of P123 / 1 M HCl was kept constant with 30 / 70 by weight and all gels were gelled and aged at 40°C for 7 d. The Si-content, the composition, and the measured times for the gelation and the phase separation are given in table 42 for the silica gels prepared with various Si-contents.

Table 41 Physicochemical data of the silica gels of the template variation in the HCl concentration range from 10^{-2} to 10^{-4} M.

samples		SAXS	N_2-sorption			Hg-Porosimetry	
	c_{HCl} /mol l^{-1}	d_{10} /nm	S^{BET} /m^2 g^{-1}	D_{BJH} /nm	t_{wall} /nm	R^{Hg} /µm	V^{Hg} /cm^3 g^{-1}
P10-90-2	10^{-2}	12.1	1247	3.5	10.5	0.1	3.2
P20-80-2	10^{-2}	11.5	746	4.0	9.3	0.3	2.8
P30-70-2	10^{-2}	11.5	739	5.7	7.6	0.3	2.7
P40-60-2	10^{-2}	12.1	977	4.5	9.5	0.1	1.9
P10-90-3	10^{-3}	12.3	966	4.2	10.0	0.1	3.6
P20-80-3	10^{-3}	12.4	1063	3.7	10.6	0.3	3.3
P30-70-3	10^{-3}	12.1	850	7.5	6.5	0.1	2.9
P40-60-3	10^{-3}	12.3	1031	5.2	9.0	0.1	2.2
P10-90-4	10^{-4}	13.2	1114	2.6	12.6	0.2	3.2
P20-80-4	10^{-4}	12.3	1010	4.1	10.1	0.2	3.1

Table 42 Composition, aging temperature T, gelation times, and the times for the phase separation of the silica gels synthesized with varying contents of Si.

samples	c_{HCl} /mol l^{-1}	T /°C	Si /wt %	P123 /wt %	HCl /wt %	t_g /min	t_{PS} /min
P1-01q	1	40°C	8.4	30	70	79	224
P30-01	1	40°C	6.3	30	70	56	221
P31-01	1	40°C	4.2	30	70	110	1715
P32-01	1	40°C	2.1	30	70	303	-

Variation of the Acid Anion

In order to investigate the influence of the acid anion on the resulting pore size regimes HNO_3, H_2SO_4, $HClO_4$, and CF_3COOH were employed besides HCl as reference. The pH-values of all acids were adjusted to 1 and the composition of Si / P123 / acid = 8.4 / 30 / 70 (by weight) was kept constant for all gels. For the preparation of the silica monoliths, 8.4 g EGMS (Si-content 10.0 wt %) were homogenized with 10 g template phase per each series and the sols were transferred to small PE vessels.

In analogy to the former gel batches, the sols were gelled and aged at 40°C for 7 d.

The pKa-values of the employed acids, the time intervals for gelation and phase separation are listed in table 7 in section 2.1.5.

Variation of the Gelation and Aging Times

For the investigation of the impact of the temperature on gelation and the formation of the hierarchical porous architecture, silica gels were gelled and aged at 40 – 90°C. For the investigation of the possibility of reducing the aging time, samples were withdrawn at each temperature after 1, 2, 3, 4, 5, 6, and 7 d. The composition of Si / P123 / 1 M HCl = 8.4 / 30 / 70 was kept constant for all silica gels. For a direct comparison, the gels were withdrawn from one batch of 55 g template phase homogenized with 48.1 g EGMS (Si-content: 9.7 wt %).

As container material, small polypropylene (PP) vessels were chosen exhibiting heat-resistance up to 100°C.

The composition, the gelation and aging temperature as well as the corresponding times for gelation and phase separation of the silica gels prepared for the investigation of the different aging temperatures are listed in table 43.

Table 43 Composition, time intervals for the gelation and phase separation of the silica gels gelled and aged at different temperatures T.

samples	c_{HCl} /*mol l*$^{-1}$	*T* /*°C*	*Si* /*wt %*	*P123* /*wt %*	*HCl* /*wt %*	t_g /*min*	t_{PS} /*min*
P1-40-x	1	40	8.4	30	70	66	184
P1-50-x	1	50	8.4	30	70	28	68
P1-60-x	1	60	8.4	30	70	27	52
P1-70-x	1	70	8.4	30	70	30	38
P1-80-x	1	80	8.4	30	70	25	30
P1-90-x	1	90	8.4	30	70	23	30

The physicochemical data of the silica gels prepared in the temperature range of 40 – 90°C after 3 and 7 days aging are listed in table 9 in section 2.1.6. The physicochemical properties of the silica gels aged for 1, 2, 4, 5, and 6 d in the temperature range of 40 – 90°C are given in table 44.

Table 44 Physicochemical properties of the silica gels gelled and aged in the range of 40 – 90°C for 1, 2, 4, 5, and 6 days.

			SAXS	*N_2-sorption*	
samples	*T* /°C	*t* /d	d_{10} /nm	*C*	S^{BET} /$m^2\ g^{-1}$
P1-40-1	40	1	9.9	169.8	638
P1-50-1	50	1	10.8	28.9	749
P1-60-1	60	1	11.5	26.9	812
P1-70-1	70	1	-	117.1	781
P1-80-1	80	1	-	62.5	880
P1-90-1	90	1	-	112.0	813
P1-40-2	40	2	10.6	191.0	691
P1-50-2	50	2	10.6	226.2	750
P1-60-2	60	2	11.5	106.7	812
P1-70-2	70	2	-	17.1	955
P1-80-2	80	2	-	63.4	880
P1-90-2	90	2	-	66.0	891
P1-40-4	40	4	10.6	56.9	718
P1-50-4	50	4	10.6	207.1	738
P1-60-4	60	4	11.5	175.3	786
P1-70-4	70	4	13.0*	173.5	860
P1-80-4	80	4	-	71.5	895
P1-90-4	90	4	-	18.5	995
P1-40-5	40	5	10.4	303.2	699
P1-50-5	50	5	10.6	211.7	753
P1-60-5	60	5	11.3	32.6	819
P1-70-5	70	5	12.6*	130.2	883
P1-80-5	80	5	-	60.9	873
P1-90-5	90	5	-	74.2	923
P1-40-6	40	6	10.5	245.1	704
P1-50-6	50	6	10.6	184.6	813
P1-60-6	60	6	11.8	115.1	889
P1-70-6	70	6	12.4*	22.8	962
P1-80-6	80	6	-	50.0	870
P1-90-6	90	6	-	64.1	999

* d_{10} is determined for a broad shoulder in the SAXS patterns.

7.2.3.2. Synthesis of Inorganic-Organic Hybrid Monoliths by Employing Pluronic P123

The inorganic–organic hybrid monoliths were synthesized in analogy to the pure inorganic silica monoliths by employing Pluronic P123 in acidic media (c(HCl) = 1 – 0.03 M) as supramolecular template and as phase separation-inducing agent.

Direct Approach via Co-Condensation

For the *in-situ* modification of the silica network, the ethylene glycol-modified silane (EGMS) was co-condensed with either the methyl- or phenyl-substituted EGMS analogon (MeGMS, PhGMS). The molar ratio of MeGMS to EGMS was varied in the range of 0 – 100 mol % at c(HCl) = 0 and 0.03 M, while the molar ratio of PhGMS to EGMS was restricted to ratios of maximum 40 mol % PhGMS. (Above 40 mol % PhGMS, no homogeneous gels could be obtained.)

The ratio of Si / P123 / 1 – 0.03 M = 8.4 / 30 / 70 (by weight) was kept constant for all gel syntheses. The Si-content of 8.4 wt % was established by combining the adequate molar amounts of EGMS and MeGMS or PhGMS, respectively.

For the synthesis of the methyl-modified silica monoliths, the determined Si-contents of the applied EGMS was 10.1 wt % and of the corresponding MeGMS wt % Si = 7.7. The ratio of MeGMS to EGMS, as well as the determined weight portions for MeGMS and EGMS are given in table 46 calculated for 20 g P123 in 0.03 M HCl.

In analogy, the Si-content of PhGMS was determined to 9.5 wt % and the employed EGMS contained 8.6 wt % Si. The ratio of PhGMS to EGMS including the applied weight portions for the synthesis of the phenyl-modified silica monoliths are listed in table 46 also calculated for 20 g P123 in 0.03 M HCl.

The average shrinkage of the diameter and the length of the monoliths are determined from their values after drying at 200°C in relation to their initial values after aging.

Table 45 Molar composition and weight portions of MeGMS and EGMS for the synthesis of the methyl-modified hybrid monoliths prepared at c(HCl) = 0.03 M including the determined average shrinkage of the monoliths' diameter and length.

samples	*c(HCl)* /*mol l*$^{-1}$	*MeGMS: EGMS*	*m(MeGMS)* /*g*	*m(EGMS)* /*g*	ΔL /%	ΔD /%
P2-1,5a	0.03	0:100	0.0	16.8	11.5	9.5
P3-1,5a	0.03	2.5:97.5	0.6	16.3	12.2	9.8
P4-1,5a	0.03	5:95	1.1	15.9	10.1	11.2
P5-1,5a	0.03	7.5:92.5	1.6	15.5	10.9	11.3
P6-1,5a	0.03	10:90	2.2	15.1	10.9	9.0
P7-1,5a	0.03	12.5:87.5	2.7	14.7	11.3	9.8
P8-1,5a	0.03	15:85	3.3	14.2	9.7	3.5
P9-1,5a	0.03	17.5:82.5	3.8	13.8	12.3	11.9
P10-1,5a	0.03	20:80	4.4	13.4	12.7	12.0
P11-1,5a	0.03	30:70	6.6	11.7	11.8	11.8
P12-1,5a	0.03	40:60	8.7	10.1	11.2	9.9
P13-1,5a	0.03	50:50	10.9	8.4	11.0	10.0
P14-1,5a	0.03	60:40	13.1	6.7	9.8	7.6
P15-1,5a	0.03	70:30	15.3	5.0	-	-
P16-1,5a	0.03	80:20	17.5	3.4	-	-
P17-1,5a	0.03	90:10	18.7	1.7	13.0	-0.5
P18-1,5a	0.03	100:0	21.9	0.0	-	-

The template phases of Pluronic P123 were pre-homogenized as described in section 7.2.3.1. and tempered at 40°C prior to their employment. To 20 g template phase the determined ratio of MeGMS (PhGMS) was added to EGMS and the mixture was homogenized on a vortex stirrer for 1 – 5 min at RT. The resulting sols were transferred to six long PMMA vessels and three PE moulds according to the description in section 7.2.3.1.

All gels were gelled and aged at 40°C for 7 or 15 d and were cured according to the procedure described in section 7.2.3.1.

Table 46 Molar composition and weight portions of PhGMS and EGMS for the synthesis of the phenyl-modified hybrid monoliths prepared at c(HCl) = 0.03 M including the determined average shrinkage of the monoliths' diameter and length.

samples	c(HCl) /mol l^{-1}	PhGMS: EGMS	m(PhGMS) /g	m(EGMS) /g	ΔL /%	ΔD /%
sh-P19-1a	0.03	0:100	0.0	19.6	11.9	14.2
sh-P20-1a	0.03	2.5:97.5	0.5	19.2	11.3	12.7
sh-P21-1a	0.03	5:95	0.9	18.7	11.5	15.6
sh-P22-1a	0.03	7.5:92.5	1.3	18.2	-	14.4
sh-P9-1a	0.03	10:90	1.8	17.7	14.7	16.5
sh-P23-1a	0.03	12.5:87.5	2.2	17.2	20.7	14.1
sh-P24-1a	0.03	15:85	2.7	16.7	14.0	15.5
sh-P25-1a	0.03	17.5:82.5	3.1	16.2	17.0	18.4
sh-P10-1a	0.03	20:80	3.6	15.7	15.3	14.3
sh-P11-1a	0.03	30:70	5.3	13.7	-	-
sh-P12-1a	0.03	40:60	7.1	11.7	-	-

The hybrid silica gels presented in table 45 and 46 were dried via the surface silylation approach including the heat treatment at 200°C in order to preserve the organic moieties on the surface as described above.

The physicochemical data of the methyl-modified hybrid monoliths prepared with 0, 5, 10, 15, 20, 30, 40, 50, and 100% MeGMS are given in table 10 in section 2.2.1.2., the properties of the not considered hybrid monoliths of this series are listed in table 47.

Table 47 Physicochemical properties of the methyl-modified hybrid silica monoliths prepared with 2.5 – 17.5 mol% and 60 – 90% MeGMS at c(HCl) = 0.03 M.

samples		SAXS	N_2-sorption			Hg-Porosimetry	
	%MeGMS /mol %	d_{10} /nm	S^{BET} /m² g^{-1}	D^{BJH} /nm	t_{wall} /nm	R^{Hg} /μm	V^{Hg} /cm³ g^{-1}
P3-1,5a	2.5	11.2	717	5.0	7.9	-	-
P5-1,5a	7.5	10.9	720	4.4	8.2	-	-
P7-1,5a	12.5	10.8	730	3.9	8.6	-	-
P9-1,5a	17.5	10.4	658	3.7	8.3	-	-
P14-1,5a	60	-	825	5.9	-	-	-
P15-1,5a	70	-	1209	-	-	-	-
P16-1,5a	80	-	979	-	-	-	-
P17-1,5a	90	-	802	-	-	-	-

The physicochemical properties of the phenyl-modified hybrid monoliths prepared with 2.5, 7.5, 12.5, and 17.5% PhGMS at c(HCl) = 0.03 M are listed in table 48.

Table 48 Physicochemical properties of the phenyl-modified hybrid silica monoliths prepared with x.5% PhGMS at c(HCl) = 0.03 M.

samples		*SAXS*	*N_2-sorption*			*Hg-Porosimetry*	
	%PhGMS /mol %	*d_{10}* /nm	*S^{BET}* /$m^2\,g^{-1}$	*D^{BJH}* /nm	*t_{wall}* /nm	*R^{Hg}* /µm	*V^{Hg}* /$cm^3\,g^{-1}$
sh-P20-1	2.5	11.0	1041	3.9	8.8	-	-
sh-P22-1a	7.5	10.0	1027	3.7	7.8	-	-
sh-P23-1a	12.5	9.7	846	3.7	7.5	-	-
sh-P25-1a	17.5	11.9	815	3.7	10.0	-	-

For the investigation of the resulting loading with methyl (phenyl) moieties by co-condensation, hybrid monoliths were synthesized at c(HCl) = 1 M by employing equal compositions of P123 / 1 M HCl = 30 / 70 (wt %). The ratios of MeGMS and PhGMS, respectively, to EGMS were varied in the range of 0 – 100 mol % for MeGMS and 0 – 30 mol % for PhGMS. The molar ratios of MeGMS to EGMS and PhGMS to EGMS including the corresponding weight portions are listed in tables 49 and 50.

After gelation and aging at 40°C for 7 or 15 d, the monoliths were cured in ethanol / HCl_{conc} (50/50 % v/v) and were subsequently washed with ethanol (2 – 3 d). In order to preserve the initial organic loading of the surface, the monoliths were subjected to a supercritical drying procedure with CO_2 at T = 40 – 50°C at p = 70 – 100 bar.

Prior to the investigation by IR-coupled TGA, all monoliths were tempered at 200°C to remove captured CO_2 and residual ethanol from the pore systems.

Table 49 Molar composition and weight portions of MeGMS and EGMS for the synthesis of methyl-modified silica monoliths prepared at c(HCl) = 1 M.

samples	*c(HCl) /mol l^{-1}*	*MeGMS: EGMS*	*m(MeGMS) /g*	*m(EGMS) /g*
P2-0a	1	0:100	0.0	16.5
P3-0a	1	2.5:97.5	0.6	16.1
P4-0a	1	5:95	1.2	15.7
P5-0a	1	7.5:92.5	1.9	15.3
P6-0a	1	10:90	2.5	14.9
P7-0a	1	12.5:87.5	3.1	14.5
P8-0a	1	15:85	3.7	14.1
P9-0a	1	17.5:82.5	4.3	13.6
P10-0a	1	20:80	5.0	13.2
P11-0a	1	30:70	7.4	11.6
P12-0a	1	40:60	9.9	9.9
P13-0a	1	50:50	12.4	8.3
P14-0a	1	60:40	14.9	6.6
P15-0a	1	70:30	17.4	5.0
P16-0a	1	80:20	19.8	3.3
P17-0a	1	90:10	22.3	1.7
P18-0a	1	100:0	24.8	0.0

Table 50 Molar composition and weight portions of PhGMS and EGMS for the synthesis of phenyl-modified monoliths prepared at c(HCl) = 1 M.

samples	*c(HCl) /mol l^{-1}*	*PhGMS: EGMS*	*m(PhGMS) /g*	*m(EGMS) /g*
sh-P1-1f	1	0:100	0	19.6
sh-P21-0a	1	5:95	0.9	18.7
sh-P9-0a	1	10:90	1.8	17.7
sh-P24-0a	1	15:85	2.7	16.7
sh-P10-0a	1	20:80	3.6	15.7
sh-P11-0a	1	30:70	5.4	13.8

The physicochemical data of the supercritically dried methyl-modified hybrid gels synthesized at c(HCl) = 1M are listed in table 51 and of the analogous treated phenyl-modified hybrid gels in table 52.

Table 51 Physicochemical properties of the supercritically dried methyl-modified hybrid silica gels prepared at 1 M HCl.

samples		SAXS	N_2-sorption			Hg-Porosimetry	
	%MeGMS /mol %	d_{10} /nm	S^{BET} /$m^2\ g^{-1}$	D^{BJH} /nm	t_{wall} /nm	R^{Hg} /μm	V^{Hg} /$cm^3\ g^{-1}$
P2-0a	0	10.8	403	5.4	7.0	0.2	2.9
P4-0a	5	10.8	526	5.4	7.0	0.3	3.5
P6-0a	10	10.5	558	5.0	7.1	0.4	3.4
P8-0a	15	10.3	638	4.7	7.2	-*	-*
P10-0a	20	9.9	531	4.4	7.0	0.2	3.5
P11-0a	30	9.4	691	4.4	6.5	0.1	3.8
P12-0a	40	8.1	733	4.7	4.7	-	-
P13-0a	50	-	855	-	-	-	-
P16-0a	80	-	568	-	-	-	-
P18-0a	100	-	373	-	-	-	-

* Not enough data points were recorded for an evaluation of the pore size distribution.

Table 52 Physicochemical properties of the supercritically dried phenyl-modified hybrid silica gels prepared at 1 M HCl.

samples		SAXS	N_2-sorption			Hg-Porosimetry	
	%PhGMS /mol %	d_{10} /nm	S^{BET} /$m^2\ g^{-1}$	D^{BJH} /nm	t_{wall} /nm	R^{Hg} /μm	V^{Hg} /$cm^3\ g^{-1}$
sh-P1-1f	0	11.5	563	6.3	7.0	0.2	2.9
sh-P21-0a	5	10.0	456	4.4	7.2	0.3	2.6
sh-P9-0a	10	9.7	355	3.9	7.3	0.3	1.8
sh-P24-0a	15	9.8	308	3.6	7.7	0.1	1.5
sh-P10-0a	20	8.3	196	3.7	5.9	-	0.8
sh-P11-0a	30	-	-	-	-	-	-

Modification via Post-synthetic Grafting

For the investigation of the possibility to achieve a higher loading of organic moieties and hence a higher degree of hydrophobicity, silica and methyl-modified hybrid silica gels were post-synthetically grafted.

As monolithic systems, pure silica gels prepared from EGMS at c(HCl) = 1 M and methyl-modified hybrid monoliths synthesized by co-condensation of MeGMS (10 mol %) and

EGMS (90 mol %) at c(HCl) = 0.03 M were chosen. In analogy to former experiments, the composition of Si / P123 / x M HCl = 8.4 / 30 / 70 (by weight) was kept constant.

For each modification series, silica monoliths were synthesized by adding 17.6 g of EGMS (EGMS: wt % Si = 9.7) to 20 g P123 / 1 M HCl.

For the analogue series of the hybrid silica gels, 2.0 g MeGMS (MeGMS: wt % Si = 8.5) and 15.7 g EGMS (EGMS: wt % Si = 9.7) were homogenized with 20 g P123 / 0.03 M HCl.

All gels were gelled and aged at 40°C for 7 d in PMMA vessels (diameter x length: 4.5 x 170 mm) and were then cured according to the procedure described in section 7.2.3.1.

For the grafting of the monoliths, three different approaches were chosen. Chloro-dodecyldimethylsilane (DDMCS, 24 h) and for comparison chlorotrimethylsilane (TMCS, 24 h) in petroleum ether were employed as sole modification agents resulting in the loading with dodecyldimethylsilyl moieties and trimethylsilyl entities on the surface. As third approach, an end-capping process was chosen for which the monoliths were first treated with DDMCS in petroleum ether (24 h) and in a second step with TMCS in petroleum ether (24 h). Between the two grafting steps, the monoliths were washed with petroleum ether (24 h) to remove unreacted DDMCS species and HCl.

The grafting agent and the volume fractions of the employed silylation reagents in petroleum ether are listed in table 53.

Subsequent to the surface modification, all monoliths were subjected to a washing procedure with petroleum ether (24 h) and ethanol (24 h) before they were dried at 200°C for the preservation of the organic moieties on the surface.

Table 53 Acid concentration and content of MeGMS for the gel synthesis and the modification including the corresponding volume fraction.

samples	*c(HCl) /mol l^{-1}*	*%MeGMS /mol %*	*silylation agent*	*silylation agent / petroleum ether*
sh-P1-1g1	1	0	TMCS	10 / 90% v/v
sh-P1-1g2	1	0	DDMCS	5 / 95% v/v
sh-P1-1g3	1	0	end-capped	TMCS 10 / 90 % v/v DDMCS 5 / 95 % v/v
P6-1,5b1	0.03	10	TMCS	10 / 90 % v/v
P6-1,5b2	0.03	10	DDMCS	5 / 95 % v/v
P6-1,5b3	0.03	10	end-capped	TMCS 10 / 90 % v/v DDMCS 5 / 95 % v/v

Variation of the Container Material

For the investigation of the influence of the container material on the macroporous framework in the boundary region of the monoliths, vessels made of poly(methyl methacrylate) (PMMA), polyethylene (PE), polycarbonate (PC) and poly(vinylidene fluoride) (PVDF) were applied as moulds.

The impact of the material was studied for hierarchically organized pure silica (100 mol % EGMS) and methyl-modified hybrid silica monoliths (10 mol % MeGMS / 90 mol % EGMS). The composition for the pure silica gels was established to Si / P123 / 10^{-1} M HCl = 8.4 / 30 / 70 (by weight). All monoliths were synthesized from one batch, by the addition of 35.6 g EGMS (EGMS: 9.4 wt % Si) to 40 g template phase (P123 / 10^{-1} M HCl).

The composition of the hybrid sol systems was Si / P123 / 0.03 M HCl = 8.4 / 30 / 70 (by weight) and the Si-content was established by combining 10 mol % MeGMS with 90 mol % EGMS. Three batches were applied for this series for which 16.1 g EGMS (EGMS: 9.4 wt % Si) combined with 1.7 g MeGMS (MeGMS: 9.9 wt % Si) were each homogenized with 20 g P123 / 0.03 M HCl.

The material and the dimensions of the applied containers are listed in table 54 for the particular sol-gel systems.

Table 54 Material and dimensions of the container applied for the investigations including the particular sol-gel system.

samples	*c(HCl) /mol l^{-1}*	*%MeGMS /mol %*	*container material*	*length x diameter /mm*
P1-2.1	10^{-1}	0	PMMA	4.5 x 170
P1-2.3	10^{-1}	0	PE	6.1 x 170
P1-2.5	10^{-1}	0	PVDF	6.0 x 280
P1-2.8	10^{-1}	0	PC	6.2 x 282
P6-1,5.1	0.03	10	PMMA	4.5 x 170
P6-1,5.3	0.03	10	PE	6.1 x 170
P6-1,5.5	0.03	10	PVDF	6.0 x 280
P6-1,5.8	0.03	10	PC	6.2 x 282

All monoliths were treated (silylation with TMCS) and dried according to the synthesis procedure described in detail in section 7.2.3.1.

7.2.3.3. Synthesis of Silica Monoliths by Employing New Diol-Modified Silanes

For the investigation of the impact of the released diol on the hierarchical architecture of the pore systems, silica monoliths were synthesized by employing 1,2-propane diol-modified silane (PGMS), 2,3-butane diol-modified silane (BDMS), and 1,2-hexane diol-modified silane (HDMS) as precursors. For comparison, EGMS-derived silica monoliths were also synthesized.

In analogy to the EGMS-derived silica monoliths described in section 7.3.2.1., an acidic Pluronic P123 phase was applied as supramolecular template and as phase separation inducing agent. The concentration of the acidic catalyst HCl was varied in the range of c(HCl) = 1 – 10^{-6} M, whereas the ratio of P123 to solvent was kept constant with P123 / x M HCl = 30 / 70 (by weight).

Structural investigations of the evolution of the organization of the P123 phase P123 / 1 M HCl = 30 / 70 in the presence of the particular diols at 40°C, suggested the reduction of the content of BDMS and HDMS in order to obtain a periodic ordering in the mesoscopic range. Thus, the composition of Si / P123 / x M = 8.4 / 30 / 70 being applied for EGMS and PGMS was varied for BDMS to Si / P123 / x M HCl =4.2 / 30 / 70 and for HDMS was adjusted to Si / P123 / x M HCl =4.5 / 30 / 70 (by weight).

In analogy to the experiments with EGMS, the P123 / x M HCl phases were pre-homogenized, and were tempered at 40°C before the adequate amount of the diol-modified precursor was added. The weight portions of each precursor were calculated with respect to 5 g template phase and resulted in 4.3 g EGMS, 5.7 g PGMS, 6.6 g BDMS, and 5.5 g HDMS for the particular Si-contents of the precursors given in table 55.

After homogenization with a vortex stirrer (1 – 5 min), the sols were transferred to small sealed-off PE vessels in which they were allowed to gel and age at 40°C for 7 – 8 d.

No curing procedure was applied, but the silica monoliths were immediately treated with TMCS in petroleum ether as described in section 7.2.3.1., whereas the extracted template phase was repeatingly removed. After washing with petroleum ether and ethanol (see section 7.2.3.1.), the monoliths were dried at 200°C.

Table 55 HCl concentration, type, and Si-content of precursor applied for the synthesis of the silica samples and the appearance of the monoliths after drying.

samples	*c(HCl) /mol l^{-1}*	*precursor*	*Si-content of precursor /wt %*	*appearance*
P1-1h	1	EGMS	9.7	turbid
P1-2d	10^{-1}	EGMS	9.7	turbid
P1-3d	10^{-2}	EGMS	9.7	turbid
P1-4d	10^{-3}	EGMS	9.7	turbid
P1-5c	10^{-4}	EGMS	9.7	turbid
P1-6c	10^{-5}	EGMS	9.7	turbid
PG3-8.4-0-8	1	PGMS	7.4	turbid
PG3-8.4-1-8	10^{-1}	PGMS	7.4	turbid
PG3-8.4-2-8	10^{-2}	PGMS	7.4	turbid
PG3-8.4-3-8	10^{-3}	PGMS	7.4	turbid
PG3-8.4-4-8	10^{-4}	PGMS	7.4	turbid
PG3-8.4-6-8	10^{-6}	PGMS	7.4	turbid
BD3-4.2-0-8	1	BDMS	3.2	turbid
BD3-4.2-2-8	10^{-2}	BDMS	3.2	transparent
BD3-4.2-3-8	10^{-3}	BDMS	3.2	transparent
BD3-4.2-4-8	10^{-4}	BDMS	3.2	transparent
BD3-4.2-6-8	10^{-6}	BDMS	3.2	transparent
HD2-4.5-0-8	1	HDMS	4.1	transparent
HD2-4.5-1-8	10^{-1}	HDMS	4.1	transparent
HD2-4.5-2-8	10^{-2}	HDMS	4.1	transparent
HD2-4.5-6-8	10^{-6}	HDMS	4.1	transparent

The physicochemical data of the silica gels prepared with PGMS and BDMS are presented in tables 19 and 20 in section 3.3. The physicochemical properties of the silica monoliths obtained from EGMS and HDMS are presented in table 56.

Table 56 Physicochemical properties of the silica monoliths prepared with EGMS (8.4 wt %) and HDMS (4.5 wt %) at different HCl concentrations.

samples		*SAXS*	*N_2-sorption*			*Hg-Porosimetry*	
	c(HCl) /mol l^{-1}	d_{10} /nm	S^{BET} /m^2 g^{-1}	D^{BJH} /nm	t_{wall} /nm	R^{Hg} /μm	V^{Hg} /cm^3 g^{-1}
P1-1h	1	11.0	1029	6.2	6.5	0.2	3.1
P1-2d	10^{-1}	11.3	875	5.7	7.4	0.2	3.2
P1-3d	10^{-2}	11.3	1061	5.8	7.3	0.2	3.1
P1-4a	10^{-3}	12.1	939	7.6	6.4	-	-
P1-5c	10^{-4}	12.4	838	-*	-	-	-
P1-6c	10^{-5}	12.1	981	7.5	6.5	-	-
HD2-4.5-0-8	1	-	582	-	-	-	-
HD2-4.5-1-8	10^{-1}	-	557	-	-	-	-
HD2-4.5-2-8	10^{-2}	-	530	-	-	-	-
HD2-4.5-6-8	10^{-6}	-	879	5.3	-	-	-

*No BJH-analysis was performed but a 5-point BET measurement.

7.2.3.4. Comparison of TEOS, Silicic Acid and Sodium Silicate to EGMS

The possibility of synthesizing hierarchically organized silica monoliths by substituting the ethylene glycol-modified silane (EGMS) by commercially available silicon source precursors such as tetraethylorthosilicate (TEOS) or sodium silicate ought to be investigated.

In analogy to the EGMS-derived monoliths, the silica gels were synthesized by employing Pluronic P123 in acidic or purely aqueous media as structure-directing agent. As catalyst for the hydrolysis and condensation reactions, HCl of varying concentrations was applied.

TEOS as Precursor

For the investigation of the substitution of EGMS by TEOS, the composition of the template phase was varied in the range of P123 / x M HCl = 8.4 / 10 / 90 – 8.4 / 40 / 60 with x = 1 – 10^{-3}. The Si-content was kept constant with 8.4 wt %. The portion of TEOS (98.0%, M =208.1 g mol^{-1}) was established to 3.1 g with respect to 5 g template phase.

Due to delayed gelation times, the TEOS-derived silica gels were allowed to gel and age at 40°C for 7 – 14 d. The composition of the TEOS-derived samples including the acid concentration, the gelation and aging times are listed in tables 57 – 59. All obtained silica

monoliths were further cured and surface modified (with TMCS) according to the procedure described in section 7.2.3.1.

Table 57 Composition, gelation and aging times of the TEOS-derived silica gels synthesized with c(HCl) = 1 M at 40°C.

samples	c_{HCl} /mol l^{-1}	t_{age} /d	*Si* /wt %	*P123* /wt %	*HCl* /wt %	t_g /min	t_{PS} /min
10-90-0TS12	1	12	8.4	10	90	1462	-
20-80-0TS7	1	7	8.4	20	80	1454	-
20-80-0TS12	1	12	8.4	20	80	"	-
30-70-0TS7	1	7	8.4	30	70	1350	-
30-70-0TS12	1	12	8.4	30	70	"	-
30-70-0TS14	1	14	8.4	30	70	"	-
40-60-0TS7	1	7	8.4	40	60	1445	-
40-60-0TS12	1	12	8.4	40	60	"	-
40-60-0TS14	1	14	8.4	40	60	"	-

Table 58 Composition, gelation and aging times of the TEOS-derived silica gels synthesized with c(HCl) = 10^{-1} M at 40°C.

samples	c_{HCl} /mol l^{-1}	t_{age} /d	*Si* /wt %	*P123* /wt %	*HCl* /wt %	t_g /min	t_{PS} /min
10-90-1TS7	10^{-1}	7	8.4	10	90	7101	-
10-90-1TS12	10^{-1}	12	8.4	10	90	"	-
20-80-1TS7	10^{-1}	7	8.4	20	80	7093	-
20-80-1TS12	10^{-1}	12	8.4	20	80	"	-
20-80-1TS14	10^{-1}	14	8.4	20	80	"	-
30-70-1TS7	10^{-1}	7	8.4	30	70	2367	-
30-70-1TS12	10^{-1}	12	8.4	30	70	"	-
30-70-1TS14	10^{-1}	14	8.4	30	70	"	-
40-60-1TS7	10^{-1}	7	8.4	40	60	2403	-
40-60-1TS12	10^{-1}	12	8.4	40	60	"	-
40-60-1TS14	10^{-1}	14	8.4	40	60	"	-

Table 59 Composition, gelation and aging times of the TEOS-derived silica gels synthesized with c(HCl) = 10^{-2} and 10^{-3} M at 40°C.

samples	c_{HCl} /mol l^{-1}	t_{age} /d	*Si* /wt %	*P123* /wt %	*HCl* /wt %	t_g /min	t_{PS} /min
10-90-2TS7	10^{-2}	7	8.4	10	90	2468	-
20-80-2TS7	10^{-2}	7	8.4	20	80	2458	-
20-80-2TS9	10^{-2}	9	8.4	20	80	"	-
30-70-2TS7	10^{-2}	7	8.4	30	70	2446	-
30-70-2TS9	10^{-2}	9	8.4	30	70	"	-
10-90-3TS7	10^{-3}	7	8.4	10	90	-	-
20-80-3TS9	10^{-3}	9	8.4	20	80	-	-
20-80-3TS16	10^{-3}	16	8.4	20	80	-	-

The physicochemical data of the silica monoliths excluded from the table 21 in section 4.3.1. are given in table 60.

Table 60 Physicochemical properties of the silica monoliths prepared with TEOS (8.4 wt %) and varied compositions of P123 / 10^{-2} and 10^{-3} M HCl at 40°C.

samples				*SAXS*	*N_2-sorption*		
	composition Si/P123/HCl	t_{age} /d	*c(HCl)* /mol l^{-1}	d_{10} /nm	S^{BET} /m^2 g^{-1}	D^{BJH} /nm	t_{wall} /nm
10-90-2TS7	8.4/10/90	7	10^{-2}	-	848	2.5	-
10-90-3TS7	8.4/10/90	7	10^{-3}	12.4	893	2.2, 4.6	12.1
20-80-2TS7	8.4/20/80	7	10^{-2}	-	796	3.5	-
20-80-2TS9	8.4/20/80	9	10^{-2}	-	944	3.7	-
20-80-3TS9	8.4/20/80	9	10^{-3}	-	726	3.3	-
30-70-2TS7	8.4/30/70	7	10^{-2}	-	1002	4.5	-
30-70-2TS9	8.4/30/70	9	10^{-2}	-	793	3.3	-

Silicic Acid and Sodium Silicate as Precursors

Sodium silicate (27 wt % SiO_2, 8 wt % Na_2O) was tested along with its protonated derivate, silicic acid. The silicic acid (pH 2) was obtained via ion exchange reaction of a diluted sodium silicate (9 wt % SiO_2) with an Amberlite IR-120 column and resulting in a Si-content of 4.5 wt % or 3.9 wt %. Due to the high dilution of the silicon source, high contents of the structure-directing agent P123 / 1 – 0 M HCl = 30 / 70 and 40 / 60 by weight were chosen as template phases, whereas the Si-content was adjusted to 4.2 wt %. The portion weights of the

template phase (including the ratio of P123 / x M HCl) and the silicic acid (according to the particular Si-content) are given in table 61.

Table 61 Weight portions of template phase and silicic acid for the particular composition and Si-content of H_4SiO_4.

samples	*m(template)* /g	*P123* /x M HCl	*Si-content* /wt %	*m(H_4SiO_4)* /g
30-70-xNW	5.0	30/70	4.5	4.7
40-60-xNW	5.0	40/60	3.9	5.5

The sample composition including the applied catalyst concentration (c(HCl)) and the time intervals for gelation, phase separation and aging are given in table 62.

Table 62 Composition, HCl concentration, times for gelation, phase separation and aging of the silicic acid –derived sol-gel systems at 40°C.

samples	c_{HCl} /mol l^{-1}	t_{age} /d	*Si* /wt %	*P123* /wt %	*HCl* /wt %	t_g /min	t_{PS} /min
30-70-0NW	1	7	4.2	30	70	>2880	>2880
30-70-1NW	10^{-1}	7	4.2	30	70	>720	>720
30-70-2NW	10^{-2}	7	4.2	30	70	315	315
30-70-3NW	10^{-3}	7	4.2	30	70	>720	>720
30-70-0NW	0	7	4.2	30	70	41	20
40-60-0NW	1	7	4.2	40	60	≤1*	≤1**
40-60-1NW	10^{-1}	7	4.2	40	60	≤1*	≤1**
40-60-2NW	10^{-2}	7	4.2	40	60	90	≤1**
40-60-3NW	10^{-3}	7	4.2	40	60	82	≤1**
40-60-0NW	0	7	4.2	40	60	74	≤1**

*immediate precipitation and formation of a slurry phase.
**the sol turned immediately turbid during homogenization.

For comparison, silica gels were also synthesized by employing the basic sodium silicate solution (27% SiO_2, 8% Na_2O, pH ~ 11). The Si-content for the synthesis was varied from 4.2 to 8.4 wt % and the composition of template phase was adjusted to P123 / 1 M = 10 / 90 and 20 / 80. The weight portions of sodium silicate were determined for the Si-content of 12.7 wt % Si with respect to 5 g template phase (table 63).

Table 63 Weight portions of template phase and sodium silicate for each applied Si-content determined for 12.7 wt % Si within the sodium silicate solution.

samples	*m(template)* /g	*P123* /1 M HCl	*Si-content* /wt %	*m(SiO_2*Na_2O)* /g
10-90-0NWG1	5.0	10/90	4.2	1.7
10-90-0NWG2	5.0	10/90	6.3	2.5
10-90-0NWG3	5.0	10/90	8.4	3.3
20-80-0NWG1	5.0	20/80	4.2	1.7
20-80-0NWG2	5.0	20/80	6.3	2.5

The composition including the corresponding time intervals for gelation, phase separation and aging of the sol-gel systems derived from sodium silicate are given in table 64.

Table 64 Composition, HCl concentration, time periods for gelation, phase separation, and aging sodium silicate-derived sol-gel systems at 40°C.

samples	c_{HCl} /mol l^{-1}	t_{age} /d	*Si* /wt %	*P123* /wt %	*HCl* /wt %	t_g /min	t_{PS} /min
10-90-0NWG1	1	7	4.2	10	90	-*	≤*1
10-90-0NWG2	1	7	6.3	10	90	-*	≤*1
10-90-0NWG3	1	7	8.4	10	90	-*	≤*1
20-80-0NWG1	1	7	4.2	20	80	-*	≤*1
20-80-0NWG2	1	7	6.3	20	80	-*	≤*1

*immediate precipitation.

The silica materials derived from silicic acid and sodium silicate solution were all aged at 40°C for 7 d.

In analogy to the EGMS-derived silica gels, all silica materials were subjected to the treatment with chlorotrimethylsilane (TMCS) in petroleum ether for 24 h and were subsequently washed with petroleum ether (24 h) and ethanol (24 h) before they were dried via slow heating from 30 – 200°C within 5 d.

7.2.3.5. PDMS-based Co-Polymers as Structure Directing Agents

For the investigation of the substitution of Pluronic P123 by commercially available PDMS-Based Co-polymers such as Tego Glide 440 and LA-S 687, the chemical and physical properties of these co-polymers were studied prior to their application.

Characterization of the PEO-PDMS-PEO based surfactants

Prior to the gel synthesis, the critical micelle concentrations of Tego Glide 440 and LA-S 687 were investigated by surface tension measurements, which were performed according to the "du Noüy" method on a DCAT 21 tensiometer in demineralised water. The reduction of the surface tension was measured with a Pt-Ir-Ring (DIN 53914) and a high-precision analytical balance, recording the maximal pulling force before the breakage of the lamella.

$$\gamma = \frac{F_{max}}{4\pi \cdot R} \cdot f_1 \qquad \textit{Equation 21}$$

γ: equilibrium surface tension

F_{max}: maximum pulling force

R: average ring radius

f_1: correction factor

The data were corrected according to Harkins and Jordan (correction factor f_1) with regard to the ring geometry with radius r, the difference of the density between the liquid and the gas phase (Δρ) to calculate the equilibrium surface tension γ. The correction factor f_1 is calculated according to equation 22.

$$f_1 = \sqrt{\frac{0.000368 \cdot \gamma_{max}}{R^2 \cdot \Delta\rho} + 0.04534 - \frac{1.670 \cdot r}{R}} \qquad \textit{Equation 22}$$

γ_{max}: maximum surface tension

R: average ring radius

r: ring wire radius,

$\Delta\rho = \rho_l - \rho_g$

The silicon content of the precursor was determined by thermogravimetric measurements in air. The heating was conducted from RT to 1000°C with a heating ramp of 10°C per min. Structural investigations were performed by spin-lock ^{29}Si-NMR and 1H-NMR in benzene-d_6 and DMSO-d_6.

Synthesis of the hierarchically organized silica monoliths

Silica gels were prepared by adding EGMS to a mixture of the PEO-PDMS-PEO based surfactants (Tego Glide 440 or LA-S 687) and either HCl of varying concentration or purely aqueous solution. The ratio by weight of Si to surfactant phase was 8.4 / 100, whereas the composition of the surfactant and HCl or H_2O phase, respectively, was varied from 10 / 90 (wt %) up to 30 / 70 (wt %). The reaction mixture was homogenized with a Vortex stirrer and the resulting sol or in some cases the resultant emulsion was sealed in polyethylene vessels for gelation and aging. All gels were aged at 40°C for 7 d.

The Si-content and the weight portion of EGMS for the different experiment series are listed in tables 65 – 67 calculated with respect to the quantity of template phase employed.

Table 65 Weight portions of EGMS determined for the particular Si-content for the composition Si / surfactant / x M HCl = 8.4 / 30 / 70 calculated with respect to 10 g surfactant phase.

samples	*c(HCl) /mol l^{-1}*	*surfactant /solvent*	*Si-content /wt %*	*m(EGMS) /g*
LAS-4.1.1	1	30/70	9.2	9.1
LAS-3.1.3	10^{-1}	30/70	9.2	9.1
LAS-2.1.3	10^{-2}	30/70	9.2	9.1
LAS-5.1.1	10^{-3}	30/70	9.2	9.1
LAS-6.1.1	10^{-4}	30/70	9.2	9.1
LAS-7.1.1	10^{-5}	30/70	9.2	9.1
LAS-8.1.1	10^{-6}	30/70	9.2	9.1
LAS-1.1.3	0	30/70	9.2	9.1
T44-4.1.1	1	30/70	9.2	9.1
T44-3.1.3	10^{-1}	30/70	9.2	9.1
T44-2.1.3	10^{-2}	30/70	9.2	9.1
T44-5.1.1	10^{-3}	30/70	9.2	9.1
T44-6.1.1	10^{-4}	30/70	9.2	9.1
T44-7.1.1	10^{-5}	30/70	8.6	9.8
T44-8.1.1	10^{-6}	30/70	8.6	9.8
T44-1.1.3	0	30/70	8.6	9.8

Table 66 Weight portions of EGMS determined for the particular Si-content for the composition Si / surfactant / x M HCl = 8.4 / 10 / 90 calculated with respect to 5 g surfactant phase.

samples	c(HCl) /mol l^{-1}	surfactant /solvent	Si-content /wt %	m(EGMS) /g
LAS-3.2.1	10^{-1}	10/90	8.9	5.1
LAS-2.2.1	10^{-2}	10/90	8.9	5.1
LAS-1.2.1	0	10/90	8.9	5.1
T44-3.2.1	10^{-1}	10/90	8.9	5.1
T44-2.2.1	10^{-2}	10/90	8.9	5.1
T44-1.2.1	0	10/90	8.9	5.1

Table 67 Weight portions of EGMS determined for the particular Si-content for the composition Si / surfactant / x M HCl = 8.4 / 20 / 80 calculated with respect to 10 g surfactant phase.

samples	c(HCl) /mol l^{-1}	surfactant /solvent	Si-content /wt %	m(EGMS) /g
LAS-1.3.1	0	20/80	8.9	10.0
T44-1.3.1	0	20/80	8.9	10.1

To preserve the monolithic gel body from cracking, the gels were treated with TMCS in petroleum ether (24 h) according to the procedure described in section 7.2.3.1. including the subsequent washing process and the heat treatment at 200°C.

The physicochemical properties obtained for the excluded silica gels prepared at c(HCl) = 1 – 10^{-2} M are given here in table 68.

Table 68 Physicochemical properties of the silica gels synthesized with Tego Glide 440 and LA-S 687 at c(HCl) = 1 – 10^{-2} M.

samples	SAXS			N_2-sorption			Hg-Porosimetry
	c_{HCl} /mol l^{-1}	q^1 /nm^{-1}	d^{1*} /nm	S^{BET} /$m^2\ g^{-1}$	V_0 /$cm^3\ g^{-1}$	D_{BJH}** /nm	R^{Hg} /µm
LAS-4.1.1	1	-	-	782	145.5	-	-
LAS-3.1.3	10^{-1}	-	-	792	156.7	-	-
LAS-2.1.3	10^{-2}	-	-	720	151.3	-	-
T44-4.1.1	0	-	-	782	145.5	-	-
T44-3.1.3	10^{-6}	-	-	675	170.5	-	-
T44-2.1.3	10^{-5}	-		846	169.6	6.5	-

To investigate the possibility of creating a hydrophobic surface by gradually decomposition of the PEO chains of the ABA siloxane surfactants, some silica gels were excluded from the silylation process. Instead these gels were washed with ethanol and were subsequently supercritically dried with CO_2 at 44°C and a pressure of 100 bar (T_c = 31°C, p_c = 73.7 bar[14]) followed by a selective heat-treatment up to 600°C, whereas samples at 200°C, 300°C and 400°C were withdrawn and analyzed.

Chapter 8

Conclusion

The focus of this work was on the synthesis of hierarchically organized silica and organically modified hybrid silica monoliths for the application as stationary phases in high performance liquid chromatography (HPLC) by employing diol-modified silanes as precursors. Monolithic materials exhibiting a hierarchical pore architecture in the macroscopic and mesoscopic range, combine the advantages of a co-continuous macroporous morphology with an organized mesopore system. These structural features allow for a high permeability and a high separation efficiency of the monolithic HPLC column at the same time. One promising approach towards hierarchically organized silica monoliths is employing structure-directing agents that can simultaneously act as template in the mesoscopic size regime and induce phase separation in the macroscopic range resulting in well-defined pore size domains.

In combination with the functionalization of the pore walls, tailored (organically modified) silica materials can be synthesized for the application as HPLC columns. Thorough investigations of the employment of lyotropic liquid crystalline (LLC) phases of Pluronic P123 in acidic aqueous media with the ethylene glycol-modified silane (EGMS) as precursor proved to be a promising synthesis strategy in order to create hierarchically organized silica

monoliths. By adjusting the synthesis parameters such as the concentration of the acid catalyst, the ratio of P123 to solvent, the gelation and aging temperature, etc. the resulting architecture of the pore size domains could be fine-tuned with respect to the desired morphological properties. For instance, the composition of the sol system Si / P123 / 1 M HCl = 8.4 / 30 / 70 by weight, which is allowed to gel and age at 40°C (t_{age} = 7 d), resulted in hierarchically organized silica monoliths exhibiting a homogeneous co-continuous macroporous framework formed by silica strands (with uniform macropores of R^{Hg}= 0.3 μm). Concomitantly, the generated mesoporous system being located within the silica strands exhibits a long-range 2D-hexagonal ordering in the mesoscopic range and a narrow pore diameter distribution of D^{BJH} = 6.3 nm which was affirmed by TEM imaging and SAXS measurements.

With regard to HPLC analysis in the Reversed Phase (RP) mode, hierarchically organized monoliths with a hydrophobic surface are required. In order to tailor the surface polarity, two different synthetic approaches were investigated in this work. The direct incorporation of phenyl and methyl entities by simultaneous preservation of a hierarchical organization of the meso- and the macropore size domains was achieved by co-condensing the particular glycol-modified organosilane (-CH_3: MeGMS, -C_6H_5: PhGMS) with EGMS. In analogy to the pure EGMS-derived silica monoliths, LLC phases of P123 in acidic media were employed as structure-directing agents. By adjusting the ratio of MeGMS and PhGMS, respectively, to EGMS, hierarchically organized hybrid silica monoliths were successfully synthesized in the range 2.5 to 20 mol % MeGMS and 2.5 to 10 mol % PhGMS with regard to a 2D-hexagonally arranged mesopore system and a co-continuous macroporous skeleton. A higher degree of loading of organic functionalities on the pore walls without affecting the hierarchical organization was achieved by post-synthetically grafting of silica and methyl-modified hybrid silica monoliths. The post-synthetic functionalization with trimethylsilyl moieties and the end-capping approach (by combining dodecyldimethylsilyl and trimethylsilyl entities on the silica surface) resulted in highly hydrophobic surfaces of the silica and the prior methyl-modified hybrid silica monoliths. Depending on the grafting agent, contact angles in the range of 127 – 135° for the loading with trimethylsilyl entities and 137 – 139° for the end-capped monoliths could be obtained affirming the high degree of hydrophobicity, whereas the ordering of the hierarchical pore size domains was simultaneously preserved.

In order to investigate the impact of the chemical nature of the released diol on the evolution of the hierarchical organization, novel diol-modified silanes were synthesized by transalkoxylation reactions of tetraethylorthosilicate (TEOS) with 1,2-propane diol, 2,3-butane diol, and 1,2-hexane diol and employed as precursors in the silica gel synthesis. The comparison with the analogue EGMS-derived experiments by retained ratio of P123 to solvent as well as the acid catalyst HCl revealed that the polarity of the released diol is a prominent factor for the evolution of the hierarchical organization. Along with increasing alkyl chain length, a transition of the mesoscopic ordering occurred from a 2D-hexagonal arrangement for ethylene glycol and 1,2-propane diol to a wormhole-like array of the mesopore system for 2,3-butane diol. Concomitantly, the resulting macroporous morphology is changed from a cellular silica network consisting of rod-shaped silica strands for ethylene glycol to a particulate morphology formed by spherical particles, which were already obtained for 1,2-propane diol.
In order to answer the question whether the employment of a diol-modified silane is crucial for the synthesis of hierarchically organized silica monoliths by employing acidic template phases of Pluronic P123 as structure directing agent, EGMS was substituted by commercially available precursors such as TEOS and sodium silicate as well as its protonated derivative, silicic acid. Either the resulting silica materials could not be obtained in the monolithic shape or did not display the hierarchical pore architecture indicating that neither TEOS nor sodium silicate or silicic acid are adequate substituents for EGMS at these synthesis conditions.

Besides the variation of the precursor, the replacement of Pluronic P123 as structure-directing agent by commercially available poly(ethylene oxide)-poly(dimethylsiloxane)-poly(ethylene oxide) (PEO-PDMS-PEO) block co-polymers such as Tego Glide 440 and LA-S 687 was investigated, whereas EGMS was retained as precursor. By employing these PDMS-based co-polymers hierarchically organized silica monoliths could be synthesized in purely aqueous solution and at low HCl concentrations ($c(HCl) \leq 10^{-4}$ M). The employment of LA-S 687 generated a hierarchy on two different length scales, a co-continuous macroporous framework and a mesoporous system being located within the macroporous skeleton. However, by employing Tego Glide 440 a third level of hierarchy was introduced. SEM imaging indicated the presence of large isolated macropores, the pore walls of which consist of a co-continuous macroporous framework with silica strands comprising the mesopore system.
In contrast to Pluronic P123, the PDMS-based amphiphilic co-polymers provide the opportunity of a direct tailoring of the silica surface polarity by gradual thermo-oxidative

decomposition of PEO segments resulting in a hydrophobic surface. This approach was successfully applied by employing Tego Glide 440 as structure-directing agent. After the thermal degradation at 200 and 300°C, the hierarchically organized silica monoliths exhibited a hydrophobic surface caused by thermally degraded PDMS-segments (T-units) within the porous systems, which was affirmed by solid-state CP-MAS ^{29}Si-NMR spectroscopic investigations.

The applicability of EGMS and MeGMS / EGMS-derived hierarchically organized (hybrid) silica monoliths as stationary phases for HPLC were studied in extensive HPLC experiments at Merck KGaA, Darmstadt. The testing involved HPLC experiments in the Normal Phase (NP) and Reversed Phase (RP) mode.

The hierarchically organized hybrid silica monoliths obtained from co-condensation of EGMS and its methyl-substituted derivative MeGMS (5 – 20 mol %) in the presence of an acidic LLC phase of Pluronic P123 as template proved to be promising candidates as stationary phases in the NP mode. The monoliths derived from 5 and 10 mol % MeGMS exhibited the best performances with respect to the separation quality. In addition, van-Deemter experiments were performed for the hybrid monolith obtained from 5 mol % of MeGMS. These investigations indicated the possibility of increasing the flow rate in the range of u = 1.5 – 3.4 mm s^{-1} for the separation of nitrobenzene and 2-nitroanisole without effectively impairing the separation efficiency (H(nitrobenzene) = 16.6 - 18.9 μm and H(2-nitroanisole) = 31.7 – 30.9 μm). In contrast to particulate columns for which rapidly increasing backpressures arise with increasing flow rates, the observed backpressures remained moderate in this flow range with pressures of 56 to 125 bar.

Among the tested hierarchically organized silica monoliths derived from sole EGMS by employing template phases of Pluronic P123 as structure-directing agents, the monolith synthesized at c(HCl) = 1 M exhibited the most astonishing separation properties. Due to its trimethylsilyl-modified silica surface, a good performance was obtained in the RP mode for the separation of a mixture of thiourea, biphenyl-2-ol, progesterone, 1-phenyl-1-hexanone, and anthracene. However, despite the reduced polarity of its silica surface, it also exhibited a sufficient separation quality in the NP-HPLC separation of toluene, nitrobenzene and 2-nitroanisole. For both HPLC experiments the arising backpressures were only 61 bar for RP-mode and 103 bar for the NP-mode separation indicating an undisturbed flow of the mobile phase within the monolithic column

Furthermore, additional separation experiments in the RP mode of more complex analyte mixtures such as the separation of a mixture of complexing agents (consisting of uracil, purpurine, and quinizarin) were performed. The corresponding chromatograms indicated a good performance and affirmed the suitability of the EGMS-derived monolith as HPLC column.

In summary, the aim of this thesis was the synthesis and characterization of hierarchically organized (hybrid) silica monoliths by employing (novel) diol-modified silanes as precursors for the application as stationary phases in HPLC, whereas a special focus was on the design of the hierarchically organized pore size domains and the tailoring of the surface properties.

References

[1] S. Altmaier, K. Cabrera, *J. Sep. Sci.* **2008**, *31*, 2551.

[2] K. Cabrera, *J. Sep. Sci.* **2004**, *27*.

[3] H. Minakuchi, K. Nakanishi, N. Soga, N. Ishizuka, N. Tanaka, *J. Chromatogr. A* **1997**, *762*, 135.

[4] K. Nakanishi, H. Minakuchi, N. Soga, N. Tanaka, *J. Sol-Gel Sci. Technol.* **1997**, *8*, 547.

[5] S. Mann, G. A. Ozin, *Nature* **1996**, *382*, 313.

[6] S. Mann, W. Shenton, M. Li, S. Connolly, D. Fitzmaurice, *Adv. Mater.* **2000**, *12*, 147.

[7] P. B. Weisz, V. J. Frilette, R. W. Maatmann, E. B. Mower, *J. Catal.* **1962**, *1*, 307.

[8] C. J. Plank, E. J. Rosinski, M. P. Howthorne, *Ind. Eng. Chem., Prod. Res. Dev.* **1964**, *3*.

[9] in *Handbook of Porous Solids* (Eds.: F. Schüth, K. S. W. Sing, J. Weitkamp), Wiley-VCH, Weinheim, **2002**.

[10] K. Unger, *Angew. Chem.* **1972**, *84*, 331.

[11] M. E. Davis, *Nature* **2002**, *417*, 813.

[12] M. E. Davis, C. Saldarriaga, C. Montes, J. Garces, C. A. Crowder, *Nature* **1988**, *331*, 698–699.

[13] N. Hüsing, S. Hartmann, in *Hybrid Nanocomposites for Nanotechnology* (Ed.: L. Merhari), Springer, New York, **2009**, pp. 131.

[14] N. Hüsing, U. Schubert, *Angew. Chem., Int. Ed.* **1998**, *37*, 22.

[15] C. T. Kresge, M. E. Leonowicz, W. J. Roth, J. C. Vartuli, J. S. Beck, *Nature* **1992**, *359*, 710.

[16] J. S. Beck, J. C. Vartuli, W. J. Roth, M. E. Leonowicz, C. T. Kresge, K. D. Schmitt, C. T. W. Chu, D. H. Olson, E. W. Sheppard, et al., *J. Am. Chem. Soc.* **1992**, *114*, 10834.

[17] T. Yanagisawa, T. Shimizu, K. Kuroda, C. Kato, *Bull. Chem. Soc. Jpn.* **1990**, *63*, 988.

[18] F. Hoffmann, M. Cornelius, J. Morell, M. Fröba, *Angew. Chem.* **2006**, *118*, 3290.

[19] J. S. Vartuli, K. D. Schmitt, C. T. Kresge, W. J. Roth, M. E. Leonowicz, S. B. McCullen, S. D. Hellring, J. S. Beck, J. L. Schlenker, D. H. Olson, E. W. Sheppard, *Chem. Mater.* **1994**, *6*, 2317.

[20] J. C. Vartuli, C. T. Kresge, W. J. Roth, S. B. McCullen, J. S. Beck, K. D. Schmitt, M. E. Leonowicz, J. D. Lutner, E. W. Sheppard, in *Advanced catalysts and nanostructured materials* (Ed.: W. R. Moser), Academic Press, San Diego **1991**.

[21] D. Zhao, Q. Huo, J. Feng, B. F. Chmelka, G. D. Stucky, *J. Am. Chem. Soc.* **1998**, *120*, 6024.

[22] R. Ryoo, J. M. Kim, C. H. Ko, C. H. Shin, *J. Phys. Chem.* **1996**, *100*, 17718.

[23] F. Kleitz, S. H. Choi, R. Ryoo, *Chem. Commun.* **2003**, 2136.

[24] F. Schüth, in *Handbook of Porous Solids, Vol. 1* (Eds.: F. Schüth, K. S. W. Sing, J. Weitkamp), Wiley-VCH, Weinheim, **2002**, pp. 533.

[25] N. F. Berk, C. J. Glinka, W. Haller, L. C. Sander, *Mater. Res. Soc. Symp. Proc.* **1990**, *166*, 409.

[26] W. Haller, *Nature* **1965**, *206*, 693.

[27] W. Haller, *J. Chromatogr. A* **1968**, *32*, 676.

[28] F. Janowski, D. Enke, in *Handbook of Porous Solids, Vol. 3* (Eds.: F. Schüth, K. S. W. Sing, J. Weitkamp), Wiley-VCH Weinheim, **2002**, pp. 1432.

[29] J. C. Lytle, A. Stein, in *Annual Reviews of Nano Research, Vol. 1* (Eds.: G. Cao, C. J. Brinker), World Scientific Publishing, **2006**, pp. 1.

[30] A. Galarneau, N. Calin, J. Iapichella, M. Barrande, R. Denoyel, B. Coasne, F. Fajula, *Chem. Mater.* **2009**, *21*, 1884.

[31] R. Cademartiri, M. A. Brook, R. Pelton, J. D. Brennan, *J. Mater. Chem.* **2009**, *19*, 1583.

[32] S. A. Davis, S. L. Burkett, N. H. Mendelson, S. Mann, *Nature* **1997**, *385*, 420.

[33] B. T. Holland, C. F. Blanford, T. Do, A. Stein, *Chem. Mater.* **1999**, *11*, 795.

[34] B. T. Holland, C. F. Blanford, A. Stein, *Science* **1998**, *281*, 538.

[35] B. Lebeau, C. E. Fowler, S. Mann, C. Farcet, B. Charleuxe, C. J. Sanchez, *J. Mater. Chem.* **2000**, *10*, 2105.

[36] O. D. Velev, T. A. Jede, R. F. Lobo, A. M. Lenhoff, *Nature* **1997**, *389*, 447.

[37] O. D. Velev, T. A. Jede, R. F. Lobo, A. M. Lenhoff, *Chem. Mater.* **1998**, *10*, 3597.

[38] K. Nakanishi, N. Soga, *J. Non-Cryst. Solids* **1992**, *139*, 14.

[39] K. Nakanishi, N. Soga, *J. Non-Cryst. Solids* **1992**, *139*, 1.

[40] K. Nakanishi, T. Amatani, S. Yano, T. Kodaira, *Chem. Mater.* **2008**, *20*, 1108.

[41] J. Babin, J. Iapichella, B. Lefevre, C. Biolley, J.-P. Bellat, F. Fajula, A. Galarneau, *New J. Chem.* **2007**, *31*, 1907.

[42] F. Carn, A. Colin, M.-F. Achard, H. Deleuze, E. Sellier, M. Birot, R. Backov, *J. Mater. Chem.* **2004**, *14*, 1370.

[43] T. Amatani, K. Nakanishi, K. Hirao, T. Kodaira, *J. Chem. Mater.* **2005**, *17*, 2114.

[44] K. Nakanishi, H. Shikata, N. Ishizuka, N. Koheiya, N. Soga, *J. High Resolut. Chromatogr.* **2000**, *23*, 106.

[45] K. Nakanishi, N. Tanaka, *Acc. Chem. Res.* **2007**, *40*, 863.

[46] D. Brandhuber, N. Huesing, C. K. Raab, V. Torma, H. Peterlik, *J. Mater. Chem.* **2005**, *15*, 1801.

[47] D. Brandhuber, H. Peterlik, N. Huesing, *J. Mater. Chem.* **2005**, *15*, 3896.

[48] D. Brandhuber, V. Torma, C. Raab, H. Peterlik, A. Kulak, N. Huesing, *Chem. Mater.* **2005**, *17*, 4262.

[49] S. Hartmann, D. Brandhuber, N. Huesing, *Acc. Chem. Res.* **2007**, *40*, 885.

[50] N. Huesing, D. Brandhuber, P. Kaiser, *J. Sol-Gel Sci. Technol.* **2006**, *40*, 131.

[51] W. Cho, B. J. Cha, H. I. Lee, J. M. Kim, K. Char, *J. Mater. Chem.* **2008**, *18*, 4971.

[52] T. Sen, G. J. T. Tiddy, J. L. Casci, M. W. Anderson, *Chem. Mater.* **2004**, *16*, 2044.

[53] P. Yang, T. Deng, D. Zhao, P. Feng, D. Pine, B. F. Chmelka, G. M. Whitesides, G. D. Stucky, *Science* **1998**, *282*, 2244.

[54] H. Zhong, G. Zhu, J. Yang, P. Wang, Q. Yang, *Microporous Mesoporous Mater.* **2007**, *100*, 259.

[55] W. Geffcken, E. Berger, Patent DE 736411, **1943**.

[56] W. Geffcken, E. Berger, Patent US 2366516, **1945**.

[57] H. Schroeder, *Phys.Thin Films* **1969**, *5*, 87.

[58] G. Wagner, *Metalloberflaeche* **2002**, *56*, 36.

[59] C. J. Brinker, G. W. Scherer, *Sol-Gel Science: The Physics and Chemistry of Sol-Gel Processing*, Academic Press, San Diego, **1990**.

[60] H. K. Schmidt, *Chemie in unserer Zeit* **2001**, *3*, 176.

[61] W. H. Stockmayer, *J. Chem. Phys.* **1943**, *11*, 45.

[62] P. J. Flory, *J. Am. Chem. Soc.* **1941**, *63*, 3083.

[63] J. F. Joanny, *Physica B* **1989**, 381.

[64] D. Stauffer, *Pure & Appl. Chem.* **1981**, *53*, 1479—1487.

[65] M. H. Ernst, R. M. Ziff, E. M. Hendriks, *J. Coll. Interfac. Sci.* **1984**, *97*, 266.

[66] J. E. Martin, D. Adolf, *Annu. Rev. Phys. Chem.* **1991**, *42*, 311.

[67] R. C. Mehrotra, R. P. Narain, *Indian J. Chem.* **1967**, *5*, 444.

[68] K. Sattler, H. Hoffmann, *Chem. Ing. Tech.* **2000**, *72*, 487.

[69] M. A. Brook, Y. Chen, K. Guo, Z. Zang, J. D. Brennan, *J. Mater. Chem.* **2004**, *14*, 1469.

[70] Y. A. Shchipunov, T. Y. Karpenko, *Langmuir* **2004**, *20*, 3882.

[71] A. Mitra, T. Imae, Y. A. Shchipunov, *J. Sol-Gel Sci. Technol.* **2005**, *34*, 127.

[72] N. Huesing, C. Raab, V. Torma, A. Roig, H. Peterlik, *Chem. Mater.* **2003**, *15*, 2690.

[73] I. Gill, A. Ballesteros, *J. Am. Chem. Soc.* **1998**, *120*, 8587.

[74] F. Schüth, *Angew. Chem. Int. Ed. Engl.* **2003**, *42*, 3604.

[75] M. Huang, A. Choudrey, P. Yang, *Chem. Commun.* **2000**, *12*.

[76] Y. Han, J. Kim, G. Stucky, *Chem. Mater.* **2000**, *12*, 2068.

[77] A. Fukuoka, Y. Sakamoto, S. Guan, S. Inagaki, N. Sugimoto, Y. Fukushima, K. Hirahara, S. Iijima, M. Ichikawa, *J. Am. Chem. Soc.* **2001**, *123*, 3373.

[78] S. H. Joo, S. J. Choi, I. Oh, J. Kwak, Z. Liu, O. Teresaki, R. Ryoo, *Nature* **2001**, *412*, 169.

[79] R. Ryoo, S. H. Joo, S. Jun, *J. Phys. Chem. B* **1999**, *103*, 7743.

[80] S. Jun, S. H. Joo, R. Ryoo, M. Kruk, M. Jaroniec, Z. Liu, T. Ohsuna, O. Terasaki, *J. Am. Chem. Soc.* **2000**, *122*, 10712.

[81] Q. Huo, D. I. Margolese, U. Ciesla, D. G. Demuth, P. Feng, T. E. Gier, P. Sieger, A. Firouzi, B. F. Chmelka, F. Schüth, G. D. Stucky, *Chem. Mater.* **1994**, *6*, 1176.

[82] Q. Huo, D. I. Margolese, U. Ciesla, P. Feng, T. E. Gier, P. Sieger, R. Leon, P. M. Petroff, F. Schueth, G. D. Stucky, *Nature* **1994**, *368*, 317.

[83] J. N. Israelachvili, D. J. Mitchell, B. W. Ninham, *J. Chem. Soc., Faraday Trans. 2* **1976**, *72*, 1525.

[84] D. A. Doshi, A. Gibaud, V. Goletto, M. Lu, H. Gerung, B. Ocko, S. Han, C. F. Brinker, *J. Am. Chem. Soc.* **2003**, *125*, 11646.

[85] K. Flodström, T. V. Cilaine, H. Amenitsch, V. Alfredsson, M. Linden, *Langmuir* **2004**, *20*, 4885.

[86] K. Flodström, H. Wennerstrom, V. Alfredsson, *Langmuir* **2004**, *20*, 680.

[87] C. Yu, J. Fan, Z. D. Bozhi, *Chem. Mater.* **2004**, *16*, 889.

[88] S. S. Soni, G. Brotons, M. Bellour, T. Narayanan, A. Gibaud, *J. Phys. Chem. B* **2006**, *110*, 15157.

[89] D. VanAn, diploma thesis, Universität Ulm (Ulm), **2007**.

[90] K. Nakanishi, R. Takahashi, N. Soga, *J. Non-Cryst. Solids* **1992**, *147-148*, 291.

[91] H. Kaji, K. Nakanishi, N. Soga, *J. Sol-Gel Sci. Technol.* **1993**, *1*, 35.

[92] K. Nakanishi, *J. Porous Mater.* **1997**, *4*, 67.

[93] K. Nakanishi, Y. Sato, Y. Ruyat, K. Hirao, *J. Sol-Gel Sci. Technol.* **2003**, *26*, 567.

[94] J.-H. Smatt, S. Schunk, M. Linden, *Chem. Mater.* **2003**, *15*, 2354.

[95] J. H. Smatt, C. Weidenthaler, J. B. Rosenholm, M. Linden, *Chem. Mater.* **2006**, *18*, 1443.

[96] K. Nakanishi, *Bull. Chem. Soc. Jpn.* **2006**, *79*, 673.

[97] K. Nakanishi, *J. Ceram. Soc. Jpn* **2007**, *115*, 169.

[98] V. Antochshuk, M. Jaroniec, *J. Phys. Chem. B* **1999**, *103*, 6252.

[99] X. Liu, L. Li, Y. Du, Z. Guo, T. Ong, Y. Cheng, S. C. Ng, Y. Yang, *J. Chromat. A* **2009**, *1261*, 7767.

[100] N. Gartmann, D. Brühweiler, *Angew. Chem. Int. Ed. Engl.* **2009**, *48*, 6354.

[101] N. Tanaka, H. Kobayashi, K. Nakanishi, H. Minakuchi, N. Ishizuka, *Anal. Chem.* **2001**, *73*, 420A.

[102] V. R. Meyer, *Praxis der Hochleistungs-Flüssigchromatographie*, Wiley-VCH, Weinheim, **2009**.

[103] F. C. Leinweber, U. Tallarek, *J. Chromatogr. A* **2003**, *1006*, 207.

[104] D. Brandhuber, Doctoral thesis, Technical University Vienna (Vienna), **2005**.

[105] K. Nakanishi, *J. Ceram. Soc. Jpn.* **2007**, *115*, 169.

[106] C. Boissiere, A. Larbot, A. v. d. Lee, P. J. Kooyman, E. Prouzet, *Chem. Mater.* **2000**, *12*, 2902.

[107] P. Schmidt-Winkel, P. Yang, D. I. Margolese, B. F. Chmelka, G. D. Stucky, *Adv. Mater.* **1999**, *11*, 303.

[108] N. Ishizuka, H. Kobayashi, H. Minakuchi, K. Nakanishi, K. Hirao, K. Hosoya, T. Ikegami, N. Tanaka, *J. Chromatogr., A* **2002**, *960*, 85.

[109] M. Meyer, Doctoral thesis, Bayreuth University (Bayreuth), **2003**.

[110] M. Meyer, A. Fischer, H. Hoffmann, *J. Phys. Chem. B* **2002**, *106*, 1528.

[111] D. H. Ripin, D. A. Evans, http://www.cchem.berkeley.edu/crbgrp/Assets/evans_pKa_table.pdf, **2005**.

[112] M.-C. Chao, C.-H. Chang, H.-P. Lin, C.-Y. Tang, C. Lin, -Y., *J. Mater. Sci.* **2009**, *44*, 6453.

[113] H. Dong, J. D. Brennan, *Chem. Mater.* **2006**, *18*, 4176.

[114] K. Nakanishi, K. Kanamori, *J. Mater. Chem.* **2005**, *15*, 3776.

[115] K. Kanamori, H. Yonezawa, K. Nakanishi, K. Hirao, H. Jinnai, *J. Sep. Sci.* **2004**, *27*, 874.

[116] P. Agren, M. Linden, J. B. Rosenholm, R. Schwarzenbacher, M. Kriechbaum, H. Amenitsch, P. Laggner, J. Blanchard, F. Schüth, *J. Phys. Chem.B* **1999**, *103*, 5943.

[117] X.-M. Wang, X.-Z. Du, C.-L. Li, X. Cao, *Appl. Surf. Sci.* **2008**, *254*, 3753.

[118] A. Sah, H. L. Castricum, A. Bliek, D. H. A. Blank, J. E. t. Elshof, *J. Membrane Sci.* **2004**, *243*, 125.

[119] D. G. LeGrand, in *Handbook of Polycarbonate Science and Technology* (Eds.: D. G. LeGrand, J. T. Bendler), Marcel Dekker, Inc., New York, **2000**, pp. 131.

[120] D. Kim, B. Kim, Y. Cho, M. Han, B.-S. Kim, *Ind. Eng. Chem. Res.* **2009**, *48*, 685.

[121] C. Fritscher, N. Hüsing, S. Bernstorff, D. Brandhuber, T. Koch, S. Geist, J. Geserick, S. Hartmann, S. Seidler, H. C. Lichtenegger, *Elettra Annual Report 2006* **2007**, 110.

[122] C. Fritscher, Doctoral thesis, Vienna University of Technology (Vienna), **2008**.

[123] D. R. Lide, in *CRC Handbook of Chemistry and Physics*, 82 ed., CRC, Boca Raton, Florida, **2001-2002**.

[124] P. Alexandridis, R. Ivanova, B. Lindman, *Langmuir* **2000**, *16*, 3676.

[125] R. Ivanova, B. Lindman, P. Alexandridis, *Langmuir* **2000**, *16*, 3660.

[126] R. Takahashi, K. Nakanishi, N. Soga, *J. Sol-Gel Sci. Technol.* **2000**, *17*, 7.

[127] K. Kanamori, K. Nakanishi, T. Hanada, *Soft Matter* **2009**, *5*, 3106.

[128] A. F. Hollemann, E. Wiberg, *Lehrbuch der Anorganischen Chemie*, 91.-100. ed., W. de Gruyter, Berlin, **1985**.

[129] L. C. Klein, *Ann. Rev. Mater. Sci.* **1985**, *15*, 227.

[130] S. A. Snow, U. C. Pernisz, R. J. Braun, *Silicon Chem.* **2006**, *3*, 1.

[131] S. A. Snow, R. E. Stevens, *Surfactant Science Series* **1999**, *86*, 137.

[132] K. Barnes, S. Gathman, D. Plante, L. Stark-Kasley, (Dow Corning Corporation, USA). Patent WO 2006113183, **2006**, p. 20.

[133] N. V. Churaev, A. P. Ershov, N. E. Esipova, R. M. Hill, V. D. Sobolev, Z. M. Zorin, *Langmuir* **2001**, *17*, 1349.

[134] K. S. Clement, K. M. Lee, L. J. Petroff, W. W. Rauscher, R. M. Wehmeyer, R. H. Whitmarsh, (Dow Corning Corporation, USA). Patent US 6987157, **2002**, p. 11

[135] H. F. Fink, *Tenside, Surfactants, Deterg.* **1991**, *28*, 306.

[136] D. T. Floyd, *Surfactant Science Series* **1999**, *86*, 181.

[137] R. M. Hill, E. W. Kaler, L. D. Ryan, J. A. Silas, (Dow Corning Corporation, USA; University of Delaware). Patent US 6013683, **2000**, p. 5.

[138] M. M. Peffly, N. A. Hall, (The Procter & Gamble Company, USA). Patent WO 2008079318, **2008**, p. 17.

[139] W. Spratte, G. Feldmann-Krane, W. Heilen, *Eur. Polym. Paint Colour J.* **1993**, *183*, 12.

[140] R. U. R. Wahl, J. R. Nicholson, J. L. Kerschner, *ACS Symp. Ser.* **2007**, *961*, 177.

[141] R. M. Hill, *Surfactant Sci. Ser.* **1999**, *86*, 1.

[142] H. Hoffmann, W. Ulbricht, *Surfactant Sci. Ser.* **1999**, *86*, 97.

[143] G. Kickelbick, J. Bauer, N. Huesing, M. Andersson, K. Holmberg, *Langmuir* **2003**, *19*, 10073.

[144] G. Kickelbick, J. Bauer, N. Huesing, M. Andersson, K. Holmberg, *Colloids Surf., A* **2005**, *254*, 37.

[145] J. Yang, G. Wegner, *Macromolecules* **1992**, *25*, 1786.

[146] J. Yang, G. Wegner, R. Koningsveld, *Colloid Polym. Sci.* **1992**, *270*, 1080.

[147] M. He, R. M. Hill, Z. Lin, L. E. Scriven, H. T. Davis, *J. Phys. Chem.* **1993**, *97*, 8820.

[148] N. Huesing, B. Launay, J. Bauer, G. Kickelbick, D. Doshi, *J. Sol-Gel Sci. Technol.* **2003**, *26*, 609.

[149] T. Amatani, K. Nakanishi, K. Hirao, T. Kodaira, *J. Chem. Mater.* **2005**, *17*, 2114.

[150] K. Nakanishi, H. Shikata, N. Ishizuka, N. Koheiya, N. Soga, *J. High Resolut. Chromatogr.* **2000**, *23*, 106.

[151] K. Nakanishi, N. Tanaka, *Acc. Chem. Res.* **2007**, *40*, 863.

[152] D. Brandhuber, N. Huesing, C. K. Raab, V. Torma, H. Peterlik, *J. Mater. Chem.* **2005**, *15*, 1801.

[153] Y. Zhou, M. Antonetti, *Chem. Commun.* **2003**, 2564.

[154] F. Carn, A. Colin, M.-F. Achard, R. Backov, *Mater. Res. Soc. Symp. Proc.* **2005**, *847*, 171.

[155] F. Carn, A. Colin, M.-F. Achard, H. Deleuze, Z. Saadi, R. Backov, *Adv. Materials* **2004**, *16*, 140.

[156] K. Nakanishi, R. Takahashi, N. Soga, *J. Non-Cryst. Solids* **1992**, *147-148*, 291.

[157] Evonik, product data sheet: TEGO® Glide 440 - slip and flow additive by Evonik Tego Chemie GmbH, **2009**.

[158] K. Shinoda, T. Nakagawa, B. Tamamushi, T. Isemura, *Colloidal Surfactants*, Academic Press, New York, **1963**.

[159] BASF, Technical Bulletin Pluronic P123, Florham Park, New Jersey, USA, **2004**.

[160] C. G. Göltner, B. Smarsly, B. Berton, M. Antonietti, *Chem. Mater.* **2001**, *13*, 1617.

[161] B. Smarsly, G. Xomeritakis, K. Yu, N. Liu, H. Fan, R. A. Assink, C. A. Drewien, W. Ruland, C. J. Brinker, *Langmuir* **2003**, *19*, 7295.

[162] H.-J. Kim, H. Matsuda, H. Zhou, I. Honma, *Adv. Mater.* **2006**, *18*, 3083.

[163] A. Bose, R. K. Gilpin, M. Jaroniec, *J. Colloid Interf. Sci.* **2000**, *226*, 131.

[164] A. Bose, R. K. Gilpin, M. Jaroniec, *J. Colloid Interf. Sci.* **2001**, *240*, 224.

[165] K. Noble, A. B. Seddon, M. L. Turner, P. Chevalier, I. A. Mackinnon, *J. Sol-Gel Sci. Technol.* **2000**, *19*, 807.

[166] K. Noble, A. B. Seddon, M. L. Turner, P. Chevalier, D. L. Ou, *J. Sol-Gel Sci. Technol.* **2003**, *26*, 419.

[167] S. Han, C. Kim, D. Kwon, *Polymer* **1997**, *38*, 317.

[168] Z. Lin, X. Han, T. Wang, S. Li, *J. Therm. Anal. Calorim.* **2008**, *91*, 709.

[169] K. A. Andrianov, *Metalorganic Polymers*, Interscience, New York, **1965**.

[170] P. R. Dvornic, in *Gelest,* (Eds.: B. Arkles, G. Larson), Gelest, Inc., Silicon Compounds: Silanes & Silicones, **2004**, pp. 419.

[171] K. Cabrera, D. Lubda, H.-M. Eggenweiler, H. Minakuchi, K. Nakanishi, *J. High Resolut. Chromatogr.* **2000**, *23*, 93.

[172] Merck, Analytical HPLC Application 031419, Darmstadt, **2008**.

[173] F. Rouquerol, J. Rouquerol, K. S. W. Sing, in *Handbook of Porous Solids, Vol. 1* (Eds.: F. Schüth, K. S. W. Sing, J. Weitkamp), Wiley-VCH, Weinheim, **2002**, pp. 236.

[174] K. S. W. Sing, D. H. Everett, R. A. W. Haul, L. Moscou, R. A. Pierotti, J. Rouquerol, T. Siemieniewska, *Pure Appl. Chem.* **1985**, *57*, 603.

[175] S. Brunauer, P. H. Emmett, E. Teller, *J. Am. Chem. Soc.* **1939**, *60*, 309.

[176] E. P. Barrett, L. G. Joyner, P. P. Halenda, *J. Am. Chem.Soc.* **1951**, *73*, 373.

[177] M. Kruk, V. Antochshuk, M. Jaroniec, A. Sayari, *J. Phys. Chem. B* **1999**, *103*, 10670.

[178] H. Giesche, in *Handbook of Porous Solids, Vol. 1* (Eds.: F. Schüth, K. S. W. Sing, J. Weitkamp), Wiley-VCH, Weinheim, **2002**, pp. 309.

[179] C. A. L. y. Leon, *Adv. Colloid Interface Sci.* **1998**, *76-77*, 341.

[180] A. Guinier, G. Fournet, *Small-Angle Scattering of X-rays*, John Wiley & Sons, Inc, New York, **1955**.

[181] J. D. F. Ramsay, in *Handbook of Porous Solids, Vol. 1* (Eds.: F. Schüth, K. S. W. Sing, J. Weitkamp), Wiley-VCH, Weinheim, **2002**, pp. 135.

[182] C. Jobke, exam thesis, Ulm University (Ulm), **2007**.

Acknowledgements

First, I would like to express a very big "Thank you" to Prof. Dr. Nicola Hüsing for her confidence in me, her constant professional support and for offering me the opportunities to look beyond my own nose at conferences and workshops.

I would like to thank Prof. Dr. Boris Mizaikoff who agreed to be the second reviser of my thesis.

I would also like to thank Dr. Karin Cabrera and Dr. Stephan Altmaier from Merck KGaA for their professional advice and support, and the HPLC measurements, which were performed at the laboratories of Merck KGaA, Darmstadt.

I would also like to thank Christian Jobke, Zhou Zhu, Sylvia Flaig, and Christos Triantafillidis for their contribution to this thesis as well as all students who helped with my work in the laboratory.

I also want to thank Andrea Feinle and Christoph Schmidtkunz for proof-reading my thesis.

From the Institute of Inorganic Chemistry I, I want to thank Cornelia Egger for the outrageous number of nitrogen sorption measurements, Thomas Fröschl (TGA) and Daniela Mannes (TGA, SAXS), Denis Jahn (SAXS), and Michael Stark, who showed a lot of patience for my many special requests of SAXS experiments.

A very special "thank you" goes to Jasmin, who was also always within earshot, when I needed her. Moreover, thanks to all members of the Institute of Inorganic Chemistry I for their chemical advice and mental support throughout the last 4 years.

I would also like to thank Dr. Udo Werz and Ulrich Ziegler for the spin-lock and the HMBC long-range ^{29}NMR experiments.

I am deeply grateful to my parents, Kurt and Angelika, and my sister Anna for their love and their constant encouragement.

And I would also like to thank my "second" family, Ursel, Alex, Jens, and "die wilden Kerle" (Linus, Jonas, and Oskar) who have welcomed me into their family from the beginning…

and especially Michael for his help and patience and for still not being fed up with me!

Sarah Hartmann

Scharnhorststr. 27
89077 Ulm, Germany
Email: s.j.hartmann@web.de
Date of birth: 17/11/1978 in Starnberg, Germany

Higher Education

05/2006 – 12/2009	**Doctoral. thesis**: Hierarchically Organized (Hybrid) Silica Monoliths for the Application as Stationary Phases in HPLC elaborated at the Institute of Inorganic Chemistry I, Ulm University, Ulm, Germany, under the supervision of Prof. Nicola Hüsing
10/1999 – 03/2006	**Studies for the Diploma Program in Chemistry** at the Ulm University, Ulm, Germany. Diploma Degree in Chemistry (1.6) **Diploma thesis**: PDMS-PEO Block Copolymere als struktur-dirigierende Agentien in der Festkörpersynthese elaborated at the Institute of Inorganic Chemistry I, Ulm University, Ulm, Germany, supervised by Prof. Nicola Hüsing.

School Education

09/1997 – 06/1999	**Maria-Theresia Gymnasium**, Augsburg, Germany. Abitur (High School Graduation, Germany)
08/1996 – 06/1997	**High School Year Abroad in Canada**. Participation in a student exchange program at Abbey High School, Abbey, Saskatchewan, Canada. Graduation from High School
09/1989 – 07/1996	**Maria-Theresia Gymnasium**, Augsburg, Germany.
09/1989 – 07/1989	**Grundschule Gessertshausen**, Germany.

Experience

Since 10/2005	**Teaching Assistant**: Practical courses in inorganic chemistry – fundamental and advanced inorganic chemistry.
Since 10/2006	**Supervision and mentoring** of diploma and scientific graduate theses at the Institute of Inorganic Chemistry I, Ulm University, Ulm, Germany.

Publications

N. Hüsing, S. Hartmann, *Inorganic-Organic Hybrid Porous Materials*. In Ed. L. Merhari: *Hybrid Nanocomposites for Nanotechnology: Electronic, Optical, Magnetic and Biomedical Applications*, Springer, New York, 2009, p. 131 - 171.

S. Hartmann, D. Brandhuber, N. Hüsing, *Glycol-Modified Silanes: Novel Possibilities for the Synthesis of Hierarchically Organized (Hybrid) Porous Materials*, Accounts of Chemical Research, 40 (9), 2007, p. 885 - 894.

Oral Contribution

S. Hartmann, N. Hüsing, *Glycol-Modified Precursors in the Preparation of Hierarchically Organized Silsesquioxane and Pure Silica Monoliths*, SGM 2008, Trzbieszowice, Poland.

Poster Contributions

S. Hartmann, Z. Zhu, S. Flaig, N. Hüsing, *New Diol-Modified Silanes as Precursors for the Synthesis of Hierarchically Organized Silica Monoliths – How Does a Change in Polarity Affect the Formation of the Different Pore Size Regimes?*, Silicon Days 2009, Vienna, Austria.

S. Hartmann, N. Hüsing, *Preparation of Hierarchically Organized Methylsilsesquioxane And Silica Monoliths By Employing Glycol-Modified Precursors,* IMMS 2008, Namur, Belgium.

J. Geserick, V.A. Du, S. Hartmann, X. Liu, C. Jobke, N. Hüsing, *Glykolat-modifizierte Precursoren in der Synthese Mesoporöser Materialien*, GdCh Konferenz 2007, Ulm, Germany.

S. Hartmann, N. Hüsing, *PDMS-PEO Copolymers in the Synthesis of Silica Monoliths Exhibiting Hierarchy on Multiple Levels*, SGS 2007, Montpellier, France.

Further Contributions

T. Nakamura, H. Yamada, Y.. Yamada, A. Gürtanyel, S. Hartmann, N. Hüsing, K. Yano, *New Strategy Using Glycol-Modified Silane to Synthesize Monodispersed Mesoporous Silica Spheres Applicable to Colloidal Photonic Crystals,* Langmuir, DOI: 10.1021/la902498p.

S. Hartmann, A. Hardy-Dessources, M. Baba, N. Hüsing, J. M. Nedelec, *Multiscale Characterization of Porous Ceramics Using a Calorimetric Approach*, IWAC03, 2008, Limoges, France.

Ulm, den 22.12.2009

Eidesstattliche Erklärung

Ich versichere hiermit, daß ich die Arbeit selbständig angefertigt habe und keine anderen als die angegebenen Quellen und Hilfsmittel benutzt sowie die wörtlich oder inhaltlich übernommenen Stellen als solche kenntlich gemacht habe.

Ulm, den 22.12.2009

_____

(Sarah Hartmann)